There are a huge number of water pollutants; one of them is dyes. The method of removing the carcinogenic dyes is based on the adsorption-desorption equilibrium mechanism. Graphene oxide (GO) has pulled in the multidisciplinary examination in the most recent decade credited to its uncommon physicochemical properties. It is used for preparing five different polymeric adsorbents. These adsorbents were characterized by using various techniques, like Fourier transform infrared spectroscopy FTIR, Field emission scanning electron microscopy FESEM, and X-ray diffraction spectroscopy XRD, as well as analysis of the surface area, pore size, and specific pore volume by Brunauer Emmett Teller and Barrett Joyner Halenda (BET & BJH Analysis). Batch experiments were performed for studying adsorption systems of GO and its prepared composites towards Congo Red CR and Bismarck Brown BB toxic dyes, and they have appeared good response to adsorb from their aqueous solutions. Adsorption isotherms were determined using the Langmuir, Freundlich, Temkin, and Dubinin–Radushkevich models.

The kinetic models, namely Pseudo-First-Order, Pseudo-Second-Order, and Intra-Particle Diffusion were employed to understand the mechanism of the adsorption process. Thermodynamic parameters were calculated and used to interpret the results and revealed that the adsorption systems were a spontaneous and endothermic process for GO and its composites. A study of the desorption process was applying for using prepared adsorbents several times while retaining its good adsorption capacity and observed that the desorption efficiency (S%) of GO is higher than that of GO-modified adsorbents.

Dr. Hadi Salman Al-Lami

Hadi Salman Al-Lami is a Professor of Polymer and Ceramic Chemistry, he is got his Ph.D. 1989 from School of Chemistry and Molecular Sciences, University of Sussex, Brighton, UK. He is currently working at the College of Science, University of Basrah.

Ali A. Abdulwahid is got his Ph.D. from the University of Basrah in 2013 where he is currently working as an Analytical chemist assistant professor at the College of Science.

Alaa Adil Mizhir Albaheli is currently working as a lecturer at the University of Basrah, College of Marine Sciences. He is recently awarded a Ph.D. degree in Analytical Chemistry, 2020.

Generis
PUBLISHING
www.generis-publishing.com

Barcode

Generis // Graphene Oxide-Grafted-Polymers Interactions with Congo red and Bismarck Brown dyes

Dr. Hadi Salman Al-Lami

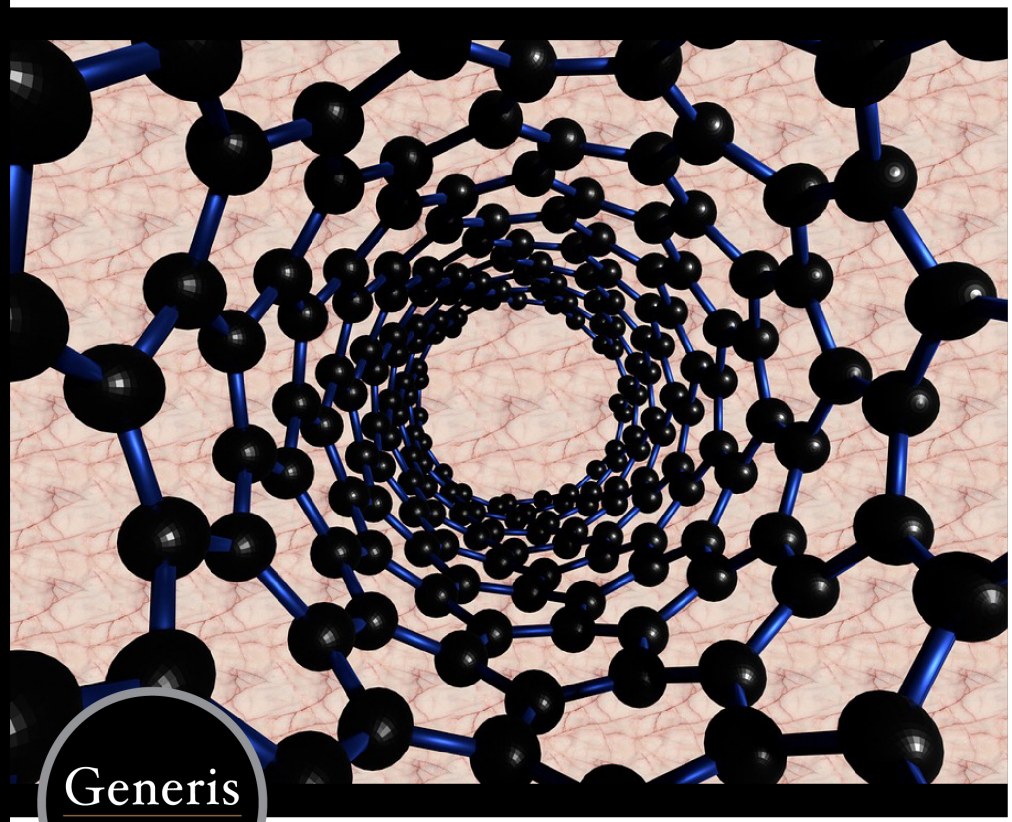

Generis
PUBLISHING

Graphene Oxide-Grafted-Polymers Interactions with Congo red and Bismarck Brown dyes

Generis
PUBLISHING

Graphene Oxide-Grafted-Polymers Interactions with Congo red and Bismarck Brown dyes

Alaa Adil Mizhir Albaheli

Title: *Graphene Oxide-Grafted-Polymers Interactions with Congo red and Bismarck Brown dyes*

Author: *Alaa Adil Mizhir Albaheli*

ISBN:

Cover image: www.pixabay.com

Publisher: Generis Publishing
Online orders: www.generis-publishing.com
Contact email: info@generis-publishing.com

Dedication

To

My dear wife and children...

My family ...
And everyone who visited my heart to leave a mark of love and a heartbeat …
Give them all this little effort …

Acknowledgments

I would like to express my sincere gratitude to the many people who have contributed to help complete this research project. First of all thanks to my supervisors ***Prof. Dr. Hadi S. Al-Lami*** *and* ***Asst. Prof. Dr. Ali A. Abdul Wahid*** *for introducing me to the interesting field of science and for providing me with the opportunity to carry out this study. I am extremely lucky to have such supervisors whose feedbacks were indispensable. They have patiently corrected me and my research would not have been possible without their help.*

I would like to convey my gratefulness and appreciation to the Head of Chemistry Department, Asst. Prof. Dr. Ali A. A. AL-Riyahee. I wish to express my sincere thanks to Asst. Prof. Dr. Baqer A. Al-Mayyahi, Prof. Dr. Hassan T. Abdul Sahib, Asst. Prof. D. Nuha H. Mzher (University of Thi-Qar), and Dr. Bassam Ashoor Rasheed (Marine Science Centre) for providing me with the necessary information and consideration and for their valuable feedback.

I am extremely grateful to my colleagues at the College of Marine Sciences, especially the Dean of the College, Prof. Dr. Hamid T. Alsaad, the Head of Applied Marine Sciences, Asst. Prof. Muayad H. M. Albehadili, and Zainab Jaafar Oudha for their support.

Having taken my last steps, I find myself obliged to thank my wife, children, and family for their continuous support. In addition, my gratitude goes to all the graduate students, especially my colleagues Huda Salim and Fadhil Neamah Abdulrida (Biology Department) and I ask Allah to bless them all.

Alaa

Abstract

There are a huge number of water pollutants; one of them is dyes. This study is based on preparing some polymeric adsorbents for the removal of carcinogenic dyes. Hummer's method with some modifications was used for preparing graphene oxide GO from graphite. Five composites were prepared by grafting GO with; 3,3′- diaminobenzidine, DAB/ethylene diamine tetraacetic acid, chitosan, CS/EDTA, and poly (n-butyl methacrylate-co-methacrylic acid) to form GO/DAB, GO/DAB/EDTA, GO/CS, GO/CS/EDTA, and GO/pBCM composites respectively.

These adsorbents were characterized by using various techniques, like Fourier transform infrared spectroscopy FTIR, Field emission scanning electron microscopy FESEM, and X-ray diffraction spectroscopy XRD, as well as analysis of the surface area, pore size, and specific pore volume by Brunauer Emmett Teller and Barrett Joyner Halenda (BET & BJH Analysis).

Batch experiments were performed for studying adsorption systems of GO and its prepared composites towards Congo Red CR and Bismarck Brown BB toxic dyes, and they have appeared good response to adsorb from their aqueous solutions. The optimization of adsorption systems started with studying the effect of pH of the dye solutions. The results showed that the optimum pH-values were varied depending on the type of the adsorbents and the nature of the adsorbed dye. It was found that pH (3.0, 7.0, 5.0, 3.0, 5.0, and 7.0) for adsorption of CR dye onto GO, GO/DAB, GO/DAB/EDTA, GO/CS, GO/CS/EDTA, and GO/pBCM respectively, and (3.0, 3.0, 5.0, 3.0, 5.0, and 3.0) for adsorption of BB dye for the same adsorbents sequence above.

The second optimized factor was the time. The results showed that the optimum times were (60, 30, 45, 45, 45, and 30 min.) for adsorption of CR dye onto GO, GO/DAB, GO/DAB/EDTA, GO/CS, GO/CS/EDTA, and GO/pBCM adsorbents respectively and (45, 30, 30, 45, 45, and 15 min.) for adsorption of BB dye for the same adsorbents series stated above. These results imply that the five prepared GO-composites needed a few times to reach the equilibrium compared with the reference (GO).

Adsorption isotherms were determined using the Langmuir, Freundlich, Temkin, and Dubinin–Radushkevich models. The Langmuir model was found to be more suitable for the experimental data than other adsorption models,

and this reflects the monolayer adsorption of CR and BB dyes onto the surface of adsorbents and assumes there are restricted and homogenous adsorption sites. The maximum adsorption values (q_{max}) were calculated using the Langmuir isotherm results. They were found (1250, 1428.5, 1438.1, 2000, 1666.6, and 1304.9 mg/g) for adsorption of CR dye onto adsorbents GO, GO/DAB, GO/DAB/EDTA, GO/CS, GO/CS/EDTA, and GO/pBCM respectively and (833.3, 1734.7, 1111.1, 920.74, 863.8, and 1000 mg/g) for adsorption of BB dye for the same adsorbents order mentioned previously. Again, these results proved that the preference for prepared GO-composites over GO.

The kinetic models, namely Pseudo-First-Order, Pseudo-Second-Order, and Intra-Particle Diffusion were employed to understand the mechanism of the adsorption process, and it fitted very well the Pseudo-Second- Order kinetic model for both CR and BB dyes onto GO and all prepared GO-composite, which relies on the assumption that chemisorption may be the rate-limiting step.

Thermodynamic parameters include enthalpy ($\Delta H°$), entropy ($\Delta S°$), free energy ($\Delta G°$), and activation energy (E_a) of the adsorption process were calculated and used to interpret the results and revealed that the adsorption systems were a spontaneous and endothermic process for GO and its composites. Also, low activation energy values (E_a<40 kJ/mol) were characteristics of the physisorption mechanism and diffusion-controlled process.

A study of the desorption process was applying for using prepared adsorbents several times while retaining its good adsorption capacity and observed that the desorption efficiency (S%) of GO is higher than that of GO-modified adsorbents.

TABLE OF CONTENTS

LIST OF FIGURES

LIST OF TABLES

LIST OF SCHEMES

1. Introduction

1.1. A Brief Introduction of Graphene Oxide GO

Nanoscience and nanotechnology fundamentally manage the combination, portrayal, investigation, and misuse of nanomaterials. Carbon, a standout amongst the most well-known molecules on Earth, happens normally in numerous structures and as a part of innumerable substances which are called allotropes of carbon. Graphene, a "wonder material" is the world's thinnest, strongest, and stiffest material, and additionally being a magnificent channel of warmth and power. It is the fundamental building square of other imperative allotropes. Graphene oxide (GO) is of awesome intrigue because of its minimal effort, simple access, and across-the-board capacity to change over to graphene. Adaptability is additionally a much-wanted element [1].

Graphene oxide (GO) is graphite that has been oxidized to sprinkle the carbon layers with oxygen atoms and after that diminished, to isolate the carbon layers totally into individual or few-layer graphene. Graphene oxide is the successful result of this oxidation is when the oxidizing operators respond with graphite, the interplanar separating between the layers of graphite is expanded. The oxidized compound would then be able to be scattered in a base arrangement, for example, water, and graphene oxide are then produced [2-4]. Many sorts of oxygen functionalities are known to exist in GO: epoxide (-O-), hydroxyl (-OH), and carboxyl (-COOH). Epoxide and hydroxyl, situated on the basal plane of GO, the real parts; carboxyl, distributed at the edges of GO, are the minor ones [5].

Graphene oxide (GO) has pulled in the multidisciplinary examination in the most recent decade credited to its uncommon physicochemical properties, what's more, its applications in vitality discussion, supercapacitor, photocatalysis, adsorbents, and so forth [6, 7]. Due to the one-of-a-kind compound exercises, phenomenal scattering properties, high surface territories, and huge measure of useful gatherings on its surfaces, GO has demonstrated remarkable sorption exhibitions for various types of environmental pollutants [8, 9].

The sp^2/sp^3 ratios in GO can be tuned by varying the oxidation degree using suitable chemical reactions. GO with a various ratio of sp^2/sp^3 domains may provide novel properties that can be useful for making several

improvements in the development of graphene-based research applications such as biosensors, supercapacitors, and optoelectronic devices, etc., With the motivation of altering the properties of GO by varying the oxidation levels, we used a modified Hummers method employing various quantities of an oxidizing agent. To date, three major methods of synthesizing GO have been used; (i) the Brodie method [10], (ii) the Staudenmaier method [11], and (iii) the Hummers method [12]. Over these methods, the Hummers method is generally considered to be the best since it has the advantage of nontoxicity compared to the former two which involve highly toxic reactions due to the liberation of toxic gases and highly reactive species [13]. In a commonplace GO, the quantity of carbon atoms bonded to oxygen exceeds the number of intact sp^2-hybridized carbon atoms. This makes GO differ from the parent graphene. From one perspective, these oxygen functionalities can be considered as deformities brought into the generally perfect graphene plane. These deformities change over electrically conductive graphene into a cover. Then again, the oxygen functionalities give GO numerous interesting properties that the parent graphene does not have. One of these properties is hydrophilicity, i.e. the capacity to be disintegrated and to shape stable colloid arrangements in water and in some low-molecular-weight alcohols. Another preferred standpoint is opening a tunable bandgap that is in charge of novel optical and electronic properties [14].

Usually, GO is thermally unstable. Upon heating even below 100˚C, GO solely decomposes possibly due to the release of the absorbed water. The major mass loss occurs at ~200˚C presumably because of decompositions of oxygen-containing groups [15, 16]. However, the removal of functional groups greatly increases the thermal stability of the RGO. When the GO is heated up to 800˚C, no significant mass loss is detected [16]. Tentatively accessible GOs are amorphous materials with huge sizes. Their stoichiometry and structures vary depending upon the techniques used for their syntheses [19]. Microscopic images [17] and Raman spectroscopy [18] have appeared that oxygen functionalities form islands and lines on the basal plane of GO, dividing the GO sheet into small in-plane aromatic domains (Figure 1.1). In this manner, the surface structures of GO are sheets of fragmental graphene with oxygen functionalizes modification [19].

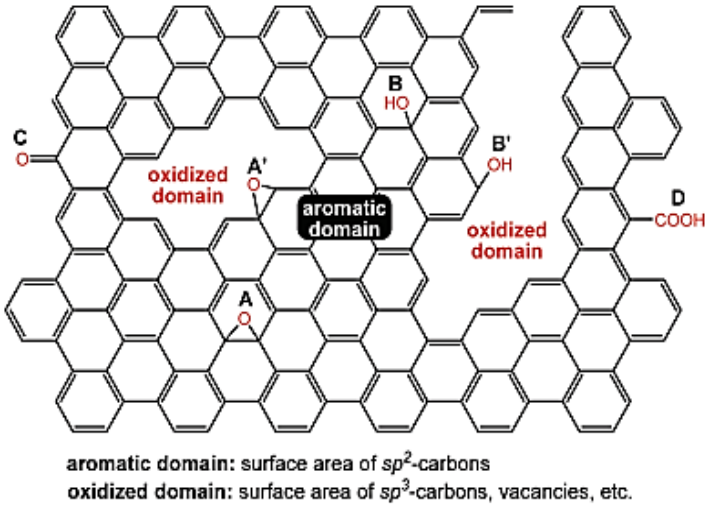

Figure 1.1. Schematic illustration of oxygen-containing groups in GO: A, epoxide located at the interior of an aromatic domain of GO; A′, epoxide located at the edge of an aromatic domain; B, hydroxyl located at the interior of an aromatic domain; B′, hydroxyl at the edge of an aromatic domain; C, carboxyl at the edge of an aromatic domain; and D, carboxyl at the edge of an aromatic domain [18]

1.2. Schemes Proposed of (GO) synthesis

1.2.1. Brodie and Staudenmaier Methods

Brodie prepared the first batch of GO when he was investigating the chemistry of graphite in 1859 [20]. When he added $KClO_3$ into a slurry of graphite in fuming HNO_3, he obtained a new batch of a compound that later determined to contain carbon, oxygen, and hydrogen. Nonetheless, his observations and conclusions were limited by theories and characterization techniques available at that time, leaving a huge space for work and improvement until today.

One of the improvements in Brodie's work was carried out by L. Staudenmaier [21, 22]. Two major changes were introduced:

i. Concentrated sulfuric acid is added to improve the acidity of the mixture.

Multiple aliquots of potassium chlorate solution are added into the reaction mixture throughout the reaction.

These changes have led to a highly oxidized GO product (composition the same as the final product that Brodie got) in a single reaction vessel, thus largely simplified the process. However, the Staudenmaier method was both times consuming and hazardous: the addition of potassium chlorate typically lasted over 1 week, and the chlorine dioxide evolved needed to be removed by an inert gas, while the explosion was a constant hazard. Therefore, further modification or development of this oxidation process was still worth investigation.

1.2.2. Hummers Method and Its Modifications

Very nearly, 60 years after the presentation of Staudenmaier's technique, physicists Hummers and Hoffman in Mellon Institution of Industrial Research built up a distinctive formula for making GO. A without water blend of concentrated sulfuric corrosive, sodium nitrate, and potassium permanganate was arranged and kept up beneath 45°C for graphite oxidation. As per their depiction, the entire oxidation process completed inside 2h, prompting the last item with a higher level of oxidation than Staudenmaier's item [23]. In any case, it was discovered that Hummers' item ordinarily has a deficiently oxidized graphite center with GO shells, and a pre-expansion procedure is useful to accomplish a higher level of oxidation. First presented by Kovtyukhova in 1999 [24]. Other reported modifications also include an increase in the amount of potassium permanganate, etc. [25]. These days, the change in Hummer's strategy is the most widely recognized formula utilized for GO planning as depicted in Scheme (1.1). The oxidation degree and yield of GO have been widely enhanced when contrasted and the simple first item is recognized by Brodie. Nevertheless, the division and cleansing procedures in the altered Hummers technique are still very convoluted and tedious.

1.2.3. The Improved Method to Synthesize GO

As the gold rush of graphene research started in 2004, GO jumped into the center of carbon nanomaterial research, and lots of publications have emerged talking about its structure, reduction, and applications. In 2010, a new recipe was introduced by Tour’s group at Rice University, which avoided the

use of sodium nitrate and increased the amount of potassium permanganate and also introduced a new acid into the reaction vessel: phosphoric acid [26].

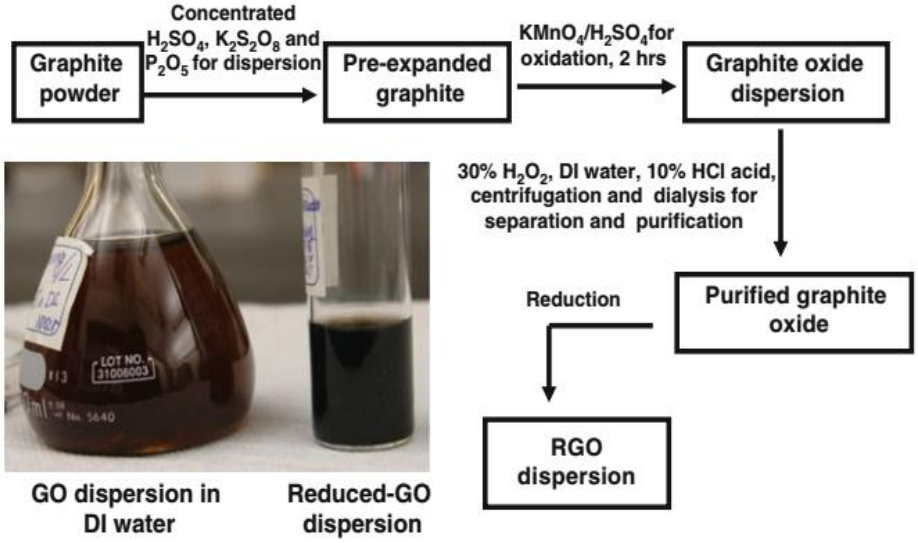

Scheme 1.1. The recipe of the most commonly used modified Hummers method for GO preparation [28]
Lower left: photographic images of the final product GO in deionized water (left) and the dispersion after hydrazine reduction with ammonia (right).

They reported a GO product with a higher degree of oxidation made by reacting graphite with six equivalents of $KMnO_4$ in a (9:1) mixture of H_2SO_4/H_3PO_4. One of the greatest focal points of this convention is the absence of $NaNO_3$, thus avoiding the generation of toxic gases such as NO_2, N_2O_4, or ClO_2 in the reaction and making it more environmentally friendly. Furthermore, phosphoric acid is believed to offer more intact graphitic basal planes and the final yield is much higher than that in the Hummers method. A comparison among these protocols is shown in Scheme (1.2)

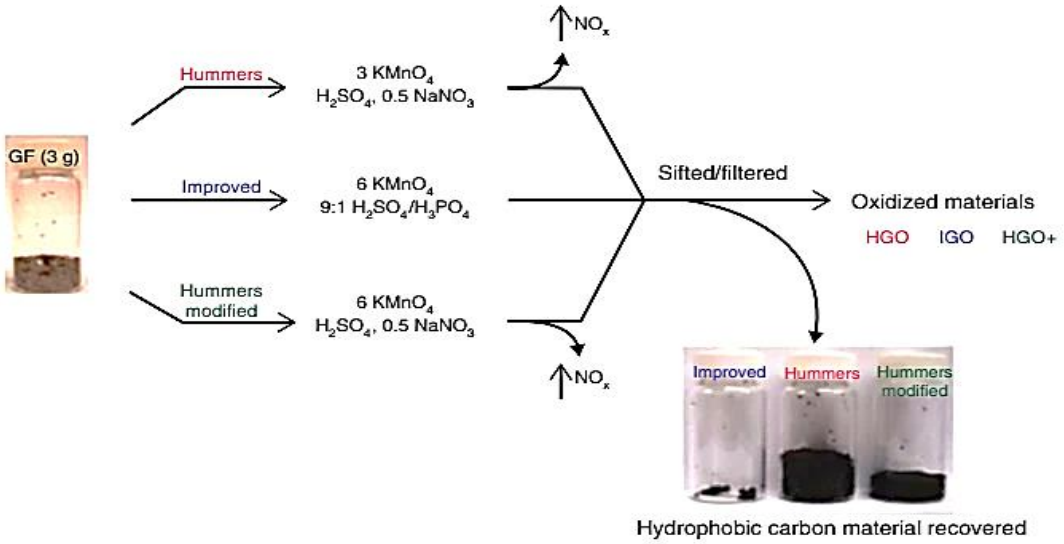

Scheme 1.2. A comparison of procedures and yields among different GO preparation recipe [16]

1.3. Functionalization of Graphene Oxide (GO)

It is well established that the densely functionalized surface of GO has provided unique opportunities for chemical modification via classic organic transformations to finely tune the material's chemical and physical properties. The methods used to derivatize GO are highly dependent on the desired application and properties such as electrical and thermal conductivity, hydrophilicity, and mechanical reinforcement. Oftentimes, functionalized derivatives of GO exhibit physical properties not found in as-synthesized GO [27]. In the broadest sense, the functionalization of GO can be divided into two categories: peripheral functionalization and basal plane functionalization. Modifications of the periphery of GO typically utilize the reactivity of the carboxylic acid groups whereas basal plane modification has traditionally harnessed the reactivity of the resident hydroxyl and epoxide groups [27].

Among different functional moieties, carboxylic acid might be the most active one, since it is mostly located on the peripheries of GO sheets. The activation of the COOH is usually led by treatment with $SOCl_2$, followed by various nucleophilic attacks with different nucleophiles (Scheme 1.3) [23, 27-29]. 1-Ethyl-3-(3-dimethylamino propyl)-carbodiimide (EDC) [30], N,N′-dicyclohexylcarbodiimide (DCC) [31], or 2-(7-aza-1-H-benzotriazole-l-yl)-

1,1,3,3,-tetramethyluronium hexafluorophosphate (HATU) [32] can also activate –COOH, and attacks by nucleophiles such as amines or hydroxyl groups are usually followed to form covalent attachments [23].

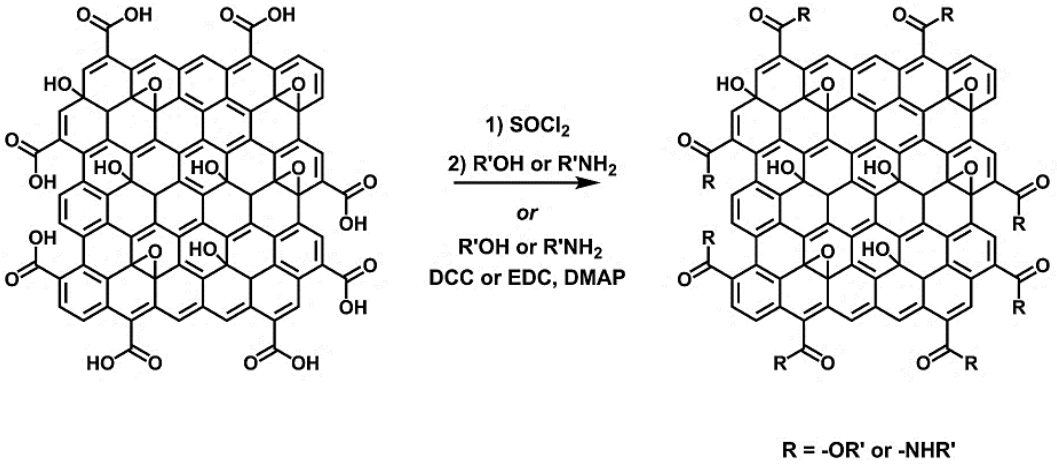

Scheme 1.3. Activation of GO's peripheral carboxylic acid groups with either $SOCl_2$ or a carbodiimide, and subsequent condensation with an alcohol or an amine [23]

For example, GO was activated with EDC and then functionalized with chitosan (M_n=3kDa). The resulting water-dispersible Chitosan–Graphene Oxide composites were then used as a system to deliver a water-insoluble drug (camptothecin) [33, 34]. Similar to GO's carboxylic acid groups, the hydroxyl groups may be functionalized using carbodiimide coupling chemistry. In this case, a surface-bound hydroxyl group on GO serves as the nucleophile and condenses with an exogenous carboxylic acid [27].

Another route to derivatize the basal carbon surface of GO is through the ring-opening of the epoxide groups. The nucleophile of choice is typically an amine, including aliphatic, aromatic, and polymeric variants. Generally, the amine is heated in the presence of exfoliated GO in a polar solvent and purification/isolation involves either filtration or centrifugation. Beyond heteroatom nucleophiles, carbanions have also been used in the same manner to open the epoxide groups [35].

The functionalization of GO via the aforementioned routes has led to complex architectures with diverse properties such as increased hydrophilicity or hydrophobicity as well as enhanced thermal stability and mechanical

robustness. As such, functionalize derivatives of GO have found applications in polymer composites, drug delivery systems, analyte sensing, and electrochemical devices [36].

1.4. Graphene Oxide-Based Polymer Composites

Polymer composites represent another area that frequently capitalizes on GO's reactivity and ability to modify the carbon material's functional groups. Graphene Oxide-based polymer composites are attractive materials in that they often possess enhanced thermal and/or mechanical stability when compared to the filler-free polymer [37].

Commonly, the dispersion of fillers within the host polymer matrices is one of the most crucial parameters in determining the effectiveness of the added fillers as well as the final characteristics achieved [38]. Graphene oxide, which is best known for its oxygen-rich functional groups (hydroxyl, carboxyl, and epoxy groups) located on the basal plane and edges, can be dispersed into individual sheets in water. Therefore, a molecular level dispersion can be achieved, providing that a common solvent is used for both GO and the polymer matrix. In contrast, the overall performance of graphene-based composites depends heavily on the interfacial adhesion between graphene oxide and polymer matrix. While the most common interactions of graphene or graphene oxide with the polymers rely mainly on the physical bindings as the strongest possible interactions, various studies utilized the oxygen functional groups which are responsible for hydrogen bonding formation to react with polymeric molecules [39].

Recently, single-layered two-dimensional graphene, which is recognized as one of the strongest materials in the world, has attracted much attention due to its excellent properties and potentially low cost in mass production [40, 41].

To harnessing the fantastic properties, graphene has been considered to incorporate into polymers, to prepare graphene or graphene oxide filled (nano-) composites, which may be offered novel and interesting structured materials for various applications [42]. However, in mass cases, graphene is not compatible with polymers. Functionalization of graphene is necessary for the improvement of the compatibility with polymers [43].

For instance, the poor distribution of graphene layers within the polymer matrix, caused by the strong force between graphene sheets and the high viscosity of polymers, is overcome by functionalizing graphene sheets with

oxygen and hydroxyl functionalities to encourage better interactions between the components [44].

Graphene/polymer (nano-) composites are commonly synthesized using in-situ polymerization. The monomer and graphene precursors are initially dissolved in a common solvent and ultra-sonicated to achieve uniform dispersion. An initiator is then added to the mixture to form the polymer. This specific technique can be expanded or varied to form a very wide range of categories and classifications, depending on the type of desired end product, as well as the selected synthesis routes. For instance, a free-radical initiator and reducing agent can be added simultaneously to induce polymerization and at the same time reduce GO to graphene, or achieve ordered layer structure of the desired composites [45-47].

1.5. Water Pollution

Water is considered polluted if some substances or condition is present to such a degree that the water cannot be used for a specific purpose. Olaniran defined water pollution to be the presence of excessive amounts of hazardous pollutants in water in such a way that it is no longer suitable for drinking, bathing, cooking, or other uses [48]. Humans generally induce water pollution. It results from actions of humans carried on to better self. These could be treated under the various activities that man engages in, which lead to pollution. The growth of the human population, industrial and agricultural practices are the major causes of pollution [49].

Heavy metal pollution has a serious threat to the survival of living biota and the physicochemical nature of the environment. Water is the natural and preferred sink for contamination and its pollution becomes an important concern for human health. Heavy metal compounds are widely used in electroplating, cement, metal processing, wood preservatives, paint and pigments, and steel fabricating industries. These industries produce large quantities of toxic wastewaters [50].

Particularly, colored organic compounds generally represent a minor fraction of the organic components of wastewaters but their color renders them esthetically unacceptable. The color of waste effluents is due to the presence of phenolic compounds such as tannins or lignins (2–3%), organic colorants (3–4%), and especially dyes and dye intermediates [51].

Organic dyes are considered as chemical contaminants for industrial wastewater. About 30% of the dyes used in industrial processes go to industrial wastewater [52]. Dyeing industries such as paper, rubber, plastic, food, leather, or textile are the main sources of industrial wastewater. The wastewater generated by these industries, with main characteristics of high salinity, high chemical oxygen demand (COD) concentrations, high temperature, high fluctuation in pH (2–12), and strong coloration is one of the most important environmental concerns [53], where many of them are toxic and carcinogenic [54].

Some of the used dyes in these industries directly or during the dyeing process are released to effluents. In the dyeing process, due to the low level of dye fiber fixation, about 10–15% of the used dyes are lost in wastewater. Eventually, generated highly colored wastewater gets its way to the environment, which is problematic because of the high visibility, resistance, and toxic impact of the dyes that exist in the wastewater [55, 56]. The presence of dyes in the water, even at low concentrations, reduces the penetration of oxygen and light, which resulted in endanger of the environment by the effect on biological cycles and photosynthetic activities. Also, they lead to toxic effects on human health such as jaundice, skin irritation, allergies, heart defects, and mutations [57]. According to the synthetic origin and complex aromatic structures of dyes, they are resistant to biological degradation. Therefore, organic dyes can remain stable under different conditions and biological processes are not able to eliminate the dyes easily and completely [58]. They may be accumulated in living tissues, causing various diseases and disorders; therefore they must be removed from wastewater before it is released into the environment before discharge [59]. Also, textile effluents constitute a major part of industrial wastewater. The release of dyes to the environment by untreated wastewater poses a serious threat to freshwater sources, aquatic life, and human beings [60].

The traditional techniques for the elimination of pollutants include; precipitation, membrane filtration, adsorption, and ion exchange, etc. [61]. Furthermore, various methods have been applied for dye removal from contaminated waters and industrial effluents, which are generally classified as chemical, physical, and biological [62].

Nevertheless, these methods show some limitations such as low efficiency, high operating costs, needing special equipment, and high sludge

production. All these limitations lead to the inadequacy of these methods for dye wastewater treatment in small-scale industries [63].

Among these methods, the adsorption technique has been used widely because it is a simple, economical, and cost-effective process for the elimination of dyes from wastewater. The adsorption process is preferred by many researchers over other methods and is widely used in wastewater treatment. Some adsorbents such as; clay minerals, oxides, and carbon materials (Graphene and Graphene Oxide) have been studied extensively to remove most pollutants like dyes and metal ions from aqueous solutions [64, 65].

1.6. Adsorption Process Principles

Adsorption is a process in which a substance (adsorbate), in the gas or liquid phase, accumulates on a solid surface. It is based on the capability of porous materials with large surfaces to selectively retain compounds on the surface of the solid (adsorbent)[66].

Adsorption is used to remove many organic pollutants, toxic compounds, dyes, and other substances of various types of water that cannot be removed by conventional methods. These components can be removed largely by adsorption on the surfaces of many porous natural materials such as activated carbon, cellulite, and other substances [67].

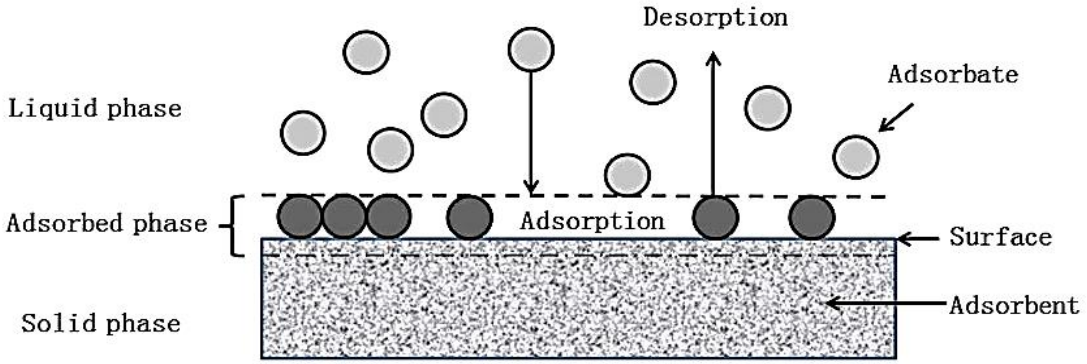

Figure 1.2. Schematic description for Basic terms of adsorption [68]

Figure (1.2) shows an adsorption example of an adsorbate contained in the liquid phase and a solid adsorbent with a highly porous surface or functional group modified surface, adsorbate from the solution will be deposited at the surface of the adsorbent due to liquid-solid intermolecular

forces of attraction. The process is reversible so that the deposited molecules will desorb from (leave) the adsorbent surface if some parameters are changed conveniently. thus, the adsorbate can be separated from the solution by adsorption and desorption [68].

Thus, absorption includes the whole matter whereas adsorption is only effective on surfaces. But both the terms are included in a single term called "*Sorption*", and the reverse of sorption is called "*Desorption*" [69].

1.6.1. Mechanism of Adsorption Process

Among the operations, the adsorption process occupies an important position in environmental remediation, since it is an efficient and economically feasible process for the treatment of wastewater containing dissolved organic pollutants [70]. In the adsorption, molecules extracted from one phase (liquid phase, adsorbate solution) and concentrated at the surface of a second phase (solid phase, adsorbent) which occurs due to an attractive force existing between the adsorbent surfaces and the adsorbate molecules.

Therefore, adsorption is a removal process where certain molecules are bound to a particle surface by either chemical or physical attraction. The process consists of three sequential steps [71]:

- Substances adsorb to the exterior of the adsorbent.
- Substances move into the adsorbent pores.
- Substances adsorb to the interior walls of the adsorbent.

While adsorption is the phenomenon of accumulation of a large number of molecular species at the surface of a solid or liquid phase in comparison to the bulk. These phenomena can be classified into two types depending on the nature of the bonding between the molecules of the adsorbate and the surface of the adsorbent, namely chemisorption and physisorption.

Both types take place when the molecules in the liquid phase become attached to the surface of the solid phase as a result of the attractive forces at the adsorbent surface overcoming the kinetic energy of the adsorbate molecules [72].

1.6.2. Categories of Adsorption

Adsorption is classified into two types depending on the nature of the bond between the adsorbent surface and the adsorbate substance [72, 73]:

(1) Physisorption; or physical adsorption occurs when, because of energy difference and/or electrical attractive forces (weak Van der Waals forces), adsorbate molecules become physically fastened to the adsorbent surface. Physisorption takes place with the formation of single or multiple layers of adsorbate on the adsorbent surface and is characterized by the low activation energy of adsorption.

(2) Chemisorption; or chemical adsorption occurs when a chemical reaction occurs between the adsorbed molecules and the adsorbent. Chemisorption takes place with the formation of a single layer of adsorbate attached to the adsorbent surface by chemical bonds. This type of interaction is strong with a covalent bond between adsorbate and the surface of the adsorbent is characterized by a high enthalpy of adsorption.

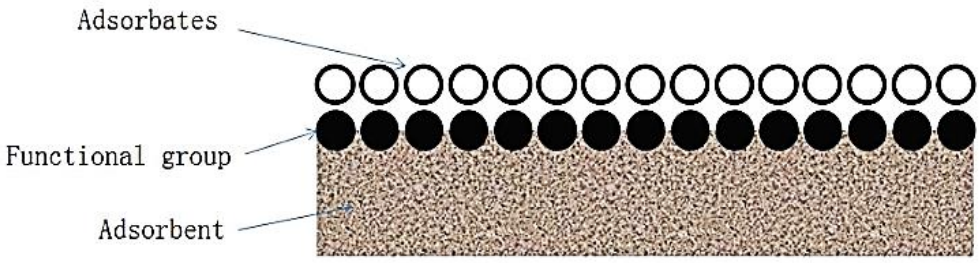

Figure 1.3. Chemical adsorption onto an adsorbent with a functional group [68]

Table 1.1. Comparison between Physical and Chemical adsorption [68]

Physical adsorption	Chemical adsorption
Low heat of adsorption (20-40 kJ/mol)	The high heat of adsorption (40-400 kJ/mol)
Van der Waal's forces	Chemical bond
Low temperature favored	High temperature favored
Does not require any activation energy	Requires activation energy
Reversible	Irreversible

1.7. Applications of Graphene Derivatives in the Adsorption Process

Numerous challenges remain for developing the fundamental understanding of graphene and graphene oxide and their composites, these materials have already been explored for a range of applications [74].

However, these materials sometimes suffer from either low adsorption capacities or efficiencies. Modified graphene or graphene oxide compounds have gradually developed important roles to resolve this problem because of enhanced active sites and abundant functional groups on the surfaces. So far, a variety of materials such as graphene compounds [75-77] have been studied during the adsorption process for removing different organic and inorganic pollutants from large volumes of aqueous solutions (aquatic environments), and the results indicated that these materials have high adsorption capacity.

Pollutant removal from the water via adsorption process on graphene-based materials has been widely used in a water purification technology because of its high efficiency and low cost [78]. For those, some inorganic and organic pollutants that strongly threaten the human body, animal, and plants, GO-based materials display strong adsorption affinity to remove them from wastewater [79, 80].

Unlike the carbon nanotubes CNTs, which require a special oxidation process to introduce hydrophilic groups for the pollutants removal, the production process of graphene oxide from graphite inherently introduces the functional groups of –COOH, –O–, and –OH on to the surface, which are favorable chemical functionalities for an ideal sorbent [81, 82]. Considering the oxygen-containing functional groups on the graphene oxide surfaces, the graphene oxide compounds should have a high sorption capacity for the adsorption of many pollutants from large volumes of aqueous solutions [83].

Studies have reported that many dyes, such as Congo red, rhodamine B, and methyl blue may have carcinogenic and mutagenic effects on animals and humans [84]. Various materials have been used to adsorb organic dyes, such as clays, mesoporous gels, organic-inorganic hybrids, magnetic particles, activated carbon, and graphene oxide, and as a new promising material GO is one of the most preferred adsorbents because of the unique layered structure, large surface area, and high adsorption capabilities of this material [85].

Gemini surfactant/GO composites have been successfully prepared using three Gemini surfactants with different tail chain lengths [86], and these composites were applied to the adsorption of Congo red dye, and from the experimental data, optimum adsorption conditions, adsorption kinetics, and isotherms were obtained. The removal process was favorable at acidic pH and reached equilibrium in ~60 min. The results showed that the pseudo-second-order model and the Langmuir adsorption isotherm were a good fit for the adsorption of Congo red onto Gemini surfactant/GO composites as adsorbents for the removal of some organic dyes in wastewater treatment (As shown in Scheme 1.4).

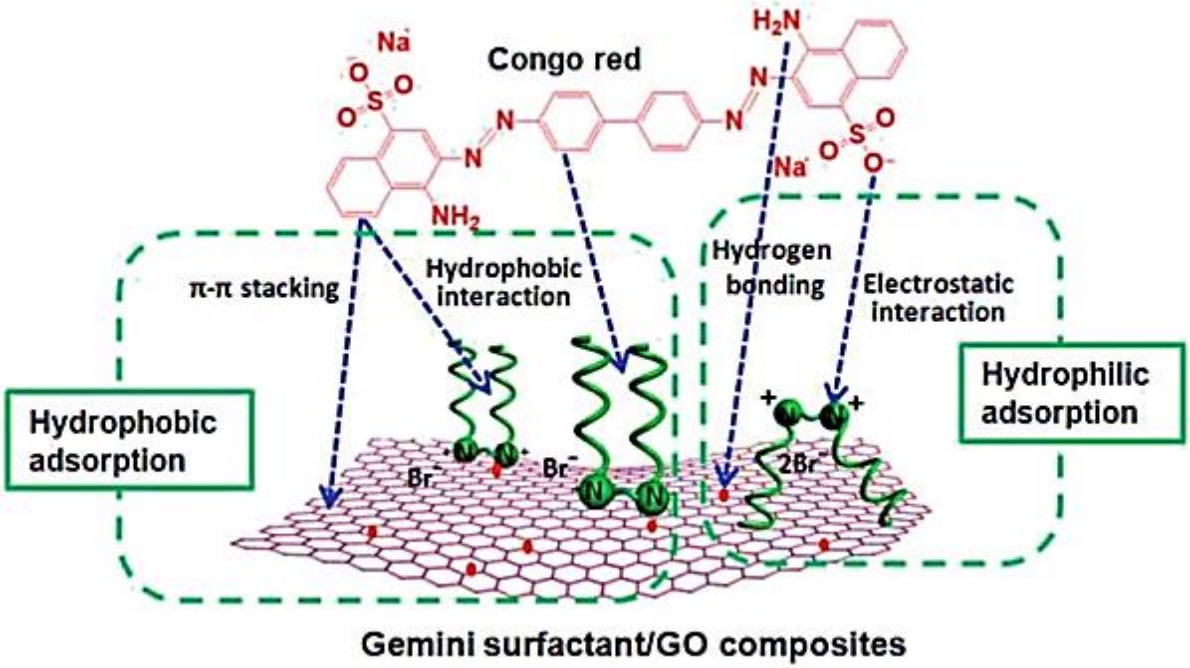

Scheme 1.4. Proposed mechanisms for adsorption of Congo red on Gemini surfactant/GO composites [86]

Recently, it was demonstrated that the silylation of GO is another efficient method to introduce efficient groups onto the surface of GO for the application of pollutants removal from water (As shown in Figure 1.4) [87].

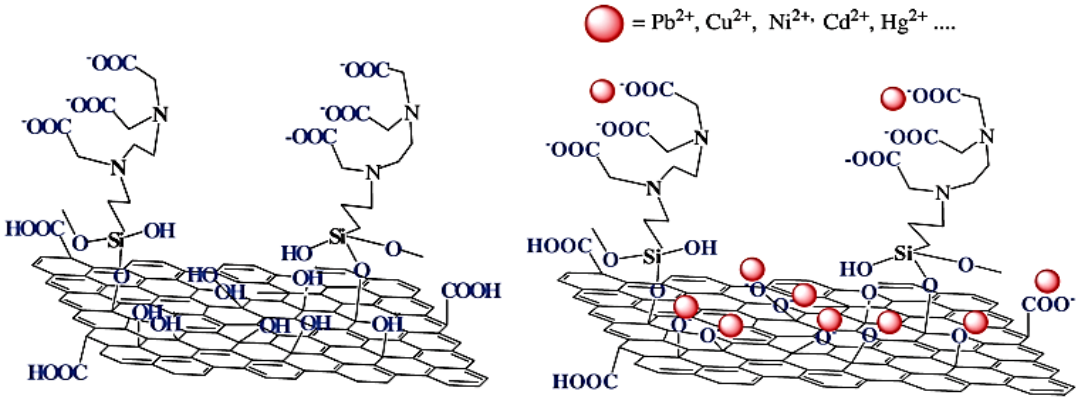

Figure 1.4. Chemical structure of EDTA-GO (left) and its interaction with pollutants (right) [87]

Important kind of harmful and toxic water pollutants are organic dyes, which has been widely used in various industrial fields, such as coating, papermaking, and textiles. One effective way to remove them is direct adsorption [88].

Until now, the adsorptive removal of toxic dyes from wastewater using several adsorbents. Therefore, GO and GO-based compounds have attracted substantial interest as highly effective adsorbents for pollutants such as organic dyes in water. Because of the surface functional groups of GO, such as oxygen-containing groups (epoxides, hydroxylic, and carboxylic groups) that was regulate the availability of the adsorption sites [89].

Recently GO and GO-based compounds have made great progress in the removal of the dye [90-92]. The adsorption characteristics of the prepared composite poly (methyl methacrylate) (PMMA)–graphene oxide (GO) were investigated for removing the study of crystal violet (CV) dye. The adsorption results revealed that the best adsorption capacity of CV dye by PMMA–GO nanocomposites occurred at pH 12. The thermodynamic parameters for CV adsorption onto the PMMA–GO composites, including the Gibbs free energy $\Delta G°$, entropy $\Delta S°$, and enthalpy $\Delta H°$ were calculated of CV dye adsorption via thermodynamic examination. Also, the adsorption process was interpreted well by the pseudo-second-order kinetic model [93].

A three-dimensional porous graphene oxide/polyacrylic acid (GO/PAA) aerogel with double network skeleton was assembled by in situ solution polymerization toward the removing of multi dyes from wastewater, such as methylene blue MB, crystal violet CV, methyl orange MO, and rhodamine B RhB, in which the adsorption capacities for CV and MB were 851.31 and 771.14 mg/g, respectively. This composite showed outstanding adsorption capacity due to the structure of the 3D double network skeleton, large specific surface area, and remarkable carboxyl group content. Langmuir isotherm and D-R models described the adsorption isotherms, and the adsorption kinetic was fitted by the pseudo-second-order kinetic model [94].

The study reported developed a novel mesoporous SiO_2 - GO hybrid material (SiO_2NH_2-GO) as a super adsorbent for organic dyes removing from water, through the condensation reaction between the amine units exposed on 3-aminopropyl functionalized silica nanoparticles and the epoxy groups on the surface of GO [95]. The maximum adsorption capacity of methylene blue, rhodamine B, and methyl violet dyes at pH 10 reaching 300, 358, and 178 mg/g respectively.

N-layer graphene oxide (nGO) was synthesized from graphite oxidation via the modified Hummers method and then functionalized with diethylenetriamine to obtain the novel n-layer amino-functionalized graphene oxide [nGO-(NH)R]. This Nano sorbent was evaluated through the adsorption of anionic Reactive Black 5 (RB5) and cationic methylene blue (MB) dyes as shown in Figure 1.5 [96]. pH effect analysis showed that adsorption of anionic RB5 was not influenced by pH changes; on the other hand, cationic MB adsorption was higher at pH 12.0. Langmuir isotherm best fitted the adsorption of both dyes onto nGO-(NH)R and showed maximum monolayer adsorption capacity of 3036.43 and 335.86 mg/g for MB and RB5 respectively. Adsorption kinetics indicated that the system reached the equilibrium state within 5 min for MB, and after 90 min for RB5. Additionally, the pseudo-second-order model was better fitted to the experimental data for the adsorption of both dyes in nGO-(NH)R. Thermodynamic parameters exhibited the spontaneous adsorption of both dyes and chemisorption behavior of RB5.

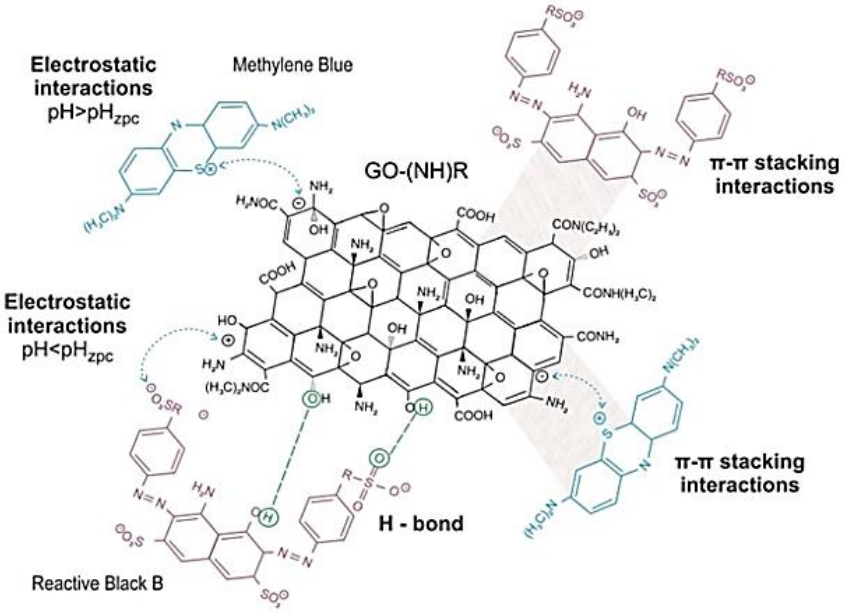

Figure 1.5. The adsorption of MB and RB5 dyes onto GO-(NH)R [96]

Intending to develop an improved adsorbent material for the treatment of printing and dyeing wastewater, a novel thiosemicarbazide functionalized graphene oxide (GO-TSC-GO) adsorbent was prepared by the condensation

reaction of the thiosemicarbazide amino group with the graphene oxide carboxyl group to apply adsorption study on printing and dyeing wastewater containing methylene blue dye [97]. The adsorption behavior was consistent with the pseudo-second-order adsorption kinetic model and Langmuir isotherm model. Thermodynamic analysis indicated an exothermic chemical adsorption reaction. The q_{max} of GO was 196.8 mg/g whereas GO-TSC-GO was 596.642 mg/g, proving that this prepared composite has very important applications for the treatment of dyeing wastewater.

The adsorption process of three cyanine dyes with different alkyl chain lengths (R_5, R_7, and R_{10}) onto graphene oxide GO nanosheets was achieved by the preparation of graphene oxide (GO) nanosheets as adsorbent. The effect of the alkyl chain length of dye molecules was investigated. It was noticed that the adsorption efficiency increased proportionally with the increase in the chain length. R_{10} has the highest q_{max} according to the Langmuir isotherm model. The thermodynamic parameters showed that the adsorption was spontaneous and endothermic. The adsorption process was attributed to the electrostatic and π-π interactions between the dyes and GO surface as shown in Scheme 1.5 [98].

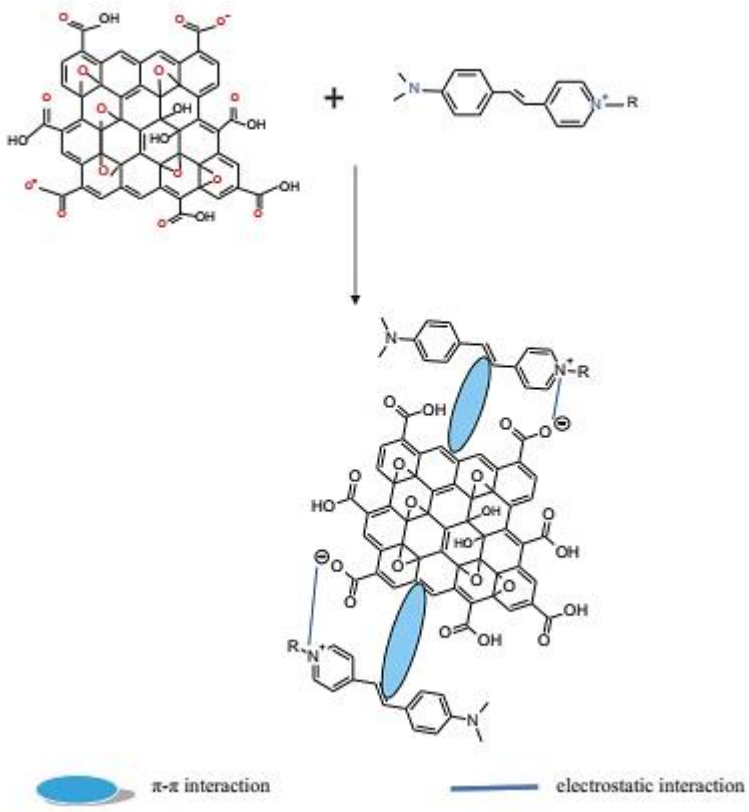

Scheme 1.5. The interaction between GO and cyanine dye [98]

The addition of graphene oxide GO into mesoporous silica SBA-15 could be successfully applied in the adsorption of the dye [99]. Their adsorption capacity and removal efficiency were evaluated for the elimination of methylene blue dye. The GO-MS compound showed the perfect capacity for removal of MB dye compared with pure SBA-15. The maximum adsorption capacity of the composite for MB dye was found to be 242 mg/g and the removal efficiency reached 100%. The adsorption capacity and removal efficiency of GO-MS were highly sensitive to the initial concentration of dye, solution temperature, and dosage of adsorbent. The thermodynamic parameters revealed that the adsorption was exothermic and spontaneous. The adsorption kinetics followed the pseudo-second-order model and the data were fitted well with the Langmuir isotherm model.

The adsorption of a methylene blue MB as a model dye pollutant, on MGO and PAA/MGO, was investigated by Zhang *et al*. [100] in a batch system. The functionalization of PAA to MGO significantly enhances the maximum adsorption capacity of MB dye from 70 mg/g on MGO to 291 mg/g (PAA/MGO). The PAA/MGO shows a high adsorption capacity of MB dye with magnetic properties for easy separation and excellent recyclability, which endows the nanocomposite with great potential for the removal of cationic organic pollutants in wastewater treatment. The binding of carboxyl groups of the PAA on GO leads to form acid anhydride groups (as illustrated in Scheme 1.6 d) may not be very stable in an aqueous solution, and the binding between PAA and hydroxyl groups on GO would dominate the grafting interaction.

Reduced graphene oxide (rGO) materials have also been used for the adsorption of many hazardous organic dyes. Nguyen *et al*. (2020) have reported the removing study of methylene blue, rhodamine B, and methyl orange dyes by the nanostructured TiO_2/ZnO/rGO (TZR) composites [101].

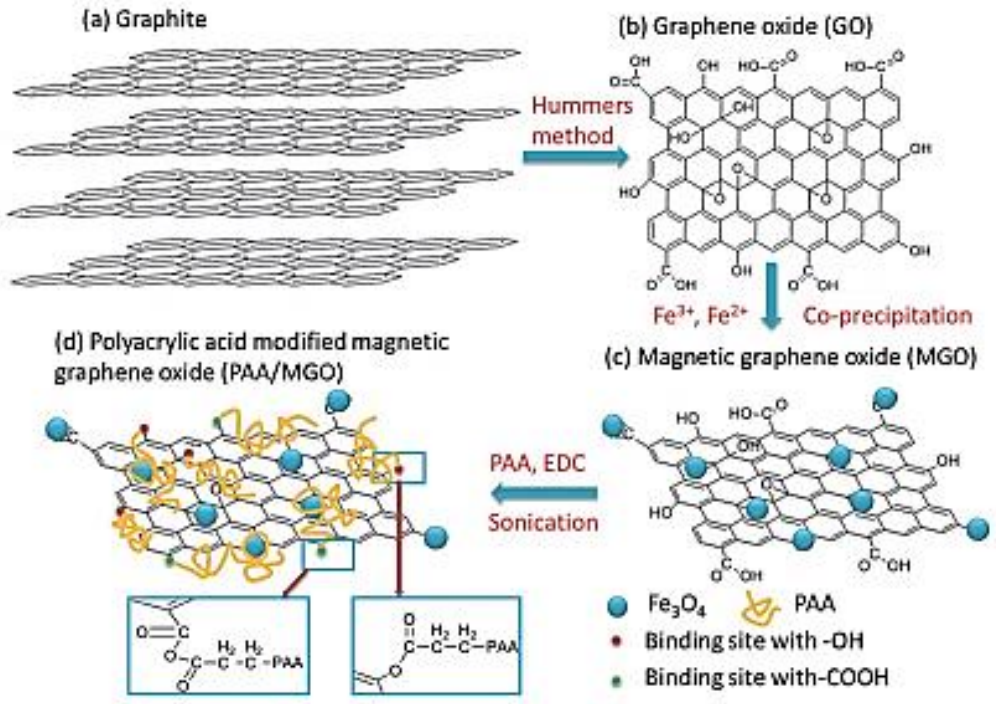

Scheme 1.6. Synthesis process for PAA/MGO composite [100]

Also, a facial synthesis of a reduced graphene oxide silver nanoparticle hybrid nanocomposite (rGO-AgNP) was carried out from aqueous extracts of Brassica nigra by the reduction of graphene oxide and silver ions simultaneously [102]. The synthesized nanocomposite acts as an agent for the removal of Direct blue-14 (DB-14) dye thereby finding its way into water treatment. The rGO-AgNP composites are effective in adsorbing dye and have a favourable effect on water treatment. The adsorption equilibrium data of DB-14 dye onto nanocomposite were found to be well fitted and in good agreement with isotherm models, confirm the efficiency of rGO-AgNP composite as an effective adsorbent for removal of dye pollutants.

1.8. The Aims of the Study

The overall aim of this research is the chemical modifications of Graphene Oxide to achieve a selective and improved adsorption process. GO-composites have also been pointed as useful adsorbents. Anionic and cationic dyes of Congo red and Bismarck Brown showed good response to adsorbs onto the prepared composites from their aqueous solutions. The key objectives of this research are shown as follows:

1. Synthesis of Graphene Oxide (GO) from the Graphite using modified Hummer's Method.

2. Modifying GO and Preparing 3,3´–Diaminobenzidine-Graphene Oxide (GO/DAB), GO/DAB–Ethylenediaminetetraacetic acid (GO/DAB/EDTA), Graphene Oxide–Chitosan (GO/CS), GOCS–Ethylenediaminetetraacetic acid (GO/CS/EDTA), and Graphene Oxide-based poly (n–butyl methacrylate–co–methacrylic acid) (GO/pBCM).

3. Investigating the adsorption removal efficiency of CR and BB dyes onto GO and GO–composites.

4. Evaluating the effects of initial concentration, pH, temperature, and contact time on the adsorption efficiency.

5. Investigating the adsorption Langmuir, Freundlich, Temkin, and D-R isotherm models of the adsorption process.

6. Investigating the adsorption kinetics; Pseudo-First-Order, Pseudo-Second-Order, and Intra-Particle Diffusion the adsorption process.

7. Investigating the thermodynamic functions of $\Delta H°$, $\Delta S°$, and $\Delta G°$ of the adsorption process, as well the activation energy E_a.

8. Desorption of dyes from the prepared adsorbents by applying several cycles of adsorption/desorption experiments using the same adsorbents.

2. The Experimental Work

2.1. Chemicals

The dyes used in this study were purchased from Sigma-Aldrich. Other used chemicals were supplied from different sources as listed in the table (2.1) for the liquid compounds, and table (2.2) for the solid compounds.

Table 2.1. The liquid chemical compounds with their purity and sources

No.	Chemical	Purity (%)	Company
1	Acetic acid	100	VWR
2	Ethanol	99.9	VWR
3	Hydrochloric acid (36%)	36.0	BDH
4	Hydrogen peroxide (30%)	30.0	Fluka
5	Methacrylic acid	99.0	Sigma Aldrich
6	Methanol	98.0	VWR
7	N,N-Dimethylformamide (DMF)	99.0	BDH
8	n-Butyl methacrylate	99.0	Sigma Aldrich
9	Phosphate Buffer Solution	-	Fluka
10	Sulfuric acid	98.0	VWR
11	Tetrahydrofuran (THF)	99.9	Fluka
12	Thionyl Chloride	97.0	BDH

Table 2.2. The solid chemical compounds with their purity and sources

No.	Chemical	Purity (%)	Company
1	1-ethyl-3-(3-dimethylaminopropyl)-carbodiimide hydrochloride (EDC)	99.0	Sigma Aldrich
2	3,3´-Diaminobenzidine (DAB)	99.0	Sigma Aldrich
3	Anhydrous Magnesium sulfate	≥ 99.5	Sigma Aldrich
4	Benzoyl Peroxide	99.0	Fluka
5	Calcium hydride	99.9	Sigma Aldrich
6	Chitosan (80 meshes ; Degree of deacetylation = 85%)	-	Sigma Aldrich
7	Ethylene diamine tetraacetic acid (EDTA)	≥ 99.5	Sigma Aldrich
8	Graphite Powder	99.99	HOPKIN & WILLIAMS
9	N,N´-dicyclohexylcarbodiimide (DCC)	99.0	Sigma Aldrich
10	Potassium Permanganate	≥ 99.0	Sigma Aldrich
11	Sodium Chloroacetate	98.0	Sigma Aldrich
12	Sodium Hydroxide	99.99	Sigma Aldrich
13	Sodium Nitrate	≥ 99.0	Sigma Aldrich

2.2. Instruments and Equipment

The physical measurements were performed using the following instruments:

1. UV-Vis spectra measurements were recorded over the range of 200-800 nm on a PG Instruments Limited (Japan), model T80 (EMC-LAB), using a cell of 0.5 cm in length.

2. FTIR spectra were recorded on Shimadzu, FTIR-8400S (Japan).

3. X-rays Diffraction XRD was performed by a Rigaku X-ray Powder Diffraction diffractometer (Japan).

4. Field Emission Scanning Electron Microscope images FESEM were recorded on FEI NOVA NanoSEM-450 (Netherlands).

5. BET Surface Area Analyzer, type Micro metrics Tri-Star's II Plus, using N_2 gas as analysis adsorptive (USA).

6. Hot plate magnetic stirrer, type VELP SCIENTIFICA-C20 (Europe).

7. Lab-Therm Lab-Shaker, Adolf Kükner Basel (Switzerland).

8. Drying Oven Vacuum, Lab TAC. Budenberg Company (Germany).

9. Centrifuge, Hettich (ZENTRIFUGEN). Type D-7200 Tuttlingen, (Germany).

10. BASIC 20 pH-meter, type E-08328 ALELLA-Barcelona, with a combined glass electrode, CRISON INSTRUMENTS, S. A. (EU).

[11] Accurate Balance Citizen Scale model CY 204, d=0.0001 g.

[12] Branson Ultrasonic™, type DHA-1000, Fisher Scientific (USA).

2.3. Drying of Organic Solvents

The organic solvents used in this study were dried by sodium wire for 24 h and then filtered and distilled. The dry solvents were obtained at their defined boiling points. The temperature-controlled at 110°C to obtain dry Tetrahydrofuran THF, and at 153°C for N,N-Dimethylformamide DMF, with ignoring the first 10% and the last 10% of the solvent volume [103]. The solvents ethanol and methanol were used as received without any further treatments.

2.4. Preparation of Adsorbents

2.4.1. Synthesis of Graphene Oxide (GO)

Modified Hummers method for synthesis Graphene Oxide GO was carried out [104-106]. This included dissolving 2.0 g of graphite and 1.0 g of $NaNO_3$ in 46.0 ml of concentrated H_2SO_4 under an ice bath. After about 15 min of stirring, 6.0 g of $KMnO_4$ was gradually added to the suspension with stirring as slowly as possible to keep the reaction temperature below 20°C. The suspension was stirred for two h and then maintained at 35°C for 30 min. 100.0 mL of deionized water was slowly poured into the suspension, resulted in a quick increase in temperature, and the temperature should be kept below 98°C. After 15 min, the suspension was further diluted to approximately 280.0 mL with warm deionized water. 20.0 mL of 30% H_2O_2 was added to remove the residual $KMnO_4$ and MnO_2 to change the color into luminous yellow. Then, the suspension was filtered and washed with a warm 5% aqueous HCl aqueous solution and deionized water, respectively, until no sulfates were detected, and the pH of the filtrate was adjusted to 7. The product, graphene oxide, was dried under vacuum at 50°C to a constant weight. Scheme (2.1) exhibits the chemical equation of the preparation method.

2.4.2. Synthesis of 3,3´-Diaminobenzidine-Graphene Oxide Composite (GO/DAB)

To synthesize 3,3´-Diaminobenzidine-Graphene Oxide composite [107], 0.5 g GO was ultrasonically dispersed in 10.0 mL distilled water for 5 min at room temperature followed by adding a mixture of 2.5 g Sodium hydroxide NaOH and 2.5 g Sodium chloroacetate $ClCH_2COONa$. The suspension was slowly stirred and ultrasonically treated for 2 h at room temperature to convert hydroxyl and epoxide functional groups in GO to carboxylic groups [106, 108]. The resulting product, carboxyl-functionalized graphene oxide (GOCOOH), was neutralized with dilute hydrochloric acid and dried under vacuum at 80°C for 24 h. A mixture of 5.0 mL thionyl chloride and 25.0 mL DMF was added to 0.5 g of GOCOOH and refluxed for 24 h at 70°C. The resulting product, acyl chloride- functioned graphene oxide (GOCOCl), was centrifuged for 8 min at 5000 rpm and thoroughly washed with THF several times, and dried in an oven at 80°C.

2.0 g DAB was added to GOCOCl and ultrasonically treated in 50.0 mL DMF for 2 h at room temperature. Afterward, the suspension was refluxed for 24 h at 110°C to carry out the reaction. GO/DAB was cooled and washed with ethanol to remove any excess of DAB and finally dried in a vacuum for 24 h. The preparation route can be represented by chemical equations shown in scheme (2.2).

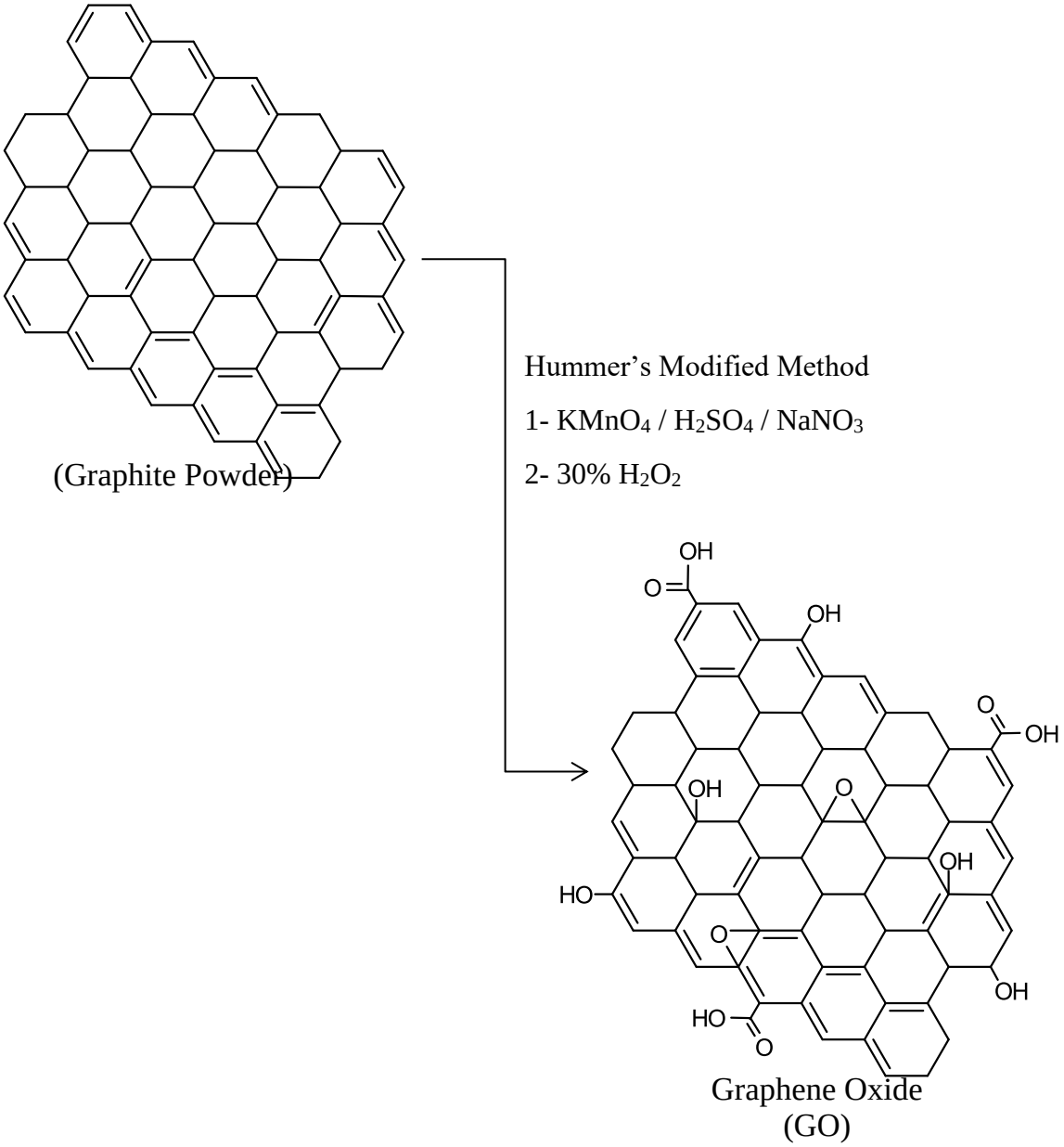

Scheme 2.1. The preparation method of Graphene Oxide GO

2.4.3. Synthesis of GO/DAB–Ethylenediaminetetraacetic Acid Composite (GO/DAB/EDTA)

For the preparation of GO/DAB/EDTA, 1.0 g GODAB was dispersed in 20.0 mL of 10% acetic acid to form GO/DAB dispersion, 6.0 g EDTA was evenly dispersed in 100.0 mL of methanol to get EDTA dispersion. Then GODAB and EDTA dispersion were mixed by mechanical rumbling and react at room temperature for 24 h. The obtained product GO/DAB/EDTA was filtered, washed twice with ultrapure water, dried at 50°C, and ground into a fine powder [109]. The chemical equation can be represented by the scheme (2.3).

2.4.4. Synthesis of Graphene Oxide-Chitosan Composite (GO/CS)

The GO/CS was prepared according to the literature with some modifications [110]. 0.5 g of GO was dispersed in 50.0 mL distilled water by ultrasonication for 3 h. A solution of 0.05 M (0.0478 g) N,N′-dicyclohexylcarbodiimide DCC was added to the GO dispersion and stirred continuously for 2 h to activate the carboxyl groups of GO [111]. The pH was adjusted to 7.0 by a 2% NaOH solution. Then, the activated GO solution with 5.0 g Chitosan CS was dispersed in 50.0 mL distilled water and 50 mL (10%) HAC by ultrasonication for 20 min. After that, the mixed solutions were stirred at 60 °C for an additional 3 h. The precipitate after filtration was washed with 10% NaOH solution and deionized water in turn until pH was about 7.0. The obtained product GO/CS was dried in a vacuum oven. Scheme (2.4) illustrates the preparation route.

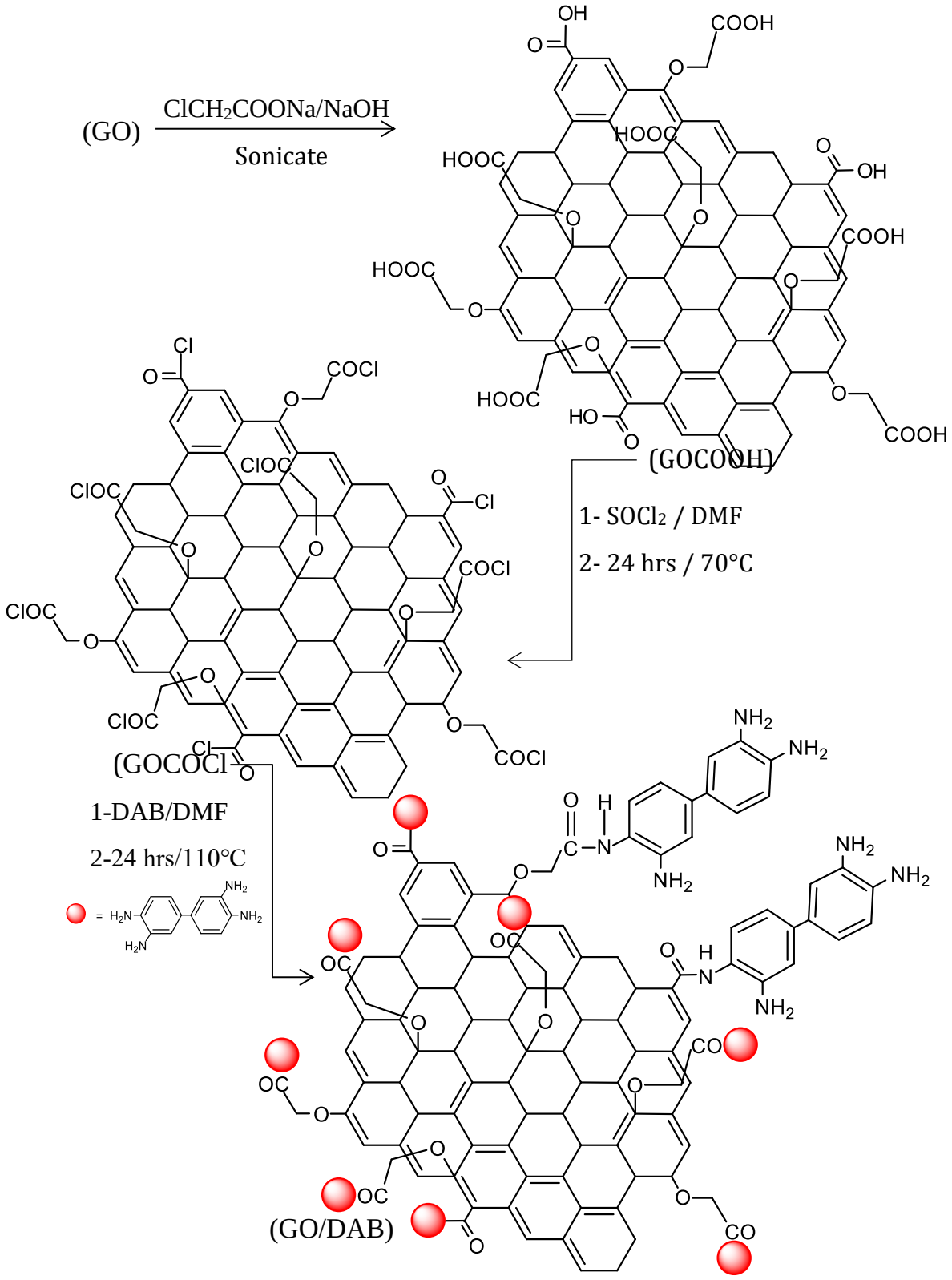

Scheme 2.2. The preparation method of GO/DAB

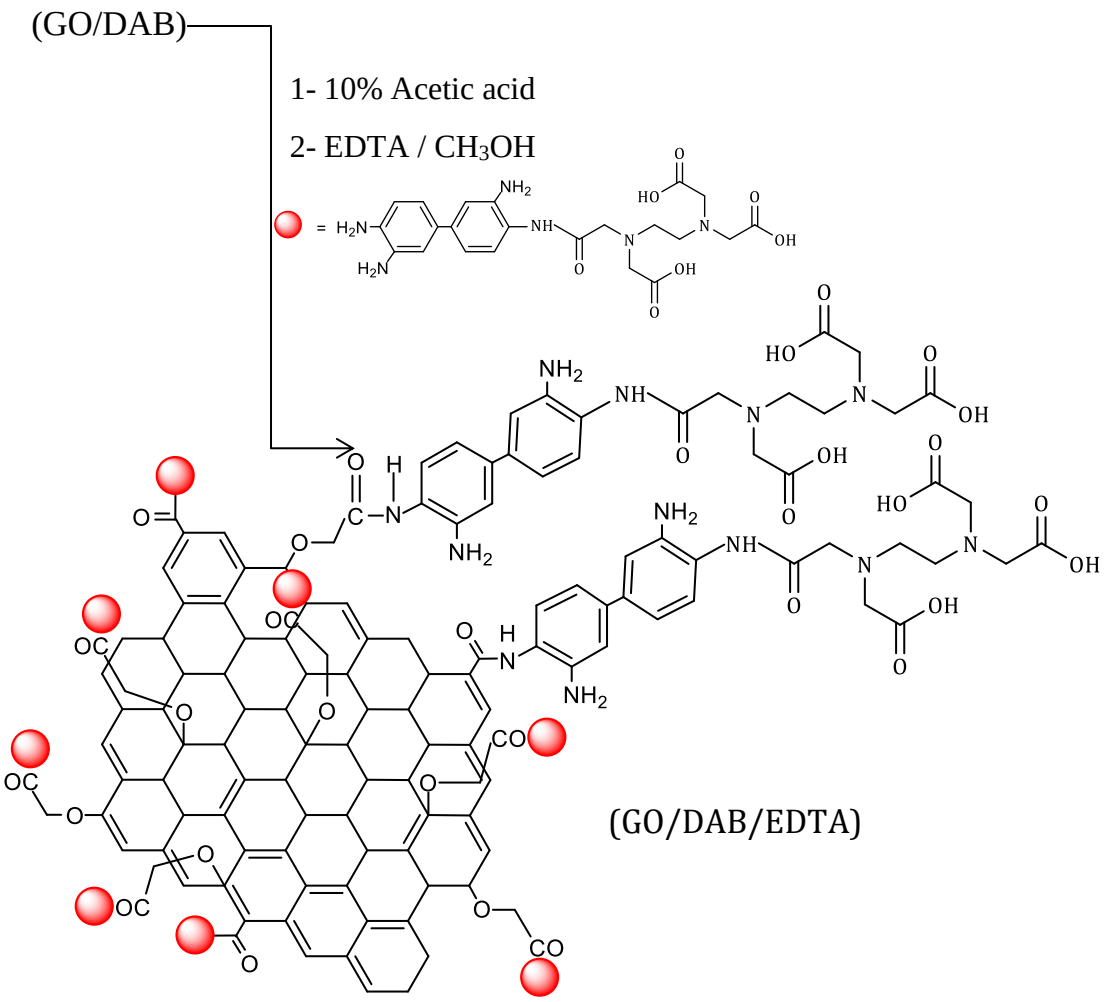

Scheme 2.3. The preparation method of GO/DAB/EDTA

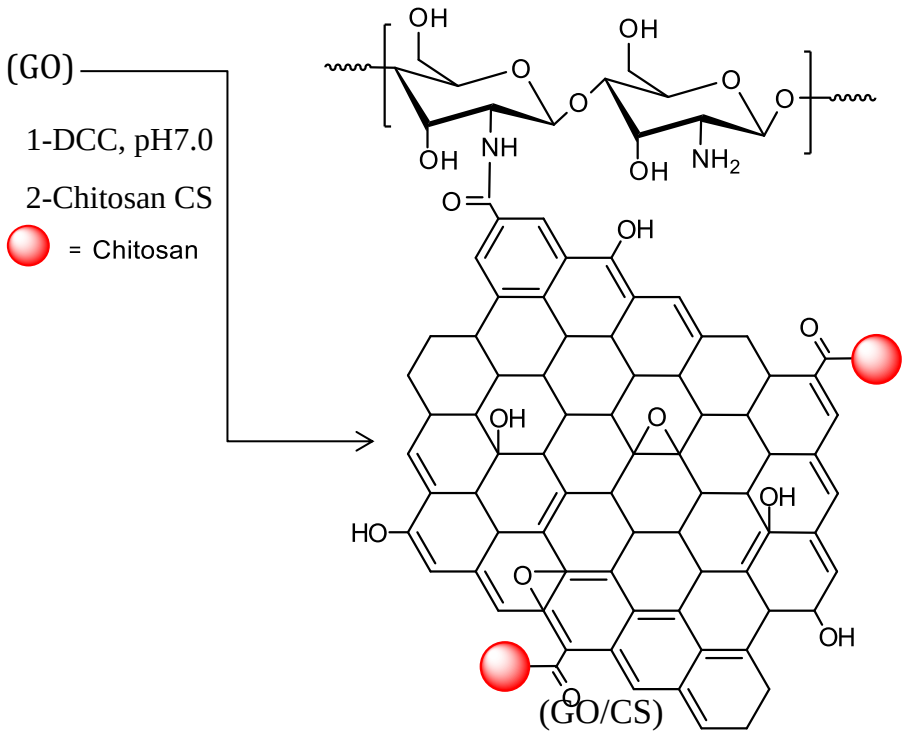

Scheme 2.4. The preparation method of GO/CS

2.4.5. Synthesis of GOCS–Ethylenediaminetetraacetic Acid Composite (GO/CS/EDTA)

The functionalization of GO/CS by EDTA was achieved using a reported method with some modifications [109]. 0.5 g GO/CS was dispersed in 20.0 mL of 10% acetic acid aqueous solution to form GO/CS dispersion, and 6.0 g EDTA was evenly dispersed in 100.0 mL of methanol for 2 h to get EDTA dispersion. The GO/CS and EDTA dispersions were mixed by mechanical rumbling and left to react at room temperature for 24 h. The obtained product GO/CS/EDTA was separated by filtration and washed twice with deionized water, dried in the vacuum oven at 50°C, and ground into a fine powder. The chemical equation can be represented by the scheme (2.5).

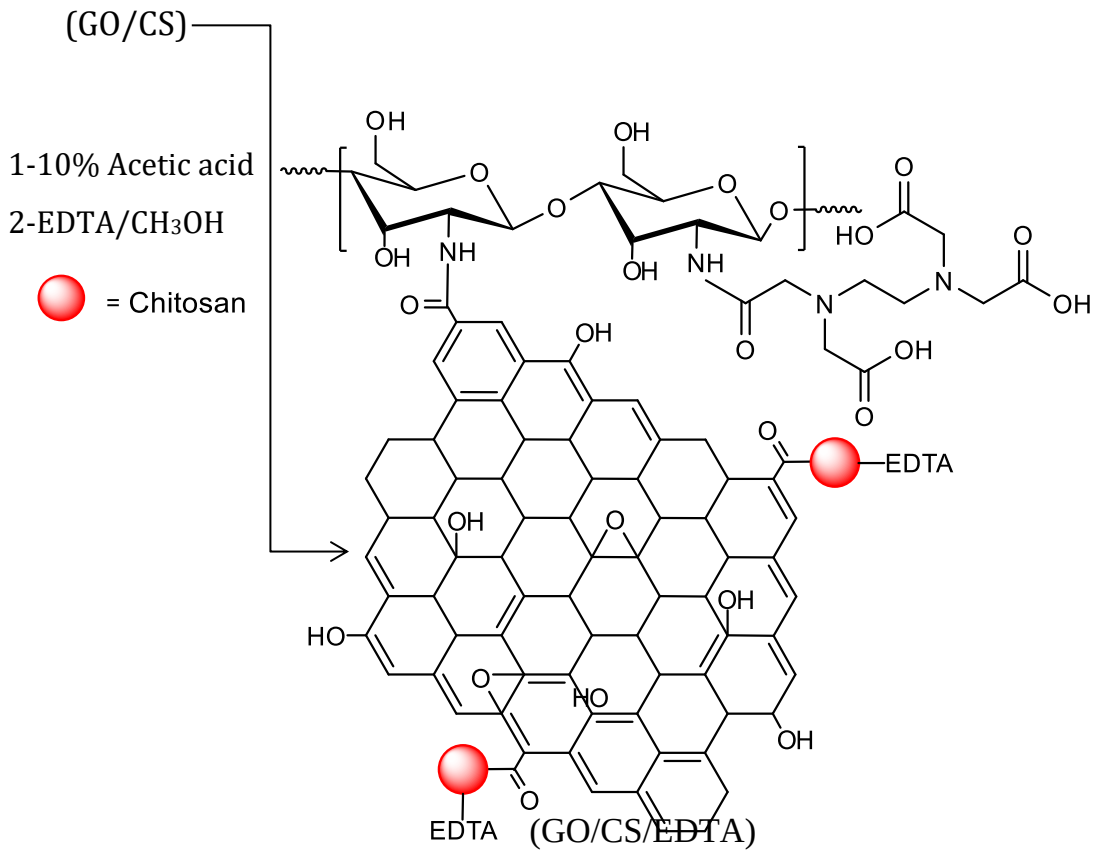

Scheme 2.5. The preparation method of GO/CS/EDTA

2.4.6. Copolymerization of n-Butyl Methacrylate/Methacrylic Acid (pBCM)

Butyl methacrylate monomer BMA was washed twice with 5% NaOH to remove inhibitor and twice with distilled water, then it was dried over anhydrous $MgSO_4$, then with Calcium hydride, and freshly vacuum distilled before copolymerization. Methacrylic acid MAA was distilled under reduced pressure before use in the copolymerization using benzoyl peroxide as initiator.

The copolymerization (as shown in scheme 2.6) was carried out in the round bottom flask of equimolar amounts of freshly distilled n-butyl methacrylate and methacrylic acid under dry N_2 gas in a water bath after adding benzoyl peroxide ($1x10^{-4}$ mole/L) at 70° [112, 113]. The copolymer

was precipitated into methanol. It was filtered and washed several times with methanol and vacuum dried at room temperature.

2.4.7. Polymerization of Graphene Oxide-Based Poly (n-butyl methacrylate-co-methacrylic acid) (GO/pBCM)

The Polymerization was carried out with some necessary changes. 0.3 g GO was dispersed in 7.5 mL of phosphate buffer solution pH 6 and ultra-sonicated for 30 min. 0.3 g pBCM and 0.03 g of 1-ethyl-3-(3-dimethyl aminopropyl)-carbodiimide hydrochloride EDC were added to the GO dispersion, and the reaction mixture was sonicated for 30 min. The mixture was stirred for an additional 24 h at room temperature. Finally, GO/pBCM composite was obtained by filtered, washed with DI water over 3 times, and dried for 24 h under vacuum as a dark grey powder [114]. The preparation route can be shown in the scheme (2.7).

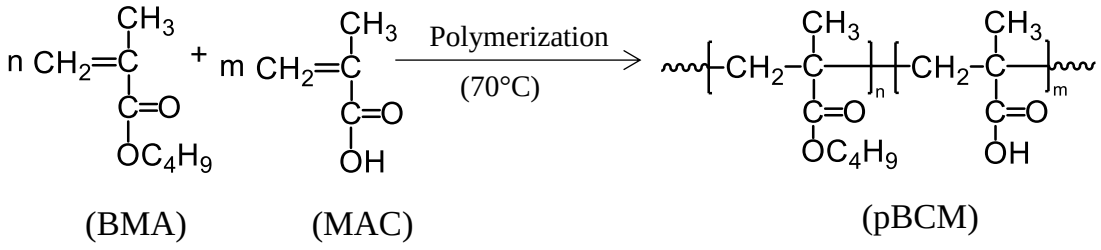

(BMA) (MAC) (pBCM)

Scheme 2.6. The preparation routes of pBCM

2.5. Analysis of the Synthesized Adsorbents

The prepared compounds in this study were characterized using FTIR, XRD, FESEM, and BET techniques. The procedures were conducted as follows.

2.5.1. Fourier Transform Infrared Spectroscopy FTIR

The FTIR spectra were analyzed to prepared compounds using an FTIR-8101M Shimadzu spectrometer (Japan) with KBr pellet in the region (400-4000 cm^{-1}) to investigate the functional groups and chemical structures. It is available at the Department of Chemistry/College of Science/University of Basrah.

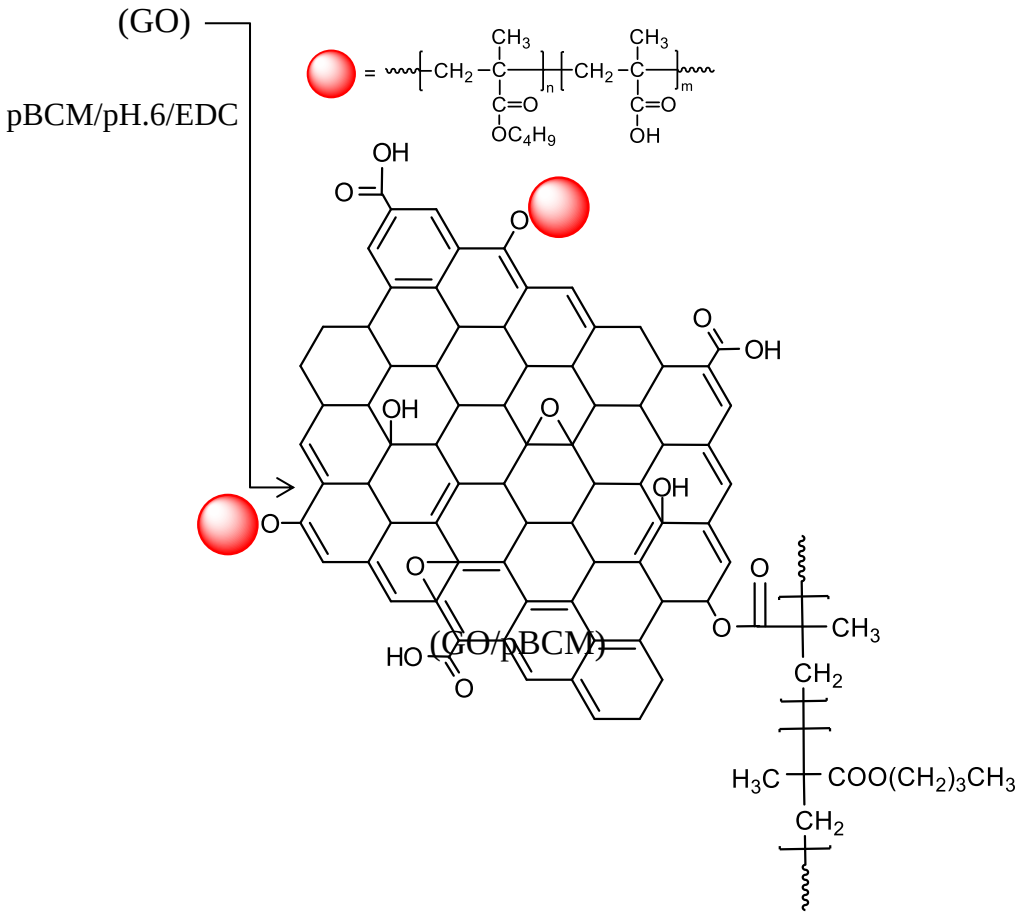

Scheme 2.7. The preparation routes of GO/pBCM

2.5.2. X-rays Diffraction Spectroscopy (XRD)

Patterns of X-ray diffraction XRD of the compounds were recorded by a Rigaku X-ray Powder Diffraction diffractometer (Japan). With a generator voltage of 20-45 kV and generator current of 2-50 mA, with scanning speed of 2 min^{-1} from 5° to 80° producing CuK_{α} radiation with a wavelength of 1.5406 Å. It is available at the Department of the Physics / University of Tehran.

2.5.3. Field Emission Scanning Electron Microscopy (FESEM)

The structure and surface morphology of the materials were identified using an FEI NOVA NanoSEM 450 Emission Scanning Electron Microscope FESEM under vacuum at an operating voltage of 10 kV. It is available at the Department of the Physics / University of Tehran.

2.5.4. Analysis of the Surface Area and the Porosity of Surface BET & BJH

Surface properties including surface area, pore size, and specific pore volume diameter were studied for surfaces of all prepared materials, by Adsorption-Desorption isotherm (Brunauer Emmett Teller BET) and pore size distribution method (Barrett Joyner Halenda BJH), using BET Surface Area Analyzer Type Micro metrics tri star II Plus (USA) using N_2 gas as analysis adsorptive. It is available at the Department of the Physics/University of Tehran.

2.6. Preparation of Dyes Solutions

Congo Red CR (FW=696.7) and Bismarck Brown BB (FW=419.31) were used as purchased without any further treatment in this study, as models of anionic and cationic azo dyes respectively, and their chemical structures are shown in Fig. 2.1. A stock solution of both dyes 1000.0 mg/L was prepared for the adsorption experiments and then the required concentrations were provided with the dilution by using deionized water.

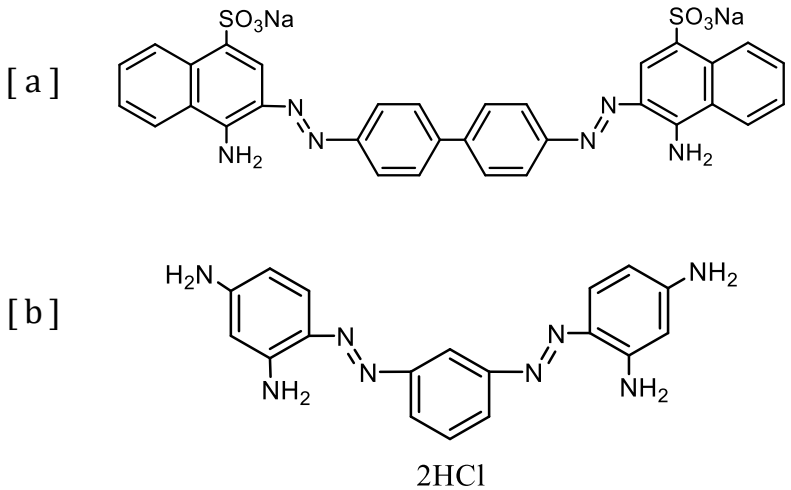

Figure 2.1. Chemical structure of; Congo Red (a), and Bismarck Brown (b) dyes [115].

2.7. Absorption Spectra of Congo Red & Bismarck Brown Dyes

The maximum wavelength (λ_{max}) of Congo Red CR and Bismarck Brown BB dyes was determined using UV-Visible spectrometer scanning in the range of 200-800 nm.

2.8. Optimization of Adsorption Experiments

2.8.1. The Initial Concentration of Dyes

To perform the optimal initial concentration of both Congo Red CR and Bismarck Brown BB dyes, different concentrations were prepared; 100, 200, 300, 400, and 500 mg/L. Adsorption Experiments were examined for each value of initial concentration by contacting a fixed 0.025 g of adsorbent with 0.1 L of dye solutions for 24 h at 27°C.

2.8.2. Acid Function pH

2.8.2.1. The effect of pH on the CR Dye

The effect of pH on the CR dye adsorption was studied at initial concentration 300.0 mg/L of adsorbents GO, GO/DAB, GO/DAB/EDTA, and GO/pBCM, and at 500.0 mg/L as initial concentration of adsorbents GO/CS and GO/CS/EDTA. 0.025 g as a fixed weight of prepared adsorbents was used with 0.1L of CR solutions for 24 h at 27°C. The pH adjusting of the CR dye solution was accomplished by using 0.10 M of Hydrochloric acid or Sodium Hydroxide solution. Adsorbents were then separated from the solution by filtration and the equilibrium concentration of reaming CR dye determined with a UV-Visible Spectrophotometer at λ_{max} 494 nm.

2.8.2.2. The effect of pH on the BB Dye

The effect of pH on the BB dye adsorption was studied at 400.0 mg/L as initial concentration of adsorbents GO, GO/DAB, GO/CS, GO/CS/EDTA, and GO/pBCM respectively, and at 200.0 mg/L of adsorbent GO/DAB/EDTA. By using 0.025 g as a fixed weight of prepared adsorbents with 0.1L of the BB solutions were used for 24 h at 27°C. The pH adjusting of the BB dye solution was accomplished by using 0.10 M of Hydrochloric acid or Sodium

Hydroxide solution. Adsorbents were then separated from the solution by filtration and the equilibrium concentration of reaming BB dye determined with a UV-Visible Spectrophotometer at λ_{max} 457 nm.

2.8.3. Contact Time of Experiments

2.8.3.1. Determination of contact time for CR Dye

To determine the equilibrium time of adsorption study, a 0.1L of 300.0 mg/L as CR initial concentration of adsorbents GO, GO/DAB, GO/DAB/EDTA, and GO/pBCM, and at 500.0 mg/L of both adsorbents GO/CS and GO/CS/EDTA, are added to a fixed 0.025 g as a known amount of prepared adsorbents. All solutions were shaken at 200.0 rpm for 1, 3, 9, 12, 15, 30, 45, 60, 75, and 90 min at room temperature. Adsorbents then separated from the solution by filtration and the equilibrium concentration of reaming CR dye determined with a UV-Visible Spectrophotometer at λ_{max} 494 nm, and optimum pH 3.0 for GO and GO/CS; 5.0 for GO/DAB/EDTA and GO/CS/EDTA; 7.0 for GO/DAB and GO/pBCM.

2.8.3.2. Determination of contact time for BB Dye

To determine the equilibrium time of adsorption study, a 0.1L of 200.0 mg/L as BB initial concentration of GO/DAB/EDTA adsorbent and at 400.0 mg/L of GO, GO/DAB, GO/CS, GO/CS/EDTA, and GO/pBCM, were added to a fixed 0.025 g as a known amount of prepared adsorbents. All solutions were shaken at 200.0 rpm for 1, 3, 9, 12, 15, 30, 45, 60, 75, and 90 min at room temperature. Adsorbents then separated from the solution by filtration and the equilibrium concentration of reaming BB dye determined with a UV-Visible Spectrophotometer at λ_{max} 457 nm, and optimum pH 3.0 for GO, GO/DAB, GO/CS, and GO/pBCM; 5.0 for GO/DAB/EDTA and GO/CS/EDTA.

2.8.4. Temperature

Three temperature degrees; 27°, 40°, and 60°C were chosen to investigate the effect of temperature on the adsorption process using a known concentration for each dye in this study.

2.9. Adsorption Isotherm

2.9.1. Adsorption Isotherm of CR Dye

The adsorption isotherms were performed for CR dye at a concentration range of (300, 325, 350, 375, 400, and 450 mg/L) with GO, GO/DAB, GO/DAB/EDTA, and GO/pBCM respectively, and at the range (500, 525, 550, 575, 600, and 650 mg/L) with both GO/CS and GO/CSEDTA. A 0.1 L of dye solution was transferred to a fixed 0.025 g of prepared adsorbent, and shaking at 27°C within a speed of 200.0 rpm at pH 3.0 for GO and GO/CS; 5.0 for GO/DAB/EDTA and GO/CS/EDTA; 7.0 for GO/DAB and GO/pBCM. Thereafter, the solutions were filtrated and the equilibrium concentration was determined by UV-Visible Spectrophotometer at λ_{max} 494 nm.

2.9.2. Adsorption Isotherm of BB Dye

For BB, the concentration range of (200, 225, 250, 275, 300, and 350 mg/L) with GO/DAB/EDTA, and the concentration range of (400, 425, 450, 475, 500, and 550 mg/L) with GO, GO/DAB, GO/CS, GO/CS/EDTA, and GO/pBCM respectively. Also, 0.1 L of dye solution at pH 3.0 for GO, GO/DAB, GO/CS, and GO/pBCM; 5.0 for GO/DAB/EDTA and GO/CS/EDTA was transferred to a fixed 0.025 g of prepared adsorbents and shaking at 27°C within a speed of 200.0 rpm. Thereafter, the solutions were filtrated and the equilibrium concentration was determined by UV- Visible Spectrophotometer at λ_{max} 457 nm.

2.10. Adsorption Kinetics

2.10.1. Adsorption Kinetics of CR Dye

Adsorption kinetic and calculating thermodynamic parameters such as standard enthalpy change $\Delta H°$, standard entropy change $\Delta S°$, and standard free energy change $\Delta G°$ of CR dye were studied. The experiments were conducted at the chosen temperatures in this study 27°, 40°, and 60°C, with a fixed 0.025 g of adsorbents in 0.1 L of CR dye solution with an initial concentration of 300.0 mg/L for GO, GO/DAB, GO/DAB/EDTA, and GO/pBCM, and 500.0 mg/L for GO/CS and GO/CS/EDTA, and the maximum adsorption capacity were found at optimum pH; 3.0 for GO and GO/CS; 5.0

for GO/DAB/EDTA and GO/CS/EDTA; 7.0 for GO/DAB and GO/pBCM, with shaking of 200.0 rpm. Finally, the solution was filtrated and the concentration was determined by UV-Visible Spectrophotometer at λ_{max} 494 nm.

2.10.2. Adsorption Kinetics of BB Dye

The adsorption Kinetic experiments of BB dye were conducted at 27°, 40°, and 60°C as the chosen temperatures in the study, with a fixed 0.025 g of each adsorbent in 0.1 L of BB dye solution with an initial concentration of 200.0 mg/L of GO/DAB/EDTA and 400.0 mg/L of GO, GO/DAB, GO/CS, GO/CS/EDTA, and GO/pBCM, and the maximum adsorption capacity was found at optimum pH 3.0 for GO, GO/DAB, GO/CS, and GO/pBCM; 5.0 for GO/DAB/EDTA and GO/CS/EDTA, with shaking of 200.0 rpm. Finally, the solution was filtrated and the concentration (C_t mg/L) was determined by UV-Visible Spectrophotometer at λ_{max} 457 nm. Also, the thermodynamic parameters of BB dye adsorption were studied at the same conditions**,** such as standard enthalpy change $\Delta H°$, standard entropy change $\Delta S°$, and standard free energy change $\Delta G°$.

2.11. Desorption Study

Desorption of the CR and BB dyes from the prepared adsorbents was carried out by applying several cycles of adsorption/desorption experiments using the same adsorbents, maximum adsorption of the dyes conducted by applying optimum agitation time, and pH-value for each adsorbent in this study. The desorption experiments were done by immersing the dye-loaded adsorbents into 100.0 mL of distilled water as eluent, and the mixture was stirred continuously at the worst pH of each system at room temperature, then the desorbed dyes were filtrated and its concentration determined by using a UV-Visible Spectrophotometer at λ_{max} of each dye.

3. Results and Discussion

3.1. Characterization of Adsorbents

This chapter deals will with the characterization of the prepared composite adsorbents based on Graphene Oxide using Fourier Transform Infrared Spectroscopy, Field Emission Scanning Electron Microscopy, X-rays Diffraction Spectroscopy, Surface area, and the surface porosity analysis.

3.2. Fourier Transform Infrared Spectroscopy (FTIR)

FTIR spectrum can provide useful information to identify the presence of certain functional groups or chemical bonds in a molecule of an interaction system. Natural graphite, graphene oxide, and its different prepared composites are characterized as KBr discs. Figures (3.1-3.7) represent the FT-IR spectra of Graphite powder, GO, GO/BAB, GO/DAB/EDTA, GO/CS, GO/CS/EDTA, and GO/pBCM respectively.

The IR spectrum of natural graphite (Figure 3.1) is nearly featureless, while that of GO exhibits prominent peaks at 3367 cm^{-1}, which corresponds to hydroxyl stretching vibration, very weak bands at 2920 cm^{-1} are due to the asymmetric stretching vibration of the C–H bond, and at 1728 cm^{-1} corresponding to the stretching vibration of the carbonyl group. While the peak at 1619 cm^{-1} was attributed to aromatic C=C stretching vibrations. Other obvious peaks at 1371, 1165, and 1027 cm^{-1} which correspond to O–H deformation vibration, asymmetric and symmetric C–O stretching vibration in the C–O–C groups are also observed and assigned [116]. The IR spectra of graphite (Figure 3.1) and GO (Figure 3.2) are significantly different, where a high number of oxygen-containing functional groups are present on the basal planes and edges of the graphene oxide sheet [117], and the differences were generally proportionate to those reported previously in the literature [118], indicating that we successfully prepared to GO. FTIR analysis of Roy Chowdhury et al. [119], Bao et al. [120], and Galpaya et al. [121] are agreed well with our results.

Surface chemical functionalization of GO was carried out by the amidation reaction between DAB amine groups and carboxylic acid sites of GO and characterized using Fourier transform infrared spectroscopy (Figure

3.3). The nature of the interaction between GO and DAB amine is confirmed by the appearance of the peaks at 1607, 1418, and 1062 cm^{-1} could be assigned to the symmetrical stretching vibration of C=O and C-N in amides, and stretching vibration of C-N in amines respectively, and intense peak at 1027 cm^{-1} of N-H stretching vibration of the amine group. This indicates a successful reaction between graphene oxide and amine has occurred [122], and the formation of amide linkages as well as the occurrence of nucleophilic substitution reactions, as proposed in the reaction mechanism. The strong and broadband at 3367 cm^{-1} (of O-H stretching vibration in GO carboxylic functional groups) became sharper and is shifted to 3417 cm^{-1} after the reaction with DAB due to removal of O-H in carboxylic groups and forming amide groups [107].

The important absorbance peaks of GO/DAB/EDTA (Figure 3.4) at 1080 cm^{-1} are caused by the stretching vibration and bending vibration of the N–H bond [123]. The broadband observed around 3423 cm^{-1} might ascribe to the O–H stretching vibration from the adsorbed H_2O on the surface of GO/DAB/EDTA and GO components [124]. The intense band at 1635 cm^{-1} was attributed to the vibrations of the C=O bond originating from carboxyl functional groups. Besides, C–OH vibration at 1410 cm^{-1} and C–H aromatic at 3017 cm^{-1} are observed in GO/DAB/EDTA [125]. Furthermore, the C-O stretching peak shifts from 1607 cm^{-1} in GO/DAB to 1635 cm^{-1} in GO/DAB/EDTA, indicating interactions exist between GO/DAB and EDTA. FTIR spectra confirmed that the prepared GO/DAB and GO/DAB/EDTA contained plentiful oxygen and nitrogen functional groups, all the functional groups could act as available adsorption sites and played an important role in the adsorption process. A new peak at 1317 cm^{-1} is due to the C-O stretching vibration of new COO^{-} groups from EDTA [126].

The IR spectrum of GO/CS composite (Figure 3.5) shows a combination of characteristic peaks of Chitosan CS and Graphene Oxide GO. So, the results implied that interactions existed between them [127]. The stretching vibration bands of the C–H at 2928, and 2852 cm^{-1} come from $–CH_3$ of Chitosan appeared, indicating that GO was successfully grafted on Chitosan. Moreover, there are some characteristic absorbance bands at 3326, 1642, and 1577 cm^{-1} which correspond to the N–H stretching vibration, C=O stretching of –NHCO–, and N–H bends of $–NH_2$ respectively [128]. A new peak at 1453 cm^{-1} that due to C-H bending, and the shift of the characteristic peak of O–H from

around 3367 to 3326 cm^{-1}, may result from the interaction between GO and CS [129, 130].

Examining the GO/CS/EDTA composite FTIR spectrum (Figure 3.6) reveals some intense changes. The intensity of the absorption peak of N–H at 3326 cm^{-1} was dramatically weakened after grafting EDTA to GO/CS. The N-H stretching vibrations above 3000 cm^{-1} were weakened and the peak at 1577 cm^{-1} of N-H bending vibrations was also disappeared after modification. A new strong peak at 1317 cm^{-1} is appeared due to the CO stretching vibration of new COO^{-} groups from EDTA [126]. Furthermore, the C=O stretching vibration peak shifts from 1642cm^{-1} in GO/CS to 1694 cm^{-1} in GO/CS/EDTA, indicating interactions exist between GO/CS and EDTA.

Moreover, some important absorbance peaks in the FTIR spectrum of GO/pBCM composite (Figure 3.7) are observed at 3176–3327 cm^{-1} as new peaks for OH stretching vibration, 1624, 1578, 1459, and 1311 cm^{-1} combining those of GO and pBCM. Furthermore, the C-O stretching vibration peak shifts from 1728 cm^{-1} in GO to 1624 cm^{-1} in GO/pBCM, and that indicating interactions exist between GO and pBCM chains [131, 132]. Also, the following new peaks can be identified, cm^{-1}; 2851–2928 of CH stretching (CH_2 and CH_3 groups), 1400–1500 of CH_2 scissoring vibration, 1311 doublet twisting bands for CH_3 deformation, 1273–1000 of C–O–C vibration in ester groups, around 900 of C–C stretching of the main chain, and around 850 of CH out of plane deformation [133].

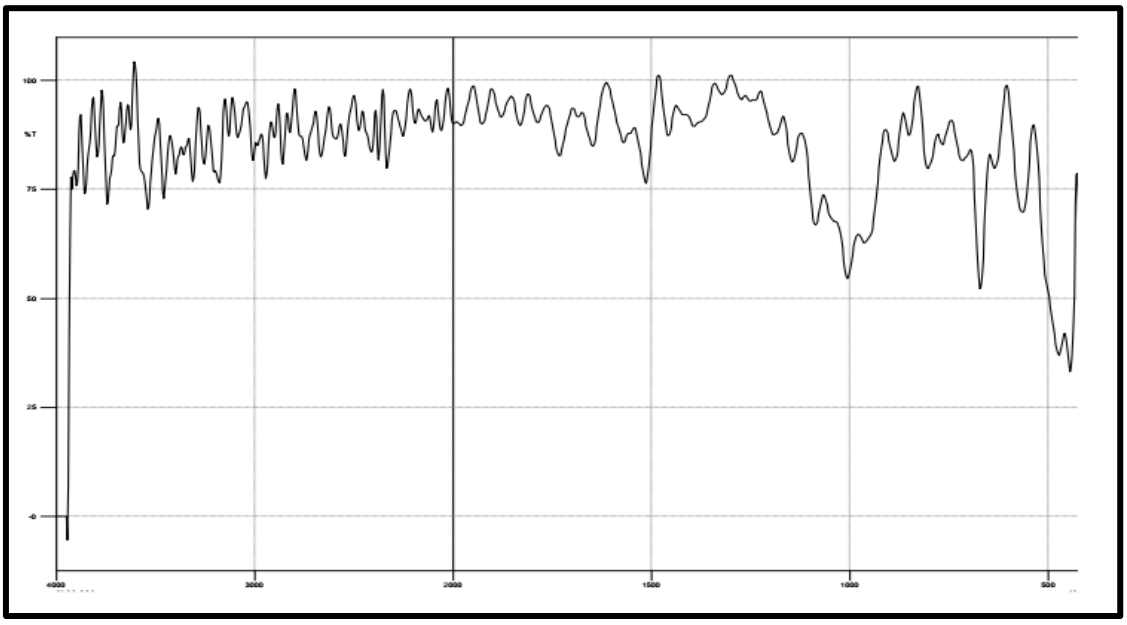

Figure 3.1. FTIR spectrum of Graphite Powder.

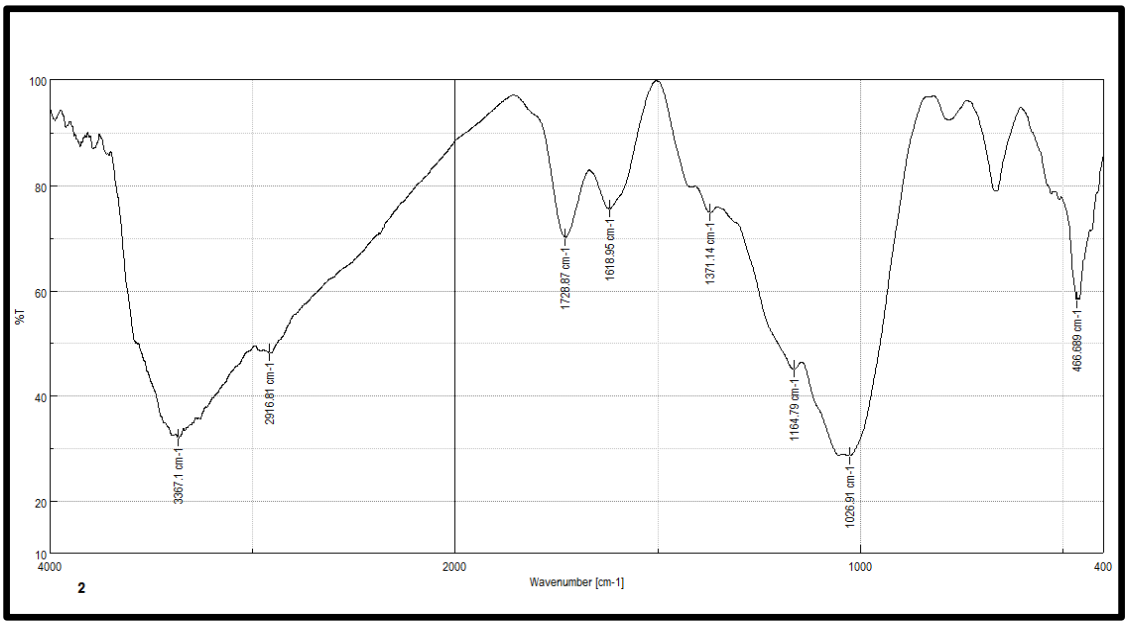

Figure 3.2. FTIR spectrum of GO adsorbent.

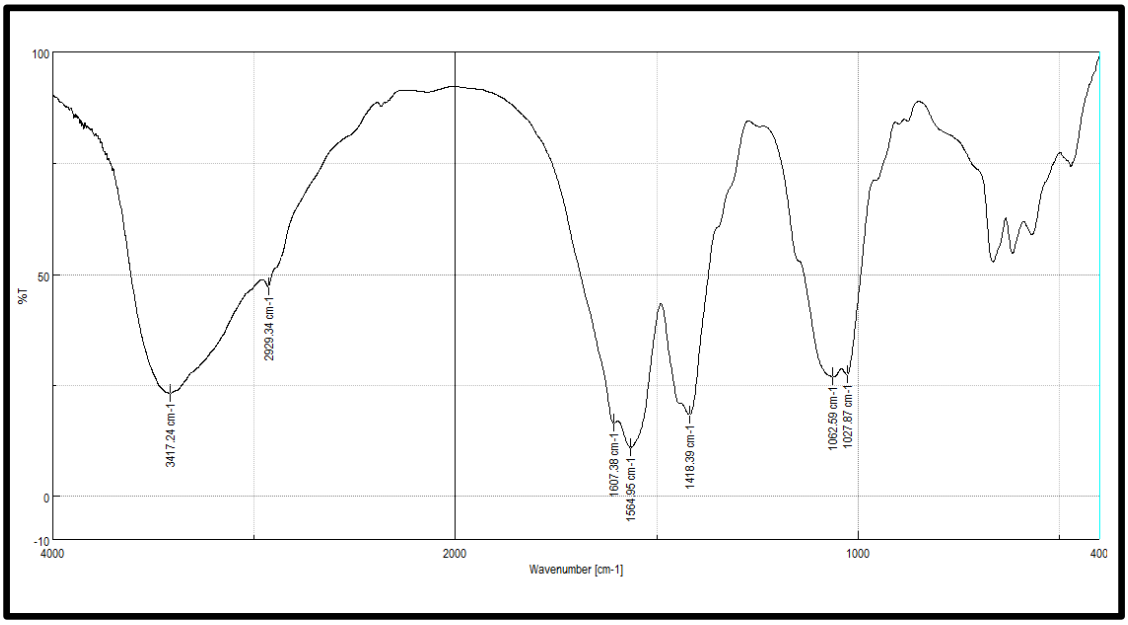

Figure 3.3. FTIR spectrum of GO/DAB adsorbent.

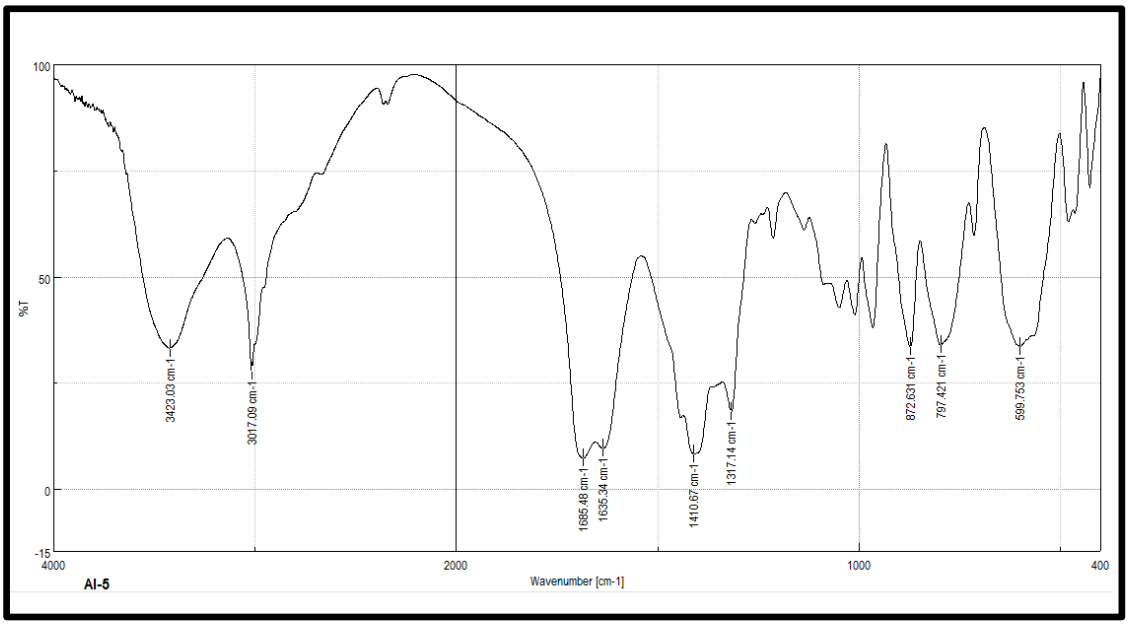

Figure 3.4. FTIR spectrum of GO/DAB/EDTA adsorbent.

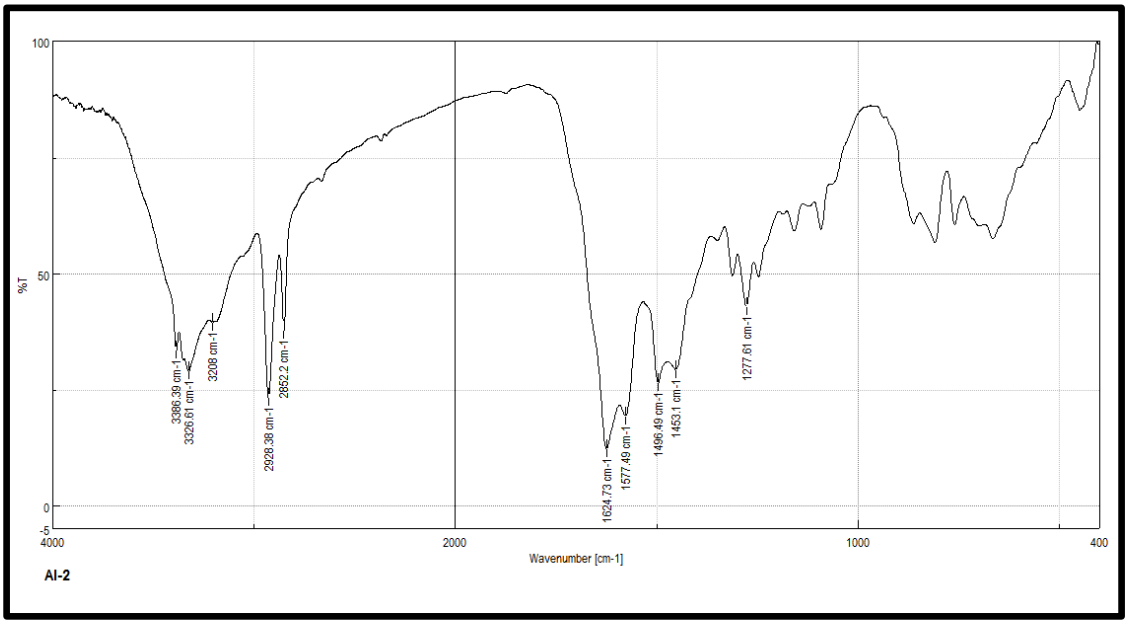

Figure 3.5. FTIR spectrum of GO/CS adsorbent.

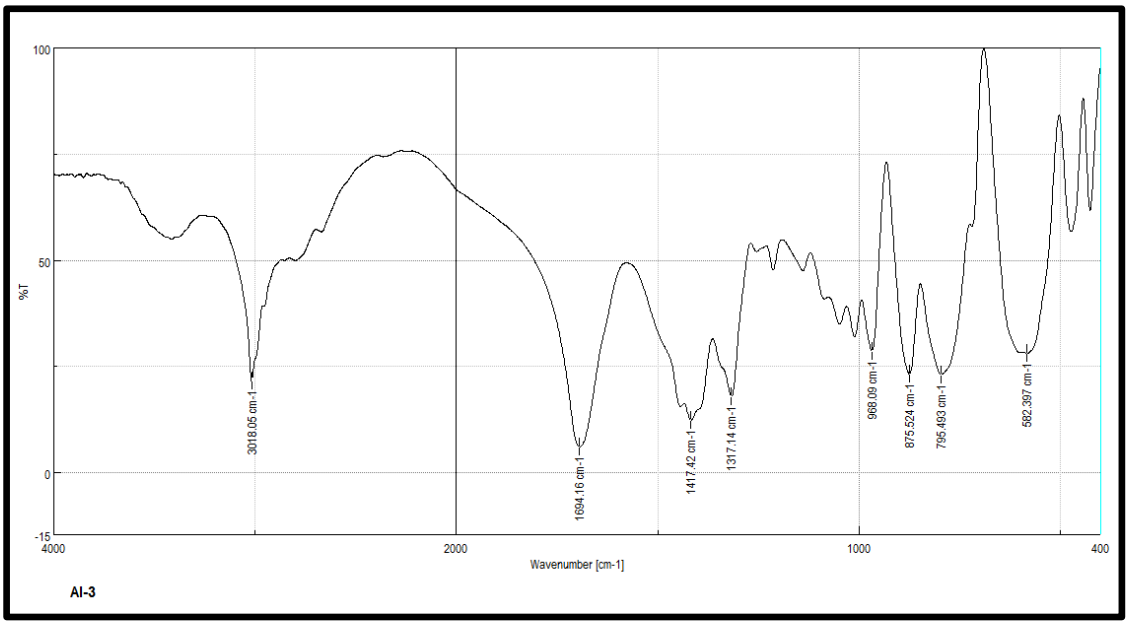

Figure 3.6. FTIR spectrum of GO/CS/EDTA adsorbent.

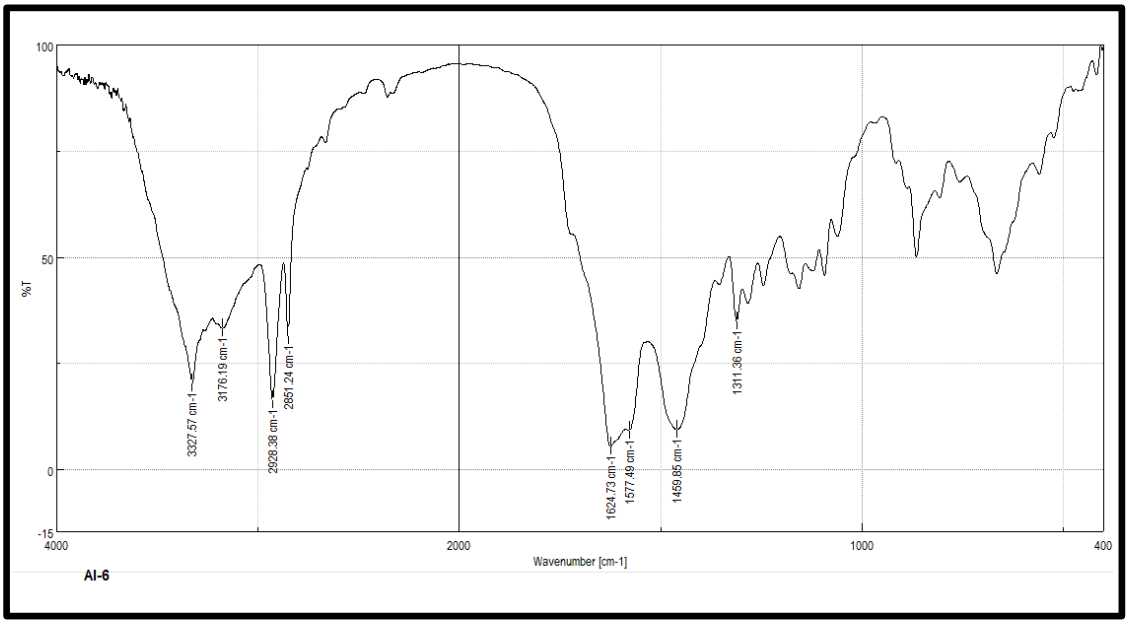

Figure 3.7. FTIR spectrum of GO/pBCM adsorbent.

3.3. Field Emission Scanning Electron Microscopy (FSEM)

Field Emission Scanning Electron Microscopy (FESEM) was used to analyze the morphological aspects, the size distribution, and the chemical composition [134]. The grain size and surface morphology were investigated for the adsorbents GO, GO/DAB, GO/DAB/EDTA, GO/CS, GO/CS/EDTA, and GO/pBCM and were obtained at 25.000× magnification and are represented in figures (3.8-3.13) respectively.

According to figure (3.8), GO adsorbent is seen as a flat sheet with some pucker on the surface which is due to deformation of graphite upon the exfoliation processes by using a strong oxidizing agent $KMnO_4$, and has well defined and interlinked three-dimensional graphene sheets, forming a porous network that resembles a loose sponge.

Figure (3.9) shows the FESEM image of GO/DAB, that appearance as quite different compared to GO adsorbent, and reveals that it is a porous structure with a large number of adsorption sites, and also observed that the surface of GO sheets is smooth and tightly packed owing to the interaction of oxygen-containing functional groups [135]. It indicates and confirms the combination of graphene oxide and 3,3´-Diaminobenzidine compound (DAB).

Furthermore, as seen in figure (3.10), the cross-section morphology of GO/DAB/EDTA adsorbent shows a surface morphology that is quite different from that of GO and GO/DAB. While there are obvious wrinkles on the surface of GO/DAB/EDTA, the surface is much smoother than either GO or GO/DAB adsorbents.

On the other hand, the illustrating figures (3.11 and 3.12) shows the adsorbents GO/CS and GO/CS/EDTA respectively, where a quite different compared to GO, it has some apparent folds and fluffy structures, assigned wrinkles, and curved surface in adsorbent GO/CS [136], and the roughness increased in adsorbent GO/DAB/EDTA images and revealed the attachment of EDTA groups [137]. This image indicates and confirms the combination of graphene oxide and chitosan as well EDTA.

Furthermore, as seen in figure (3.13), the cross-section morphology of GO/pBCM showed that the surface was also very compact, indicating that GO sheets were dispersed homogeneously in the polymer matrix, which also indicates the development of strong hydrogen bond interactions between graphene oxide and copolymer [138].

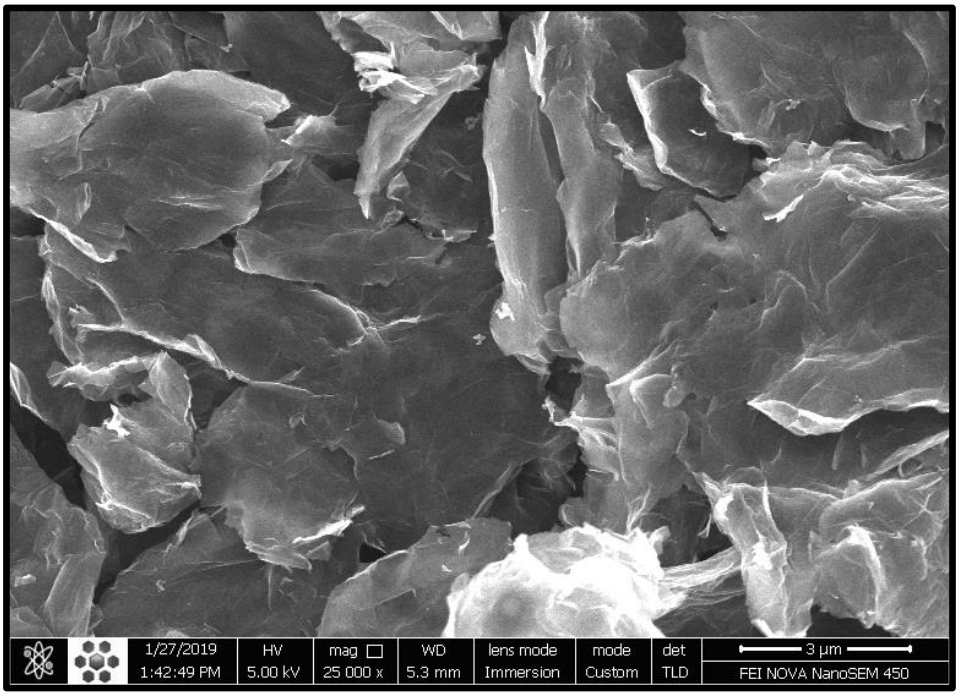

Figure 3.8. FESEM images at magnification 25000 of GO adsorbent.

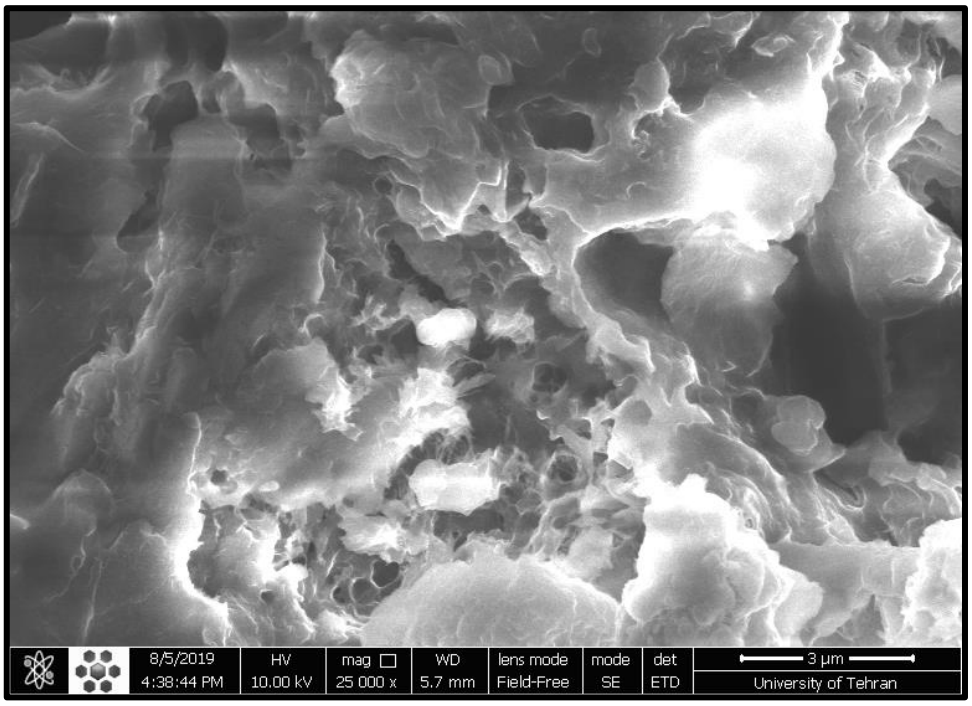

Figure 3.9. FESEM images at magnification 25000 of GO/DAB adsorbent.

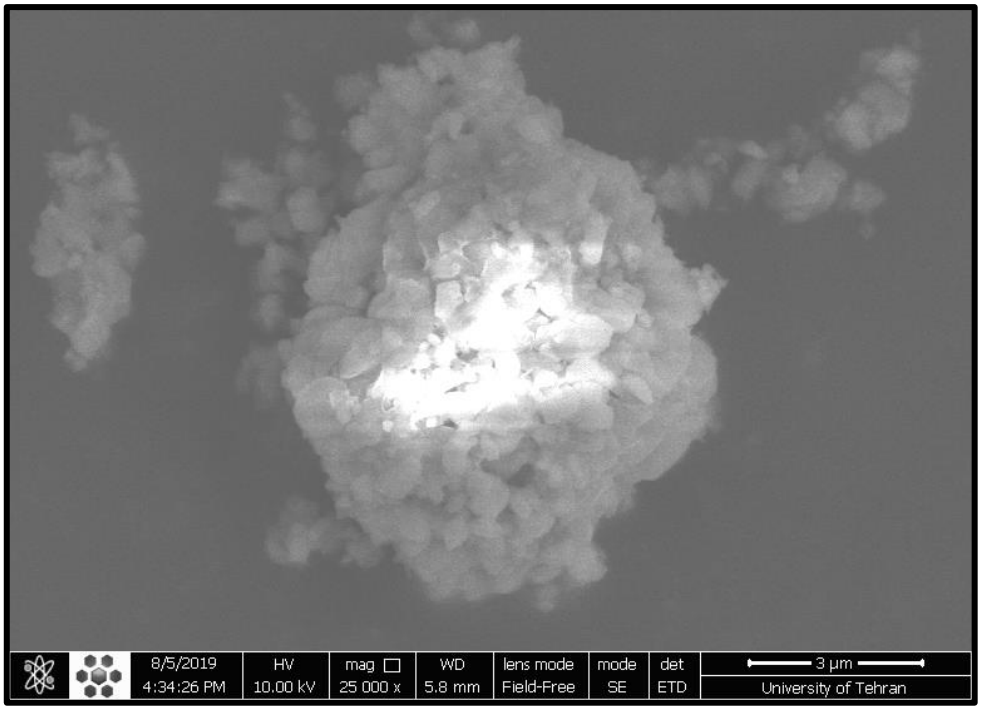

Figure 3.10. FESEM images at magnification 25000 of GO/DAB/EDTA adsorbent.

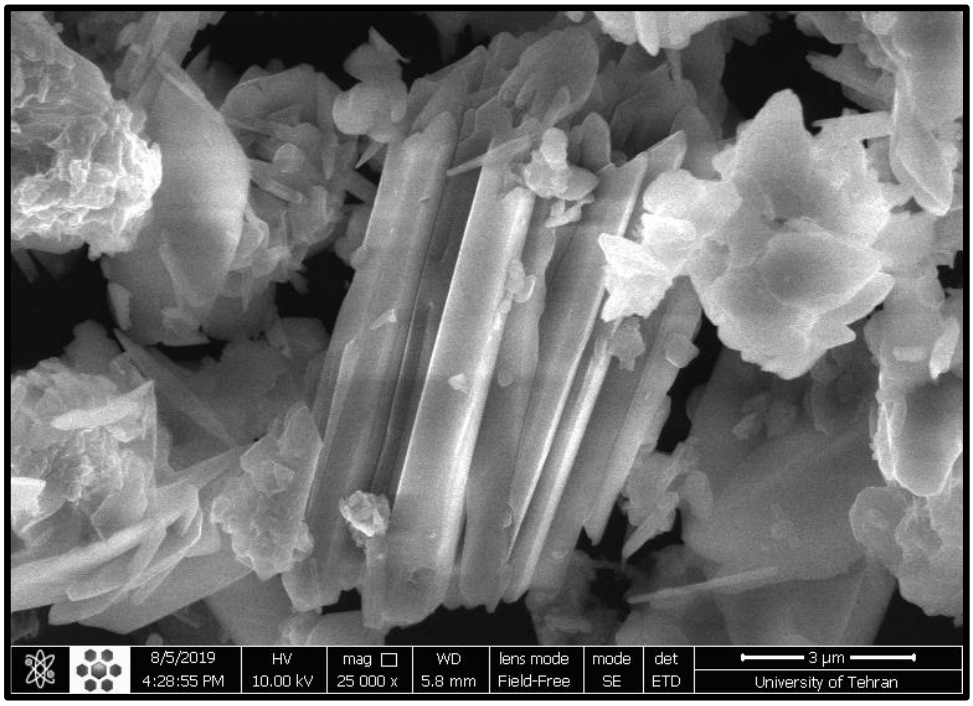

Figure 3.11. FESEM images at magnification 25000 of GO/CS adsorbent.

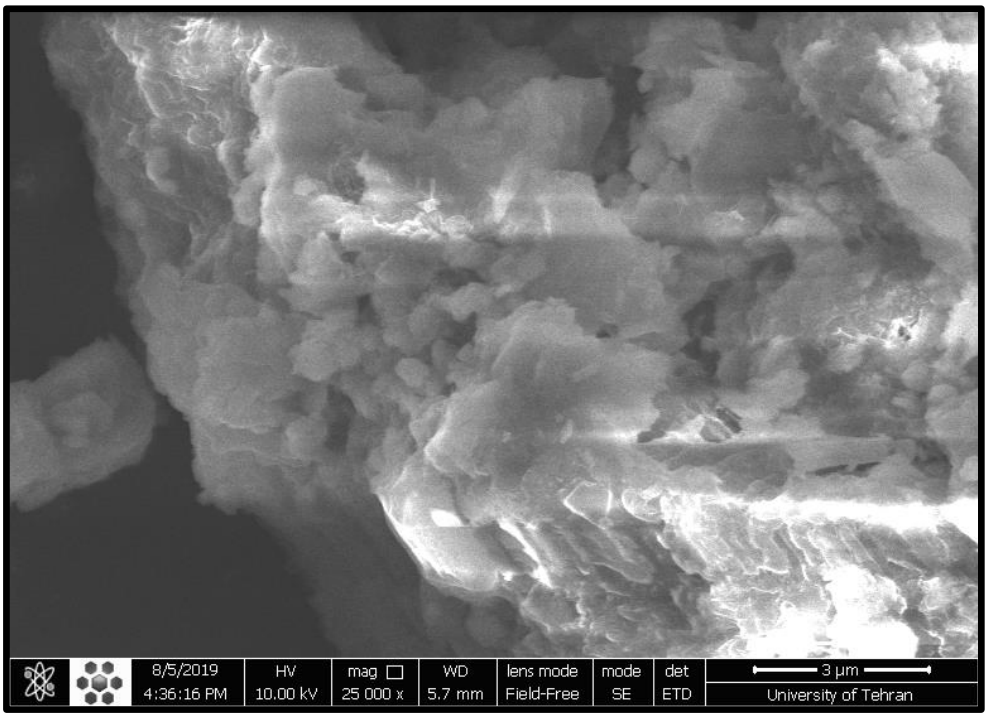

Figure 3.12. FESEM images at magnification 25000 of GO/CS/EDTA adsorbent.

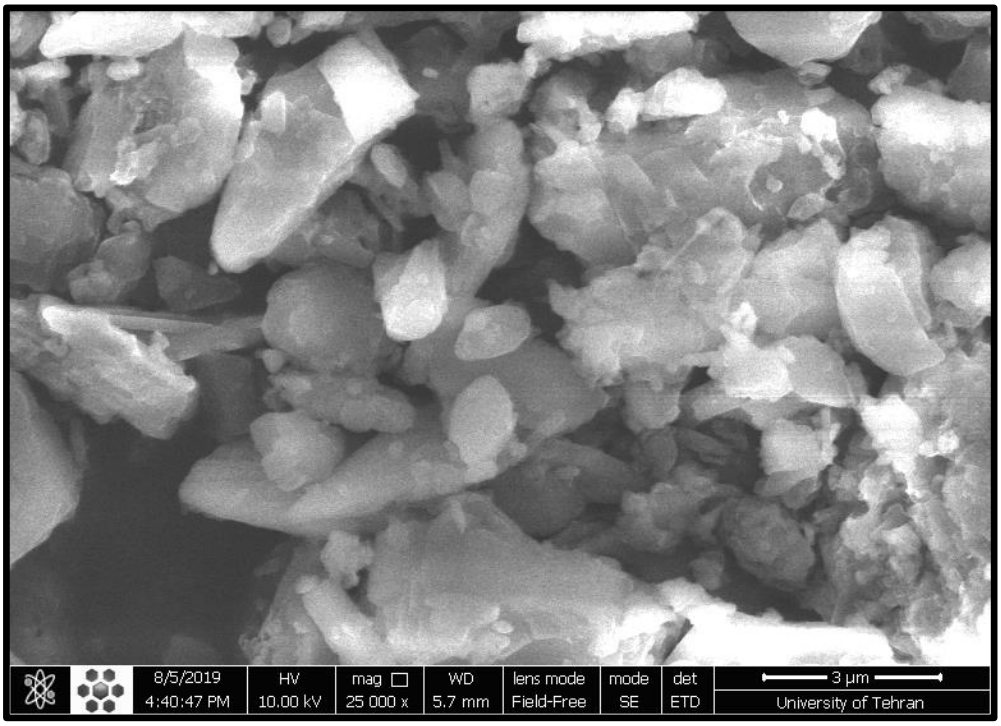

Figure 3.13. FESEM images at magnification 25000 of GO/pBCM adsorbent.

3.4. X-rays Diffraction Spectroscopy (XRD)

X-rays diffraction (XRD) is a commonly used technique to determine the structural arrangement of atoms or molecules in a crystalline material. Powder XRD has been routinely used to investigate the crystalline structure of graphite and related carbon materials. Also; XRD is a fast, non-destructive technique, and can often provide an unambiguous sample determination [139]. When it's combined with calculations of interplanar spacing, the number of coherent graphene layers may be estimated, and therefore indicate the degree of exfoliation.

The XRD patterns of prepared adsorbents GO, GO/DAB, GO/DABEDTA, GO/CS, GO/CS/EDTA, and GO/pBCM are shown in Figures (3.14-3.19) respectively.

The XRD pattern of natural graphite has a sharp diffraction peak at 2θ (26.25°), corresponding to an interlayer distance of (0.34 nm), which is following the reported value [140]. As for the GO powder sheet, Figure (3.14) shows a sharp peak at the 2θ position (~9.55°), which corresponds to an interlayer distance of (0.924 nm). The enlarged interlayer distance is attributed

to the presence of oxygen-containing functional groups on the GO sheet and suggests the successful oxidation of natural graphite using concentrated acids and $KMnO_4$ [141].

After functionalization of GO with DAB, many new peaks have appeared (Figure 3.15), the most important of those peaks are centered at 2θ (17.3°, 31.6°, 37.8°, and around 45.0°). In the GO-functioned with DAB, we observed weak peaks appearing nearly at 2θ (7.7° and 9.0°), which is lower than that of graphene oxide (9.55°). This could imply that the interplanar spacing of GO functioned with DAB was broadened due to possible intercalation of DAB, and that GO was fully exfoliated by treatment with DAB. Therefore, the XRD pattern also confirms the formation of DAB grafting on the surfaces of graphene oxide [142].

On the other hand, the GO peak disappears as shown in the XRD pattern of GO/DAB/EDTA (Figure 3.16), and other new characteristic peaks can be seen, these new bands corresponding to the chemically converted of the functioned graphene oxide into GO/DAB/EDTA, and at the same time indicating that GO sheet is uniformly an interaction with EDTA without agglomeration.

Meanwhile, after modifying GO with chitosan CS many broad peaks were appearing at 2θ between (~10.57°) and (~21.63°) as shown in figure (3.17) confirming the suitable attachment of CS to GO surface and indicating that there are mainly physical interaction but scarcely chemical reaction between CS and GO [143]. Due to the peak overlapping, no peak related to GO in XRD patterns of GO/CS. The peak at 2θ (9.44°) of GO/CS matched with that of pure GO, results from the remaining stacked GO sheets in the GO/CS [127].

The wide-angle XRD pattern was presented to investigate the prepared adsorbent GO/CS/EDTA (Figure 3.18). The diffraction peaks at 2θ = 22.21, 24.69, 32.25, and 37.21 represented as new peaks, also the diffraction peak around 17.87 might belong to the EDTA [109]. These characteristic diffraction peaks confirmed the formation of GO/CS/EDTA.

The peak characteristic of GO disappears in the XRD pattern of GO/pBCM composite (Figure 3.19), indicating that the graphene oxide GO sheet is uniformly dispersed in the pBCM matrix without agglomeration [117]. On the other hand, some new characteristic peaks at 2θ 31.69°, 37.89°, and 45.47° are also observed in the XRD pattern of the GO/pBCM composite (Figure 3.19).

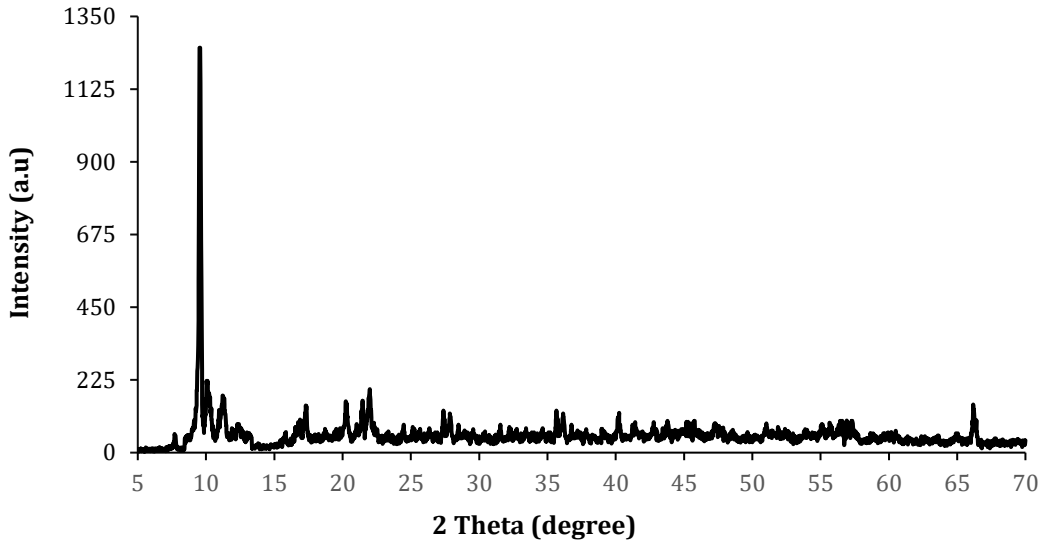

Figure 3.14. X-rays Diffraction pattern of adsorbent GO.

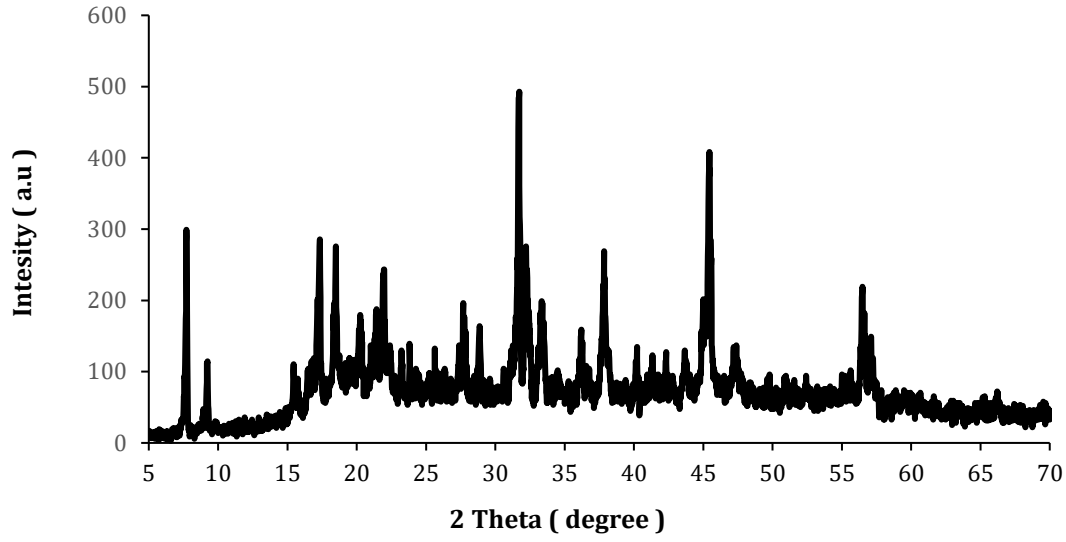

Figure 3.15. X-rays Diffraction pattern of adsorbent GO/DAB.

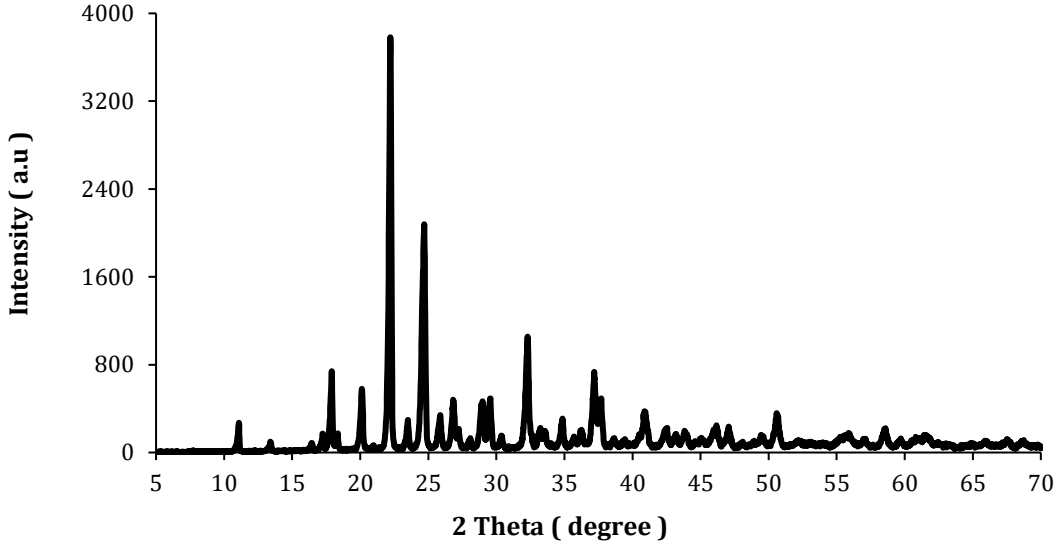

Figure 3.16. X-rays Diffraction pattern of adsorbent GO/DAB/EDTA.

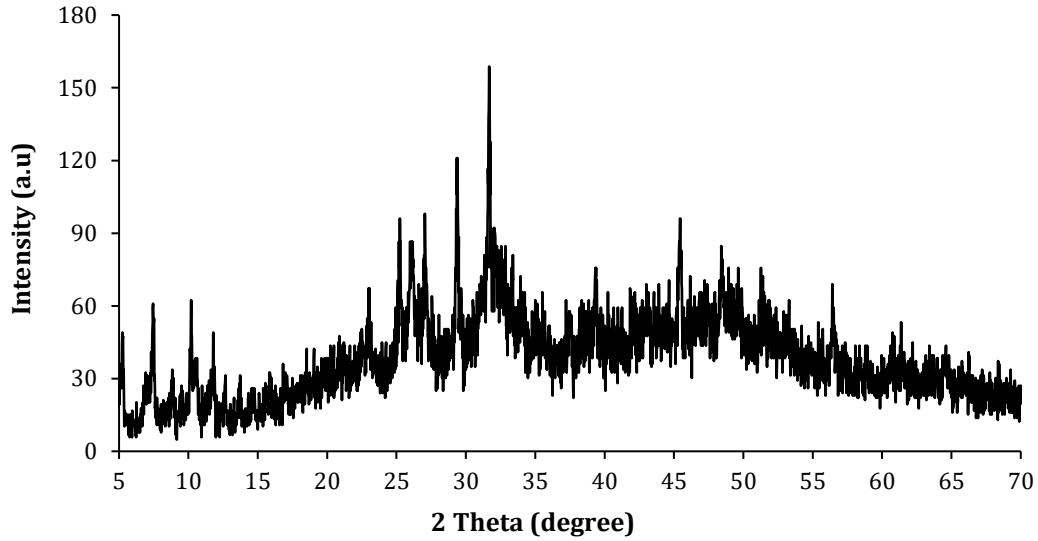

Figure 3.17. X-rays Diffraction pattern of adsorbent GO/CS.

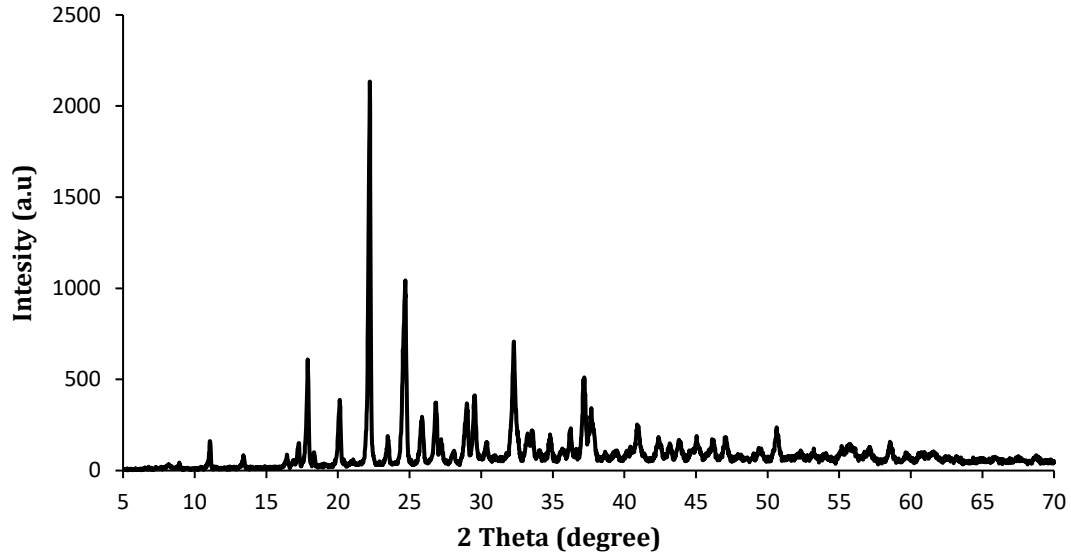

Figure 3.18. X-rays Diffraction pattern of adsorbent GO/CS/EDTA.

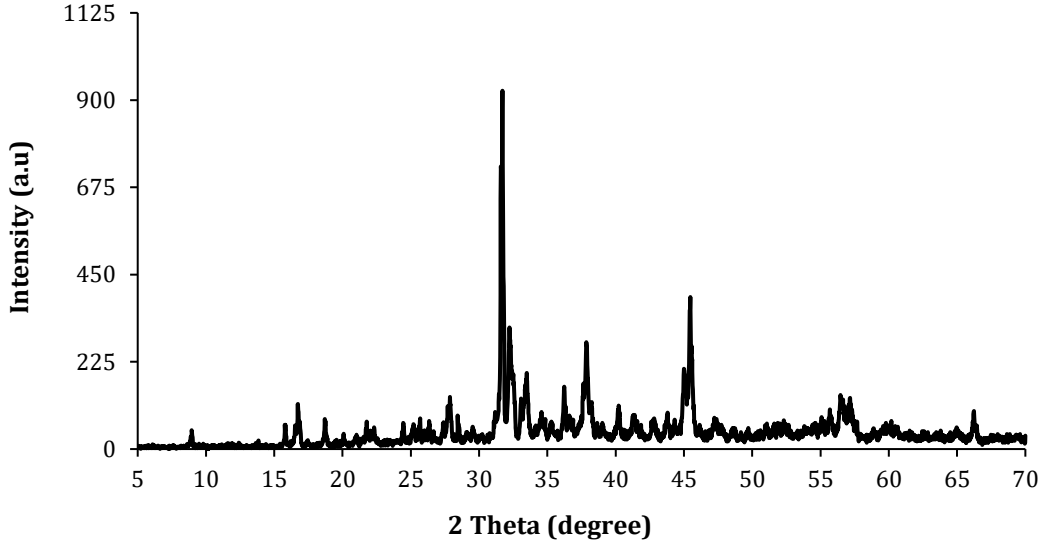

Figure 3.19. X-rays Diffraction pattern of adsorbent GO/pBCM.

3.5. Analysis of the Surface Area and the Porosity of Surface (BET & BJH)

Brunauer Emmett Teller BET analysis provides precise specific surface area evaluation of compounds by N_2 multilayer adsorption measured as a

function of relative pressure using a fully automated Analyzer [144]. This technique includes evaluations of the external area and pore area to determine the total surface area in m^2/g and profitable significant data for the adsorption processes.

Barrett Joyner Halenda BJH analysis can also be employed to determine pore size and specific pore volume using adsorption and desorption techniques. This technique characterizes pore size distribution independent of the external area due to the particle size of the compounds [145]. Figures (3.20-3.25) illustrate BET isotherms of the adsorbents; GO, GO/DAB, GO/DAB/EDTA, GO/CS, GO/CS/EDTA, and GO/pBCM respectively. All the obtained data that belongs to the BET and BJH techniques of the absorbents in our study are arranged in Table (3.1).

From BET isotherms of the prepared adsorbents (according to the classification of the International Union of Pure and Applied Chemistry IUPAC) are IV type, which indicates that the process is multilayer adsorption of these adsorbents [146]. It was found from BET & BJH as shown in table 3.1, the adsorbent GO has a surface area of 10.4477 $m^2\ g^{-1}$, total pore volume 0.000866 $cm^3\ g^{-1,}$ and average pore width (4V/A by BJH) 9.8143 nm. And through the value of the pore diameter, it is noted that the adsorbent GO was classified within Mesoporous (containing pores 2-50 nm in width) materials [147]. The particle size of these materials can affect its adsorption of adsorbate besides the influence of pore volume and surface area.

Table 3.1. Surface area analysis for prepared adsorbents

Property	GO	GO/DAB	GO/DAB/E	GO/CS	GO/CS/E	GO/pBCM
Surface area (m^2/g)*	10.4477	3.2782	3.4764	4.5763	2.6176	2.6848
Pore volume (cm^3/g)**	0.000866	0.001184	0.001477	0.001508	0.000952	0.001176
Pore diameter (nm)**	9.8143	18.9132	13.6247	16.7407	10.2146	10.0968

Isotherm type	IV	IV	IV	IV	IV	IV
Type of pore	Meso porous	Meso porous	Meso porous	Meso porous	Meso porous	Meso porous

***Determined by the BET method, **Determined by BJH method**

Furthermore, the textural properties of the other prepared adsorbents GO/DAB, GO/DAB/EDTA, GO/CS, GO/CS/EDTA, and GO/pBCM were also characterized by the BET method as shown in Figures (3.21-3.25) respectively also the corresponding pore size distribution of obtained by BJH method. As a note in the mentioned figures, all these adsorbents show similar behavior to those of type IV, which also indicates the presence of mesoporous materials [147]. The particle size of these adsorbents can also play its role in the adsorption of the dye besides the influence of pore volume and surface area.

Moreover, Table (3.1) presents the specific surface area, pore volume, and pore size (diameter) of other prepared adsorbents. It observes that GO adsorbents had higher surface area compared to other adsorbents, also the pore size and pore volume of GO adsorbents were smaller than those other adsorbents. Although the smallest surface area of the other prepared adsorbents, its adsorption capacities were larger than of GO adsorbent (*we will refer to an explanation of this in detail later in chapter four*), maybe because of the larger pore size and pore volume of these adsorbents. Thus, it could be inferred that the interactions between functional groups of GO adsorbent and dyes molecules occurred on the surface of GO. On the other hand, the active sites inside of the pore for the other adsorbents were well accessible to the CR and BB dyes molecules, and this gave good results for adsorption capacities.

In general, the adsorption behavior in mesoporous materials is determined by the adsorbent-adsorptive interactions and by the interactions between the molecules in the condensed state. In this case, the initial monolayer-multilayer adsorption on the mesoporous walls.

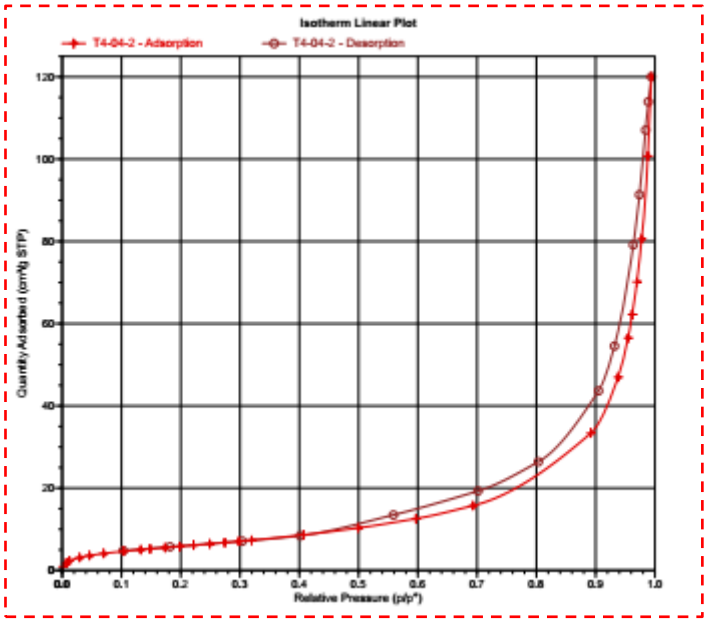

Figure 3.20. The N_2 adsorption-desorption isotherms of GO.

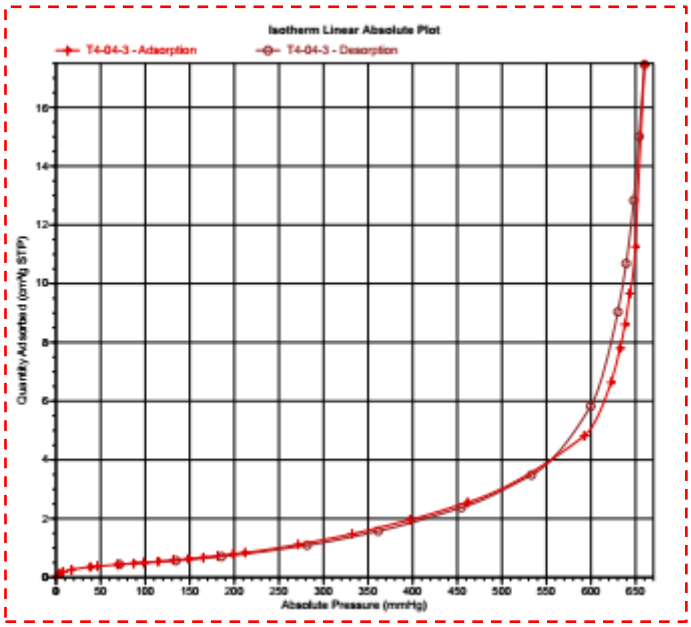

Figure 3.21. The N_2 adsorption-desorption isotherms of GO/DAB.

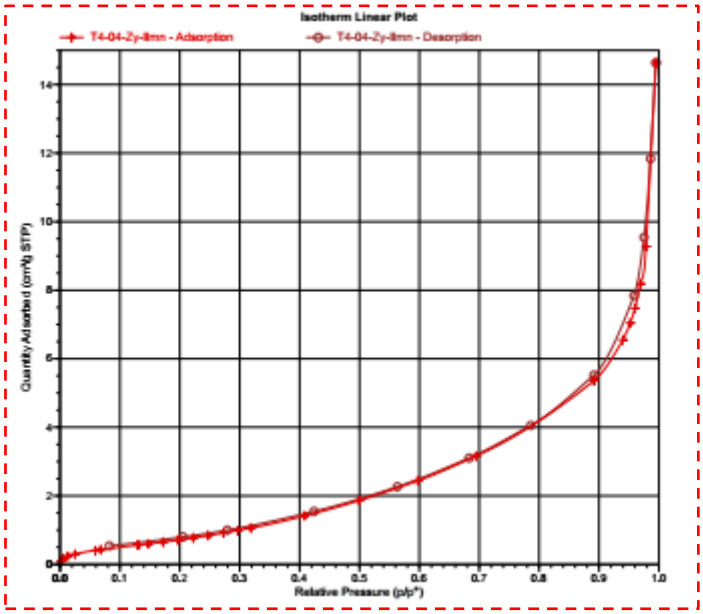

Figure 3.22. The N_2 adsorption-desorption isotherms of GO/DAB/EDTA.

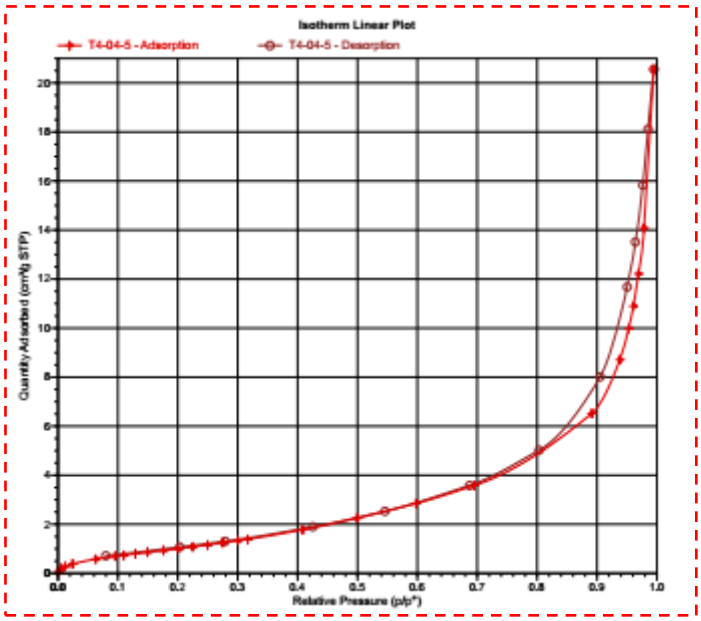

Figure 3.23. The N_2 adsorption-desorption isotherms of GO/CS.

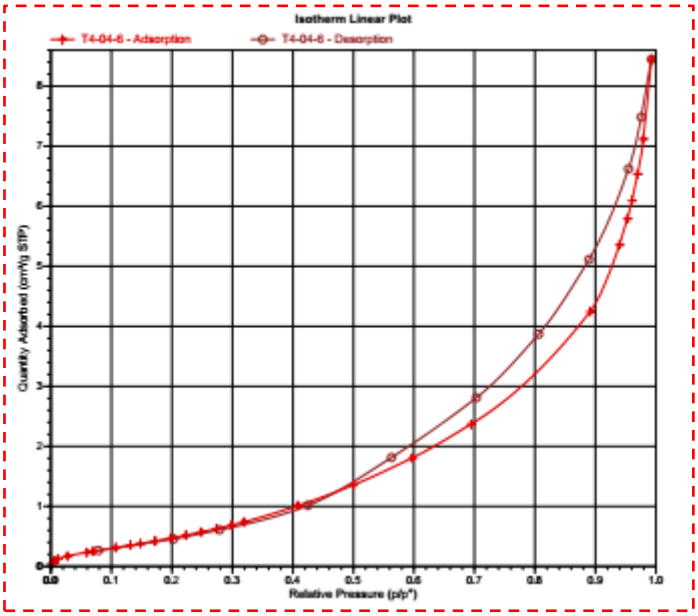

Figure 3.24. The N_2 adsorption-desorption isotherms of GO/CS/EDTA.

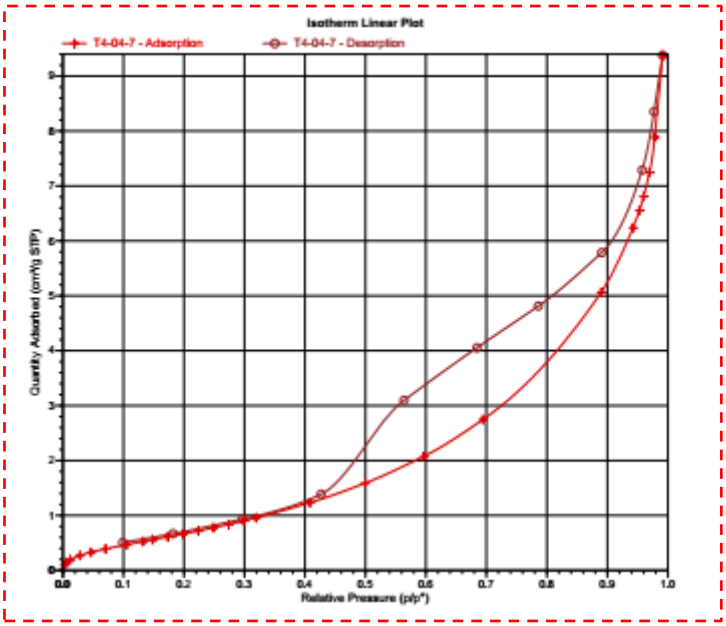

Figure 3.25. The N_2 adsorption-desorption isotherms of GO/pBCM.

4. Adsorption Experiment Study

4.1. Batch Adsorption Experiments

The adsorption experiments were carried out using a 0.1L of dyes solution with chosen initial concentration to each adsorbent by contacting an 0.025 g as a fixed weight of adsorbents for each value of initial concentration, and the solutions were shaken at 200.0 rpm for 24 hrs at 27°C, the resulting suspensions were filtration. The equilibrium concentration was determined for each dye using a UV-Visible Spectrophotometer at λ_{max} 494 nm for CR dye and λ_{max} 457 nm for BB dye.

The amount of the CR and BB dyes on the prepared adsorbents were calculated from the difference in dye concentration in the aqueous phase before and after adsorption, using the equation 4.1 [148]:

$$\mathbf{q_e = \frac{(C_o - C_e)\, V}{m}} \quad \ldots\ldots (\mathbf{4.1})$$

Where C_0 and C_e (mg/L) are the initial and equilibrium concentrations of dyes in the solution, V (L) is the volume of dyes solution, m (g) is the mass of the used adsorbents in the experiment, and q_e (mg/g) is the amount of adsorbed dyes per gram of adsorbents (adsorption capacity).

4.2. Optimization of Adsorption Experiments of Dyes

4.2.1. Initial Concentration of CR & BB Dyes

To perform the optimal initial concentration of CR and BB dyes, different concentrations are prepared; 100, 200, 300, 400, 500, and 600 mg/L. The 300.0 mg/L as an optimum initial concentration of CR dye is used for GO, GO/DAB, GO/DAB/EDTA, and GO/pBCM, and 500.0 mg/L for GO/CS and GO/CS/EDTA adsorbents. Likewise, BB dye is recorded 200.0 mg/L as the optimum initial concentration for GO/DAB/EDTA, and for the rest of adsorbents; i.e. GO, GO/DAB, GO/CS, GO/CS/EDTA, and GO/pBCM, is recorded 400.0 mg/L as an optimum initial concentration.

4.2.2. The Effect of pH on the CR & BB Dyes

The pH is an important factor that influences the solution chemistry of dyes, complexation by organic or inorganic ligands, precipitation, and

hydrolysis. pH also influences the speciation and availability of dyes for adsorption [149]. The effect of pH on the adsorption capacities of prepared adsorbents was studied at an optimum initial concentration of both CR & BB dyes, Figures (4.1 and 4.2) illustrates pH which adjusted at the range (3.0–12.0) influence of the adsorption capacities for CR and BB dyes onto GO, GO/DAB, GO/DAB/EDTA, GO/CS, GO/CS/EDTA, and GO/pBCM at 27°C.

Figure (4.1) shows a sharp decrease in the adsorption of CR dye with increasing pH from 3.0 to 7.0. A lower qmax is found, for both adsorbents GO and GO/CS at the pH ranging from 9.0 to 12.0. However, the optimum pH for adsorption depends on the types of adsorbate and adsorbent. The free electron pair of nitrogen on amine groups is responsible for the adsorption of adsorbates on chitosan adsorbents. Acidic media results in the protonation of amine groups and enhances the cationic potential of chitosan, thereby, improving the adsorption process [150]. Therefore, the pH is kept at 3.0 for the next optimization experiment for GO and GO/CS.

Figure (4.1); also revealed that the best working pH value is found to be 7.0 for the better adsorption of CR dye by GO/DAB and GO/pBCM. For both adsorbents, a sharp increase of CR adsorption is observed when the pH increases from 3.0 to 7.0, while, lower adsorption capacity is found in the pH range from 9.0 to 12.0 for the same adsorbents. Thus, in the further followed experiments, the pH was kept at 7.0, and similar results have been reported for the removal of CR dye by sorption onto aniline propyl silica aerogel [151].

Similar behavior is observed for CR dye adsorption onto adsorbents GO/DAB/EDTA and GO/CS/EDTA. Where the adsorption depends on the extent of protonation of the carboxylic groups in the graphene oxide and carboxyl and carbonyl groups of the EDTA [152]. Figure (4.1) shows that the adsorption efficiency is lower in acidic media (pH 3.0) for both adsorbents GO/DAB/EDTA and GO/CS/EDTA, and an increase of CR dye adsorption when pH value increased from 3.0 to 5.0 for both adsorbents. Therefore, pH 5.0 is optimized for adsorption CR dye by these adsorbents. After that, the lower adsorption capacity is found at a pH range from 7.0 to 12.0 also for the adsorbents GO/DAB/EDTA and GO/CS/EDTA.

The adsorption process is dependent on the pH of the solution since it affects the adsorbent surface charge and the degree of protonation of the functional groups [153]**.** With the increasing pH values, the adsorption of CR dye on GO and GOCS tends to decrease, due to the rising electrostatic repulsion between the anionic dye adsorbate species and negatively charged

adsorbent surfaces. Also, lower adsorption at alkaline pH due to the presence of excess OH^- ions destabilizing anionic dye and competing with the dye anions for the adsorption sites. Low pH leads to an increase in H^+ ion concentration in the system, the surface of adsorbents acquires a positive charge by absorbing H^+ ions, and hence more amount of anionic dye adsorption takes place. Similar behavior was observed for CR dye adsorption on agricultural stable waste-based activated carbon [154].

Figure (4.2) illustrates the pH influence of the adsorption capacities at different pH values ranging from 3.0 to 12.0 for BB dye adsorption by the prepared adsorbents. As shown in this figure, the adsorption capacity of BB dye increases with increasing the pH from 3.0 to 5.0 and decreases slightly when solution pH is above 5.0. The maximum adsorption capacities were 600.9 and 668.17 mg/g at pH 5.0 for adsorbents GO/DAB/EDTA and GO/CS/EDTA respectively. So, the best pH value for the adsorption of BB dye by these adsorbents is pH 5.0. A decrease in adsorption was observed with an increase in pH values after that, where the adsorption capacity decreased from 600.9 mg/g at pH 5.0 to 160.60 and 39.36 mg/g at pH 9.0 and 12.0 respectively for adsorbent GO/DAB/EDTA at 200.0 mg/L optimum initial concertation's.

The influence of pH on the solution concentrations of the BB dye tested after adsorption onto GO, GO/DAB, GO/CS, and GO/pBCM is presented in Figure 4.2. The results obtained indicate that the optimum pH value for the adsorption process was dependent on the type of adsorbate employed. Thus, for mention adsorbents, adsorption capacity appeared to be most effective at pH 3.0. Irrespective of nature, where the q_{max} recorded in 708.5, 1322.0, 702.0, and 741.2 mg/g for GO, GO/DAB, GO/CS, and GO/pBCM respectively. Therefore, a decrease in adsorption capacity occurred with increasing pH values, and consequently, pH 3.0 was chosen for further analysis of adsorption experiments.

Notably, the surface of all adsorbents contains different functional groups such as carboxylic and amine groups, so that, the change in pH values of dye solution will affect the ionization of these functional groups in adsorbent compounds [155, 156].

Because of that, the conclusion that the electrostatic attraction between the adsorbents and CR and BB dyes is not the sole adsorption mechanism in our study. Instead, the interaction between adsorbate and the basic functional group (which were added to the surface of adsorbent during the chemical

modification of Graphene Oxide) on the surface of the prepared adsorbents may play a more prominent role.

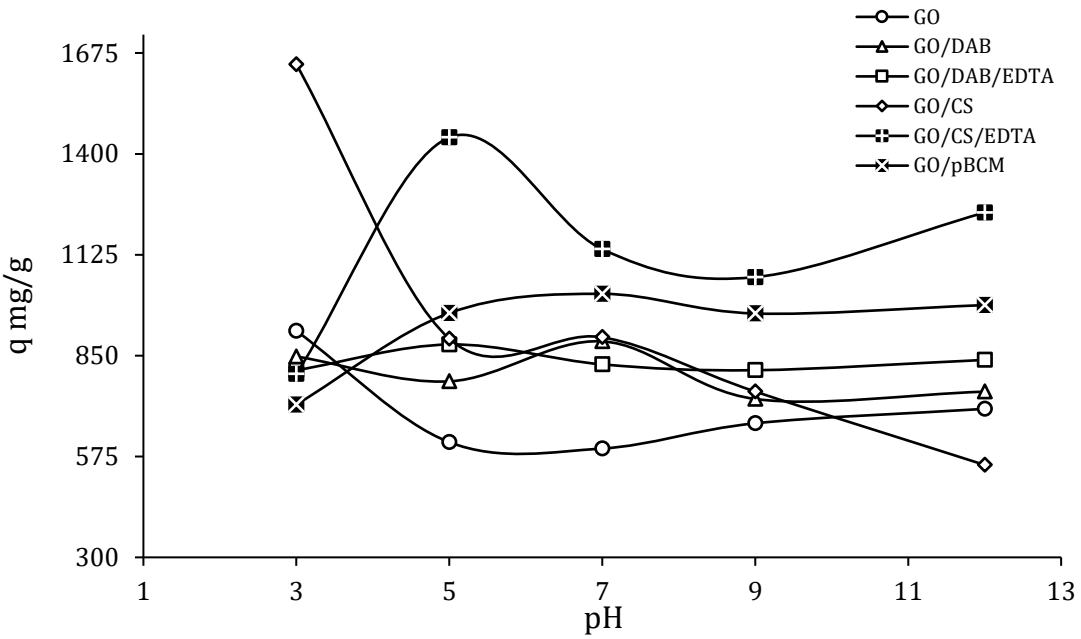

Figure 4.1. Effect of pH on the adsorption of Congo Red CR onto Adsorbents at 27°C

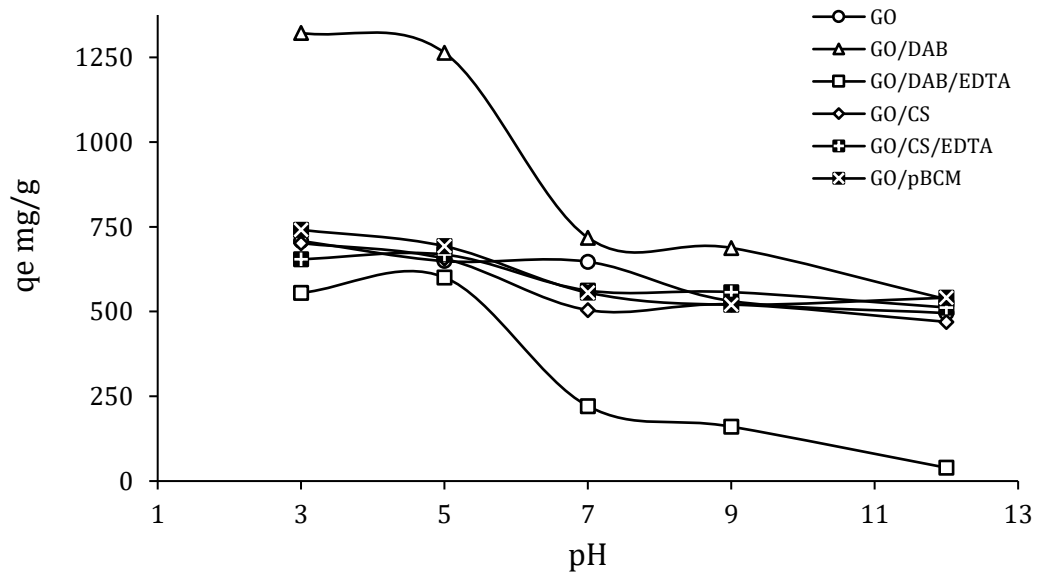

Figure 4.2. Effect of pH on the adsorption of Bismarck Brown BB onto Adsorbents at 27°C

Table (4.1) summarized the optimization pH for adsorption of CR and BB dyes onto prepared adsorbents.

Table 4.1. Optimization pH for adsorption of CR and BB dyes onto prepared adsorbents.

Dyes	Optimized pH- values					
	GO	GO/DAB	GO/DAB/EDTA	GO/CS	GO/CS/EDTA	GO/pBCM
CR	3.0	7.0	5.0	3.0	5.0	7.0
BB	3.0	3.0	5.0	3.0	5.0	3.0

4.2.3. The effect of Contact Time and Temperatures on CR & BB Dyes

The duration time before the adsorption experiment study reaches equilibrium is called agitation time [157]. Therefore, the contact time between adsorbate and adsorbent plays an important role in the adsorption process, and the time needed to attain equilibrium is very important to predict the performance and feasibility of an adsorbent for a process [158].

The effect of agitation time on the adsorption of CR and BB dyes onto the prepared adsorbents GO, GO/DAB, GO/DAB/EDTA, GO/CS, GO/CS/EDTA, and GO/pBCM are shown in Figures (4.3-4.8) and Figures (4.9-4.14) respectively, at the initial concertation of each adsorbent and optimum pH in three different temperatures 27, 40, and 60°C.

Figure (4.3) reveals that the adsorption of CR has rapidly increased from (1-60 min.), then the equilibrium is attained within (60-90 min.) for GO adsorbent. While Figures (4.4 and 4.8) show a rapid increase for GO/DAB and GO/pBCM receptively from (1–30 min.), then the equilibrium is reached within (30–60 min.). In addition, the behavior of CR dye adsorption by adsorbents GO/DAB/EDTA, GO/CS, and GO/CS/EDTA are shown in Figures (4.5-4.7) respectively has rapidly increased from (1-45 min.), and then the equilibrium is achieved within (45–75 min.).

The adsorption capacity for adsorbents GO, GO/DAB, GO/DAB/EDTA, GO/CS/EDTA, and GO/pBCM are increased as temperature rising from 27 to 60°C, except the adsorption capacity for GO/CS adsorbent that decreased with increasing temperature from 27 to 60°C. Thus, the optimum agitation times for all the followed experiments were chosen as 60 min. for adsorption of CR

dye by GO, 30 min. for GO/DAB and GO/pBCM, and 45 min. for adsorption of CR dye onto GO/DAB/EDTA, GO/CS, and GO/CS/EDTA adsorbents.

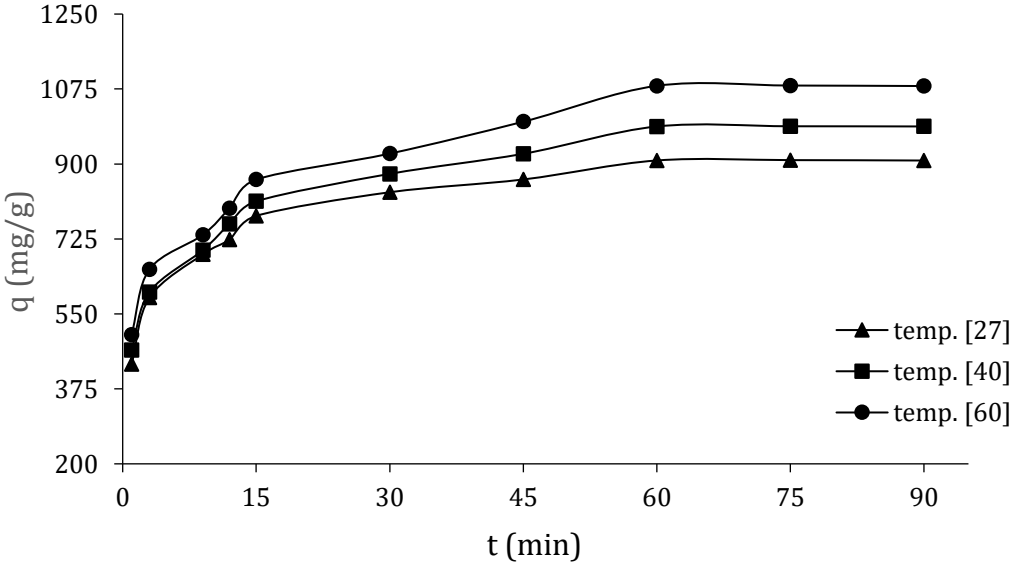

Figure 4.3. Agitation time effect of the CR dye adsorption onto GO at different temperatures

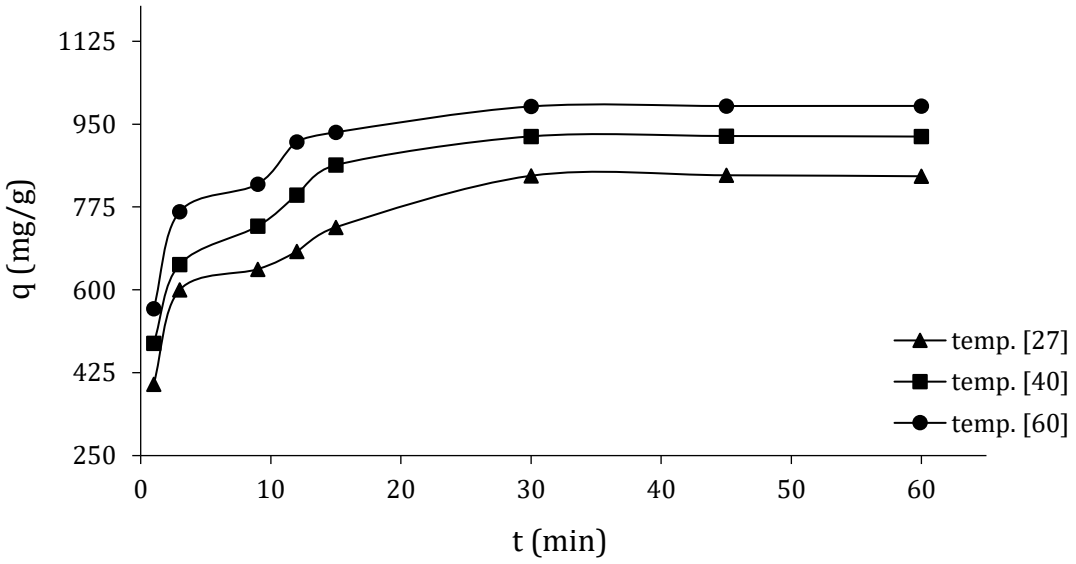

Figure 4.4. Agitation time effect of the CR dye adsorption onto GO/DAB at different temperatures

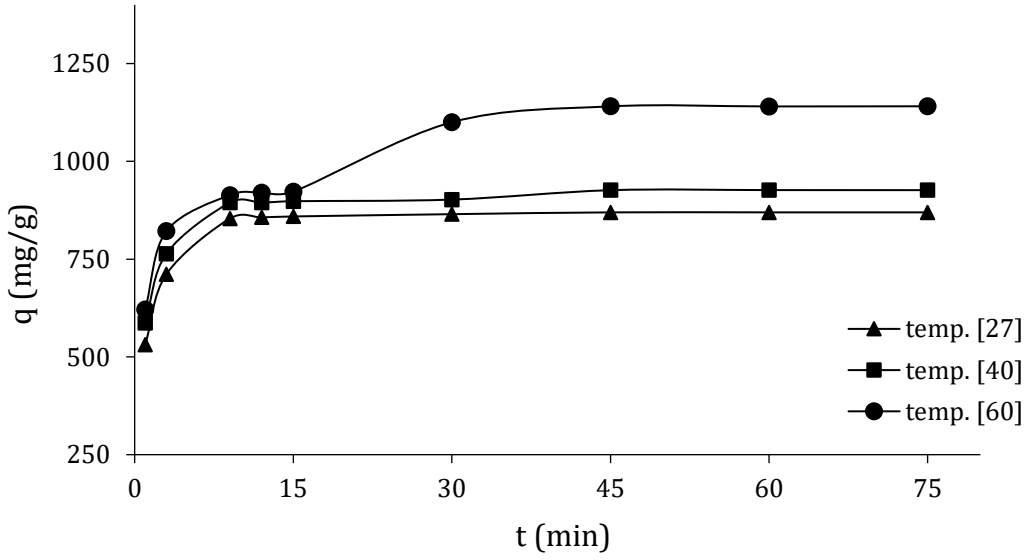

Figure 4.5. Agitation time effect of the CR dye adsorption onto GO/DAB/EDTA at different temperatures

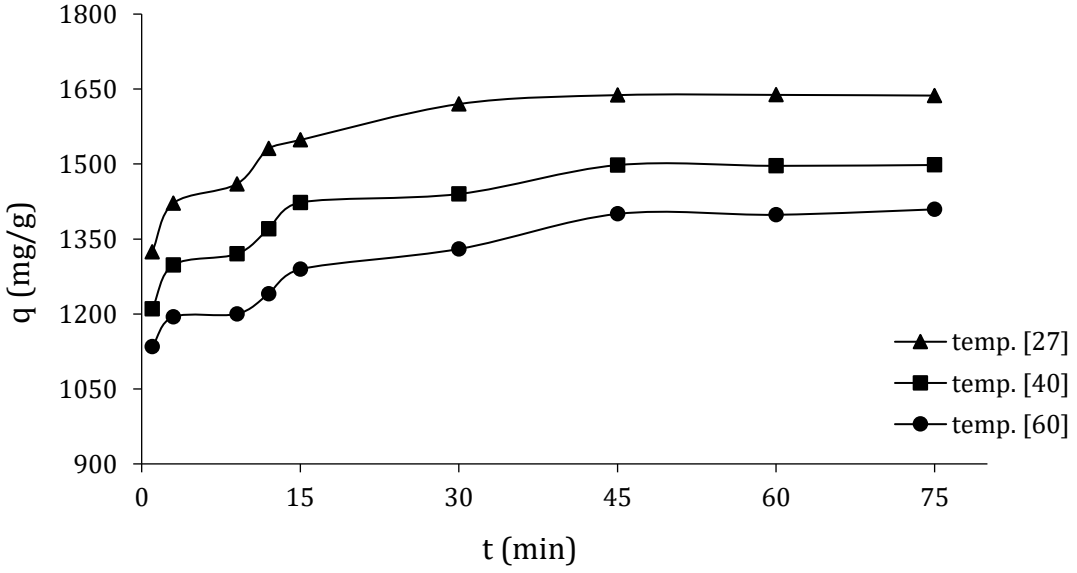

Figure 4.6. Agitation time effect of the CR dye adsorption onto GO/CS at different temperatures

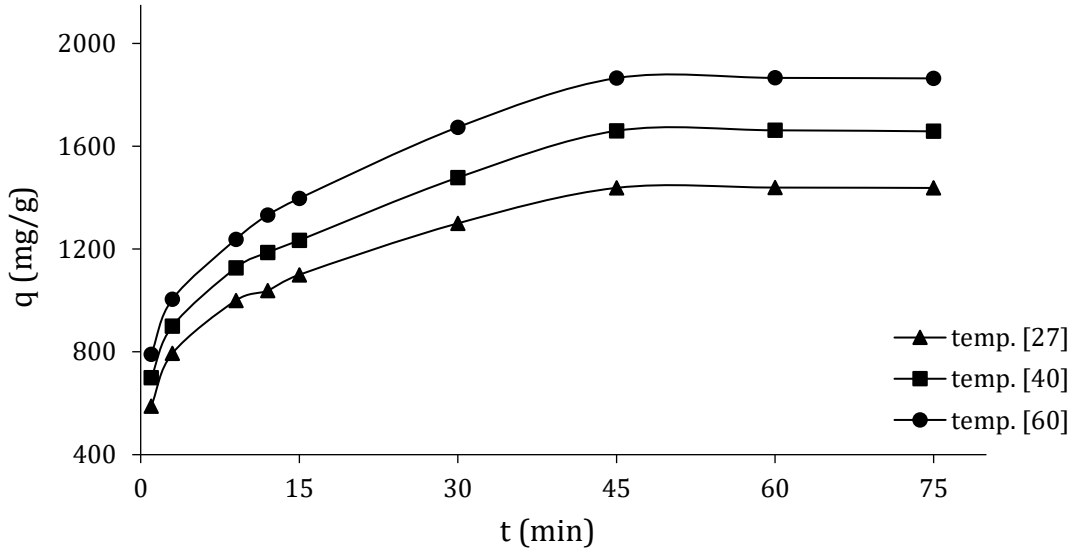

Figure 4.7. Agitation time effect of the CR dye adsorption onto GO/CS/EDTA at different temperatures

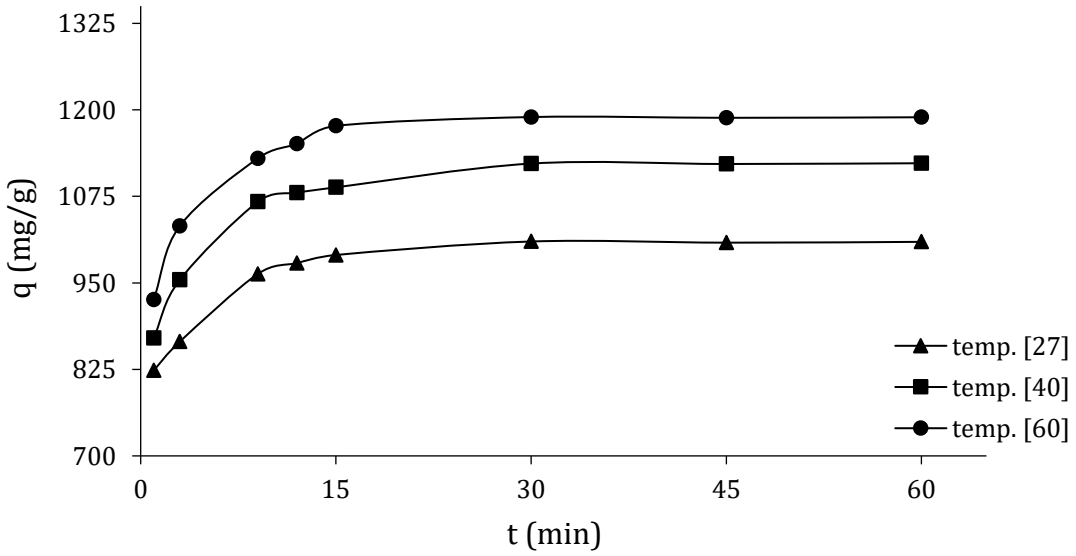

Figure 4.8. Agitation time effect of the CR dye adsorption onto GO/pBCM at different temperatures

On the other hand, the effect of agitation time on the adsorption of BB dye onto all prepared adsorbents is shown in Figures (4.9-4.14). They illustrate a rapid increase from (1-45 min.), and then the equilibrium is reached within contact time (45-75 min.) for GO, GO/CS, and GO/CS/EDTA, while GO/DAB and GO/DAB/EDTA adsorbents (Figures 4.10 and 4.11 receptively) showed a rapid increase from (1-30 min), and then the equilibrium is attained within the next (30-60 min).

In addition, the behavior of BB dye adsorption by GO/pBCM as shown in Figure (4.14) has rapidly increased from (1-15 min.), and then the equilibrium was achieved within (15-45 min.).

The adsorption capacity for all adsorbents GO, GO/DAB, GO/DAB/EDTA, GO/CS, GO/CS/EDTA, and GO/pBCM were increased as temperature rising from 27 to 60°C and this tendency for adsorption capacities are expected. Thus, the optimum agitation times for all further experiments were chosen as 15 min. for adsorption of BB dye by GO/pBCM, 30 min. for adsorbents GO/DAB and GO/DAB/EDTA, and 45 min. for adsorption of BB dye onto GO, GO/CS, and GO/CS/EDTA adsorbents.

Table 4.2. The optimization contact time for adsorption of CR and BB Dyes onto prepared adsorbents.

Dyes	Optimized Contact time					
	GO	GO/DAB	GO/DAB/EDTA	GO/CS	GO/CS/EDTA	GO/pBCM
CR	60	30	45	45	45	30
BB	45	30	30	45	45	15

From the time optimization experiments for CR and BB dyes onto synthesized adsorbents, it is observed that the required time to reach equilibrium for GO is more than the time for other prepared modified GO (i.e. GO/DAB, GO/DAB/EDTA, GO/CS, GO/CS/EDTA, and GO/pBCM). In addition, it can be seen that the reducing of required time for equilibrium was combined with the increasing of (q_{max}-value) for all modified GO with a comparison of GO only, thus leading to the importance of the modifications.

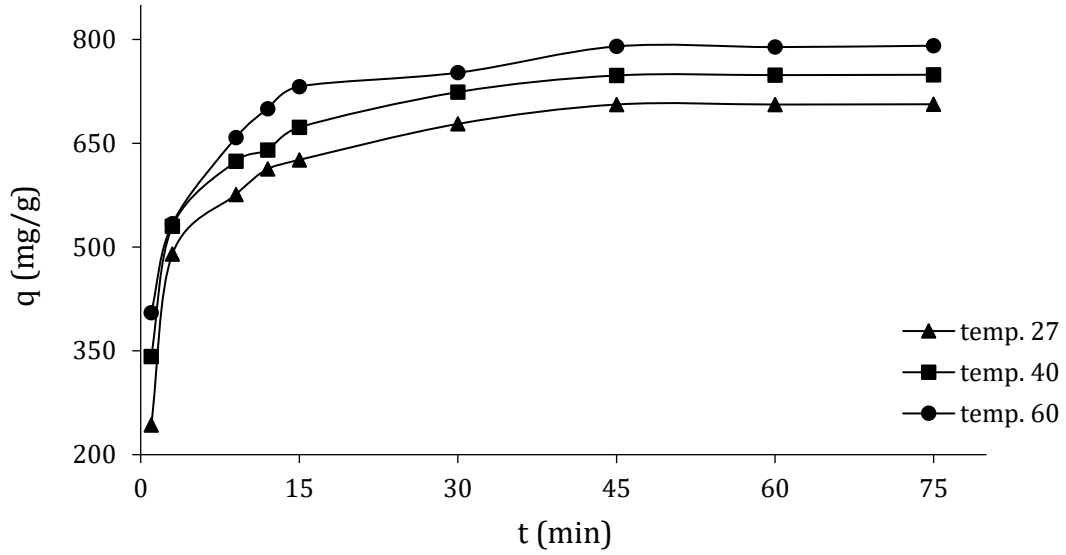

Figure 4.9. Agitation time effect of the BB dye adsorption onto GO at different temperatures

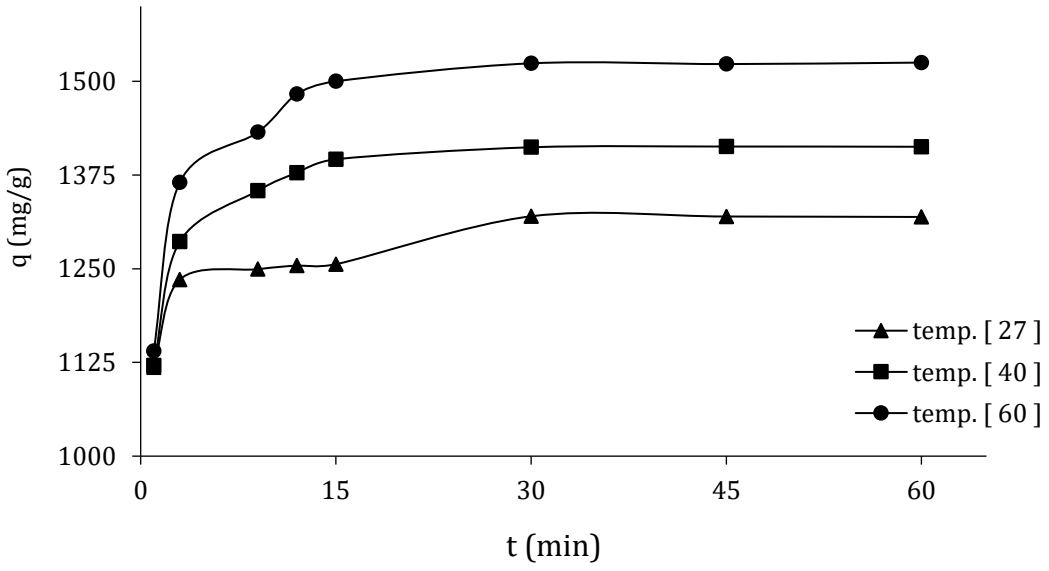

Figure 4.10. Agitation time effect of the BB dye adsorption onto GO/DAB at different temperatures

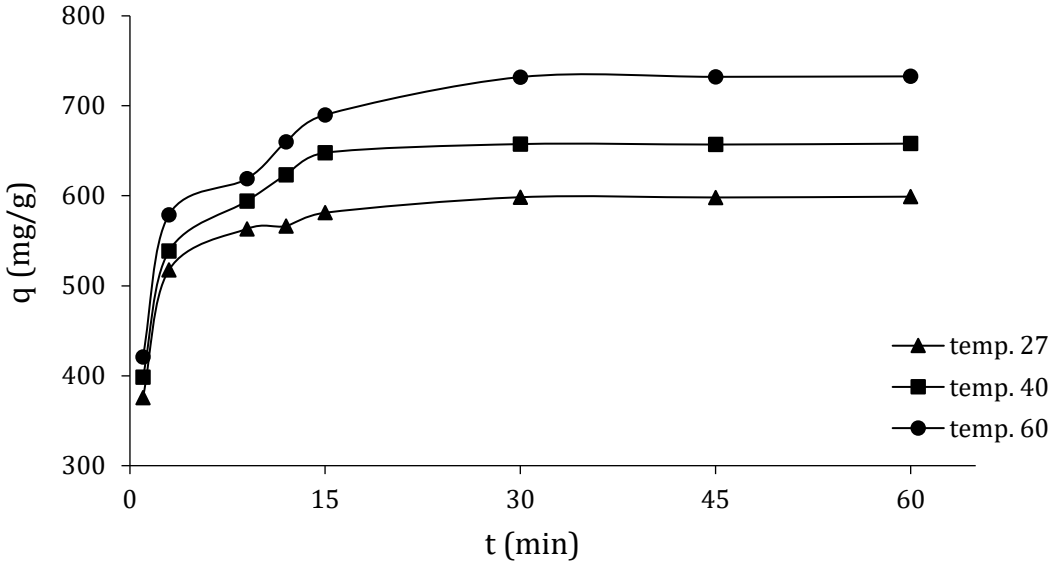

Figure 4.11. Agitation time effect of the BB dye adsorption onto GO/DAB/EDTA at different temperatures

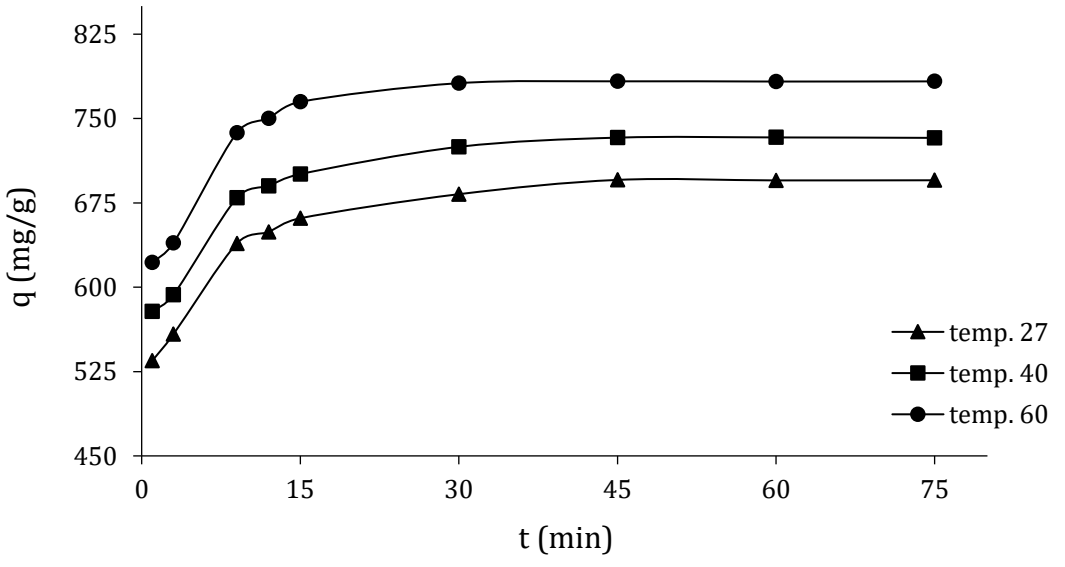

Figure 4.12. Agitation time effect of the BB dye adsorption onto GO/CS at different temperatures

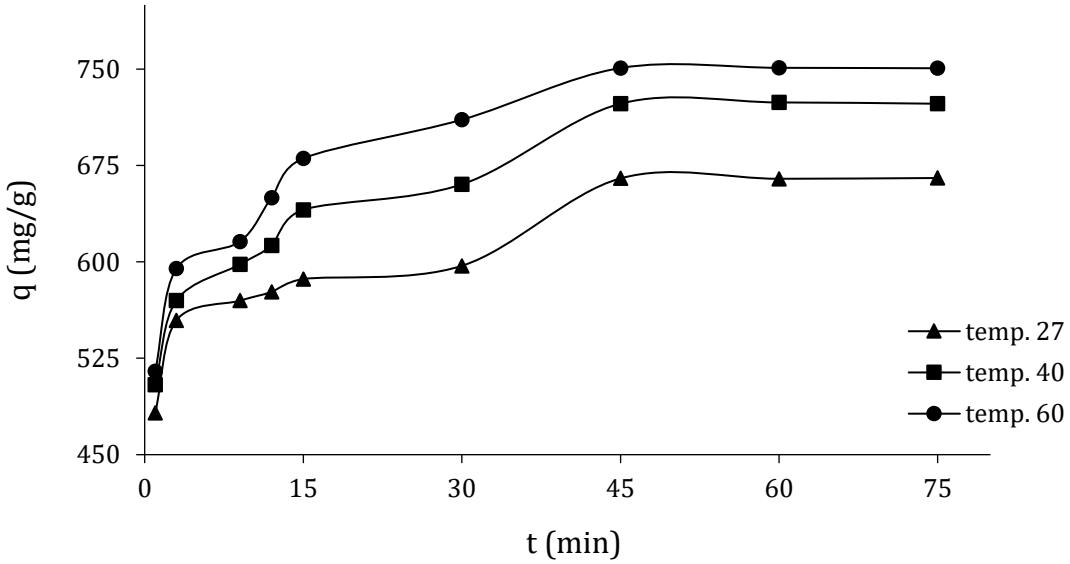

Figure 4.13. Agitation time effect of the BB dye adsorption onto GO/CS/EDTA at different temperatures

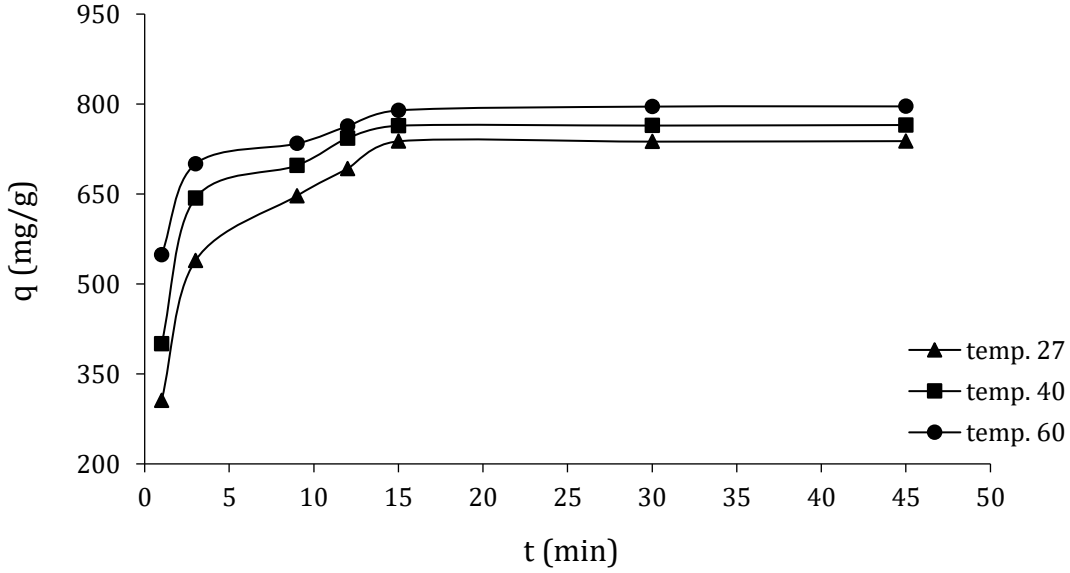

Figure 4.14. Agitation time effect of the BB dye adsorption onto GO/pBCM at different temperatures

4.2.4. Adsorption Isotherm of CR & BB Dyes

The adsorption isotherm shows the distribution of molecules between solid and liquid phases at an equilibrium state. The analysis of isotherm data by fitting them to different isotherm models is an essential important step in finding the most suitable model that can be used to describe the adsorption process [159]. To analyze the experimental adsorption results, there are several isotherm models to describe the isotherm data. In this study, Langmuir, Freundlich, Temkin, and Dubinin–Radushkevich models are employed.

4.2.4.1. Langmuir Isotherm

The Langmuir model depends upon the maximum adsorption that coincides with the saturated monolayer of adsorbate (liquid molecules) on the adsorbent (solid surface). The linearized form of the Langmuir model is given as follows [160].

$$\frac{\mathbf{C_e}}{\mathbf{q_e}} = \frac{\mathbf{1}}{(\mathbf{q_{max}}.\mathbf{k_L})} + \frac{\mathbf{C_e}}{\mathbf{q_{max}}} \quad \ldots\ldots (\mathbf{4.2})$$

Where Ce (mg/L) the dye equilibrium concentration; q_{max} (mg/g) the adsorption capacity required to complete monolayer on the adsorbent surface; q_e (mg/g) the amount of adsorbate per unit mass of adsorbent at equilibrium (mg/g); k_L (L/mg) Langmuir constant that relates to the energy of adsorption process, and when plotting C_e/q_e versus C_e, the slope of a plot equal to $(1/q_{max})$ and intercept equal to $(1/q_{max} . k_L)$

Langmuir equation is valid for monolayer adsorption of the adsorbate onto the surface of the adsorbent and assumes there are restricted and homogenous adsorption sites [161]. Hall *et al.* noted that the essential characteristics of a Langmuir isotherm can be expressed in terms of dimensionless constant separation factor or equilibrium parameter R_L [162] which is defined by:

$$\mathbf{R_L} = \frac{\mathbf{1}}{\mathbf{1} + (\mathbf{k_L}.\mathbf{C_e})} \quad \ldots\ldots (\mathbf{4.3})$$

R_L is indicative of the isotherm shape and predicts whether a sorption system to be either favorable ($0<R_L<1$), unfavorable ($R_L>1$), or irreversible ($R_L=0$) [163]. Figures (4.15 and 4.16) give the plots of the Langmuir isotherms of CR and BB dyes adsorbed onto GO, GO/DAB, GO/DAB/EDTA, GOCS, GO/CS/EDTA, and GO/pBCM respectively, and Table (4.3) displays q_{max}, k_L,

R_L and the correlation coefficient R^2 results for the Langmuir isotherms for the adsorption of these dyes by the prepared adsorbents.

Table 4.3. Langmuir isotherm parameters for adsorption of CR Dye onto Adsorbents at 27°C

Adsorbents	Dyes							
	CR				BB			
	q_{max}	k_L	R_L	R^2	q_{max}	k_L	R_L	R^2
GO	1250.0	0.0312	0.6063	0.9987	833.33	0.1263	0.0994	0.9988
GO/DAB	1428.5	0.0177	0.1579	1.0	1734.7	0.0425	0.0554	0.9929
GO/DAB/EDTA	1438.1	0.0178	0.1573	0.9969	1111.1	0.0238	0.0948	0.9993
GO/CS	2000.0	0.0450	0.0425	0.9994	920.74	0.0531	0.0449	0.9958
GO/CS/EDTA	1666.6	0.0612	0.0316	0.9999	863.88	0.0491	0.0483	0.9958
GO/pBCM	1304.9	0.0672	0.0472	0.9992	1000.0	0.0900	0.0270	0.9989

k: (L/mg), q_{max}: (mg/g)

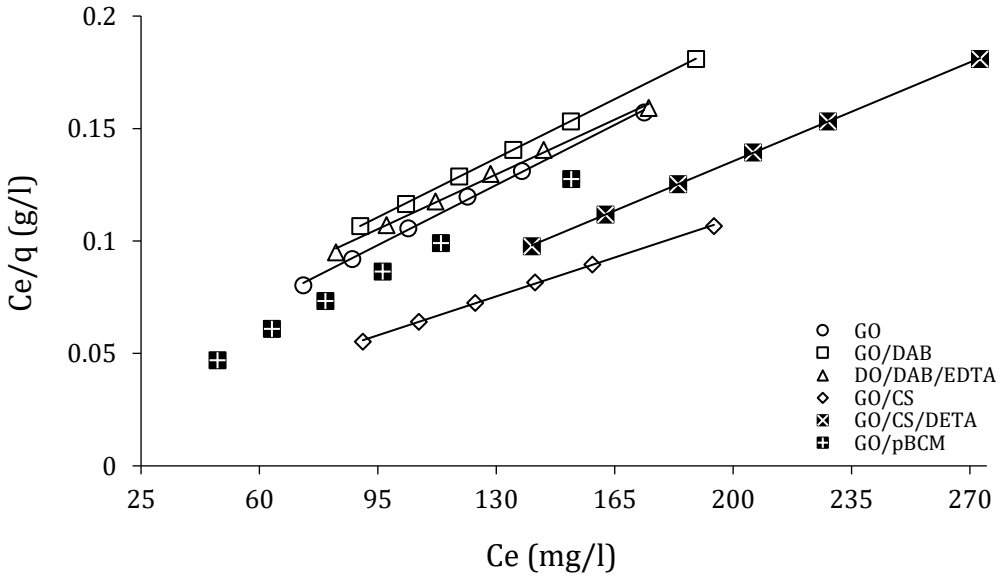

Figure 4.15. Langmuir adsorption isotherm of CR dye onto Adsorbents at 27°C

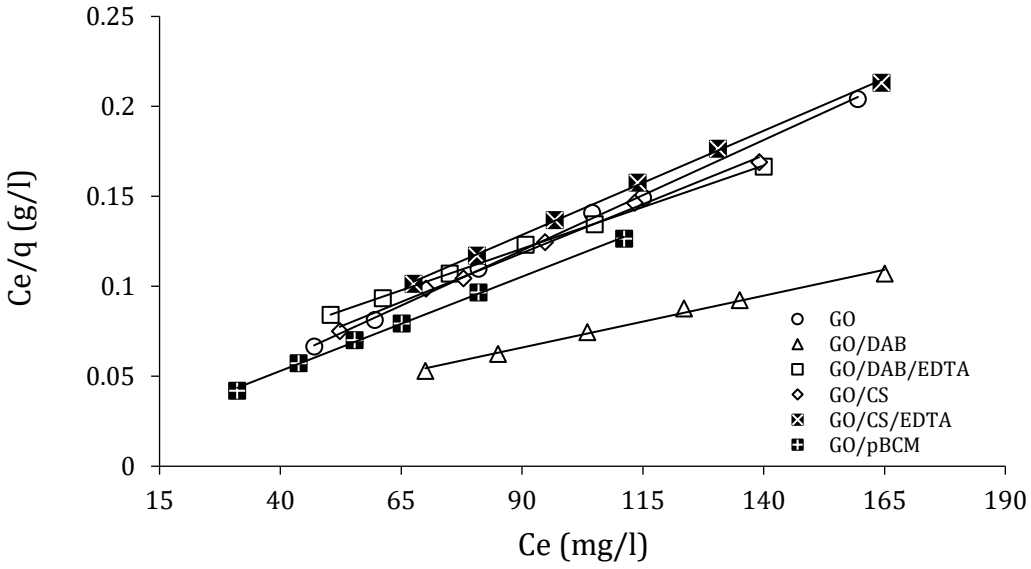

Figure 4.16. Langmuir adsorption isotherm of BB dye onto Adsorbents at 27°C

The obtained correlation coefficients R^2 for the Langmuir (as shown in Table 4.3) are $1 \geq R^2 \geq 0.9969$ for CR dye and $0.9993 \geq R^2 \geq 0.9929$ for BB dye. This describes the participation of the chemisorption mechanism in the adsorption process of dyes on the prepared adsorbents. In addition, to determine whether the adsorption process is favorable or unfavorable for the Langmuir isotherm model, the values of constant separation factor R_L, defined in the equation (4.3), are all between one and zero, implying the presence of a favorable condition for adsorption process of the prepared adsorbents by CR ($0.0316 \leq R_L \leq 0.6063$) and BB ($0.0270 \leq R_L \leq 0.0994$) dyes. Besides that, the R_L values of the adsorbents shown in Table (4.3) are lower than those of graphene oxide for both dyes, which indicates these prepared adsorbents from GO have a higher affinity towards CR and BB dyes.

This also indicates the formation of a monolayer of adsorbate molecules onto the homogeneous surface of the prepared adsorbent. Because we're inspired by the complexity of dye adsorption processes, it could say there was a tendency for chemical adsorption existing between functional groups of

prepared adsorbents and dyes [164, 165]. In addition, the results show that the q_{max} of the prepared adsorbents has values higher than graphene oxide; this indicates the ability and high efficiency of these adsorbents to absorb the CR and BB dyes from their aqueous solutions by the adsorption process.

4.2.4.2. Freundlich Isotherm

Freundlich isotherm model is based on a heterogeneous exponentially decaying distribution, which fits well with the tail portion of the heterogeneous distribution of adsorbent [166, 167]. The general Freundlich isotherm empirical equation is given by:

$$\ln q_e = \ln k_F + \frac{1}{n} \ln C_e \quad \ldots\ldots (4.4)$$

Where k_F (L/mg) is a constant for the adsorption or distribution coefficient and represents the amount of dye adsorbed onto adsorbents at the equilibrium concentration, and 1/n is the empirical parameter correlated to the intensity of the adsorption process or the surface heterogeneity of the adsorbent. A favorable adsorption process occurs with values between 0 and 1 [168].

Figures (4.17 and 4.18) represent the plots of the Freundlich adsorption isotherms of CR and BB dyes adsorbed onto GO, GO/DAB, GO/DAB/EDTA, GO/CS, GO/CS/EDTA, and GO/pBCM respectively, and Table (4.4) lists k_F, 1/n, and the correlation coefficient R^2 is determined from the linear plot of lnqe versus lnCe.

Freundlich isotherm considers the heterogeneous surface of the adsorbents, and the results indicated that the Freundlich model fit the experimental data less than the Langmuir model since the R^2 values are $0.9931 \leq R^2 \leq 0.9993$ and $0.9004 \leq R^2 \leq 0.9926$ for CR and BB dyes respectively as shown in Table (4.4). Nevertheless, these coefficient correlation values show good linearity.

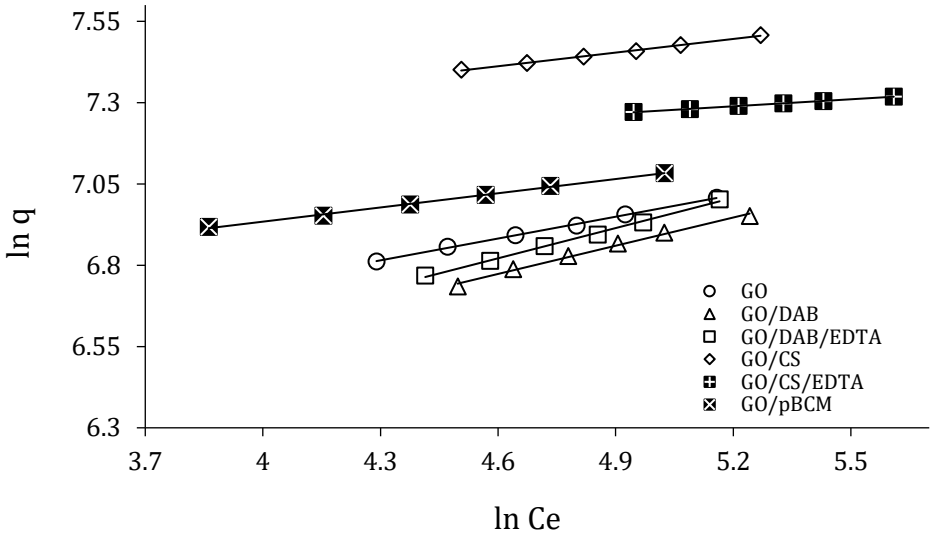

Figure 4.17. Freundlich adsorption isotherm of CR dye onto Adsorbents at 27°C

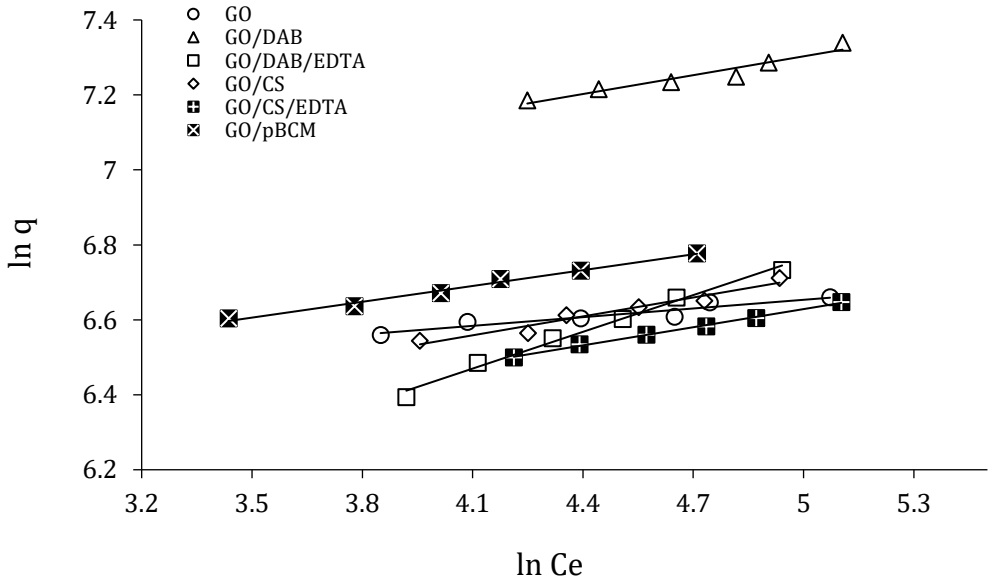

Figure 4.18. Freundlich adsorption isotherm of BB dye onto Adsorbents at 27°C

Table 4.4. Freundlich isotherm parameters for adsorption of CR and BB Dyes onto Adsorbents at 27°C

Adsorbents	Dyes					
	CR			BB		
	k_F	1/n	R^2	k_F	1/n	R^2
GO	348.278	0.2236	0.9982	527.158	0.7720	0.9004
GO/DAB	231.042	0.2892	0.9931	642.329	0.1676	0.9273
GO/DAB/EDTA	220.478	0.3099	0.9962	169.051	0.3268	0.9907
GO/CS	877.608	0.1380	0.9981	353.966	0.1682	0.9492
GO/CS/EDTA	1006.67	0.7020	0.9993	337.782	0.1612	0.9926
GO/pBCM	573.237	0.1457	0.9975	451.918	0.1407	0.9882

k: (L/mg)

Also, the results showed that k_F ranged from 220.478 to 1006.67 and from 169.051 to 642.329 $L.mg^{-1}$ for CR and BB dyes respectively, while 1/n values ranged from 0.1380 to 0.7020 for CR dye and from 0.1407 to 0.7720 for BB dye as shown in Table 4.4, which reflect the strength and practicality of the adsorption process. The 1/n values of CR dye are relatively close to BB dye is less than one, suggesting favorable adsorption of dyes on adsorbents, and in the current study, it becomes more heterogeneous as its value gets closer to zero [169].

4.2.4.3. Temkin Isotherm

The Temkin isotherm (the third isotherm studied for the adsorption of CR and dyes onto the prepared adsorbents) is based on the assumption that the heat of adsorption of all the molecules in a layer decreases linearly with coverage due to adsorbent-adsorbate (dyes) interactions and that the adsorption is characterized by a uniform distribution of the binding energies up to some maximum binding energy [170, 171].

The equation of the Temkin isotherm can be expressed in linear form as [172]:

$$\mathbf{q_e = B_T \ln A_T + B_T \ln C_e} \quad \ldots\ldots (\mathbf{4.5})$$

Where B_T (Temkin constant) =RT/b_T, T (K°) is absolute temperature, R (8.314 J/mol. K) is the universal gas constant, b_T (kJ/mol) is related to the heat of adsorption, and A_T (L/mg) is the equilibrium constant coinciding to the maximum binding energy. The plots of q_e versus lnC_e for the Temkin model

are shown in Figures (4.19 and 4.20) for the adsorption of CR and BB dyes onto prepared adsorbents respectively. The values of B_T and A_T are determined from the slope and intercept, and are given with the correlation coefficient R^2 for the Temkin isotherm in Table (4.5).

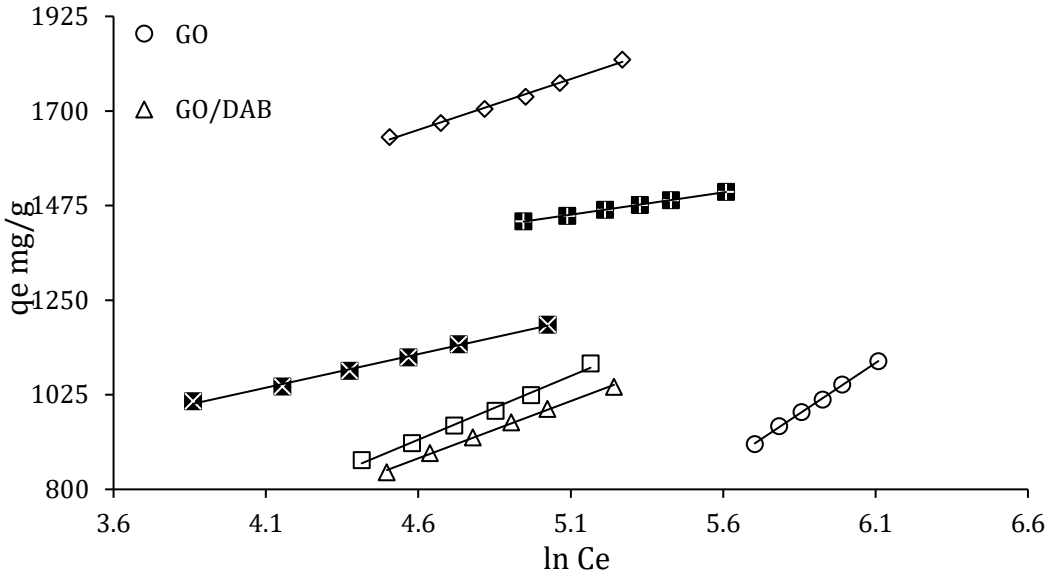

Figure 4.19. Temkin adsorption isotherm of CR dye onto Adsorbents at 27°

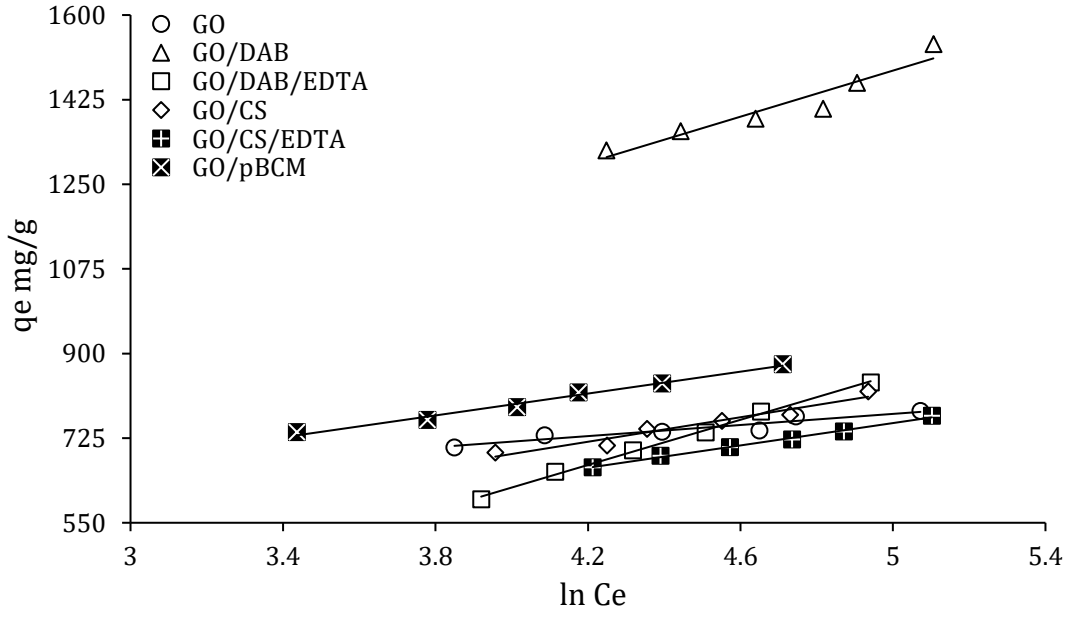

Figure 4.20. Temkin adsorption isotherm of BB dye onto Adsorbents at 27°C

Table (4.5) shows the values of correlation coefficient R^2 in Temkin isotherm for the adsorption of CR and BB dyes by adsorbents; GO, GO/DAB, GO/DAB/EDTA, GO/CS, GO/CS/EDTA, and GO/pBCM, and they are found lower than that of the Langmuir and Freundlich isotherm models, indicating the adsorption data doesn't fit well to the Temkin isotherm model.

Table 4.5. Temkin isotherm parameters for adsorption of CR and BB Dyes onto Adsorbents at 27°C

Adsorbents	Dyes					
	CR			BB		
	b_T	A_T	R^2	b_T	A_T	R^2
GO	23.548	45.607	0.9967	34.455	49.078	0.8989
GO/DAB	9.172	4.0061	0.9975	10.477	3.4390	0.9163
GO/DAB/EDTA	8.238	4.8022	0.9918	10.687	3.7902	0.9968
GO/CS	10.327	9.4826	0.9951	19.700	4.3268	0.9440
GO/CS/EDTA	5.169	55.074	0.9989	21.603	4.6947	0.9949
GO/pBCM	15.621	11.266	0.9958	22.062	20.592	0.9859

b_T: (J/mol), A_T: (L/mg)

According to the Temkin isotherm model (chosen to estimate the adsorption potentials of the adsorbent for adsorbing the adsorbate molecule), there is a non-linear increase in the heat of adsorption for both dyes in the layers, which is may attribute to different adsorbent–adsorbate interactions. Likewise, the correlation coefficients are ($0.9918 \leq R^2 \leq 0.9989$) and ($0.8989 \leq R^2 \leq 0.9968$) for CR and BB dyes respectively, indicate that the data partially satisfied Temkin adsorption isotherm and show good linearity which is an indication of the interaction between CR and BB dyes and the prepared adsorbents as listed in Table (4.5).

The Temkin constant b_T related to the heat of adsorption was also calculated, and the results show that these values were decreased for all

adsorbents compared to the values of GO (for both CR and BB dyes). Whereas, the smaller values of b_T for all prepared adsorbents suggest that the adsorption of both dyes was favorable, and the positive values indicating endothermic adsorption [173].

4.2.4.4. Dubinin–Radushkevich Isotherm

The Dubinin–Radushkevich (D-R) isotherm is an empirical model initially conceived for the adsorption of subcritical vapors onto micropore solids following a pore-filling mechanism. It is generally applied to express the adsorption mechanism [174]. Even it has a similar approach to Langmuir isotherm by rejecting the homogenous surface or constant adsorption potential; D-R version is more general than the Langmuir version in exploring adsorption isotherm, and the D-R isotherm model equation can be linearized in the following equation [175]:

$$\mathbf{ln q_e = ln q_{max} - \beta \varepsilon^2} \quad \ldots\ldots (\mathbf{4.6})$$

Where q_{max} (mg/g) is the D-R monolayer capacity, β (mol^2/kJ^2) is a constant related to adsorption energy, and ε is the Polanyi potential which is associated with the equilibrium concentration as shown in the equation [176]:

$$\boldsymbol{\varepsilon = RTln\left(1 + \frac{1}{C_e}\right)} \quad \ldots\ldots (\mathbf{4.7})$$

Where R (kJ mol^{-1} K^{-1}) is the universal gas constant, T the temperature in Kelvin, and C_e (mg/L) is the equilibrium concentration of adsorbate in solution. A plot of the amount of the prepared adsorbents in the form of lnq_e vs. ε^2 is shown in Figures (4.21 and 4.22) for the adsorption of CR and BB dyes onto prepared adsorbents.

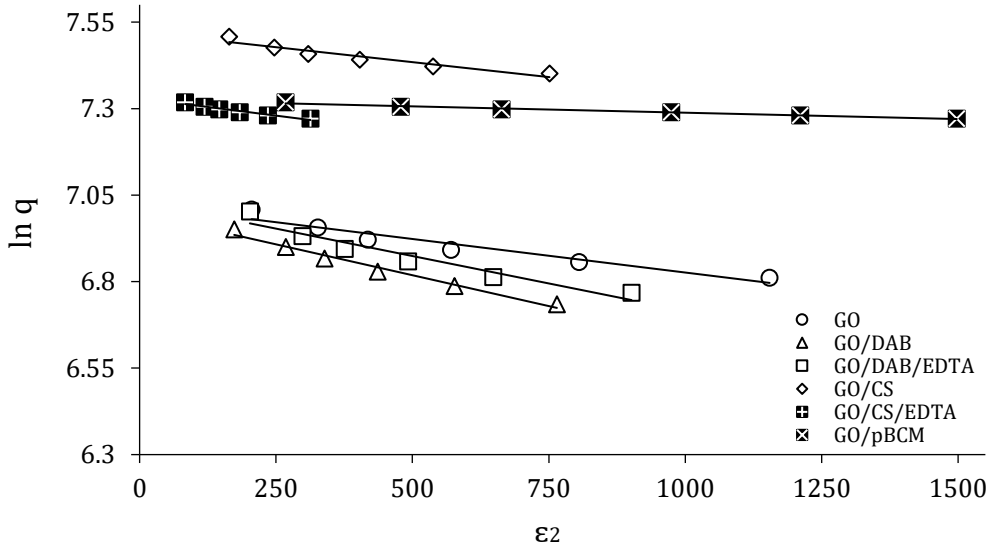

Figure 4.21. D-R adsorption isotherm of CR dye onto Adsorbents at 27°

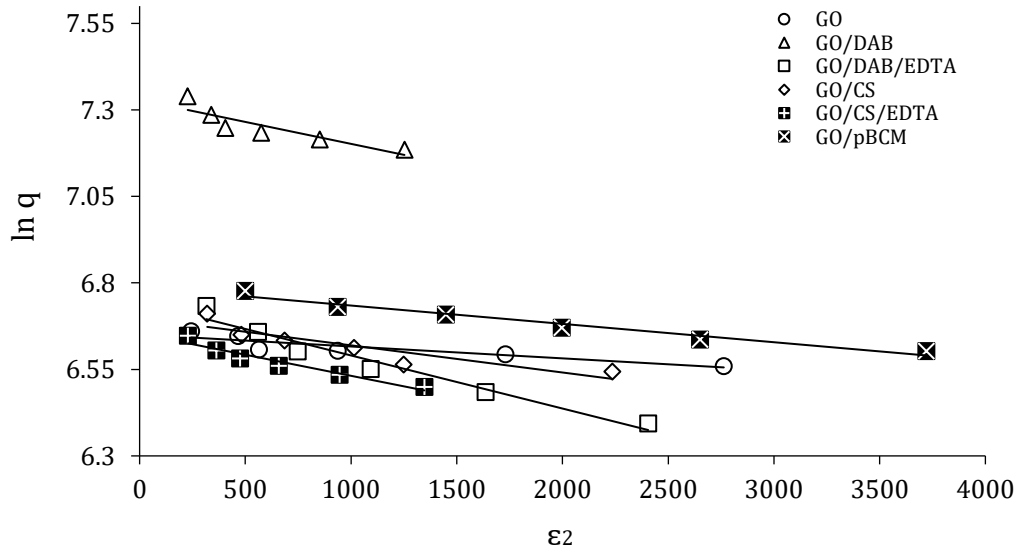

Figure 4.22. D-R adsorption isotherm of BB dye onto Adsorbents at 27°

The constants, such as q_{max} and β were determined from the intercept and the slope respectively. This approach is usually applied to distinguish the physical and chemical adsorption process [177], through the mean free energy E per molecule of adsorbate (for removing a molecule from its location in the sorption space to the infinity) can be computed by the relationship [178]:

$$\mathbf{E} = \frac{\mathbf{1}}{\sqrt{\mathbf{2}\,\boldsymbol{\beta}}} \quad \ldots\ldots (\mathbf{4.8})$$

From the linear plot of the D-R isotherm model; q_{max}, β (mol^2/kJ^2), E (kJ/mole), and R^2 are determined and listed in Table (4.6) for the adsorption of CR and BB dyes by the prepared adsorbents GO, GO/DAB, GO/DAB/EDTA, GO/CS, GO/CS/EDTA, and GO/pBCM respectively.

Table 4.6. D-R isotherm parameters for adsorption of CR and BB Dyes onto Adsorbents at 27°C

Adsorbents	Dyes							
	CR				BB			
	q_{max}	β	E	R^2	q_{max}	β	E	R^2
GO	1118.9	2E-04	50.78	0.9332	772.78	3E-05	120.73	0.8127
GO/DAB	1093.2	4E-04	35.35	0.9798	1523.8	1E-04	62.79	0.7901
GO/DAB/EDTA	1132.6	3E-04	40.82	0.9284	848.94	2E-04	57.11	0.9566
GO/CS	1845.6	2E-04	53.80	0.9238	1523.4	1E-04	62.79	0.7901
GO/CS/EDTA	1525.0	2E-04	49.87	0.9512	775.30	1E-04	64.09	0.9287
GO/pBCM	1499.8	2E-05	168.16	0.8463	857.13	3E-05	135.08	0.8244

q_{max}: (mg/g); β: (mol^2/kJ^2); E: (kJ/mol)

The adsorption behavior might have predicted the physical adsorption in the range of (1–8 kJ/mol) of the mean adsorption energy, and the chemical adsorption in more than (8 kJ/mol) of the mean adsorption energy E [179, 180]. As shown in Table (4.3) the values of the mean adsorption energies (E) calculated using Equation (4.8) of the CR and BB dyes onto adsorbents; GO,

GO/DAB, GO/DAB/EDTA, GO/CS, GO/CS/EDTA, and GO/pBCM are 35.35 to 168.1 and from 57.11 to 135.0 kJ/mol respectively, indicated that the adsorptions of both CR and BB dyes onto these prepared adsorbents were predominant on the chemisorption process [181, 182]. A comparison of the correlation coefficients R^2 of D-R isotherm (0.8463-0.9798 and 0.7901-0.9287) for adsorption of CR and BB dyes onto the prepared adsorbents respectively, reveals the fact that the adsorption behavior is not fit quite well with corresponding to the other, especially Langmuir and Freundlich isotherm models.

ased on the linear plot obtained from the D-R isotherm model and as shown in Table (4.3); the q_{max} values are determined to be (1039.2-1845.6 and 772.78-1523.8) mg/g for adsorption of CR and BB dyes respectively, and these values were close to the maximum monolayer coverage capacity q_{max} which is calculated by the Langmuir isotherm model.

Consequently, comparing the values of R^2 exhibit that they fit linearly with most of the equations of adsorption isotherms, and they are good for studying the adsorption of both CR and BB dyes on the adsorbents within the used initial concentration range, although they fit better with the Langmuir isotherm equation, in additional of R_L data of this isotherm.

Also, through the adsorption isotherms study, it is found that the adsorption process behavior of both dyes on the prepared adsorbents obeys the chemisorption process.

4.2.5. Adsorption Kinetics of CR & BB Dyes

Kinetics data help to depict dye uptake rates, which control the residence time of adsorbate at the solid-liquid interface and give valuable information for adsorption process designing [183]. Also, the experimental kinetic curves can be assessed using many various models [16, 184]. Therefore, in this study the appropriateness of pseudo-first-order, pseudo-second-order, and intra-particle diffusion is tested to interpret the mechanism of CR & BB dye adsorption onto the prepared adsorbents GO, GO/DAB, GO/DAB/EDTA, GOCS, GO/CS/EDTA, and GO/pBCM.

4.2.5.1. The Pseudo-First-Order Model

The first model was pseudo-first-order, is one of the most widely used equations for the sorption of solute from a liquid solution [185], and the mathematical expression of this model given by the equation (4.9):

$$\ln q_{e-}q_t = \ln q_1 - k_1 t \quad \ldots\ldots (4.9)$$

Where q_t and q_1 (mg/g) are the amounts of dye adsorbed at time t and the maximum adsorption capacity for the pseudo-first-order respectively. k_1 (min^{-1}) is the pseudo-first-order rate constant for adsorption. A plotting of (lnq_e-q_t) against (t) will result in a straight line of the slope of k_1 and intercept of lnq_e.

Figures (4.23-4.28 and 4.29-4.34) show the pseudo-first-order equations for both CR and BB dyes respectively at different temperatures (27, 40, and 60°C), and Table (4.7) gives the values of k_1, q_1, and R^2 for the pseudo-first-order equations.

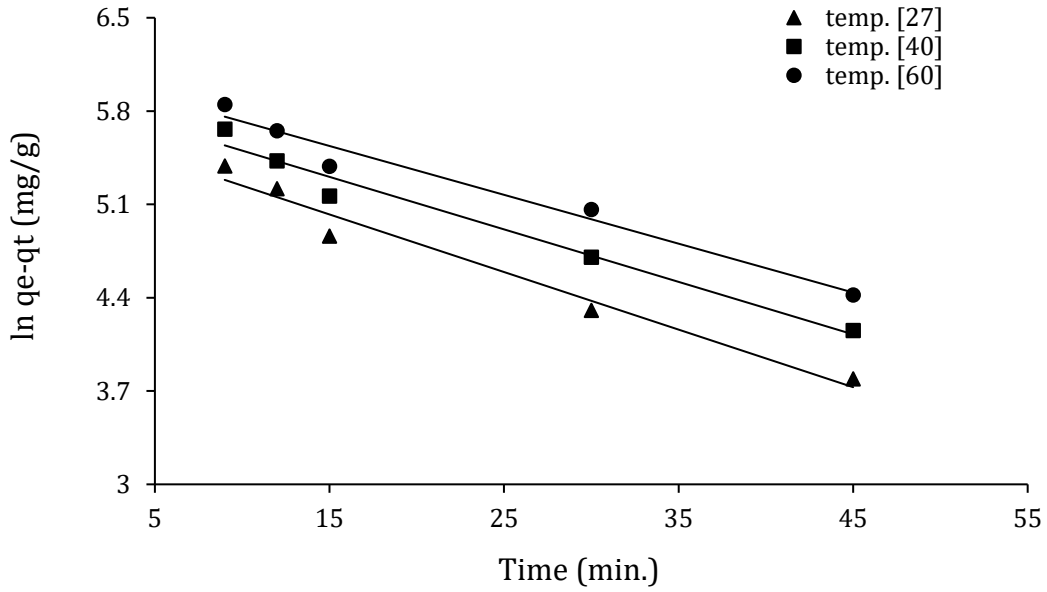

Figure 4.23. Pseudo-First-Order plot for the adsorption of CR dye onto GO at 27°C, 40°C, and 60°C

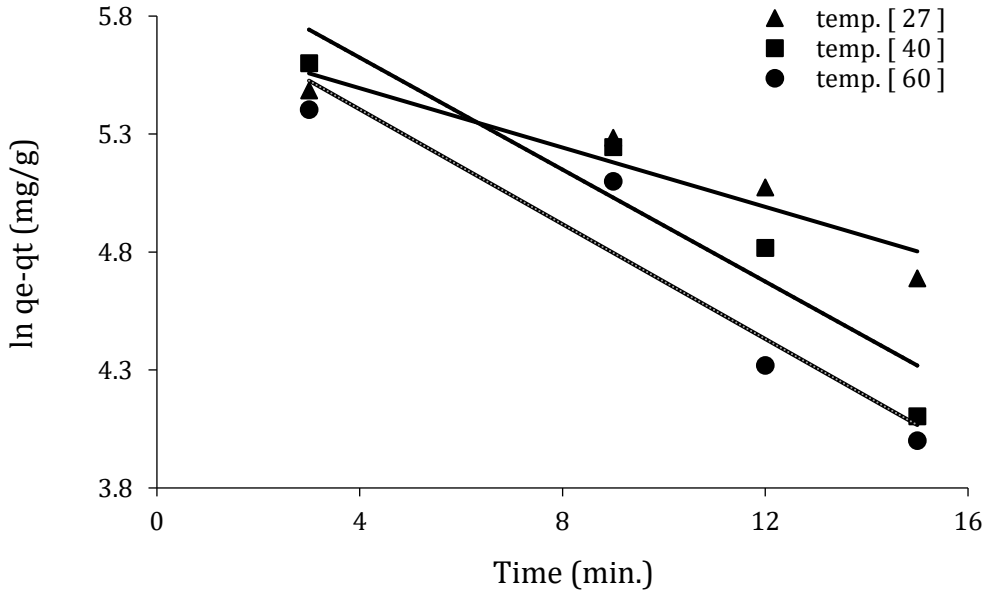

Figure 4.24. Pseudo-First-Order plot for the adsorption of CR dye onto GO/DAB at 27°C, 40°C, and 60°C

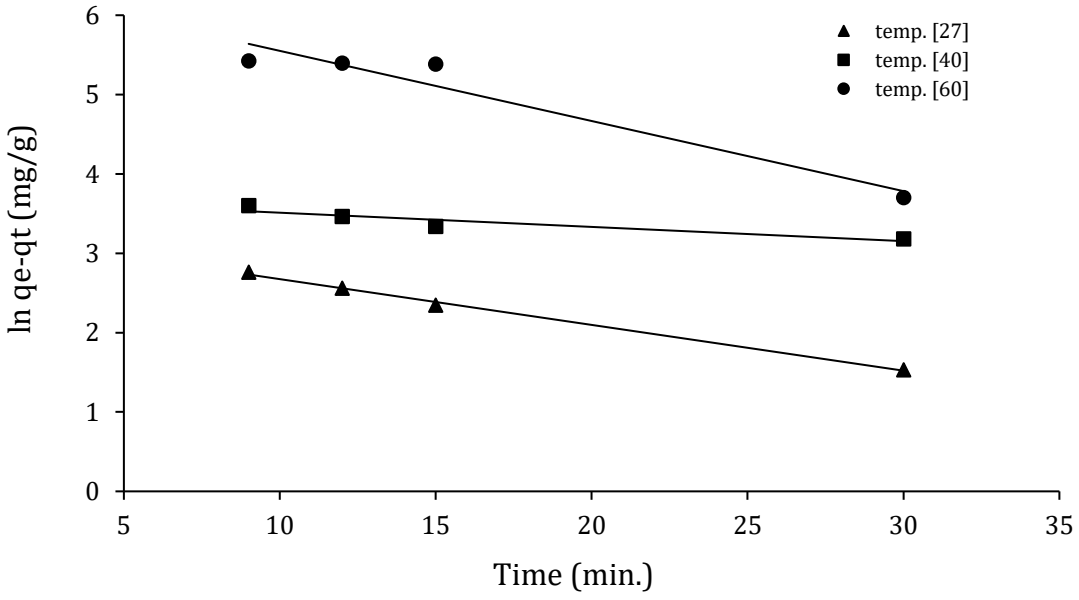

Figure 4.25. Pseudo-First-Order plot for the adsorption of CR dye onto GO/DAB/EDTA at 27°C, 40°C, and 60°C

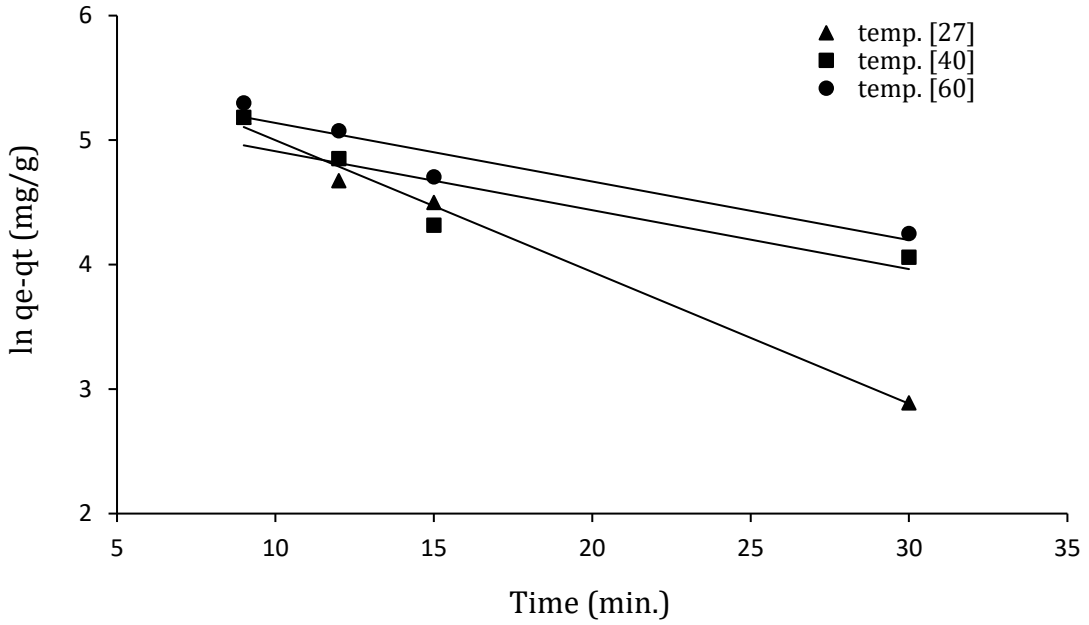

Figure 4.26. Pseudo-First-Order plot for the adsorption of CR dye onto GO/CS at 27°C, 40°C, and 60°C

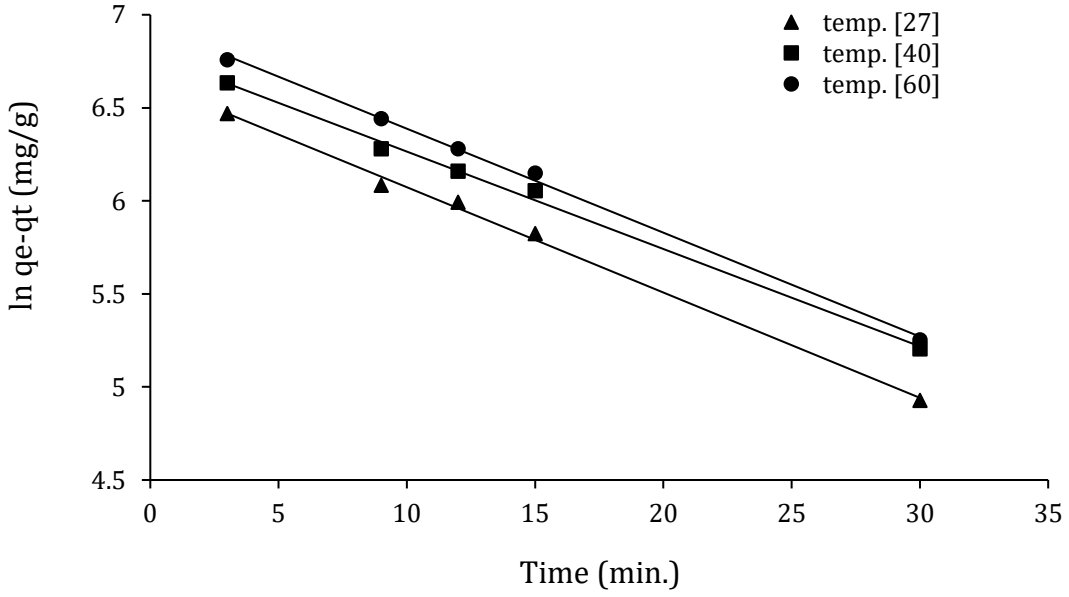

Figure 4.27. Pseudo-First-Order plot for the adsorption of CR dye onto GO/CS/EDTA at 27°C, 40°C, and 60°C

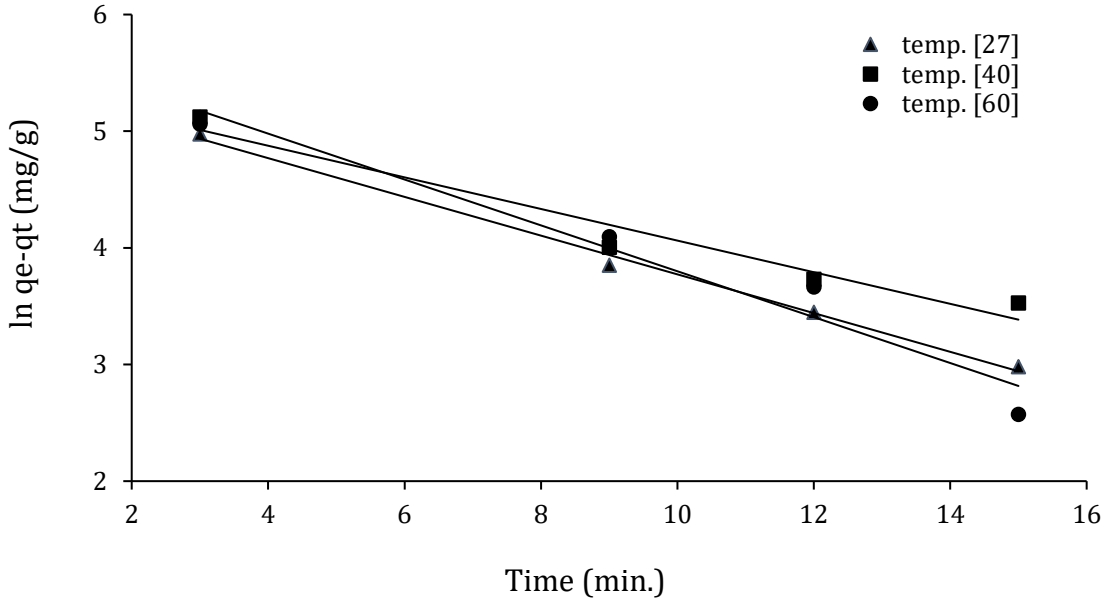

Figure 4.28. Pseudo-First-Order plot for the adsorption of CR dye onto GO/pBCM at 27°C, 40°C, and 60°C

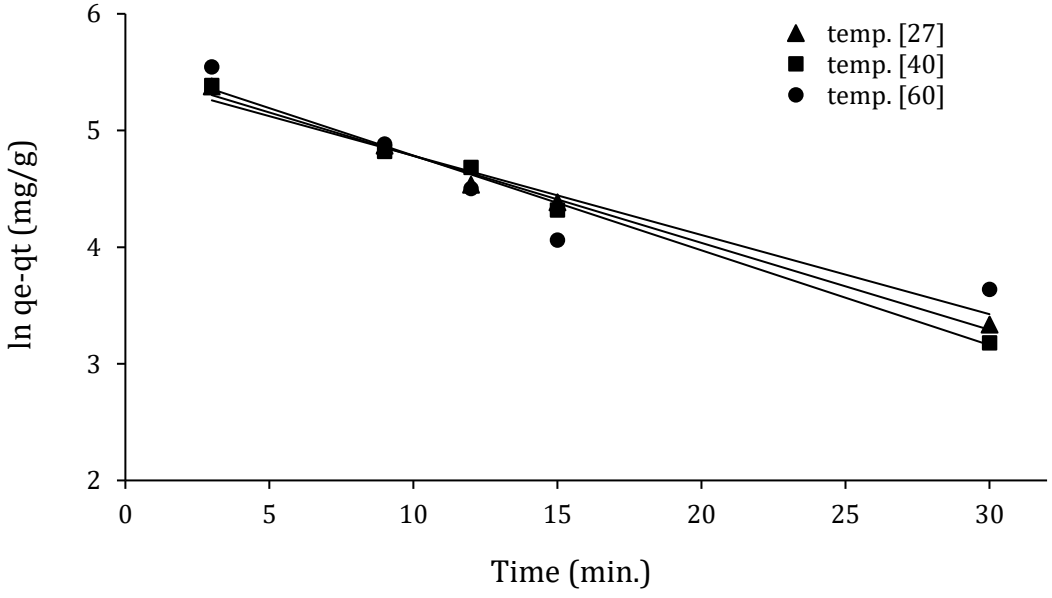

Figure 4.29. Pseudo-First-Order plot for the adsorption of BB dye onto GO at 27°C, 40°C, and 60°C

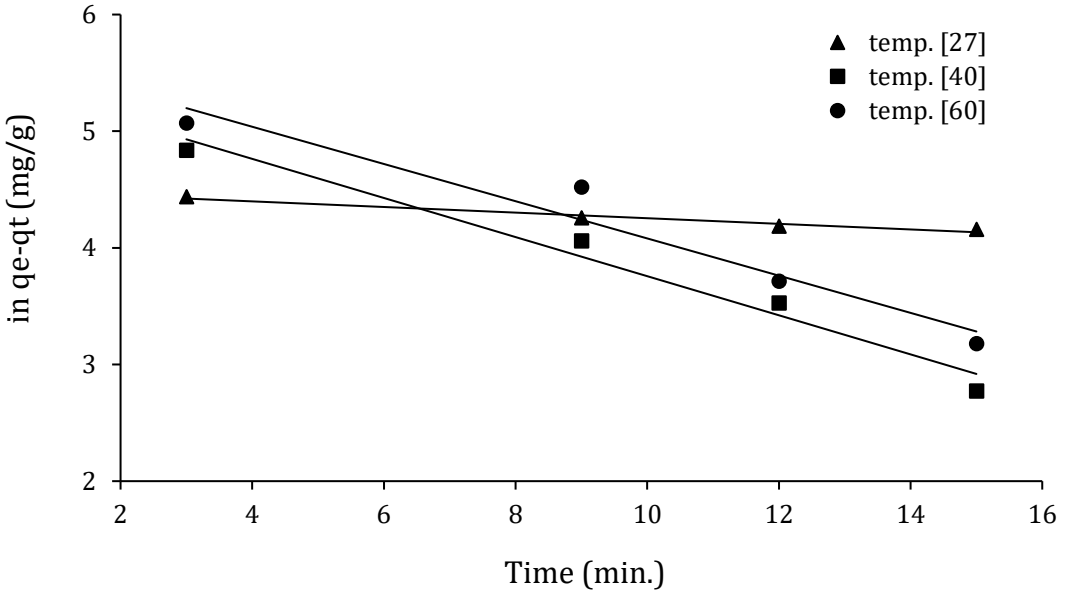

Figure 4.30. Pseudo-First-Order plot for the adsorption of BB dye onto GO/DAB at 27°C, 40°C, and 60°C

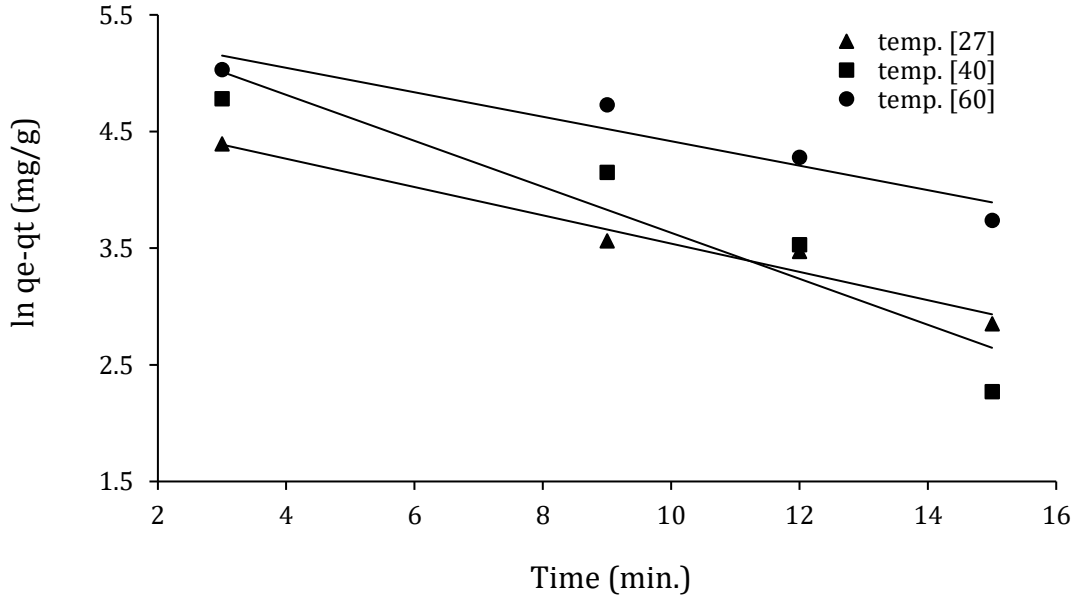

Figure 4.31. Pseudo-First-Order plot for the adsorption of BB dye onto GO/DAB/EDTA at 27°C, 40°C, and 60°C

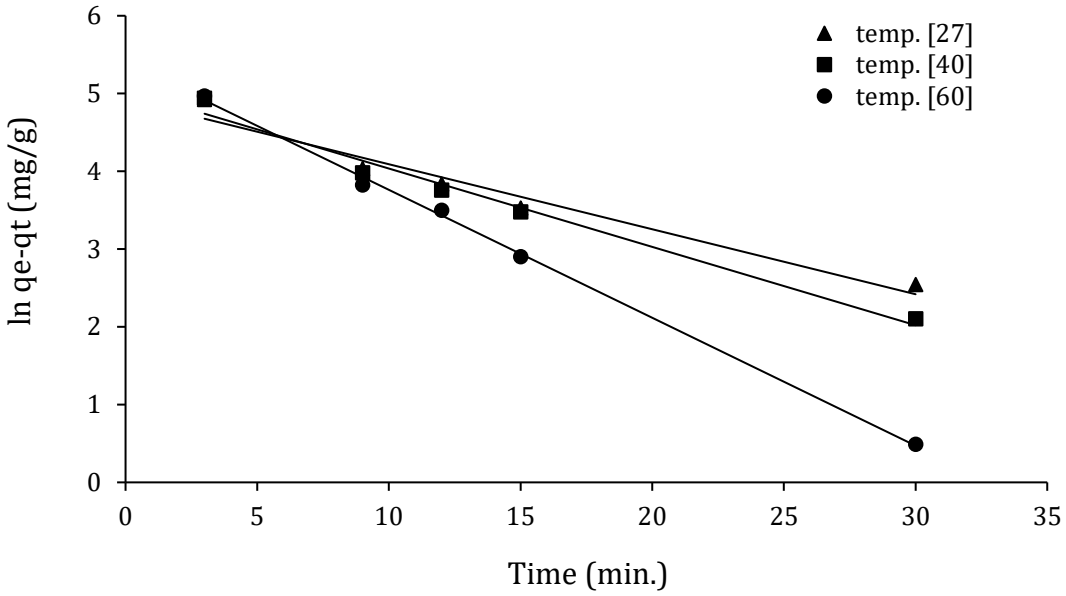

Figure 4.32. Pseudo-First-Order plot for the adsorption of BB dye onto GO/CS at 27°C, 40°C, and 60°C

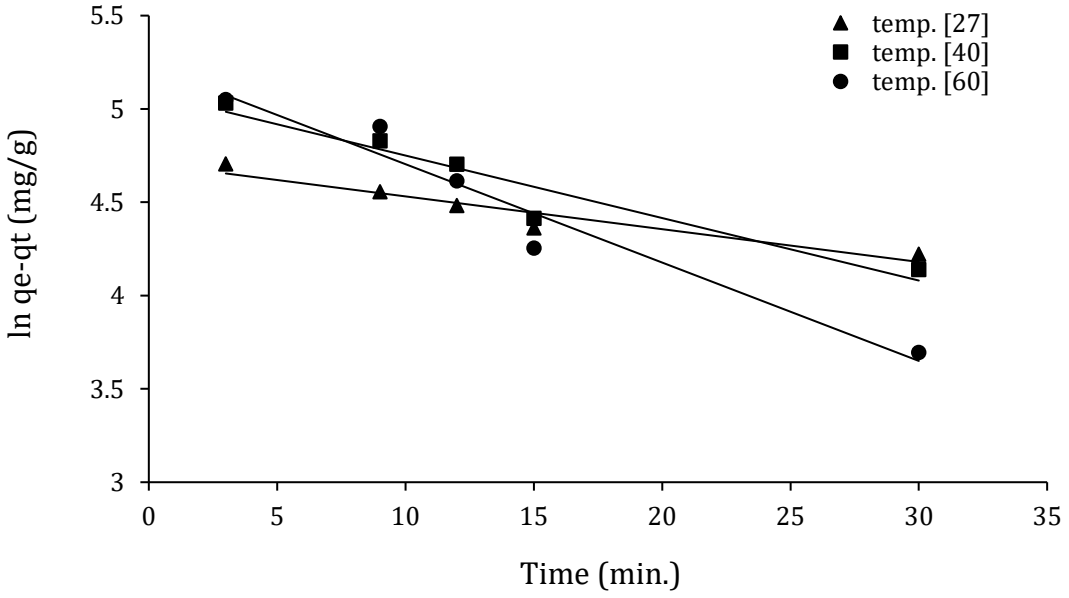

Figure 4.33. Pseudo-First-Order plot for the adsorption of BB dye onto GO/CS/EDTA at 27°C, 40°C, and 60°C

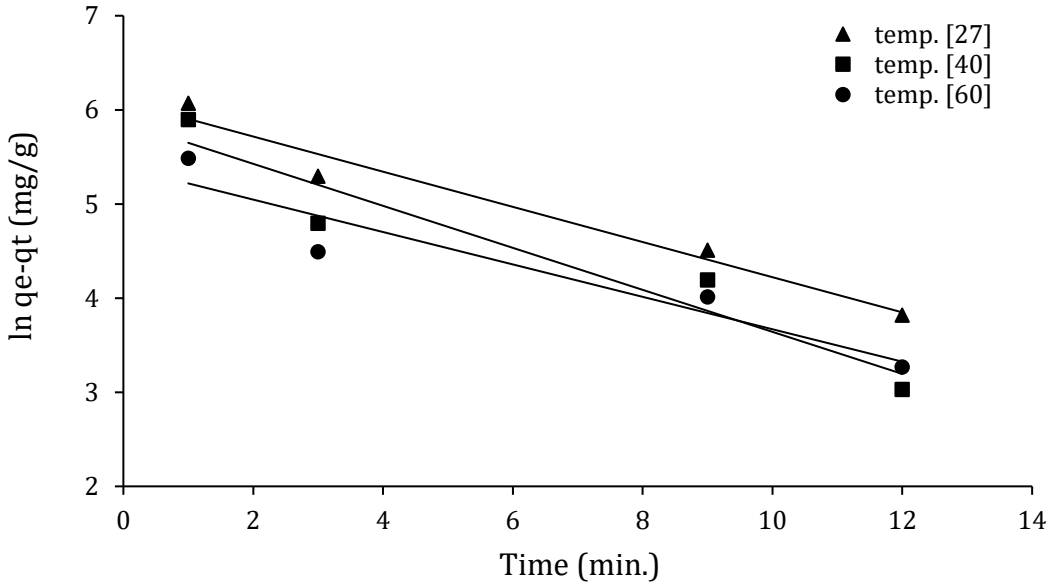

Figure 4.34. Pseudo-First-Order plot for the adsorption of BB dye onto GO/pBCM at 27°C, 40°C, and 60°C

All the other kinetic data for adsorption of CR and BB dyes onto the prepared adsorbents GO, GO/DAB, GO/DAB/EDTA, GO/CS, GO/CS/EDTA, and GO/pBCM under different temperatures (i.e. 27, 40, and 60°C) are calculated from the related plots for the pseudo-first-order model and are summarized in Table (4.7).

Table 4.7. Pseudo-First-Order parameters for adsorption of CR and BB dyes onto prepared adsorbents at different temperatures

Adsorbents	Tem.	CR Dye			BB Dye		
		k_1	q_1	R_1^2	k_1	q_1	R_1^2
GO	27	0.0432	290.84	0.9711	0.0745	251.36	0.9922
	40	0.0394	364.05	0.9747	0.0812	251.36	0.9960
	60	0.0366	440.58	0.9704	0.0679	235.61	0.8633
GO/DAB	27	0.0629	312.93	0.8962	0.0241	89.550	0.9653

	40	0.1187	445.23	0.8928	0.1676	228.88	0.9738
	60	0.1216	361.83	0.9039	0.1596	291.8	0.9484
GO/DAB/EDTA	27	0.0577	25.818	0.9969	0.1212	115.75	0.9611
	40	0.0179	40.056	0.8670	0.1971	271.13	0.8886
	60	0.0884	623.09	0.9402	0.1049	236.39	0.9099
GO/CS	27	0.1058	427.22	0.9932	0.0836	137.93	0.9583
	40	0.0473	217.93	0.7570	0.1007	154.90	0.9811
	60	0.047	272.68	0.9128	0.1645	222.85	0.9982
GO/CS/EDTA	27	0.0566	764.55	0.9965	0.0176	110.71	0.9180
	40	0.0523	887.31	0.9691	0.0335	161.59	0.9256
	60	0.0559	1039.40	0.9891	0.0527	186.97	0.9495
GO/pBCM	27	0.166	228.83	0.9950	0.1868	441.55	0.9667
	40	0.1355	228.83	0.9516	0.2232	355.34	0.9153
	60	0.1967	319.16	0.9634	0.1722	219.44	0.9033

k_1: (min^{-1}), q: (mg/g), Temperature: (°C)

4.2.5.2. The Pseudo-Second-Order Model

The second kinetic model was pseudo-second-order, which shows the rate based on the sorption equilibrium capacity in the adsorbent and not on the

concentration of the adsorbate [186]. This can be represented by the equation (4.10):

$$\frac{t}{q_t} = \frac{1}{k_2 . q_2^2} + \frac{t}{q_2} \quad \ldots\ldots (4.10)$$

Where q_2 (mg/g) is the maximum adsorption capacity for the pseudo-second-order and k_2 (g mg^{-1} min^{-1}) is the equilibrium rate constant for pseudo-second-order adsorption. Values of q_2 and k_2 are calculated from the plotting of (t/q_t) against (t) from the slope and intercept, as shown in Figures (4.35-4.40 and 4.41-4.46) for CR and BB dyes respectively.

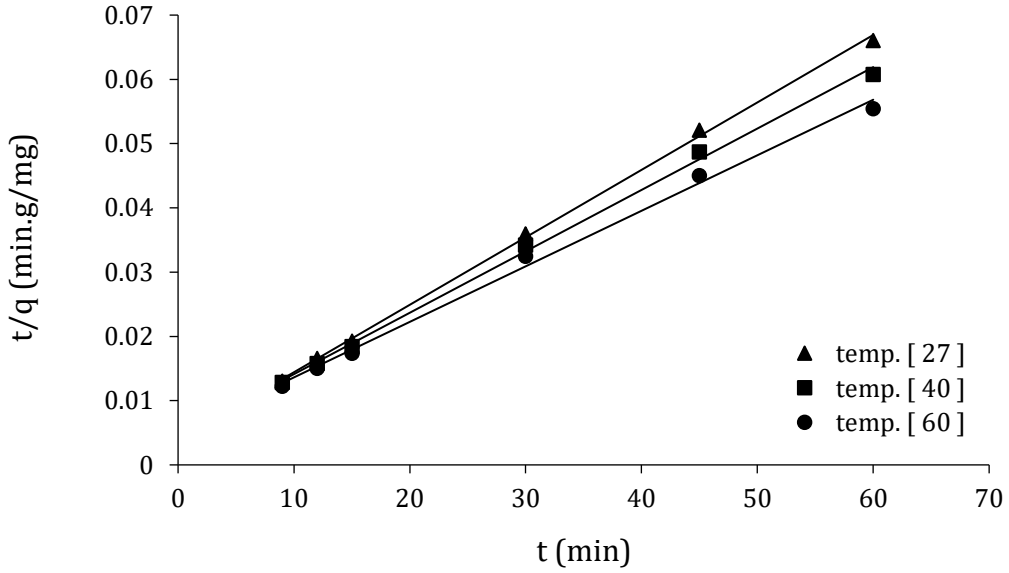

Figure 4.35. Pseudo-Second-Order plot for the adsorption of CR dye onto GO at 27°C, 40°C, and 60°C

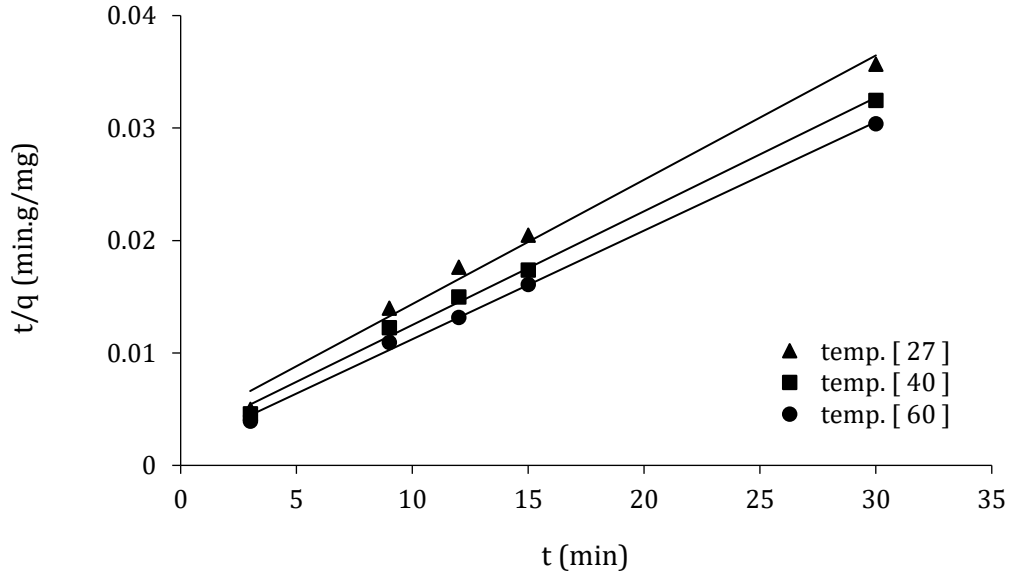

Figure 4.36. Pseudo-Second-Order plot for the adsorption of CR dye onto GO/DAB at 27°C, 40°C, and 60°C

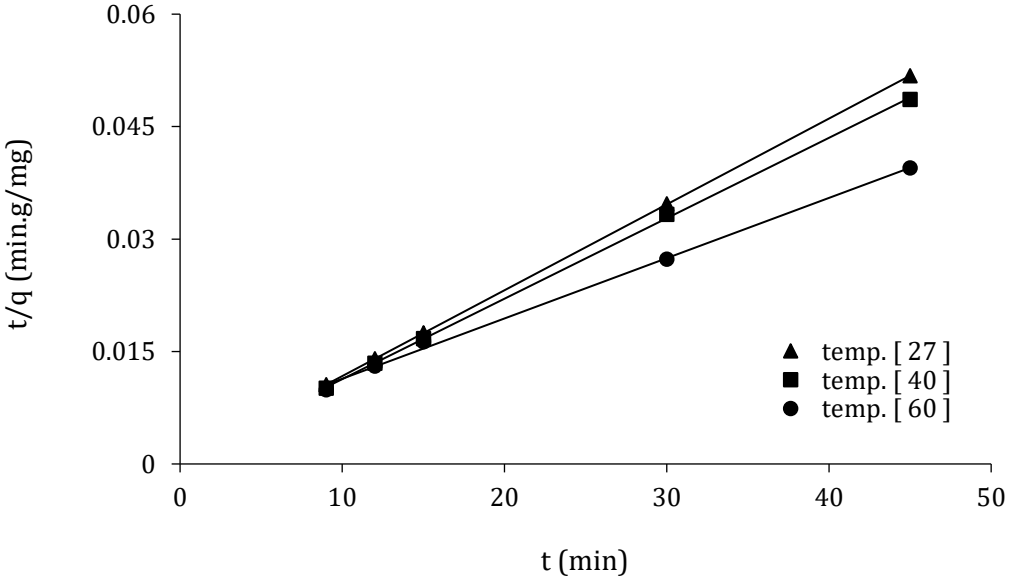

Figure 4.37. Pseudo-Second-Order plot for the adsorption of CR dye onto GO/DAB/EDTA at 27°C, 40°C, and 60°C

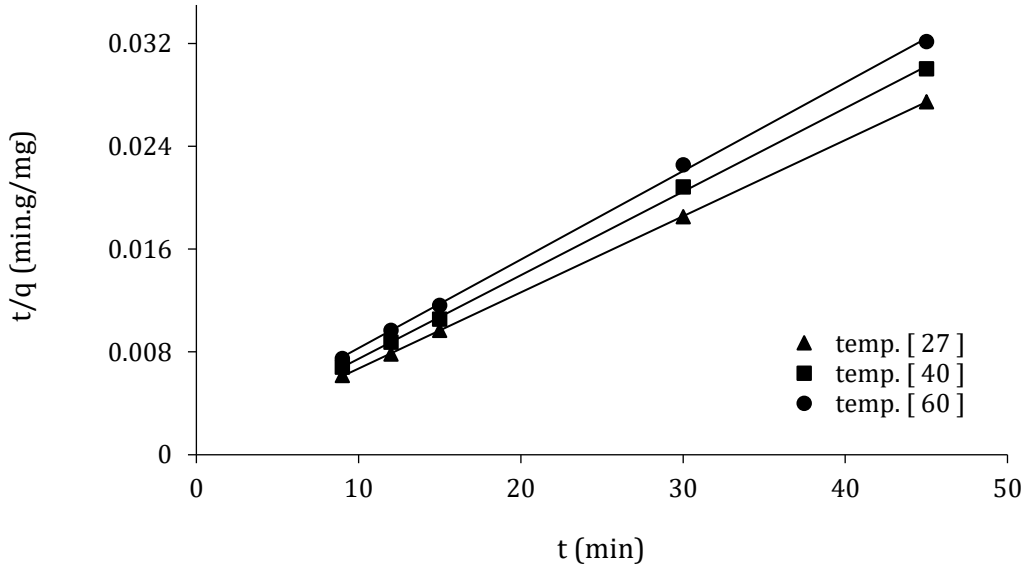

Figure 4.38. Pseudo-Second-Order plot for the adsorption of CR dye onto GO/CS at 27°C, 40°C, and 60°C

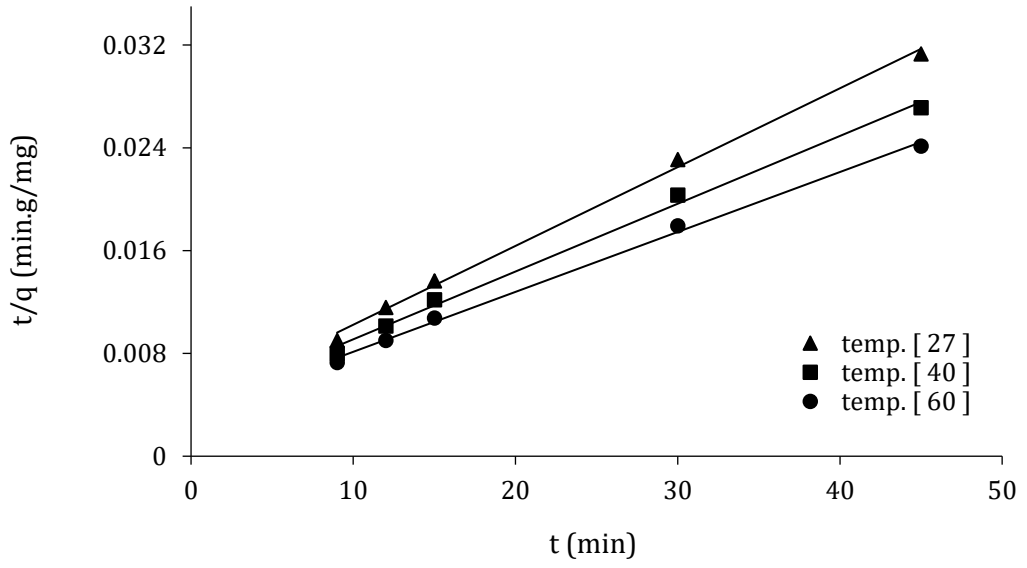

Figure 4.39. Pseudo-Second-Order plot for the adsorption of CR dye onto GO/CS/EDTA at 27°C, 40°C, and 60°C

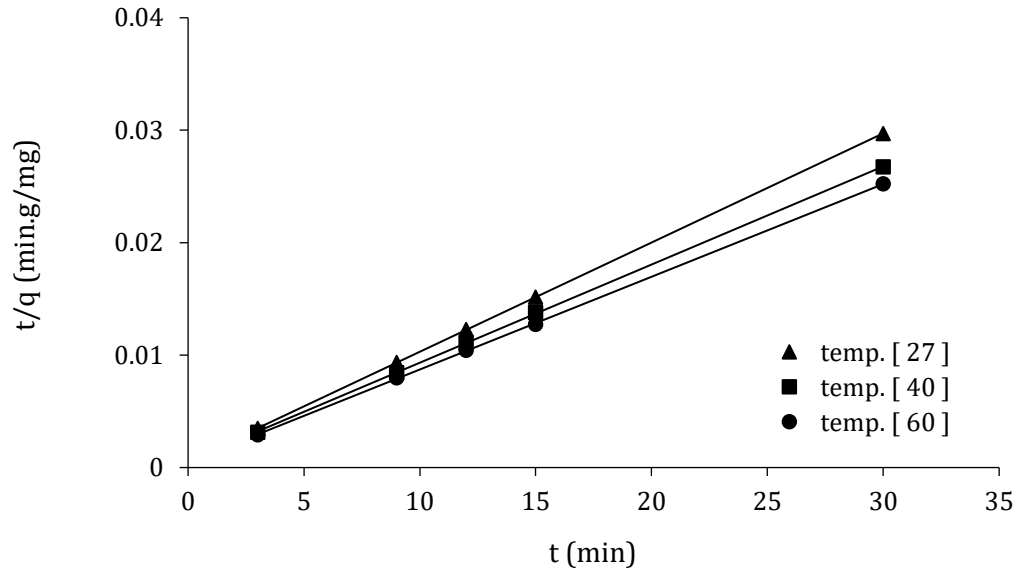

Figure 4.40. Pseudo-Second-Order plot for the adsorption of CR dye onto GO/pBCM at 27°C, 40°C, and 60°

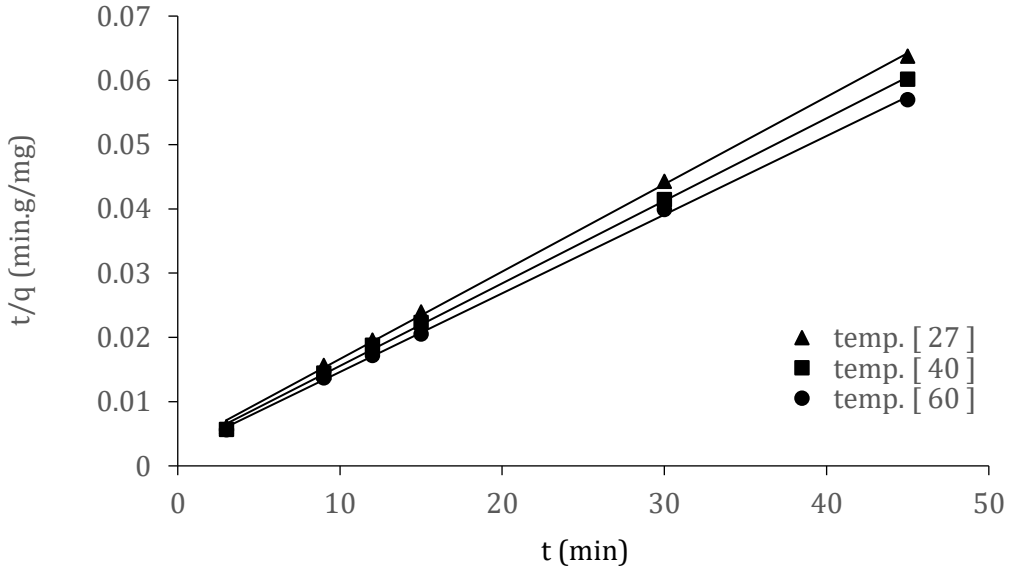

Figure 4.41. Pseudo-Second-Order plot for the adsorption of BB dye onto GO at 27°C, 40°C, and 60°

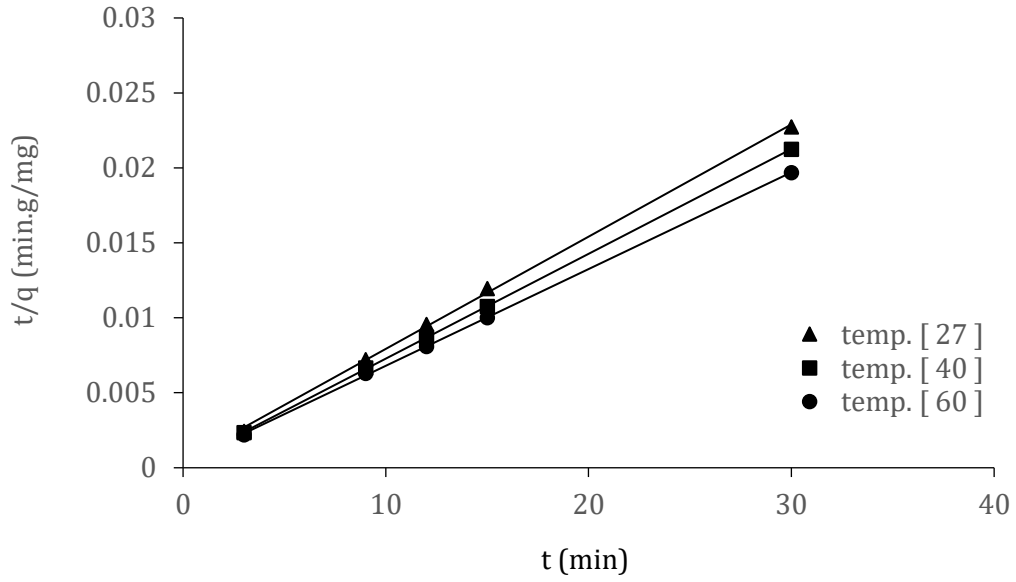

Figure 4.42. Pseudo-Second-Order plot for the adsorption of BB dye onto GO/DAB at 27°C, 40°C, and 60°

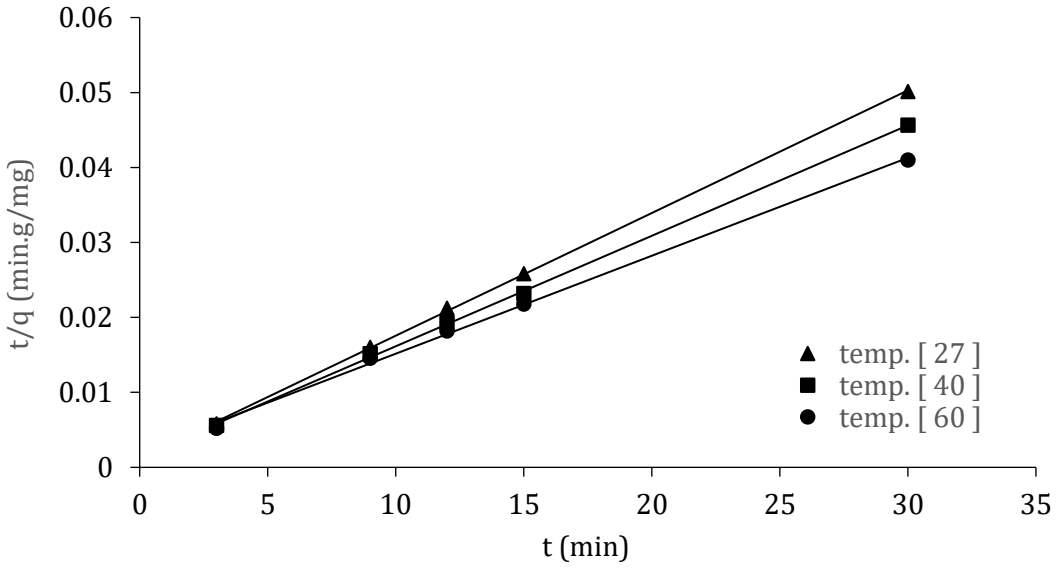

Figure 4.43. Pseudo-Second-Order plot for the adsorption of BB dye onto GO/DAB/EDTA at 27°C, 40°C, and 60°

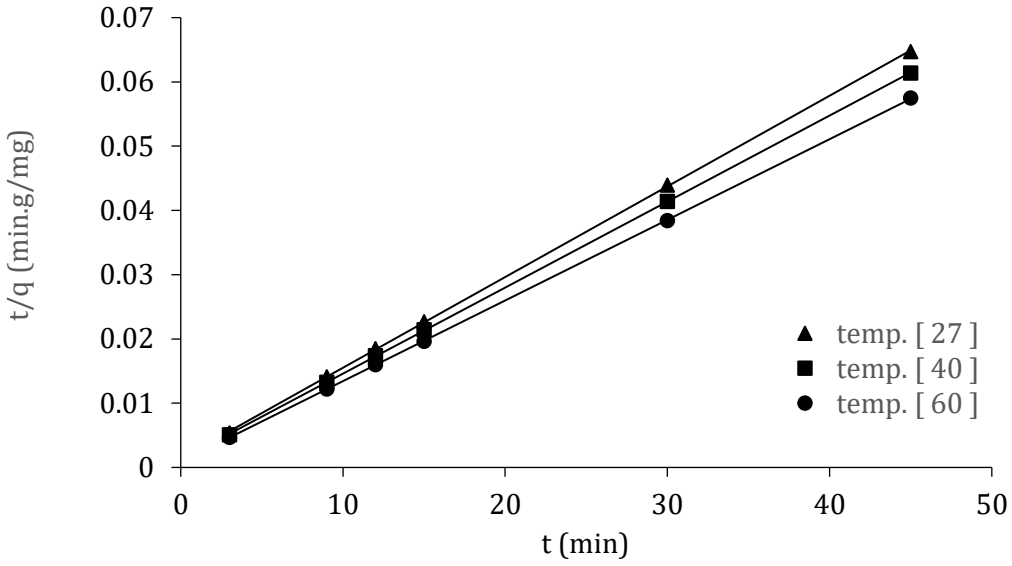

Figure 4.44. Pseudo-Second-Order plot for the adsorption of BB dye onto GO/CS at 27°C, 40°C, and 60°

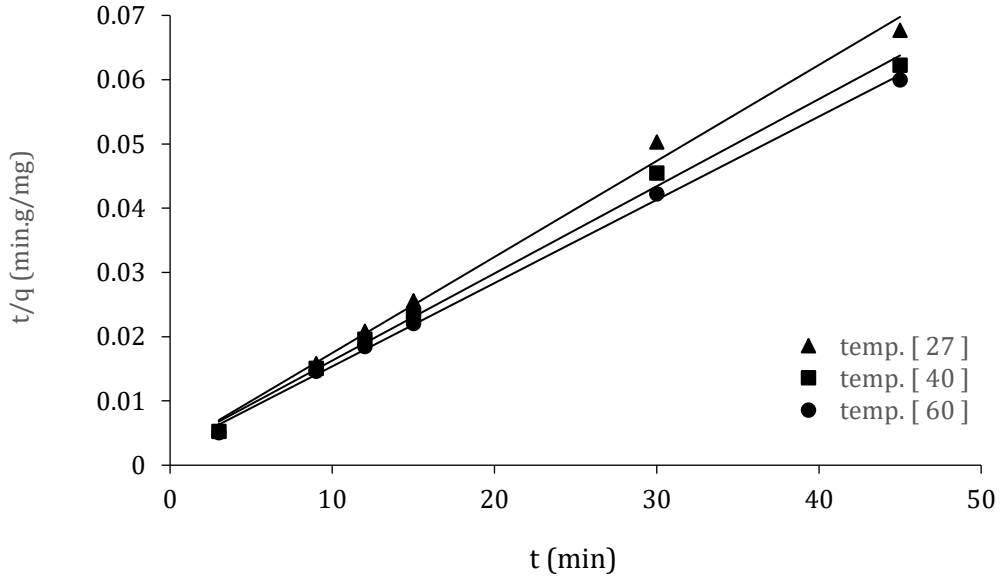

Figure 4.45. Pseudo-Second-Order plot for the adsorption of BB dye onto GO/CS/EDTA at 27°C, 40°C, and 60°

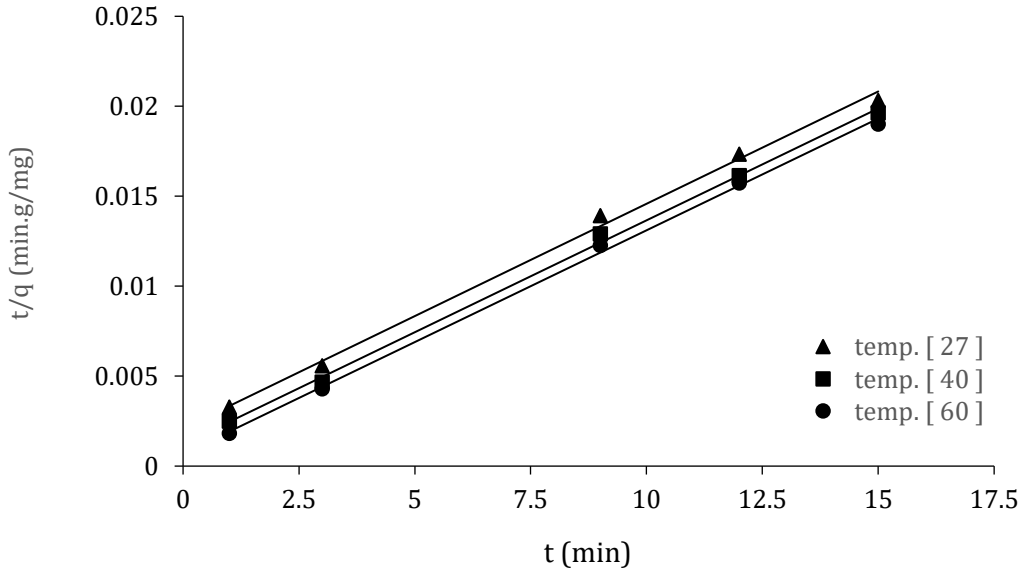

Figure 4.46. Pseudo-Second-Order plot for the adsorption of BB dye onto GO/pBCM at 27°C, 40°C, and 60°

All the various kinetic data for adsorption of CR and BB dyes onto the prepared adsorbents GO, GO/DAB, GO/DAB/EDTA, GO/CS, GO/CS/EDTA, and GO/pBCM under the different temperatures in this study (27, 40, and 60°C) are calculated from the related plots for the pseudo-second-order model and are summarized in Table (4.8).

Table 4.8. Pseudo-Second-Order parameters for adsorption of CR and BB dyes onto prepared adsorbents at different temperatures

Adsorbents	Temp.	CR Dye			BB Dye		
		k_2	q_2	R_2^2	k_2	q_2	R_2^2
GO	27	0.00026	953.28	0.9990	0.00065	735.17	0.9992
	40	0.00022	1046.4	0.9980	0.00063	778.38	0.9993
	60	0.00016	1157.1	0.9957	0.00060	816.78	0.9993
GO/DAB	27	0.00037	904.73	0.9991	0.00123	1335.9	0.9992

	40	0.00042	988.95	0.9980	0.00163	1430.8	1.0000
	60	0.00063	1035.1	0.9959	0.00280	1550.1	0.9999
GO/DAB/EDTA	27	0.00403	873.47	1.0000	0.00213	611.15	0.9998
	40	0.00202	932.11	0.9997	0.00161	678.62	0.9995
	60	0.00019	1243.9	0.9978	0.0004	765.32	0.9979
GO/CS	27	0.00060	1687.2	0.9999	0.00140	708.66	0.9999
	40	0.00049	1452.0	0.9995	0.00141	746.93	1.0000
	60	0.00035	1428.5	0.9992	0.00144	796.71	1.0000
GO/CS/EDTA	27	8.8E-05	1630.5	0.9971	0.00090	669.30	0.9992
	40	6.6E-05	1896.1	0.9955	0.00073	737.14	0.9959
	60	2.9E-05	2144.2	0.9972	0.00070	771.71	0.9982
GO/pBCM	27	0.00167	1029.7	1.0000	0.00069	800.96	0.9967
	40	0.00135	1145.5	0.9999	0.00120	803.91	0.9983
	60	0.00128	1212.7	0.9998	0.00280	804.70	0.9986

k_2: (g mg^{-1} min^{-1}), q: (mg/g), Temperature: (°C)

4.2.5.3. The Intra-Particle Diffusion Model

Intra-particle diffusion was the last model tested in this study, and the rate constant for intra-particle diffusion was obtained using Weber–Morris equation given as follows [187]:

$$q_t = \left(k_p . t^{\frac{1}{2}}\right) + C \quad \ldots\ldots (4.11)$$

Where C is the intercept, and k_p (mg g $^{-1}$ min $^{-1/2}$) is the intra-particle diffusion rate constant that equal to the plotting slope between (q_t) versus ($t^{-1/2}$). Figures (4.47-4.52 and 4.53-4.58) display the intra-particle diffusion equations for adsorption of CR and BB dyes at the different temperatures (27, 40, and 60°C), and the Table (4.9) gives k_p and C values.

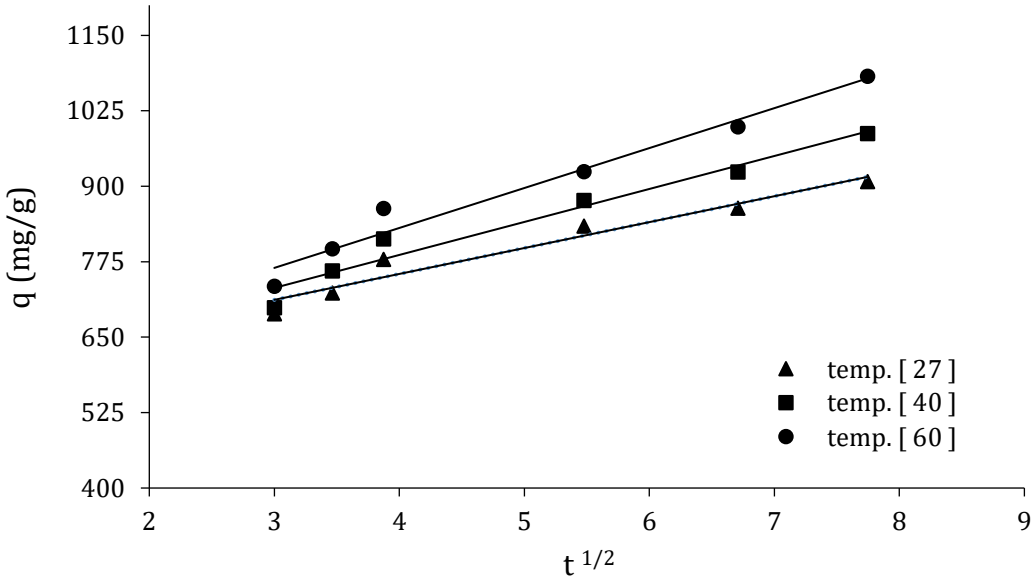

Figure 4.47. Intra-particle Diffusion plot for the adsorption of CR dye onto GO at 27°C, 40°C, and 60°C

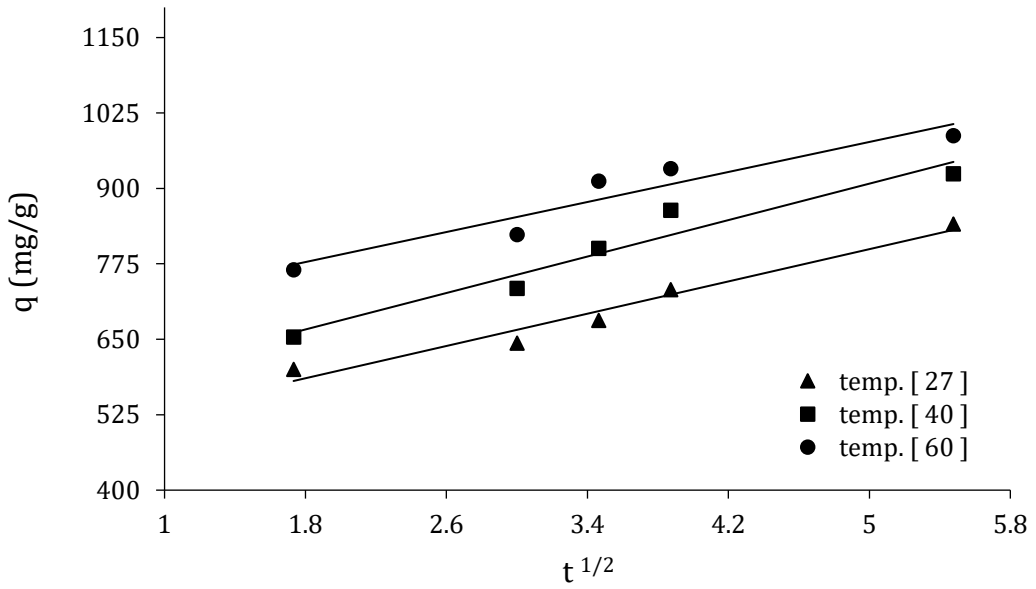

Figure 4.48. Intra-particle Diffusion plot for the adsorption of CR dye onto GO/DAB at 27°C, 40°C, and 60°C

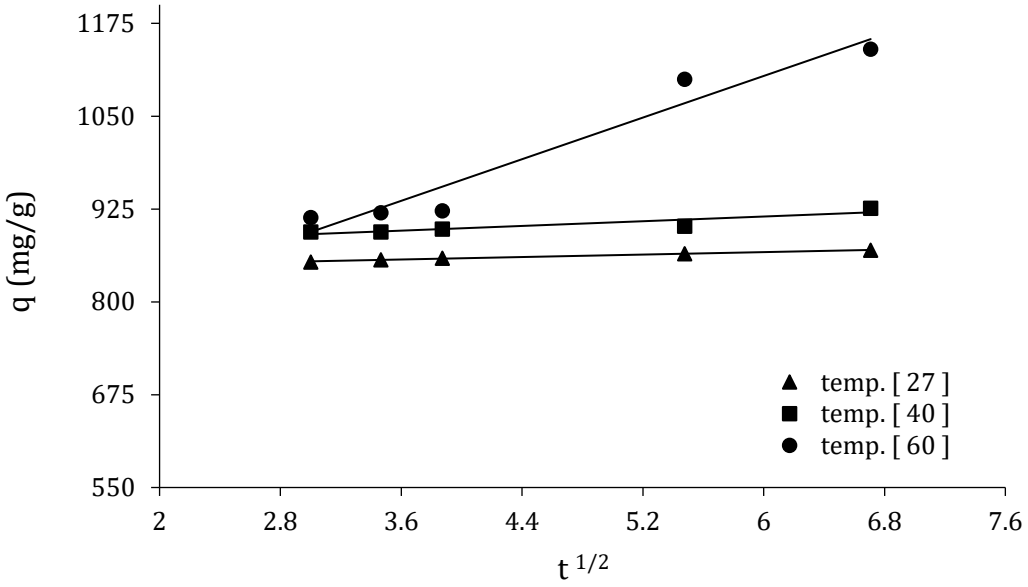

Figure 4.49. Intra-particle Diffusion plot for the adsorption of CR dye onto GO/DAB/EDTA at 27°C, 40°C, and 60°C

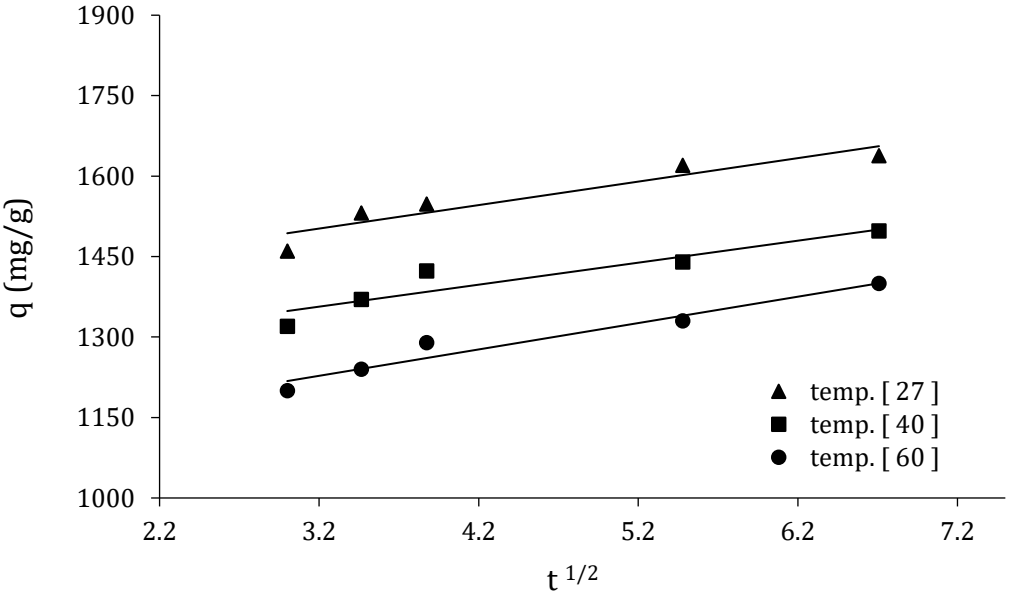

Figure 4.50. Intra-particle Diffusion plot for the adsorption of CR dye onto GO/CS at 27°C, 40°C, and 60°C

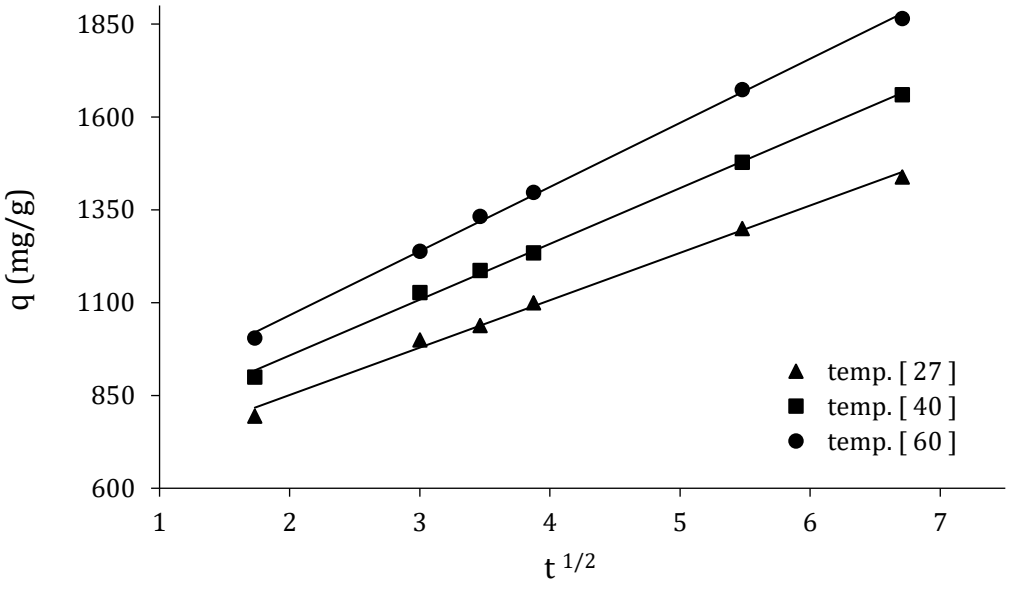

Figure 4.51. Intra-particle Diffusion plot for the adsorption of CR dye onto GO/CS/EDTA at 27°C, 40°C, and 60°C

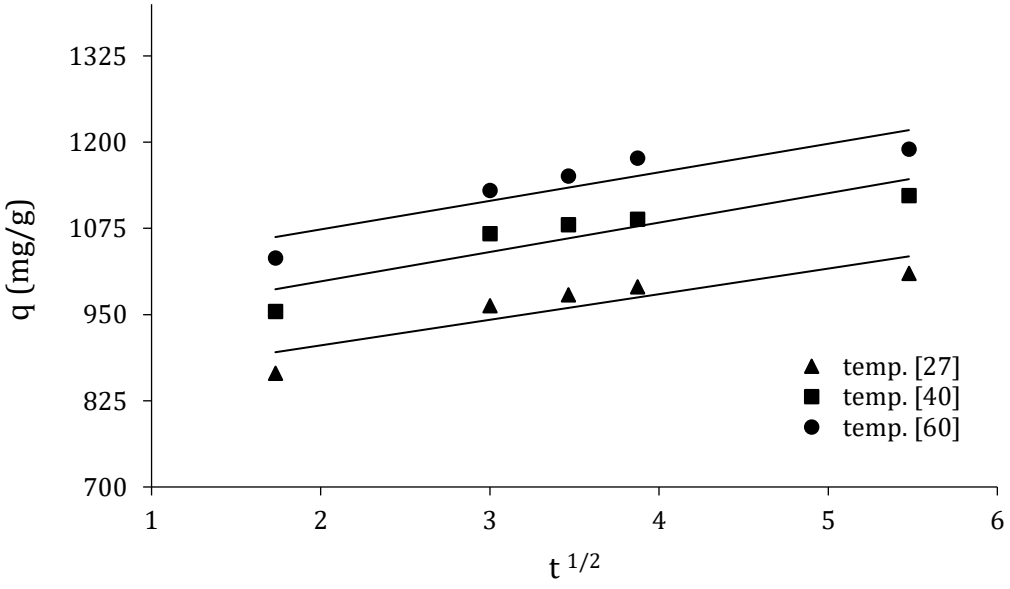

Figure 4.52. Intra-particle Diffusion plot for the adsorption of CR dye onto GO/pBCM at 27°C, 40°C, and 60°C

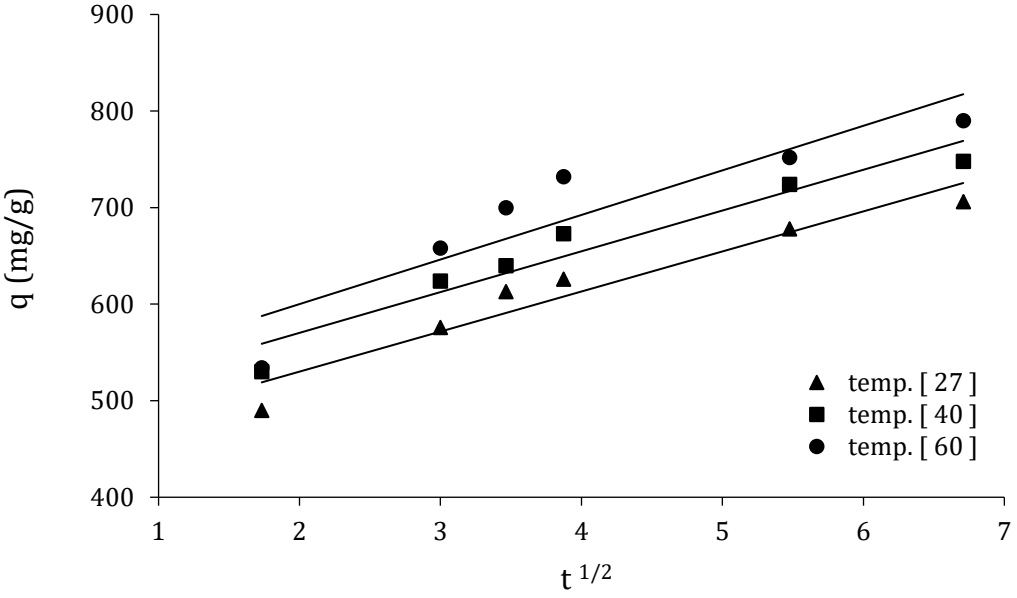

Figure 4.53. Intra-particle Diffusion plot for the adsorption of BB dye onto GO at 27°C, 40°C, and 60°C

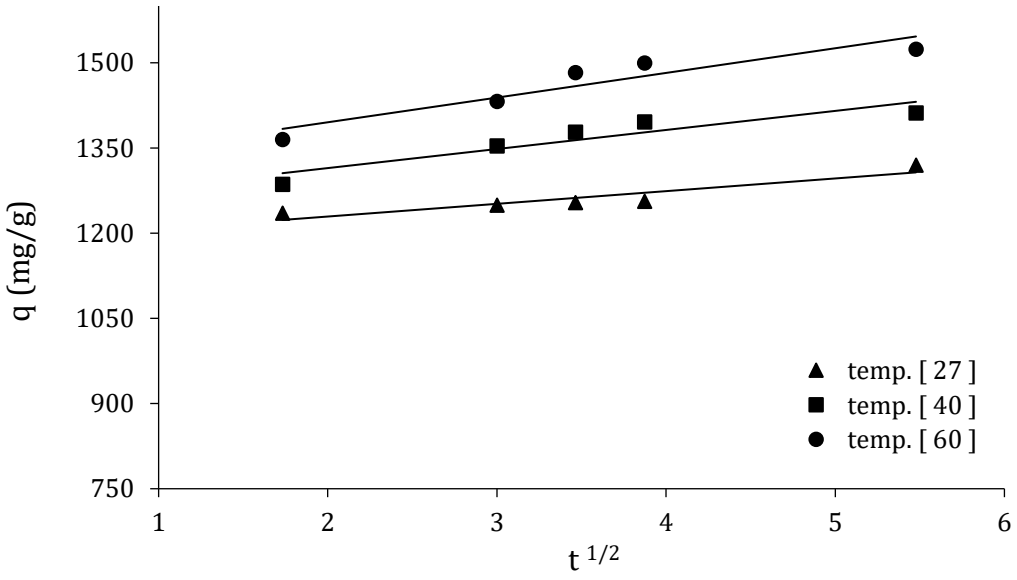

Figure 4.54. Intra-particle Diffusion plot for the adsorption of BB dye onto GO/DAB at 27°C, 40°C, and 60°C

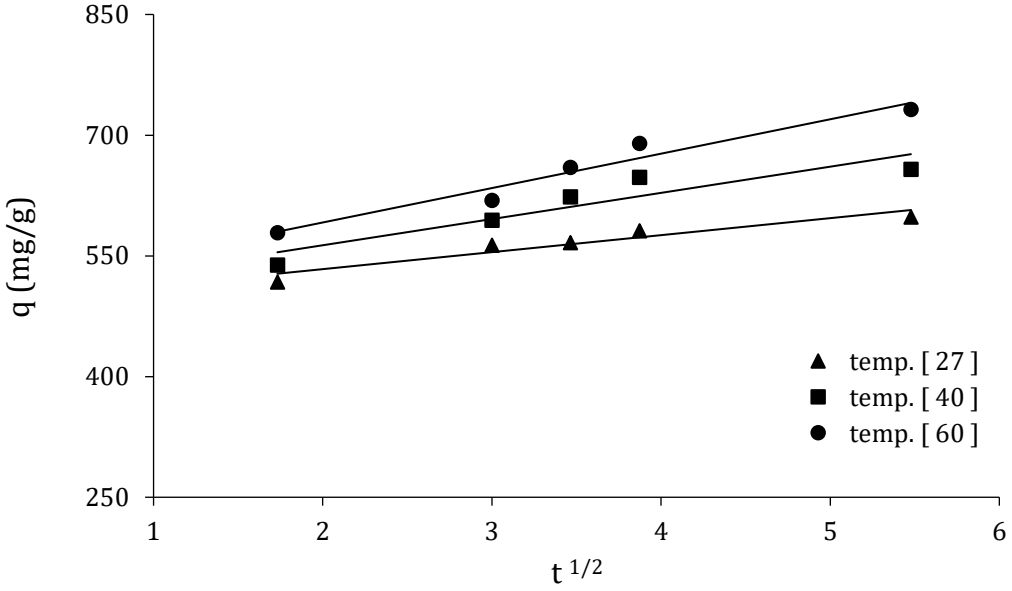

Figure 4.55. Intra-particle Diffusion plot for the adsorption of BB dye onto GO/DAB/EDTA at 27°C, 40°C, and 60°C

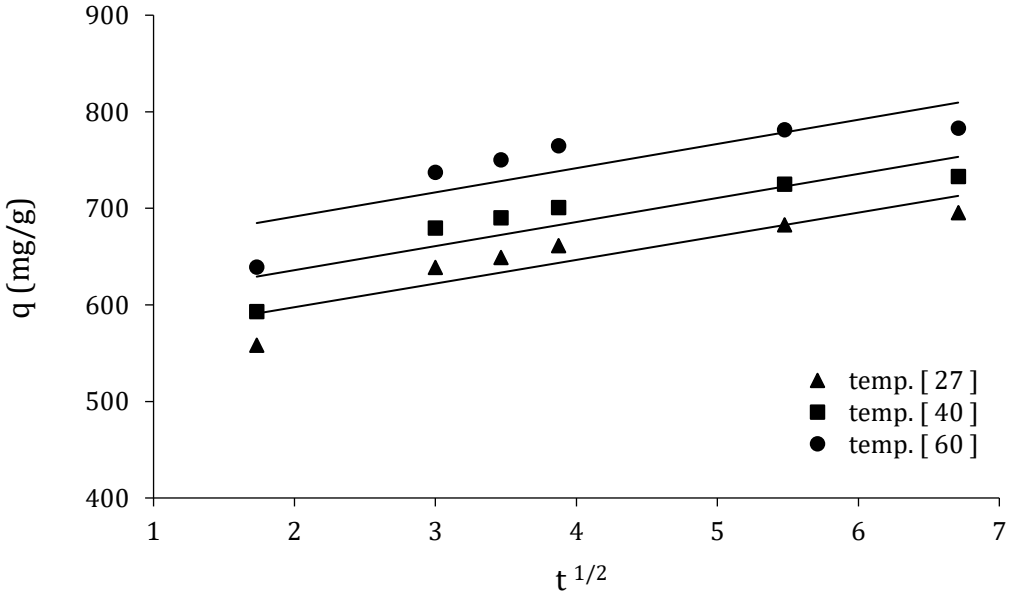

Figure 4.56. Intra-particle Diffusion plot for the adsorption of BB dye onto GO/CS at 27°C, 40°C, and 60°C

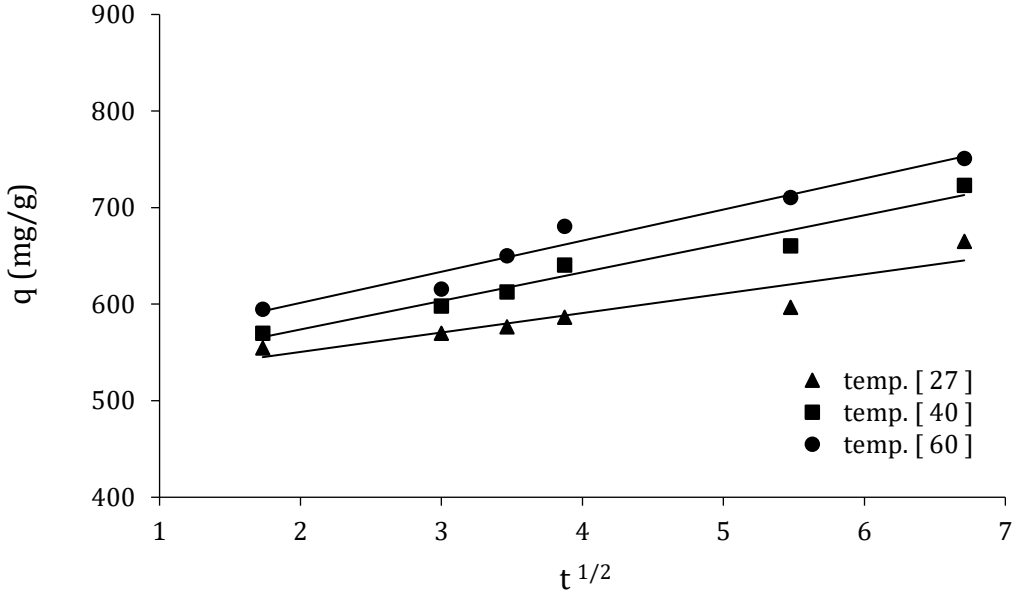

Figure 4.57. Intra-particle Diffusion plot for the adsorption of BB dye onto GO/CS/EDTA at 27°C, 40°C, and 60°C

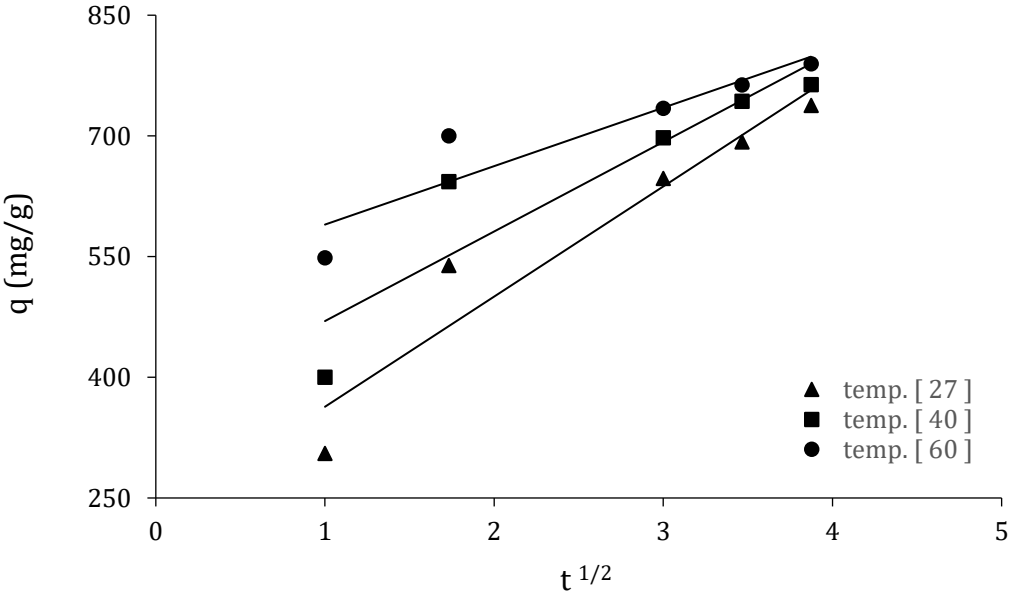

Figure 4.58. Intra-particle Diffusion plot for the adsorption of BB dye onto GO/pBCM at 27°C, 40°C, and 60°C

All the various kinetic data for adsorption of CR and BB dyes onto the prepared adsorbents GO, GO/DAB, GO/DAB/EDTA, GO/CS, GO/CS/EDTA, and GO/pBCM under the different temperatures in this study (27, 40, and 60°C) are calculated from the related plots for the Intra-Particle Diffusion model and are summarized in Table (4.9).

Table 4.9. Intra-particle Diffusion parameters for adsorption of CR and BB dyes onto prepared adsorbents at different temperatures

Adsorbents	Temp	CR Dye			BB Dye		
		k_p	C	R_p^2	k_p	C	R_p^2
GO	27	42.932	580.0	0.9489	42.492	437.12	0.9430
	40	54.661	587.6	0.9575	44.027	468.99	0.9645
	60	66.193	596.1	0.9666	47.118	491.50	0.9076
GO/DAB	27	66.842	465.5	0.9636	22.347	1184.6	0.8588
	40	75.495	530.4	0.9404	33.560	1247.4	0.8621
	60	62.184	666.0	0.9080	43.441	1308.4	0.8741
GO/DAB/EDTA	27	4.127	842.1	0.9449	22.347	491.23	0.9112
	40	7.922	867.3	0.8372	33.560	498.05	0.8552
	60	70.053	883.8	0.9845	43.441	505.93	0.9526
GO/CS	27	43.783	1362.1	0.8869	24.499	548.20	0.8133
	40	41.004	1225.5	0.8687	24.703	587.35	0.7730

	60	40.164	1070.4	0.9493	26.249	673.39	0.7331
GO/CS/EDTA	27	127.57	545.8	0.9950	20.130	510.23	0.8608
	40	150.20	657.1	0.9978	29.568	514.63	0.9614
	60	172.64	720.6	0.9985	32.212	536.91	0.9599
GO/pBCM	27	37.108	831.1	0.8008	136.91	226.48	0.9198
	40	40.622	912.8	0.8274	111.33	358.58	0.8383
	60	41.401	990.6	0.8161	72.628	517.18	0.8579

k_p: (mg g^{-1} $min^{-1/2}$), Temperature: (°C)

The rate-limiting steps for the adsorption process use to be defined by the expression of kinetic adsorption models [188]. the pseudo-first-order kinetic model most widely used models in the literature were applied to analyze the dye's adsorption data [189]. This model assumes diffusion steps are involved in rate controlling for dye removal from the solution.

The obtained correlation coefficients R^2 for these kinetic adsorption model are ≤0.9969 and ≤0.9982 for CR and BB dyes respectively, indicating that the data obtained from the study at different time interval does not fit the rate equation better than the second-order rate equation [190], as we will notice in Table (4.8).

The pseudo-first and pseudo-second models are compared for their fitness for dyes adsorption by adsorbents. Accepted kinetic models for the adsorption process can be characterized by common validity tests:

i. a high correlation coefficient R^2, indicating the applicability and reliability of a given kinetic model;

ii. a close agreement between the calculated and the experimental equilibrium capacities values [191].

As listed in Table (4.7), the low correlation coefficients of the pseudo-first-order kinetics model, for examples (R^2 = 0.7570 and 0.8670 at 40°C) for

CR dye onto GO/CS and GO/DAB/EDTA respectively, and (R^2 = 0.8633 at 60°C and 0.8886 at 40°C) for BB dye adsorption by GO and GO/CS/EDTA respectively. As well, lacking matching of calculated and experimental q_{max} values of adsorbents toward both dyes leading to concluded that this kinetic model did not explain the adsorption process.

The high correlation coefficients ($0.9955 \leq R^2 \leq 1.0$) as shown in Table (4.8) and close matching in the values of calculated and experimental q_{max} when applying the pseudo-second-order kinetics model imply the fitting of this model for both dyes adsorption systems. The rate constants k_2 of the adsorption processes for CR and BB dyes did not always increase with increasing temperature, and similar findings between rate constants and the temperature were reported in the literature [192, 193].

These facts suggest that the adsorption of both dyes by the prepared adsorbents favorably which relies on the assumption chemisorption process [194, 195].

The fitting of a pseudo-second-order kinetic model confirmed by the D–R isotherm model suggests that the adsorption systems were chemisorption.

The kinetic data of adsorption of dyes onto the prepared adsorbents are also analyzed using an intra-particle diffusion model, and as seen from Table (4.9), the obtained correlation coefficients R^2 = 0.8008–0.9985 and 0.7331–0.9645 over the whole time of a range of CR and BB dyes respectively, but they did not pass through the origin of the coordinates, this indicates that intra-particle diffusion is not the only rate-limiting step of the studied adsorption process of both dyes, and diffusion control may be involved in the adsorption process study. Also, it's observed in the same table that the values of k_P increased with increasing temperatures for the adsorption process of both dyes onto the most adsorbents, while these values decrease by increasing the used temperature in GOCS adsorbent by using the CR dye because the active sites on the surfaces of this adsorbent have occupied of the adsorbate material (dyes). The values of the constants C were nonzero of the adsorption process by both dyes on all prepared adsorbents as shown in Table (4.9), also the constant C values are increased with the increasing of temperature, while in GOCS it decreases with increasing temperature by using CR dye, this means that the adsorption process does not require heat to disengage, and according to the intraparticle diffusion equation the dye will transfer from its aqueous solution to the adsorbent surface and then it will permeate to the pores on these surfaces.

4.2.6. Adsorption Thermodynamics of CR & BB Dyes

The investigation of thermodynamic functions; the change of standard enthalpy ΔH°, the change of standard entropy ΔS°, the change of standard free energy ΔG°, and the activation energy E_a is essential to understanding the basic of adsorption reactions [196]. The adsorption thermodynamic experiments were conducted at different temperatures 300.15, 313.15, and 333.15 K.

The important thermodynamic parameters can be determined from the thermodynamic distribution coefficient (Equilibrium constant) K_L values were calculated according to the following equation [197]:

$$\mathbf{K_L = \frac{C_a}{C_e}} \quad \ldots\ldots (\mathbf{4.12})$$

Where C_a is the equilibrium concentration of dye on the adsorbents (mg/g) and C_e is the concentration of dye in the solution (mg/L). The results of thermodynamic studies make it conceivable to understand the feasibility of the adsorption process and to get helpful data about fundamental parameters of adsorption, such as ΔH° and ΔS° that can be calculated by Van't Hoff plots [198], based on the equation (4.10):

$$\mathbf{\ln K_L = \frac{\Delta S^\circ}{R} - \frac{\Delta H^\circ}{RT}} \quad \ldots\ldots (\mathbf{4.13})$$

Where R is the universal gas constant (8.314 J/mol K), and T (K) is the absolute temperature, plotting of ($\ln K_L$) versus (1/T) leading to calculate ΔH° (kJ/mol) from the slope and ΔS° (J/mol/K) from intercept, as shown in Figures (4.59-4.64) and (4.65-4.70) for adsorption of CR and BB dyes respectively onto the prepared adsorbents GO, GO/DAB, GO/DAB/EDTA, GO/CS, GO/CS/EDTA, and GO/pBCM.

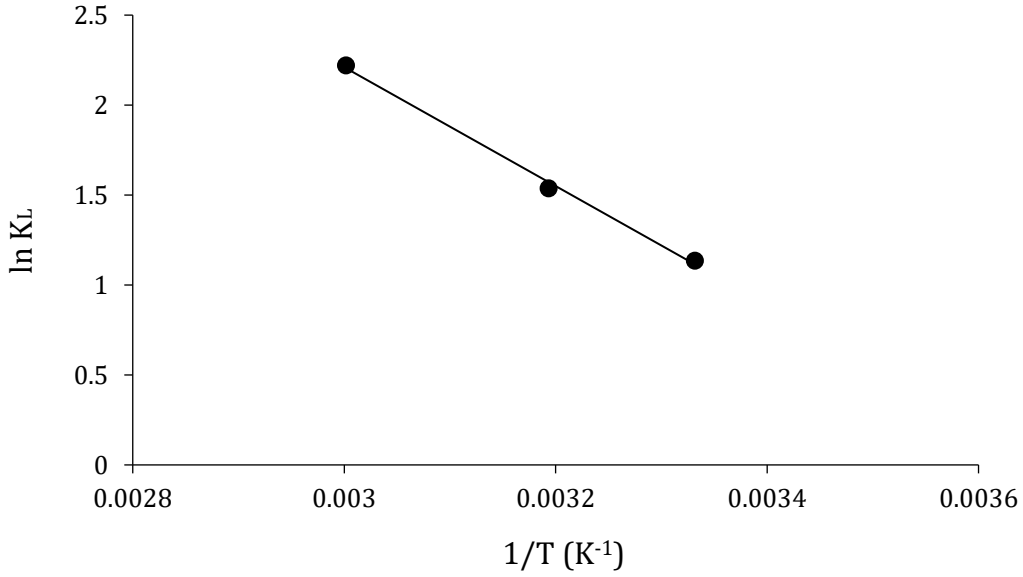

Figure 4.59. Plot of lnKL vs. 1/T for estimation of Thermodynamic Parameters for the adsorption of CR dye onto GO

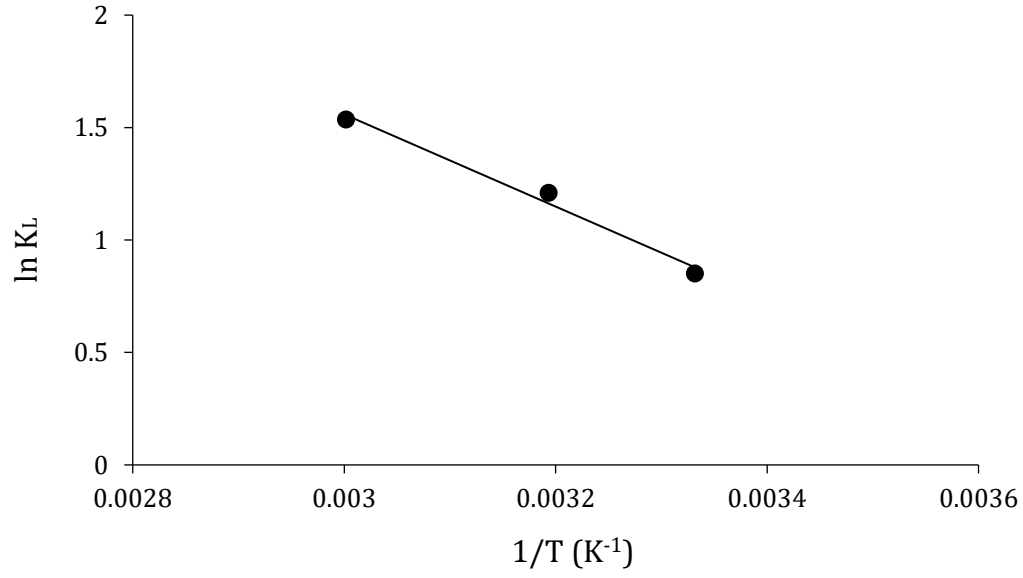

Figure 4.60. Plot of lnKL vs. 1/T for estimation of Thermodynamic Parameters for the adsorption of CR dye onto GO/DAB

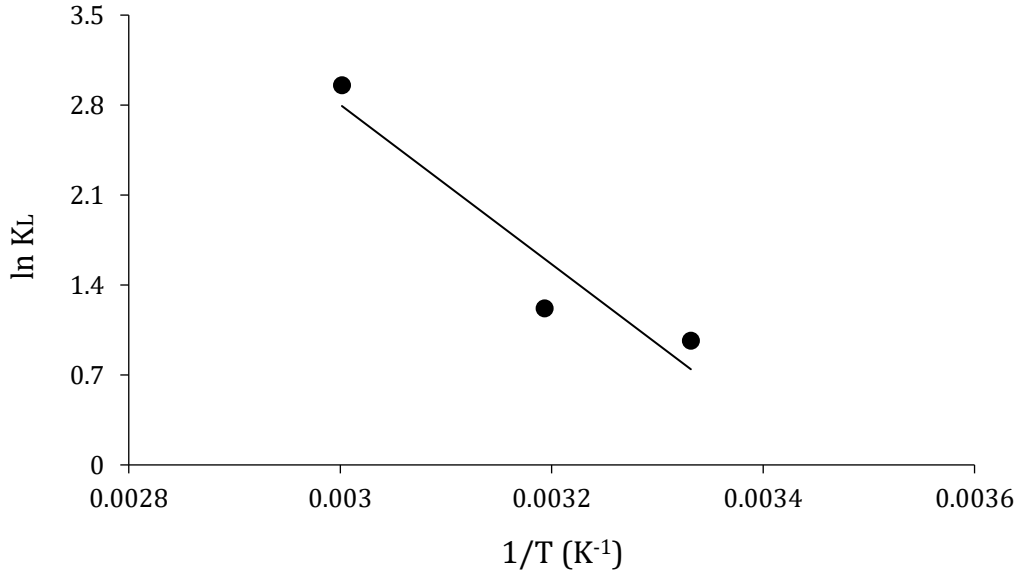

Figure 4.61. Plot of lnKL vs. 1/T for estimation of Thermodynamic Parameters for the adsorption of CR dye onto GO/DAB/EDTA

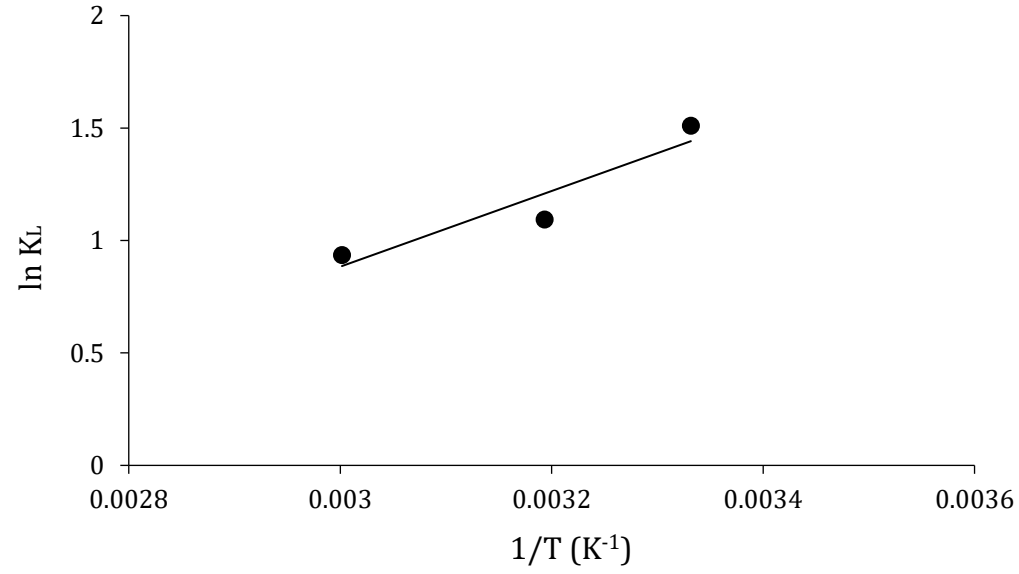

Figure 4.62. Plot of lnKL vs. 1/T for estimation of Thermodynamic Parameters for the adsorption of CR dye onto GO/CS

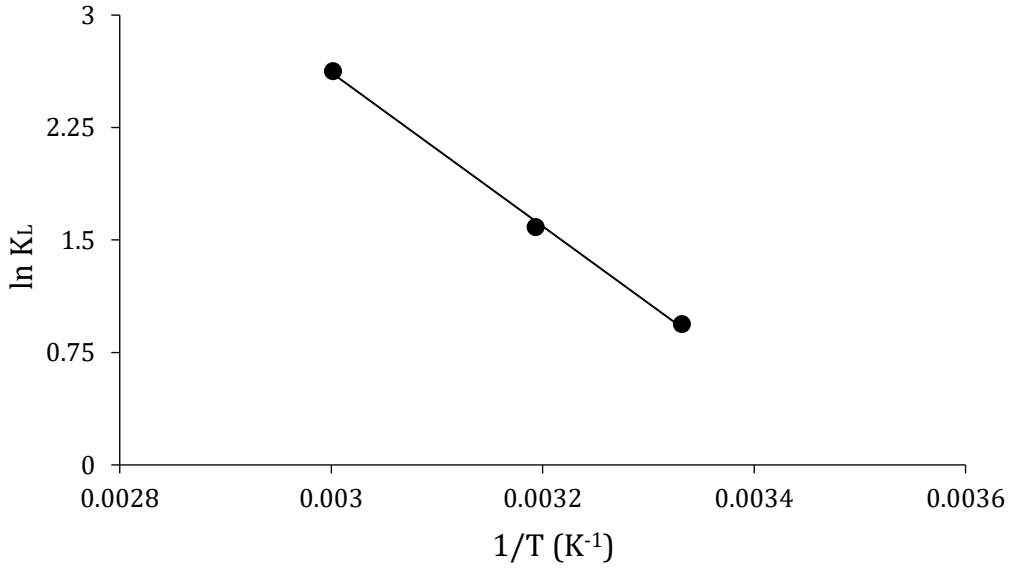

Figure 4.63. Plot of lnKL vs. 1/T for estimation of Thermodynamic Parameters for the adsorption of CR dye onto GO/CS/EDTA

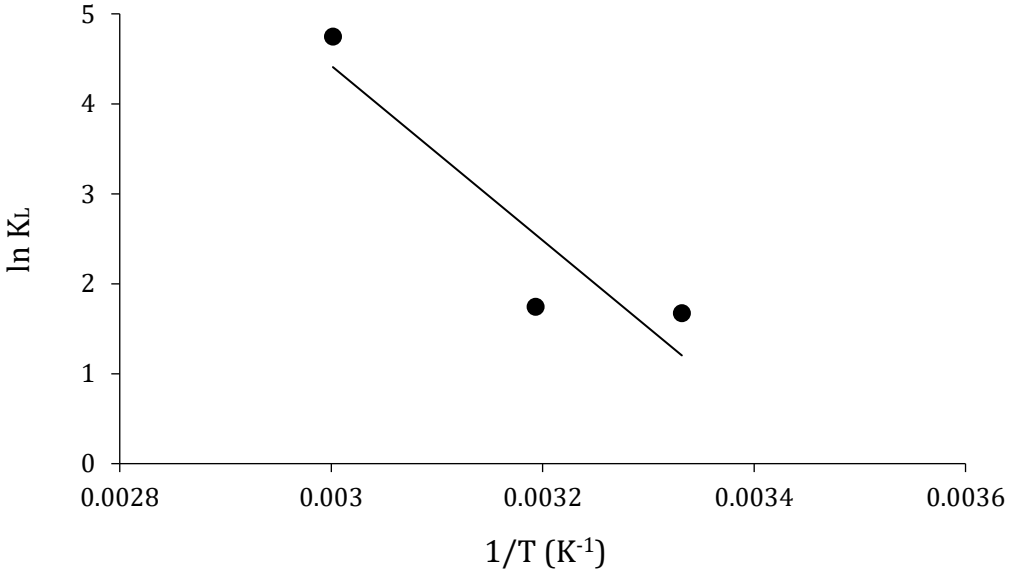

Figure 4.64. Plot of lnKL vs. 1/T for estimation of Thermodynamic Parameters for the adsorption of CR dye onto GO/pBCM

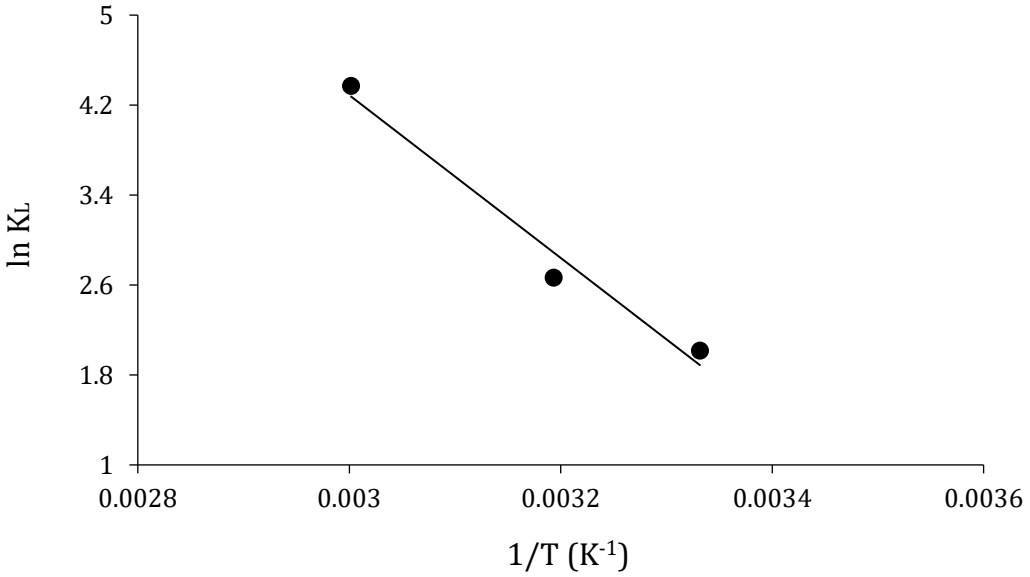

Figure 4.65. Plot of lnKL vs. 1/T for estimation of Thermodynamic Parameters for the adsorption of BB dye onto GO

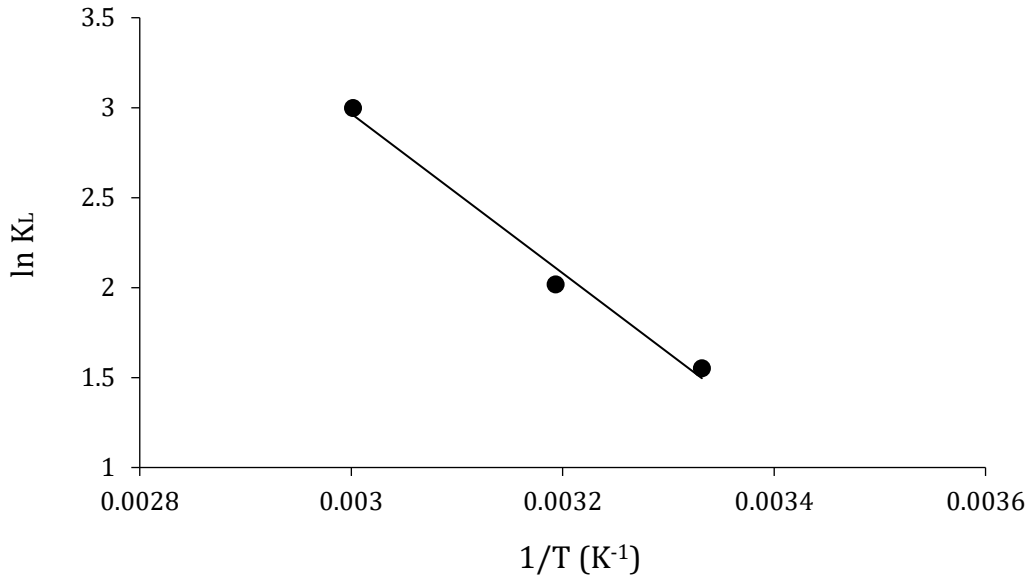

Figure 4.66. Plot of lnKL vs. 1/T for estimation of Thermodynamic Parameters for the adsorption of BB dye onto GO/DAB

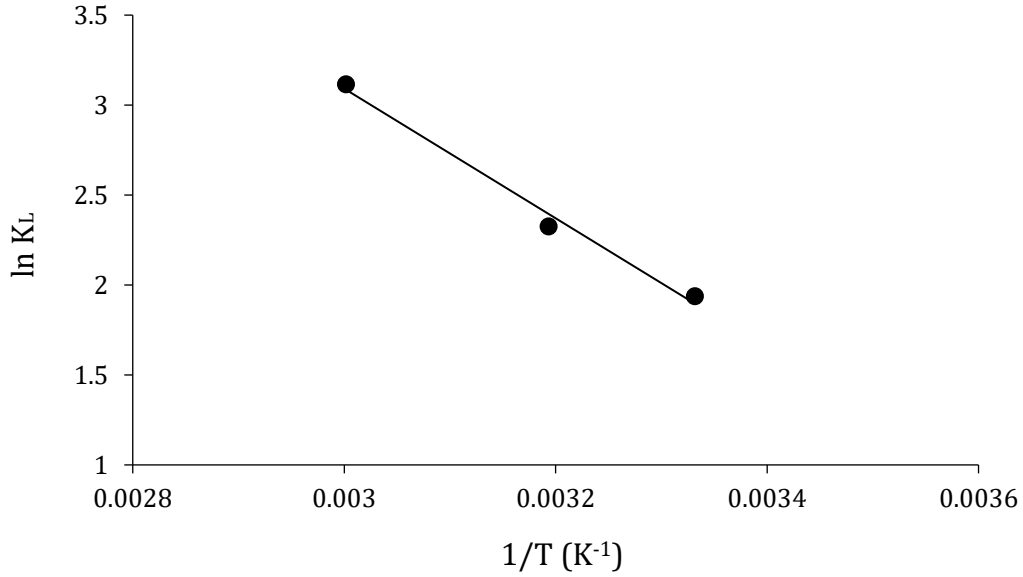

Figure 4.67. Plot of lnKL vs. 1/T for estimation of Thermodynamic Parameters for the adsorption of BB dye onto GO/DAB/EDTA

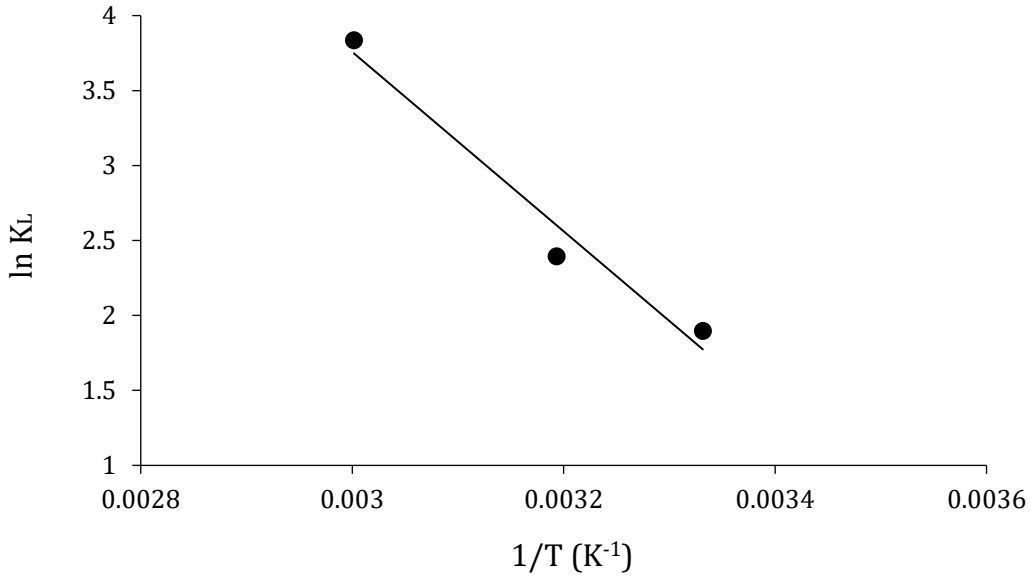

Figure 4.68. Plot of lnKL vs. 1/T for estimation of Thermodynamic Parameters for the adsorption of BB dye onto GO/CS

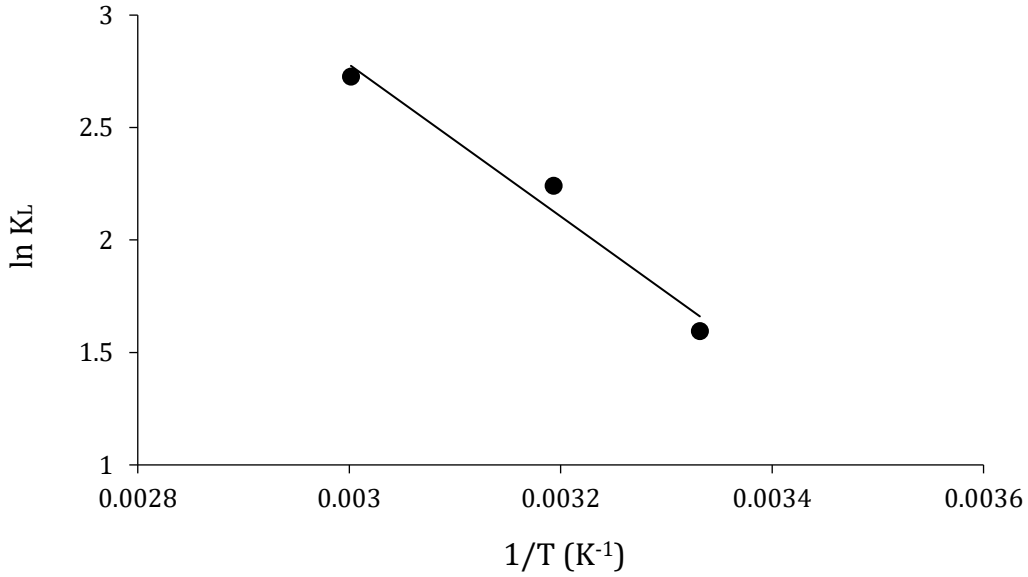

Figure 4.69. Plot of lnKL vs. 1/T for estimation of Therشmodynamic Parameters for the adsorption of BB dye onto GO/CS/EDTA

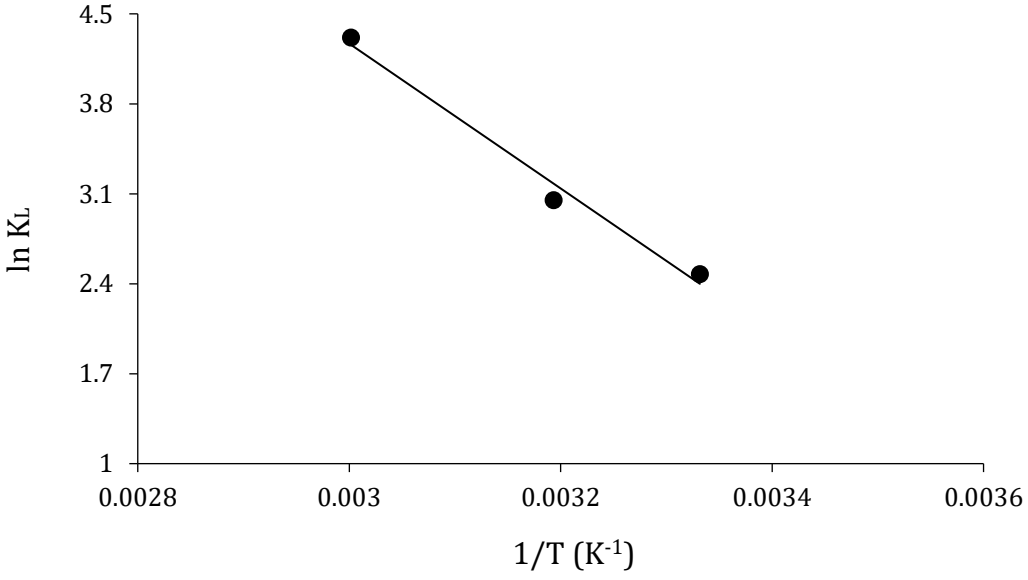

Figure 4.70. Plot of lnKL vs. 1/T for estimation of Thermodynamic Parameters for the adsorption of BB dye onto GO/pBCM

The standard Gibbs free energy ΔG° (kJ/mol) values are computed for each temperature used in the study (300.15, 313.15, and 333.15 K) of both

dyes adsorption processes from the following Helmholtz relation equation [199]:

$$\Delta G^{\circ} = \Delta H^{\circ} - T\Delta S^{\circ} \quad \ldots\ldots (4.14)$$

The activation energy E_a (kJ/mol) of the adsorption process representing the minimum energy that reactants must have for the reaction to proceed [200], and it was calculated from the Arrhenius equation, as shown by the following relationship [201]:

$$\ln K = \ln A - \frac{E_a}{RT} \quad \ldots\ldots (4.15)$$

Where K (g mg^{-1} min^{-1}) is the rate constant obtained from the pseudo-second-order kinetic model in an adsorption system of both CR and BB dyes for all prepared adsorbents, because the adsorption analyses based on the constant obtained from the linearized plots (R^2), and A is the Arrhenius factor. When (lnK) is plotted against (1/T) as shown in Figures (4.71-4.76 and 4.77-4.82), a straight line with a slope of ($-E_a/R$) is obtained for CR and BB dye adsorption respectively onto the prepared adsorbents GO, GO/DAB, GO/DAB/EDTA, GO/CS, GO/CS/EDTA, and GO/pBCM.

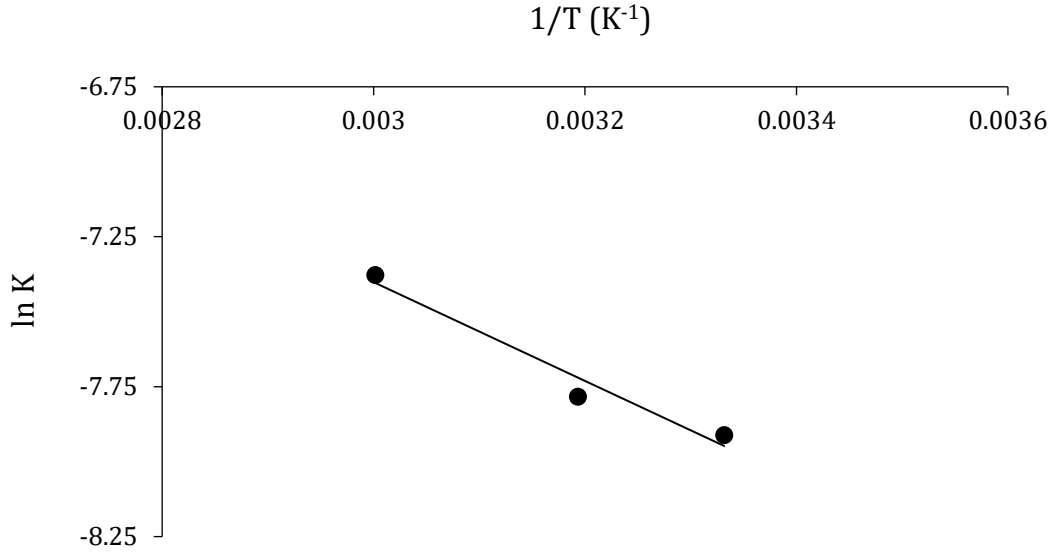

Figure 4.71. Plot of lnK vs. 1/T for estimation of Activation Energy Ea for the adsorption of CR dye onto GO

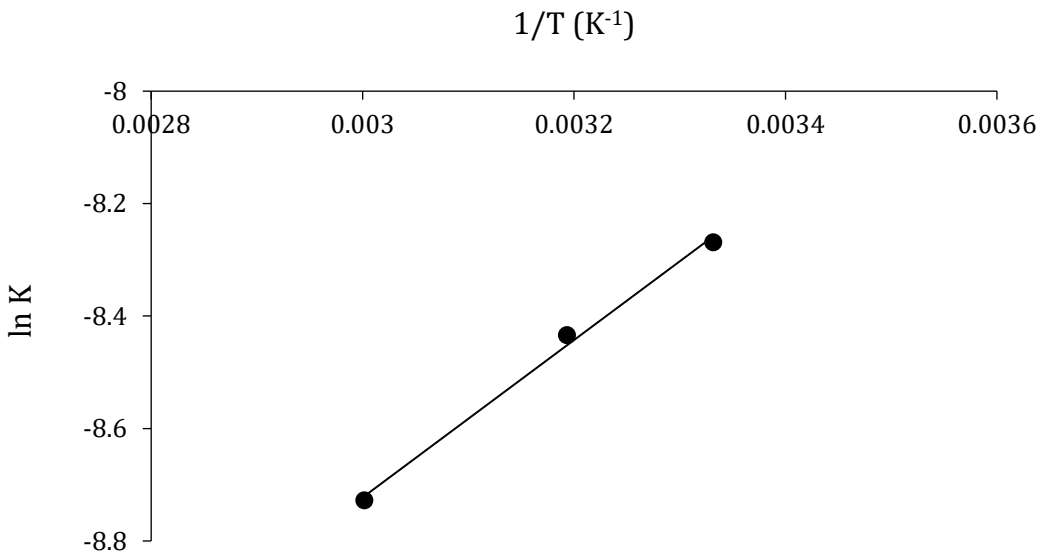

Figure 4.72. Plot of lnK vs. 1/T for estimation of Activation Energy Ea for the adsorption of CR dye onto GO/DAB

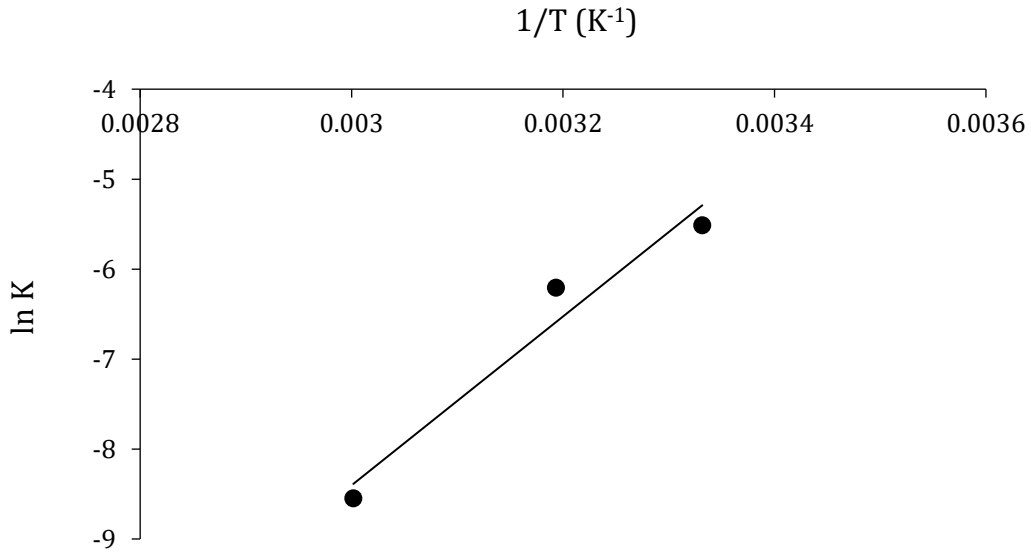

Figure 4.73. Plot of lnK vs. 1/T for estimation of Activation Energy Ea for the adsorption of CR dye onto GO/DAB/EDTA

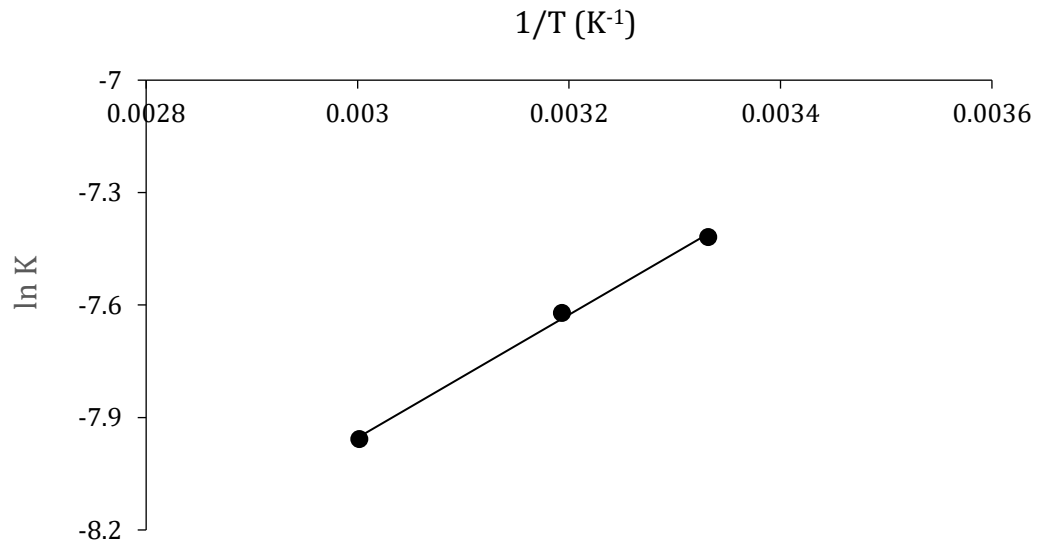

Figure 4.74. Plot of lnK vs. 1/T for estimation of Activation Energy Ea for the adsorption of CR dye onto GO/CS

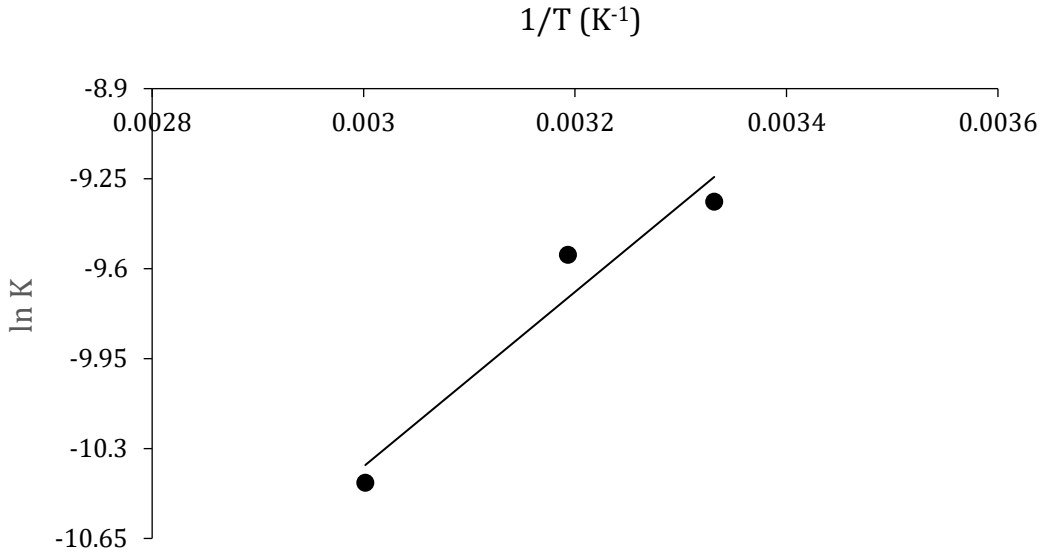

Figure 4.75. Plot of lnK vs. 1/T for estimation of Activation Energy Ea for the adsorption of CR dye onto GO/CS/EDTA

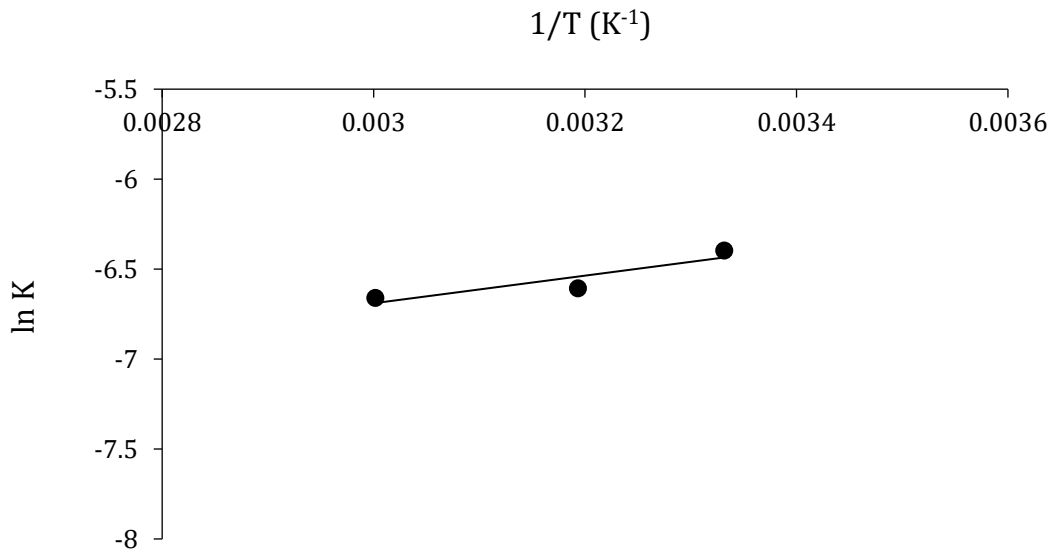

Figure 4.76. Plot of lnK vs. 1/T for estimation of Activation Energy Ea for the adsorption of CR dye onto GO/pBCM

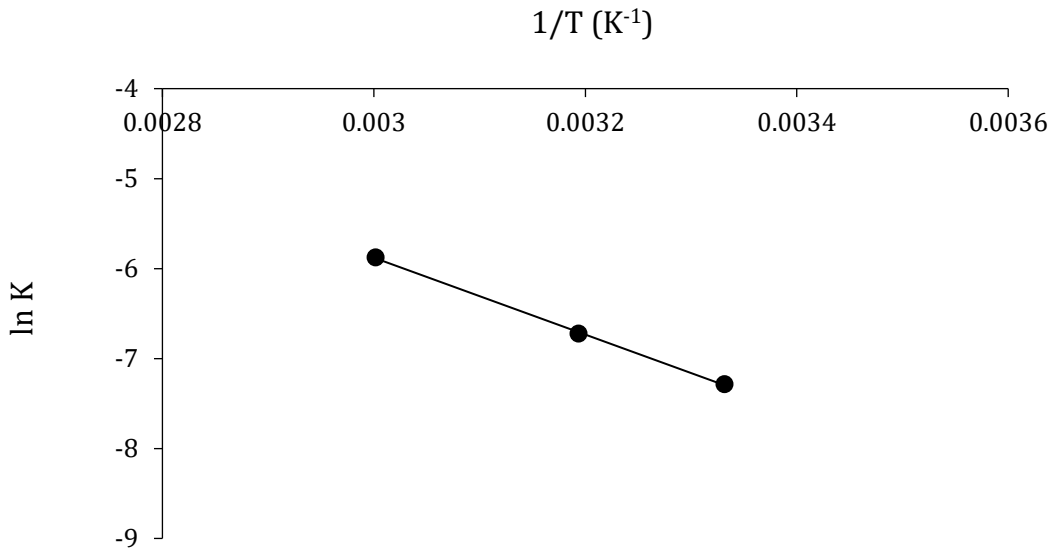

Figure 4.77. Plot of lnK vs. 1/T for estimation of Activation Energy Ea for the adsorption of BB dye onto GO

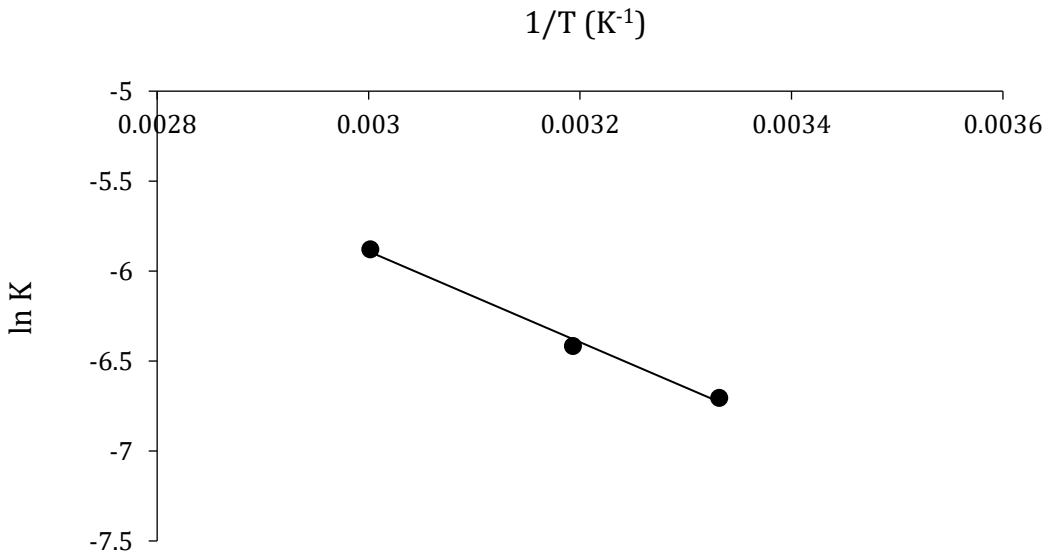

Figure 4.78. Plot of lnK vs. 1/T for estimation of Activation Energy Ea for the adsorption of BB dye onto GO/DAB

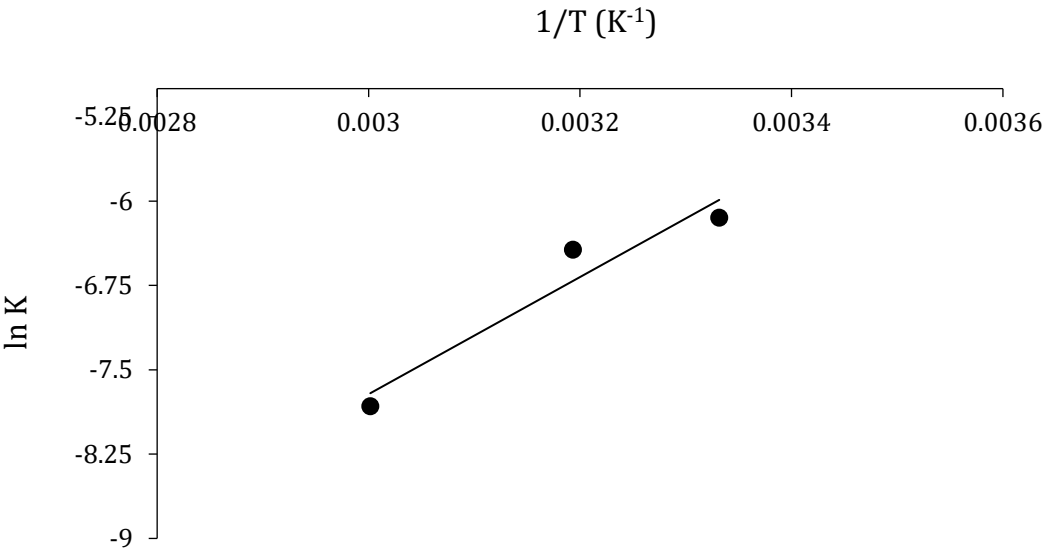

Figure 4.79. Plot of lnK vs. 1/T for estimation of Activation Energy Ea for the adsorption of BB dye onto GO/DAB/EDTA

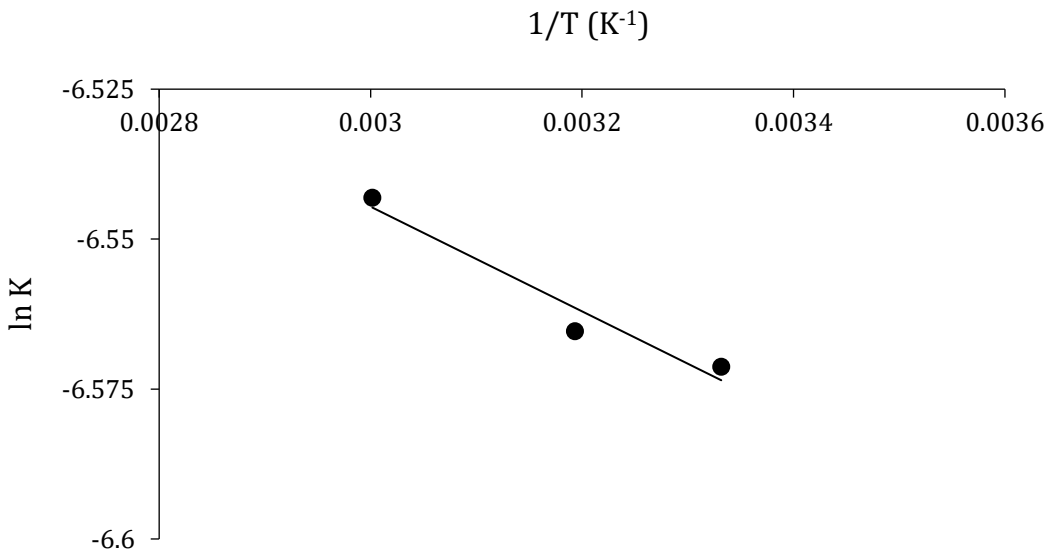

Figure 4.80. Plot of lnK vs. 1/T for estimation of Activation Energy Ea for the adsorption of BB dye onto GO/CS

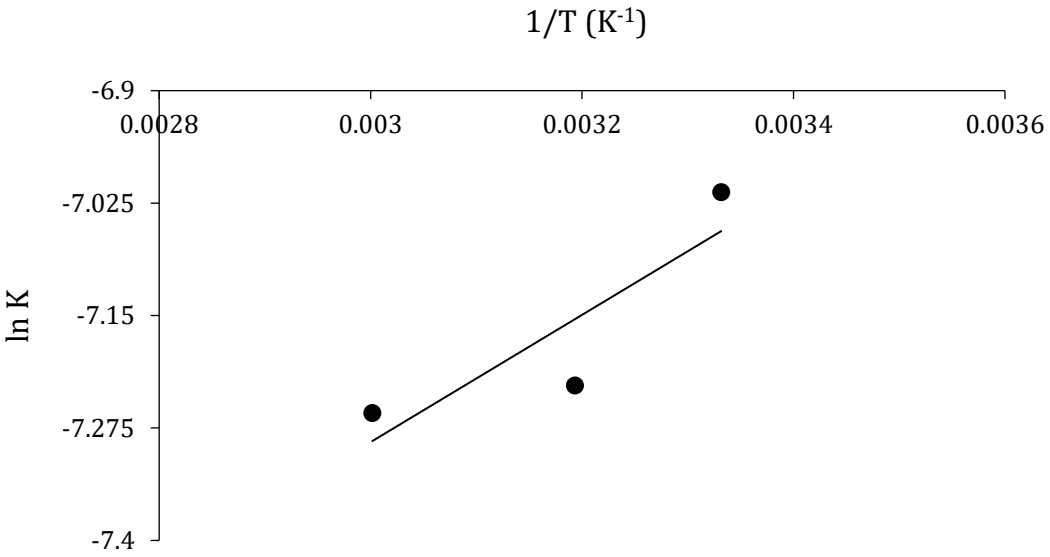

Figure 4.81. Plot of lnK vs. 1/T for estimation of Activation Energy Ea for the adsorption of BB dye onto GO/CS/EDTA

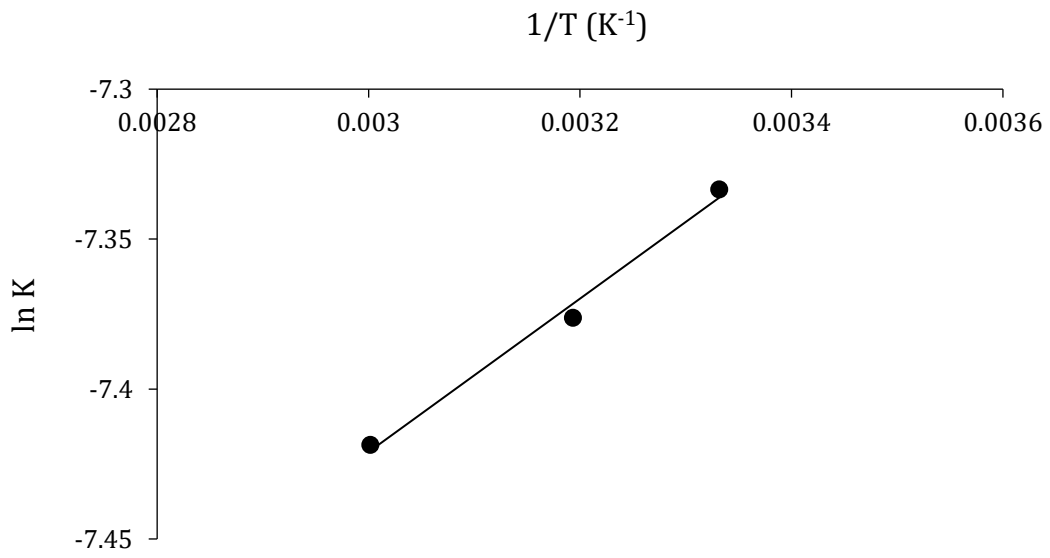

Figure 4.82. Plot of lnK vs. 1/T for estimation of Activation Energy Ea for the adsorption of BB dye onto GO/pBCM

The values of thermodynamic parameters in our current study; ΔH°, ΔS°, ΔG°, and E_a calculated from the equations were listed in Table (4.10) for adsorption of CR and BB dyes onto the prepared adsorbents GO, GO/DAB, GO/DAB/EDTA, GO/CS, GO/CS/EDTA, and GO/pBCM

Table 4.10. Thermodynamic parameters for adsorption of CR & BB dyes onto prepared adsorbents at different temperatures

Dye	Adsorbent	Temp.	ΔH°	ΔS°	- ΔG°	Ea
CR Dye	GO	300.15	27.462	100.766	2.782	13.963
		313.15			4.092	
		333.15			6.107	
	GO/DAB	300.15	17.052	64.118	2.193	-11.642
		313.15			3.026	
		333.15			4.309	
	GO/DAB/EDTA	300.15	51.600	178.103	1.856	-78.013
		313.15			4.172	
		333.15			7.734	
	GO/CS	300.15		-34.622	3.597	

		313.15	-13.989		3.147	-13.641
		333.15			2.454	
	GO/CS/EDTA	300.15	42.644	149.964	2.286	-28.232
		313.15			4.232	
		333.15			7.226	
	GO/pBCM	300.15	80.738	279.001	3.003	-6.380
		313.15			6.630	
		333.15			12.210	
BB Dye	**GO**	300.15	60.175	216.172	4.709	35.524
		313.15			7.519	
		333.15			11.843	
	GO/DAB	300.15	36.856	216.172	28.028	20.973
		313.15			30.838	
		333.15			35.126	
	GO/DAB/EDTA	300.15	29.954	115.565	4.732	-43.310
		313.15			6.234	
		333.15			8.545	
	GO/CS	300.15	49.732	180.439	4.426	0.7255
		313.15			6.771	
		333.15			10.380	
	GO/CS/EDTA	300.15	28.063	107.309	4.144	-5.879
		313.15			5.539	
		333.15			7.686	
	GO/pBCM	300.15	46.857	176.066	5.988	-2.126
		313.15			8.277	
		333.15			11.799	

Temp: (°K), ΔH°, ΔG° & E_a: (kJ/mol), ΔS°: (J/mol/ K)

All parameters listed in Table (4.10) are the actual indicator for practical applications of the dye adsorption process. ΔG° indicates that whether the reaction is spontaneous or non-spontaneous, ΔH° determines the exothermic and the endothermic nature of the dyes adsorption process, and ΔS° reveals the high or low degree of disorder at the solid-liquid interface during the dyes adsorption process.

The calculated thermodynamic parameters showed the positive values of enthalpy changes ΔH° for adsorption of CR dye onto prepared adsorbents GO,

GO/DAB, GO/DAB/ESTA, GO/CS/EDTA, and GO/pBCM, likewise for the adsorption of BB dye onto the all prepared adsorbents indicating that the adsorption processes were endothermic, also the positive value of entropy ΔS° of both the dyes onto the same adsorbents suggests an increase in the randomness at the (adsorbents/solution) interface and an affinity towards dyes [202]. This is because of the increase in mobility of adsorbate ions present in the solution while raising the temperature.

While the prepared adsorbent GO/CS with CR dye shows negative values of both the change of standard enthalpy ΔH° (-13.989 kJ/mol) and standard entropy ΔS° (-34.622 J/mol/K), indicating that the adsorption process is exothermic and the mobility of CR dye as adsorbate onto GO/CS becomes more limited as compared with that of this in the solution [203].

The obtained values of Gibbs free energy change ΔG° at the three different temperatures were less than zero for the adsorption of both CR and BB dyes by all prepared adsorbents in this study, denoting the behavior of adsorption processes is spontaneous and feasible [203].

Negative values of ΔG° (as shown in Table 4.10) reveal that the adsorption process of both dyes on the prepared adsorbents is a spontaneous reaction at any temperature. This implies that the adsorption system does not require an external energy source. And (as shown in Table 4.10) the values of ΔG° for GO/CS adsorbent with CR dye are also negative and it's increased by increasing the temperature shows that the process is also spontaneous and more favorable at a lower temperature.

The low values of activation energy (E_a<40 kJ/mol) for all the prepared adsorbents with CR and BB dyes (as shown in Table 4.10) are characteristics of the physisorption and diffusion-controlled process [204], showing that the adsorption process of both dyes ($E_{a\,CR}$ = −78.010 to 13.693 and $E_{a\,BB}$ = −34.310 to 35.524 kJ/mol) by the prepared adsorbents is governed by physisorption mechanism involving Van der Waals forces between the charged sites of the dyes and the surface of the adsorbents. Therefore, these results indicate that the adsorption processes of both dyes onto adsorbents are diffusion-controlled and physical.

It was reported that the ΔG° for physisorption was generally in the range of (−20 to Zero) kJ/mol, the physisorption together with chemisorption between (−80 and −20 kJ/mol), and chemisorption within (−400 to −80) kJ/mol [205, 206].

The calculated ΔG° between (−1.856 and −12.210) kJ/mol suggested that the adsorption of CR and BB dyes on the prepared adsorbents could be regarded as physical adsorption processes at studied temperatures. Excepting the values of ΔG° for GO/BAD adsorbent with BB dye are recorded as (−28.028 to −35.126) kJ/mol at the temperatures used in this study, shows the physicochemical adsorption process that implied both chemical bond and Van der Waals forces were formed between the dye and surface of the adsorbent.

As a result, the adsorption process gives an impression as a chemical and physical behavior, where the adsorption process might be chemisorption as shown previously in the isotherm study (Langmuir and D-R) and physisorption through the thermodynamic study, therefore this is meaning that the adsorption process of CR and BB dyes onto adsorbents was physiochemical adsorption approach.

4.2.7. Desorption Experiment of CR & BB Dyes

To make the adsorption process more economical, it was expedient to regenerate both adsorbents and dyes, which could be recycled further [207]. The desorption process studies are also important to understand the adsorption mechanism of adsorbate onto an adsorbent. Desorption is primarily performed to remove the reversible adsorbate molecules on the adsorbent and to regenerate the adsorbents [208].

The efficiency of the dyes desorption removal (%S) was calculated by the following equation [209]:

$$\mathbf{S} = \frac{\mathbf{C_d . V_d}}{\mathbf{q_e . W}} \times \mathbf{100\%} \quad \ldots\ldots (\mathbf{4.16})$$

Where q_e (mg/g) is the equilibrium amount of dye adsorbed on the adsorbent; C_d (mg/L) is the dye concentration in solution after desorption, and V_d (ml) is the volume of the eluent (Desorbent reagent).

Tables (4.11 and 4.12) shows the adsorption-desorption process of both dyes from the prepared adsorbents using distilled water as desorption agent for three cycles, where the decreasing of adsorption efficiency from cycle one to cycle three were (31.13, 32.45, 29.51, 34.25, 34.12, and 37.07%) for CR dye, and were (37.70, 34.79, 35.72, 34.02, 35.45, and 31.10%) for BB dye that's adsorbed from prepared adsorbents; GO, GO/DAB, GO/DAB/EDTA, GO/CS, GO/CS/EDTA, and GO/pBCM respectively. That is means that these adsorbents could be used several times while retaining their good adsorption capacity, and a relatively low percentage of the desorption values (S%)

suggests that both dyes were chemisorbed onto the surface of GO-modified adsorbents compared to graphene oxide [210].

Table 4.11. Adsorption/Desorption for CR dye onto prepared adsorbents

Cycle No.	GO		GO/DAB		GO/DAB/E		GO/CS		GO/CS/E		GO/pBCM	
	q_e	%S	q_e	%S	q_e	%S	q_e	%S	q_e	%S	q_e	%S
1	1050.31	81.32	1096.82	68.48	1168.22	77.03	1668.77	64.92	1886.82	75.73	1196.61	72.41
2	841.66	70.33	863.41	55.93	958.98	68.14	1321.34	54.80	1541.24	66.67	990.62	63.87
3	723.33	62.11	740.68	44.07	823.74	57.04	1097.08	43.81	1318.17	55.14	753.02	52.20

Table 4.12. Adsorption/Desorption for BB dye onto prepared adsorbents

Cycle No.	GO		GO/DAB		GO/DAB/E		GO/CS		GO/CS/E		GO/pBCM	
	q_e	%S	q_e	%S	q_e	%S	q_e	%S	q_e	%S	q_e	%S
1	745.11	79.01	1501.44	70.73	755.09	66.51	788.07	72.71	755.87	68.01	764.43	73.18
2	532.55	71.52	1121.81	63.41	557.03	60.67	593.08	69.05	560.16	65.23	599.63	67.40
3	464.13	68.30	979.06	51.91	485.35	48.33	519.91	66.00	487.90	63.76	526.63	54.82

q_e: (mg/g), %S: Desorption system

A desorption study gives a good explanation of the significant characteristics of an appropriate adsorbent for practical applications. Besides, the regeneration of adsorbent generally leads to the recovery of dyes, reuse of adsorbent in the adsorption study, and cost of the adsorption process [211]. Where, the desorption percentages (%S) of GO were (81.32% to 62.11%) and (79.01% to 68.30%) from first to the third cycle for both CR and BB dyes

respectively, and these desorption percentages were higher than of the other five adsorbents that derived from GO i.e.; GO/DAB, GO/DAB/EDTA, GO/CS, GO/CS/EDTA, and GO/pBCM, and this may be attributed to the sufficient functional groups in this derivatives (the adsorption sites) with compared with GO.

The adsorbents GO/BAD, GO/BAD/EDTA, GO/CS, GO/CS/EDTA, and GO/pBCM were having more functional groups, thus they show a lower %S, and this led to understanding the importance of functional groups in this adsorbents understudy for both dyes.

5. Conclusions and Recommendations

5.1. Conclusions

The conclusions of our work are summarized in the followings points;

1. Graphene Oxide and its composites are successfully prepared from Graphite powder at suitable conditions.

2. Graphene Oxide-Composites used as adsorbents with modified surfaces revealed high adsorption efficiency and high ability to remove Congo Red and Bismarck Brown dyes from their aqueous solutions.

3. The study showed that the adsorption efficiency of these compounds depends on:

(i) pH
(ii) Agitation Time
(iii) Temperature

4. The results reveal the adsorption at the equilibrium follows Langmuir isotherm.

5. The kinetic data for adsorption of both dyes onto prepared adsorbents obeyed the Pseudo-Second Order model.

6. The investigation of $\Delta H°$ and $\Delta G°$ indicate that the adsorption of both dyes onto prepared adsorbents is Endothermic (expect GOCS adsorbent with CR dye) and Spontaneous.

7. The mean adsorption energy (E) from the Dubinin-Radushkevich isotherm and the activation energy (E_a) from the Arrhenius equation indicated that the adsorption process might be the dual nature of physisorption and chemisorption, and was predominant in the chemisorption process of both dyes on prepared adsorbents.

8. The desorption-adsorption study showed good reusability and stability of the prepared adsorbents after the third cycle.

5.2. Recommendations

The present work introduced the successful preparation of Graphene Oxide-composites. The surfaces of these compounds have been used to adsorb

two dyes of CR and BB from their aqueous solutions. Suggested future work for more insights and application are as follows;

1. Preparing more GO-composite by grafted GO with some biodegradable polymers which are considered environmentally friendly because of their biodegradability, especially in the form of nanocomposites (EFPNCs).

2. Impregnated prepared GO-composites with magnetic nanoparticles such as Fe_3O_4, $CdFe_2O_4$, and others to enhance their adsorption efficiency and gaining magnetic filtration benefits.

3. Impregnated prepared GO-composites with quantum-dots nanoparticles such as ZnS, CdS, and others to enhance their adsorption efficiency.

4. Using the prepared GO-composites to remove heavy element ions such as iron, lead, manganese, mercury, cadmium, and other ions.

5. Using the prepared GO-composites to remove pollutant hydrocarbons such as detergents, pesticides, and others.

6. Applying another analytical approach to removing dyes onto GO and the prepared GO-composites such as solid-phase extraction (SPE).

7. Study the adsorption of some pollutant gases such as CO_2 and NO_X onto prepared GO-composites.

References

[1] P.B. Arthi G, L. Bd, A Simple Approach to Stepwise Synthesis of Graphene Oxide Nanomaterial, Journal of Nanomedicine & Nanotechnology, 06 (2015).

[2] B. Ankamwar, F. Surti, Water Soluble Graphene Synthesis, Chemical Science Transactions, 1 (2012) 500-507.

[3] F. Ban, S. Majid, N. Huang, H. Lim, Graphene oxide and its electrochemical performance, Int. J. Electrochem. Sci, 7 (2012) 4345-4351.

[4] H. Xu, Q. Yang, F. Li, L. Tang, S. Gao, B. Jiang, X. Zhao, L. Wang, C. Fan, A graphene-based platform for fluorescent detection of SNPs, Analyst, 138 (2013) 2678-2682.

[5] Q. Wu, Y. Sun, P. Ma, D. Zhang, S. Li, X. Wang, D. Song, Gold nanostar-enhanced surface plasmon resonance biosensor based on carboxyl-functionalized graphene oxide, Anal Chim Acta, 913 (2016) 137-144.

[6] X. Wang, Y. Liu, H. Pang, S. Yu, Y. Ai, X. Ma, G. Song, T. Hayat, A. Alsaedi, X. Wang, Effect of graphene oxide surface modification on the elimination of Co (II) from aqueous solutions, Chem. Eng. J., 344 (2018) 380-390.

[7] X. Ren, Q. Wu, H. Xu, D. Shao, X. Tan, W. Shi, C. Chen, J. Li, Z. Chai, T. Hayat, New insight into GO, cadmium (II), phosphate interaction and its role in GO colloidal behavior, Environmental science & technology, 50 (2016) 9361-9369.

[8] S. Yu, X. Wang, Y. Ai, Y. Liang, Y. Ji, J. Li, T. Hayat, A. Alsaedi, X. Wang, Spectroscopic and theoretical studies on the counterion effect of Cu (II) ion and graphene oxide interaction with titanium dioxide, Environmental Science: Nano, 3 (2016) 1361-1368.

[9] S. Yu, X. Wang, W. Yao, J. Wang, Y. Ji, Y. Ai, A. Alsaedi, T. Hayat, X. Wang, Macroscopic, spectroscopic, and theoretical investigation for the interaction of phenol and naphthol on reduced graphene oxide, Environmental science & technology, 51 (2017) 3278-3286.

[10] B.C. Brodie, XIII. On the atomic weight of graphite, Philosophical Transactions of the Royal Society of London, 149 (1859) 249-259.

[11] L. Staudenmaier, Verfahren zur darstellung der graphitsäure, Berichte der deutschen chemischen Gesellschaft, 31 (1898) 1481-1487.

[12] W.S. Hummers Jr, R.E. Offeman, Preparation of graphitic oxide, Journal of the American chemical society, 80 (1958) 1339-1339.

[13] K. Krishnamoorthy, M. Veerapandian, K. Yun, S.-J. Kim, The chemical and structural analysis of graphene oxide with different degrees of oxidation, Carbon, 53 (2013) 38-49.

[14] A.M. Dimiev, S. Eigler, Graphene oxide: fundamentals and applications, John Wiley & Sons2016.

[15] X. Gao, D.-e. Jiang, Y. Zhao, S. Nagase, S. Zhang, Z. Chen, Theoretical insights into the structures of graphene oxide and its chemical conversions between graphene, Journal of Computational and Theoretical Nanoscience, 8 (2011) 2406-2422.

[16] S. Stankovich, D.A. Dikin, R.D. Piner, K.A. Kohlhaas, A. Kleinhammes, Y. Jia, Y. Wu, S.T. Nguyen, R.S. Ruoff, Synthesis of graphene-based nanosheets via chemical reduction of exfoliated graphite oxide, carbon, 45 (2007) 1558-1565.

[17] J. Paredes, S. Villar-Rodil, A. Martínez-Alonso, J. Tascon, Graphene oxide dispersions in organic solvents, Langmuir, 24 (2008) 10560-10564.

[18] Y. Liang, D. Wu, X. Feng, K. Müllen, Dispersion of graphene sheets in organic solvent supported by ionic interactions, Advanced Materials, 21 (2009) 1679-1683.

[19] X. Gao, J. Jang, S. Nagase, Hydrazine and thermal reduction of graphene oxide: reaction mechanisms, product structures, and reaction design, The Journal of Physical Chemistry C, 114 (2009) 832-842.

[20] S. Kim, S. Zhou, Y. Hu, M. Acik, Y.J. Chabal, C. Berger, W. De Heer, A. Bongiorno, E. Riedo, Room-temperature metastability of multilayer graphene oxide films, Nature Materials, 11 (2012) 544.

[21] P. Sun, F. Zheng, M. Zhu, K. Wang, M. Zhong, D. Wu, H. Zhu, Realizing synchronous energy harvesting and ion separation with graphene oxide membranes, Scientific reports, 4 (2014) 5528.

[22] A.V. Talyzin, T. Hausmaninger, S. You, T. Szabó, The structure of graphene oxide membranes in liquid water, ethanol and water-ethanol mixtures, Nanoscale, 6 (2014) 272-281.

[23] W. Gao, Graphene oxide: reduction recipes, spectroscopy, and applications, Springer2015.

[24] R. Joshi, P. Carbone, F.C. Wang, V.G. Kravets, Y. Su, I.V. Grigorieva, H. Wu, A.K. Geim, R.R. Nair, Precise and ultrafast molecular sieving through graphene oxide membranes, science, 343 (2014) 752-754.

[25] W. Gao, L.B. Alemany, L. Ci, P.M. Ajayan, New insights into the structure and reduction of graphite oxide, Nature Chemistry, 1 (2009) 403.

[26] H.W. Kim, H.W. Yoon, S.-M. Yoon, B.M. Yoo, B.K. Ahn, Y.H. Cho, H.J. Shin, H. Yang, U. Paik, S. Kwon, Selective gas transport through few-layered graphene and graphene oxide membranes, Science, 342 (2013) 91-95.

[27] D.R. Dreyer, A.D. Todd, C.W. Bielawski, Harnessing the chemistry of graphene oxide, Chemical Society Reviews, 43 (2014) 5288-5301.

[28] X.-Z. Tang, W. Li, Z.-Z. Yu, M.A. Rafiee, J. Rafiee, F. Yavari, N. Koratkar, Enhanced thermal stability in graphene oxide covalently functionalized with 2-amino-4, 6-didodecylamino-1, 3, 5-triazine, Carbon, 49 (2011) 1258-1265.

[29] Z.-B. Liu, Y.-F. Xu, X.-Y. Zhang, X.-L. Zhang, Y.-S. Chen, J.-G. Tian, Porphyrin, and fullerene covalently functionalized graphene hybrid materials with large nonlinear optical properties, The Journal of Physical Chemistry B, 113 (2009) 9681-9686.

[30] O. Akhavan, E. Ghaderi, Toxicity of graphene and graphene oxide nanowalls against bacteria, ACS nano, 4 (2010) 5731-5736.

[31] X. Fan, W. Peng, Y. Li, X. Li, S. Wang, G. Zhang, F. Zhang, Deoxygenation of exfoliated graphite oxide under alkaline conditions: a green route to graphene preparation, Advanced Materials, 20 (2008) 4490-4493.

[32] L.J. Cote, F. Kim, J. Huang, Langmuir− Blodgett assembly of graphite oxide single layers, Journal of the American Chemical Society, 131 (2008) 1043-1049.

[33] L. Feng, X. Yang, X. Shi, X. Tan, R. Peng, J. Wang, Z. Liu, Polyethylene glycol and polyethyleneimine dual-functionalized nano-graphene oxide for photothermally enhanced gene delivery, Small, 9 (2013) 1989-1997.

[34] J.T. Robinson, S.M. Tabakman, Y. Liang, H. Wang, H. Sanchez Casalongue, D. Vinh, H. Dai, Ultrasmall reduced graphene oxide with high near-infrared absorbance for photothermal therapy, Journal of the American Chemical Society, 133 (2011) 6825-6831.

[35] W.R. Collins, E. Schmois, T.M. Swager, Graphene oxide as an electrophile for carbon nucleophiles, Chem. Commun., 47 (2011) 8790-8792.

[36] D. Chen, H. Feng, J. Li, Graphene oxide: preparation, functionalization, and electrochemical applications, Chemical reviews, 112 (2012) 6027-6053.

[37] T. Kuilla, S. Bhadra, D. Yao, N.H. Kim, S. Bose, J.H. Lee, Recent advances in graphene-based polymer composites, Progress in polymer science, 35 (2010) 1350-1375.

[38] J. Liang, Y. Huang, L. Zhang, Y. Wang, Y. Ma, T. Guo, Y. Chen, Molecular-level dispersion of graphene into poly (vinyl alcohol) and effective reinforcement of their nanocomposites, Advanced Functional Materials, 19 (2009) 2297-2302.

[39] W. Chee, H. Lim, N. Huang, I. Harrison, Nanocomposites of graphene/polymers: a review, Rsc Advances, 5 (2015) 68014-68051.

[40] C. Lee, X. Wei, J.W. Kysar, J. Hone, Measurement of the elastic properties and intrinsic strength of monolayer graphene, Science, 321 (2008) 385-388.

[41] C. Gómez-Navarro, M. Burghard, K. Kern, Elastic properties of chemically derived single graphene sheets, Nano letters, 8 (2008) 2045-2049.

[42] S. Stankovich, D.A. Dikin, G.H. Dommett, K.M. Kohlhaas, E.J. Zimney, E.A. Stach, R.D. Piner, S.T. Nguyen, R.S. Ruoff, Graphene-based composite materials, nature, 442 (2006) 282.

[43] Y. Lin, J. Jin, M. Song, Preparation and characterization of covalent polymer functionalized graphene oxide, J. Mater. Chem., 21 (2011) 3455-3461.

[44] H.-B. Zhang, W.-G. Zheng, Q. Yan, Y. Yang, J.-W. Wang, Z.-H. Lu, G.-Y. Ji, Z.-Z. Yu, Electrically conductive polyethylene terephthalate/graphene nanocomposites prepared by melt compounding, Polymer, 51 (2010) 1191-1196.

[45] S. Bose, T. Kuila, M.E. Uddin, N.H. Kim, A.K. Lau, J.H. Lee, In-situ synthesis and characterization of electrically conductive polypyrrole/graphene nanocomposites, Polymer, 51 (2010) 5921-5928.

[46] F. Wu, Y. Lu, G. Shao, F. Zeng, Q. Wu, Preparation of polyacrylonitrile/graphene oxide by in situ polymerization, Polymer International, 61 (2012) 1394-1399.

[47] K.S. Choi, F. Liu, J.S. Choi, T.S. Seo, Fabrication of free-standing multilayered graphene and poly (3, 4-ethylene dioxythiophene) composite films with enhanced conductive and mechanical properties, Langmuir, 26 (2010) 12902-12908.

[48] N. Olaniran, Environment and Health: An Introduction, Environment and Health. Lagos. Macmillan Nig. Pub. Co for NCF, (1995) 34-151.

[49] S.K. Singh, Water Pollution: Sources, Effects, and Control Measures, Journal of Agroecology and Natural Resource Management, 3 (2016) 64-66.

[50] C. Raji, T. Anirudha, Chromium (VI) adsorption by sawdust carbon: Kinetics and equilibrium, (1997).

[51] M.V. Tuttolomondo, G.S. Alvarez, M.F. Desimone, L.E. Diaz, Removal of azo dyes from water by sol-gel immobilized Pseudomonas sp, J. of Environ. Chem. Eng., 2 (2014) 131-136.

[52] E. Brillas, C.A. Martínez-Huitle, Decontamination of wastewaters containing synthetic organic dyes by electrochemical methods. An updated review, App. Catal. B: Environ., 166 (2015) 603-643.

[53] D. El-Mekkawi, H. Galal, Removal of a synthetic dye “Direct Fast Blue B2RL” via adsorption and photocatalytic degradation using low-cost rutile

and Degussa P25 titanium dioxide, Journal of hydro-environment research, 7 (2013) 219-226.

[54] A. Gürses, M. Açıkyıldız, K. Güneş, M.S. Gürses, Colorants in health and environmental aspects, Dyes Pigments, Springer2016, pp. 69-83.

[55] A. Demirbas, Agricultural-based activated carbons for the removal of dyes from aqueous solutions: a review, J. Hazard. Mater., 167 (2009) 1-9.

[56] N. Ali, A. Hameed, S. Ahmed, Physicochemical characterization and bioremediation perspective of textile effluent, dyes, and metals by indigenous bacteria, J. Hazard. Mater., 164 (2009) 322-328.

[57] G. Crini, Non-conventional low-cost adsorbents for dye removal: a review, Bioresour. Technol., 97 (2006) 1061-1085.

[58] S.P. Buthelezi, A.O. Olaniran, B. Pillay, Textile dye removal from wastewater effluents using bioflocculants produced by indigenous bacterial isolates, Molecules, 17 (2012) 14260-14274.

[59] W.W. Ngah, M. Hanafiah, Removal of heavy metal ions from wastewater by chemically modified plant wastes as adsorbents: a review, Bioresour. Technol., 99 (2008) 3935-3948.

[60] S. Sathian, M. Rajasimman, G. Radha, V. Shanmugapriya, C. Karthikeyan, Performance of SBR for the treatment of textile dye wastewater: Optimization and kinetic studies, Alexandria Engineering Journal, 53 (2014) 417-426.

[61] M.M. Matlock, B.S. Howerton, D.A. Atwood, Chemical precipitation of lead from lead battery recycling plant wastewater, Industrial & engineering chemistry research, 41 (2002) 1579-1582.

[62] G. Ratnamala, K. Brajesh, Biosorption of removal navy blue dye from an aqueous solution using pseudomonas putida, International Journal of Science, Environment and Technology, 2 (2013) 80-89.

[63] M. Kobya, E. Demirbas, E. Senturk, M. Ince, Adsorption of heavy metal ions from aqueous solutions by activated carbon prepared from apricot stone, Bioresour. Technol., 96 (2005) 1518-1521.

[64] B. Fonseca, H. Figueiredo, J. Rodrigues, A. Queiroz, T. Tavares, Mobility of Cr, Pb, Cd, Cu and Zn in a loamy sand soil: A comparative study, Geoderma, 164 (2011) 232-237.

[65] X. Tan, Q. Fan, X. Wang, B. Grambow, Eu (III) sorption to TiO2 (anatase and rutile): batch, XPS, and EXAFS studies, Environmental science & technology, 43 (2009) 3115-3121.

[66] D. Garg, Adsorptive removal of dyes from aqueous solution using Cu-BTC and Commercial Activated Carbon, 2012.

[67] C.R. Williamson, M.D. Picard, Petrology of carbonate rocks of the Green River Formation (Eocene), Journal of Sedimentary Research, 44 (1974).

[68] S. Jiulong, Development of inorganic-organic hybrid materials for wastewater treatment, 2014.

[69] F.S. Abbas, Dyes removal from wastewater using agricultural waste, Advances in Environmental Biology, 7 (2013) 1019-1026.

[70] A.M.K. Aljebori, A.N. Alshirifi, Effect of different parameters on the adsorption of textile dye maxilon blue GRL from aqueous solution by using white marble, Asian journal of chemistry, 24 (2012) 5813.

[71] F.M. Mohammed, Modelling and design of water treatment processes using adsorption and electrochemical regeneration, The University of Manchester (United Kingdom), 2011.

[72] H.D. Beyene, The potential of dye removal from textile wastewater by using different treatment technology. A review, Int J Environ Monit Anal, 2 (2014) 347-353.

[73] W. McCabe, J. Smith, P. Harriot, Fluid flow phenomena, Unit Operations of Chemical Engineering (JC Warren L. McCabe eds.), (2005) 45-67.

[74] J.R. Potts, D.R. Dreyer, C.W. Bielawski, R.S. Ruoff, Graphene-based polymer nanocomposites, Polymer, 52 (2011) 5-25.

[75] V. Chandra, J. Park, Y. Chun, J.W. Lee, I.-C. Hwang, K.S. Kim, Water-dispersible magnetite-reduced graphene oxide composites for arsenic removal, ACS nano, 4 (2010) 3979-3986.

[76] V. Chandra, K.S. Kim, Highly selective adsorption of Hg^{2+} by polypyrrole–reduced graphene oxide composite, Chem. Commun., 47 (2011) 3942-3944.

[77] G. Zhao, L. Jiang, Y. He, J. Li, H. Dong, X. Wang, W. Hu, Sulfonated graphene for persistent aromatic pollutant management, Advanced Materials, 23 (2011) 3959-3963.

[78] J. Zhao, L. Liu, F. Li, Graphene oxide: physics and applications, Springer2015.

[79] Z. Liu, J.T. Robinson, X. Sun, H. Dai, PEGylated nanographene oxide for delivery of water-insoluble cancer drugs, Journal of the American Chemical Society, 130 (2008) 10876-10877.

[80] L. Zhang, J. Xia, Q. Zhao, L. Liu, Z. Zhang, Functional graphene oxide as a nanocarrier for controlled loading and targeted delivery of mixed anticancer drugs, small, 6 (2010) 537-544.

[81] G. Gollavelli, C.-C. Chang, Y.-C. Ling, Facile synthesis of smart magnetic graphene for safe drinking water: heavy metal removal and disinfection control, ACS Sustainable Chemistry & Engineering, 1 (2013) 462-472.

[82] H. Gao, Y. Sun, J. Zhou, R. Xu, H. Duan, Mussel-inspired synthesis of polydopamine-functionalized graphene hydrogel as reusable adsorbents for water purification, ACS applied materials & interfaces, 5 (2013) 425-432.

[83] G. Zhao, J. Li, X. Ren, C. Chen, X. Wang, Few-layered graphene oxide nanosheets as superior sorbents for heavy metal ion pollution management, Environmental science & technology, 45 (2011) 10454-10462.

[84] P. Kush, K. Deori, A. Kumar, S. Deka, Efficient hydrogen/oxygen evolution and photocatalytic dye degradation and reduction of aqueous Cr (VI) by surfactant-free hydrophilic Cu 2 ZnSnS 4 nanoparticles, Journal of Materials Chemistry A, 3 (2015) 8098-8106.

[85] M. Hui, P. Shengyan, H. Yaqi, Z. Rongxin, Z. Anatoly, C. Wei, A highly efficient magnetic chitosan “fluid” adsorbent with a high capacity and fast

adsorption kinetics for dyeing wastewater purification, Chem. Eng. J., 345 (2018) 556-565.

[86] S. He, X. Liu, P. Yan, A. Wang, J. Su, X. Su, Preparation of Gemini surfactant/graphene oxide composites and their superior performance for Congo red adsorption, RSC advances, 9 (2019) 4908-4916.

[87] S. Hou, S. Su, M.L. Kasner, P. Shah, K. Patel, C.J. Madarang, Formation of highly stable dispersions of silane-functionalized reduced graphene oxide, Chemical Physics Letters, 501 (2010) 68-74.

[88] L. Zhou, C. Gao, W. Xu, Magnetic dendritic materials for highly efficient adsorption of dyes and drugs, ACS applied materials & interfaces, 2 (2010) 1483-1491.

[89] J. Su, S. He, Z. Zhao, X. Liu, H. Li, Efficient preparation of cetyltrimethylammonium bromide-graphene oxide composite and its adsorption of Congo red from aqueous solutions, Colloids Surf., A: Physico. Eng. Asp., 554 (2018) 227-236.

[90] Q. Zhao, X. Zhu, B. Chen, Stable graphene oxide/poly (ethyleneimine) 3D aerogel with tunable surface charge for high-performance selective removal of ionic dyes from water, Chem. Eng. J., 334 (2018) 1119-1127.

[91] A. Molla, Y. Li, B. Mandal, S.G. Kang, S.H. Hur, J.S. Chung, Selective adsorption of organic dyes on graphene oxide: theoretical and experimental analysis, Appl. Surf. Sci., 464 (2019) 170-177.

[92] A. Abd-Elhamid, E.A. Kamoun, A.A. El-Shanshory, H.M. Soliman, H. Aly, Evaluation of graphene oxide-activated carbon as effective composite adsorbent toward the removal of cationic dyes: composite preparation, characterization and adsorption parameters, Journal of Molecular Liquids, 279 (2019) 530-539.

[93] M. Rajabi, K. Mahanpoor, O. Moradi, Thermodynamic and kinetic studies of crystal violet dye adsorption with poly (methyl methacrylate)–graphene oxide and poly (methyl methacrylate)–graphene oxide–zinc oxide nanocomposites, Journal of Applied Polymer Science, 136 (2019) 47495.

[94] Q. Han, W. Li, Z. Zhou, Z. Fang, L. Chen, Z. Xu, X. Qian, Graphene Oxide/Polyacrylic acid-based double network skeleton for enhanced cationic dye adsorption, Polymer-Plastics Technology and Materials, 58 (2019) 1638-1648.

[95] W. Czepa, D. Pakulski, S. Witomska, V. Patroniak, A. Ciesielski, P. Samorì, Graphene oxide-mesoporous SiO2 hybrid composite for fast and efficient removal of organic cationic contaminants, Carbon, 158 (2020) 193-201.

[96] T.J.M. Fraga, Z.S.B. de Souza, D.M. dos Santos Fraga, M.N. Carvalho, E.M.P. de Luna Freire, M.G. Ghislandi, M.A. da Motta Sobrinho, Comparative approach towards the adsorption of Reactive Black 5 and methylene blue by n-layer graphene oxide and its amino-functionalized derivative, Adsorption, 26 (2020) 283-301.

[97] J. Bu, L. Yuan, N. Zhang, D. Liu, Y. Meng, X. Peng, High-efficiency adsorption of methylene blue dye from wastewater by a thiosemicarbazide functionalized graphene oxide composite, Diamond and Related Materials, 101 (2020) 107604.

[98] A.S. Elsherbiny, A.H. Gemeay, M.A. Salem, Adsorption efficiency of graphene oxide towards cyanine dyes with different alkyl chain lengths, Sep. Sci. Technol., (2020) 1-9.

[99] T.-H. Liou, M.-H. Lin, Characterization of graphene oxide supported porous silica for effectively enhancing adsorption of dyes, Sep. Sci. Technol., 55 (2020) 431-443.

[100] J. Zhang, M.S. Azam, C. Shi, J. Huang, B. Yan, Q. Liu, H. Zeng, Poly (acrylic acid) functionalized magnetic graphene oxide nanocomposite for removal of methylene blue, RSC Advances, 5 (2015) 32272-32282.

[101] C.H. Nguyen, M.L. Tran, T.T. Van Tran, R.-S. Juang, Enhanced removal of various dyes from aqueous solutions by UV and simulated solar photocatalysis over TiO2/ZnO/rGO composites, Sep. Purif. Technol., 232 (2020) 115962.

[102] C. Karthik, N. Swathi, D. Caroline, Green synthesized rGO-AgNP hybrid nanocomposite–An effective antibacterial adsorbent for photocatalytic

removal of DB-14 dye from aqueous solution, J. of Environ. Chem. Eng., 8 (2020) 103577.

[103] W.L.F. Armarego, C. Chai, C.L.L. Chai, I. Books24x7, Knovel, Purification of Laboratory Chemicals, Butterworth-Heinemann2003.

[104] A.O. da Silva, R.P. Weber, S.N. Monteiro, A.M. Lima, G.S. Faria, W.O. da Silva, S.d.S.A. Oliveira, K.G. de Castro Monsores, W.A. Pinheiro, Effect of graphene oxide coating on the ballistic performance of aramid fabric, J. Mater. Res. Technol., (2020).

[105] C. Shen, E. Barrios, M. McInnis, J. Zuyus, L. Zhai, Fabrication of graphene aerogels with heavily loaded metallic nanoparticles, Micromachines, 8 (2017) 47.

[106] R.L. White, C.M. White, H. Turgut, A. Massoud, Z.R. Tian, Comparative studies on copper adsorption by graphene oxide and functionalized graphene oxide nanoparticles, Journal of the Taiwan Institute of Chemical Engineers, 85 (2018) 18-28.

[107] M. Ghorbani, A. Shams, O. Seyedin, N.A. Lahoori, Magnetic ethylene diamine-functionalized graphene oxide as a novel sorbent for removal of lead and cadmium ions from wastewater samples, Environ. Sci. Pollut. Res., 25 (2018) 5655-5667.

[108] P. Kumar, A. Bansiwal, N. Labhsetwar, S.L. Jain, Visible light assisted photocatalytic reduction of CO 2 using a graphene oxide supported heteroleptic ruthenium complex, Green Chemistry, 17 (2015) 1605-1609.

[109] L. Cui, Y. Wang, L. Gao, L. Hu, L. Yan, Q. Wei, B. Du, EDTA functionalized magnetic graphene oxide for removal of Pb (II), Hg (II) and Cu (II) in water treatment: Adsorption mechanism and separation property, Chem. Eng. J., 281 (2015) 1-10.

[110] L. Li, C. Luo, X. Li, H. Duan, X. Wang, Preparation of magnetic ionic liquid/chitosan/graphene oxide composite and application for water treatment, Int. J. Biol. Macromol., 66 (2014) 172-178.

[111] D. Depan, B. Girase, J. Shah, R. Misra, Structure–process–property relationship of the polar graphene oxide-mediated cellular response and

stimulated growth of osteoblasts on hybrid chitosan network structure nanocomposite scaffolds, Acta Biomater., 7 (2011) 3432-3445.

[112] R. Islamova, O. Golovochesova, Y.B. Monakov, I. Utepova, A. Musikhina, O. Chupakhin, Effect of heterocyclic derivatives of ferrocene on free-radical polymerization of methyl methacrylate and styrene, Polym. Sci. Ser. B., 52 (2010) 637-647.

[113] L. Yakimtsova, E. Egorova, Y.I. Matusevich, K. Selevich, A. Kurtikova, Preparation and thermal degradation of methyl methacrylate-methacrylic acid copolymers, Russ. J. Appl. Chem., 82 (2009) 1636-1643.

[114] J. Liu, G. Liu, W. Liu, Preparation of water-soluble β-cyclodextrin/poly (acrylic acid)/graphene oxide nanocomposites as new adsorbents to remove cationic dyes from aqueous solutions, Chem. Eng. J., 257 (2014) 299-308.

[115] R.W. Sabnis, Handbook of biological dyes and stains: synthesis and industrial applications, John Wiley & Sons2010.

[116] M. Bera, P. Gupta, P.K. Maji, Facile one-pot synthesis of graphene oxide by sonication assisted mechanochemical approach and its surface chemistry, Journal of nanoscience and nanotechnology, 18 (2018) 902-912.

[117] M. Zhong, Y.-T. Liu, X.-M. Xie, Self-healable, super-tough graphene oxide–poly (acrylic acid) nanocomposite hydrogels facilitated by dual cross-linking effects through dynamic ionic interactions, J. Mater. Chem. B, 3 (2015) 4001-4008.

[118] J. Ma, P. Cai, W. Qi, D. Kong, H. Wang, The layer-by-layer assembly of polyelectrolyte functionalized graphene sheets: a potential tool for biosensing, Colloids Surf., A: Physico. Eng. Asp., 426 (2013) 6-11.

[119] D.R. Chowdhury, C. Singh, A. Paul, Role of graphite precursor and sodium nitrate in graphite oxide synthesis, RSC Advances, 4 (2014) 15138-15145.

[120] C. Bao, L. Song, W. Xing, B. Yuan, C.A. Wilkie, J. Huang, Y. Guo, Y. Hu, Preparation of graphene by pressurized oxidation and multiplex reduction and its polymer nanocomposites by masterbatch-based melt blending, J. Mater. Chem., 22 (2012) 6088-6096.

[121] D. Galpaya, M. Wang, G. George, N. Motta, E. Waclawik, C. Yan, Preparation of graphene oxide/epoxy nanocomposites with significantly improved mechanical properties, Journal of Applied Physics, 116 (2014) 053518.

[122] D.L. Pavia, G.M. Lampman, G.S. Kriz, J.A. Vyvyan, Introduction to spectroscopy, Cengage Learning2008.

[123] R.-r. Shan, L.-g. Yan, K. Yang, S.-j. Yu, Y.-f. Hao, H.-q. Yu, B. Du, Magnetic Fe3O4/MgAl-LDH composite for effective removal of three red dyes from aqueous solution, Chem. Eng. J., 252 (2014) 38-46.

[124] R. Extremera, I. Pavlovic, M. Pérez, C. Barriga, Removal of acid orange 10 by calcined Mg/Al layered double hydroxides from water and recovery of the adsorbed dye, Chem. Eng. J., 213 (2012) 392-400.

[125] L. Cui, X. Guo, Q. Wei, Y. Wang, L. Gao, L. Yan, T. Yan, B. Du, Removal of mercury and methylene blue from aqueous solution by xanthate functionalized magnetic graphene oxide: sorption kinetic and uptake mechanism, J. Colloid Interface Sci., 439 (2015) 112-120.

[126] C. Zhao, L. Ma, J. You, F. Qu, R.D. Priestley, EDTA-and amine-functionalized graphene oxide as sorbents for Ni (II) removal, Desal. Water Treat., 57 (2016) 8942-8951.

[127] W.M. El Rouby, A.A. Farghali, M. Sadek, W.F. Khalil, Fast Removal of Sr (II) From Water by Graphene Oxide and Chitosan Modified Graphene Oxide, J. Inorg, Organomet. Polym. Mater., 28 (2018) 2336-2349.

[128] L. Zhang, H. Luo, P. Liu, W. Fang, J. Geng, A novel modified graphene oxide/chitosan composite used as an adsorbent for Cr (VI) in aqueous solutions, Int. J. Biol. Macromol., 87 (2016) 586-596.

[129] H. Ge, Z. Ma, Microwave preparation of triethylenetetramine modified graphene oxide/chitosan composite for adsorption of Cr (VI), Carbohydr. Polym., 131 (2015) 280-287.

[130] L. Liu, C. Li, C. Bao, Q. Jia, P. Xiao, X. Liu, Q. Zhanc, Preparation and characterization of chitosan, Talanta, 93 (2012) 350-357.

[131] S. Park, K.-S. Lee, G. Bozoklu, W. Cai, S.T. Nguyen, R.S. Ruoff, Graphene oxide papers modified by divalent ions—enhancing mechanical properties via chemical cross-linking, ACS nano, 2 (2008) 572-578.

[132] H.P. Cong, P. Wang, S.H. Yu, Highly elastic and super stretchable graphene oxide/polyacrylamide hydrogels, Small, 10 (2014) 448-453.

[133] C. Babaç, G. Güven, G. David, B.C. Simionescu, E. Pişkin, Production of nanoparticles of methyl methacrylate and butyl methacrylate copolymers by microemulsion polymerization in the presence of maleic acid terminated poly (N-acetylethylenimine) macromonomers as cosurfactant, European polymer journal, 40 (2004) 1947-1952.

[134] S. Khorrami, Z. Abdollahi, G. Eshaghi, A. Khosravi, E. Bidram, A. Zarrabi, An improved method for fabrication of Ag-GO nanocomposite with controlled anti-cancer and anti-bacterial behavior; a comparative study, Scientific reports, 9 (2019) 1-10.

[135] H.-L. Ma, Y. Zhang, Q.-H. Hu, D. Yan, Z.-Z. Yu, M. Zhai, Chemical reduction and removal of Cr (VI) from acidic aqueous solution by ethylenediamine-reduced graphene oxide, J. Mater. Chem., 22 (2012) 5914-5916.

[136] S. Kumar, J. Koh, Physiochemical and optical properties of chitosan based graphene oxide bionanocomposite, Int. J. Biol. Macromol., 70 (2014) 559-564.

[137] M. Mahmoudian, E. Nozad, M. Hosseinzadeh, Characterization of EDTA functionalized graphene oxide/polyethersulfone (FGO/PES) nanocomposite membrane and using for elimination of heavy metal and dye contaminations, 폴리머, 42 (2018) 434-445.

[138] Y. Huang, M. Zeng, J. Ren, J. Wang, L. Fan, Q. Xu, Preparation and swelling properties of graphene oxide/poly (acrylic acid-co-acrylamide) super-absorbent hydrogel nanocomposites, Colloids Surf., A: Physico. Eng. Asp., 401 (2012) 97-106.

[139] B.K. Saikia, R.K. Boruah, P.K. Gogoi, A X-ray diffraction analysis on graphene layers of Assam coal, Journal of chemical sciences, 121 (2009) 103-106.

[140] G. Liu, L. Wang, B. Wang, T. Gao, D. Wang, A reduced graphene oxide modified metallic cobalt composite with superior electrochemical performance for supercapacitors, RSC Advances, 5 (2015) 63553-63560.

[141] T.N. Blanton, D. Majumdar, Characterization of X-ray irradiated graphene oxide coatings using X-ray diffraction, X-ray photoelectron spectroscopy, and atomic force microscopy, Powder Diffr., 28 (2013) 68-71.

[142] A.N. Abd, A.H. Al-Agha, M.A. Alheety, Addition of some primary and secondary amines to graphene oxide, and studying their Effect on Increasing its Electrical Properties, Baghdad Science Journal, 13 (2016) 1.

[143] D. Han, L. Yan, W. Chen, W. Li, Preparation of chitosan/graphene oxide composite film with enhanced mechanical strength in the wet state, Carbohydr. Polym., 83 (2011) 653-658.

[144] S. Lowell, J.E. Shields, M.A. Thomas, M. Thommes, Characterization of porous solids and powders: surface area, pore size and density, Springer Science & Business Media2012.

[145] S. Lowell, J.E. Shields, Powder surface area and porosity, Springer Science & Business Media2013.

[146] Z. Pei, L. Li, L. Sun, S. Zhang, X.-q. Shan, S. Yang, B. Wen, Adsorption characteristics of 1, 2, 4-trichlorobenzene, 2, 4, 6-trichlorophenol, 2-naphthol and naphthalene on graphene and graphene oxide, Carbon, 51 (2013) 156-163.

[147] F.J. Sotomayor, K.A. Cychosz, M. Thommes, F. Sotomayor, Characterization of micro/mesoporous materials by physisorption: Concepts and case studies, Acc. Mater. Surf. Res, 3 (2018) 34-50.

[148] P. Pauletto, J. Gonçalves, L. Pinto, G. Dotto, N. Salau, Single and competitive dye adsorption onto chitosan-based hybrid hydrogels using artificial neural network modeling, J. Colloid Interface Sci., 560 (2020) 722-729.

[149] R. Han, W. Zou, Z. Zhang, J. Shi, J. Yang, Removal of copper (II) and lead (II) from aqueous solution by manganese oxide coated sand: I. Characterization and kinetic study, J. Hazard. Mater., 137 (2006) 384-395.

[150] L. Zhang, Y. Zeng, Z. Cheng, Removal of heavy metal ions using chitosan and modified chitosan: A review, Journal of Molecular Liquids, 214 (2016) 175-191.

[151] F.A. Pavan, S.L. Dias, E.C. Lima, E.V. Benvenutti, Removal of Congo red from aqueous solution by aniline-propyl silica xerogel, Dyes Pigments, 76 (2008) 64-69.

[152] I.E.M. Carpio, J.D. Mangadlao, H.N. Nguyen, R.C. Advincula, D.F. Rodrigues, Graphene oxide functionalized with ethylenediamine triacetic acid for heavy metal adsorption and anti-microbial applications, Carbon, 77 (2014) 289-301.

[153] R.W. Peters, Chelant extraction of heavy metals from contaminated soils, J. Hazard. Mater., 66 (1999) 151-210.

[154] C. Namasivayam, D. Kavitha, Removal of Congo Red from water by adsorption onto activated carbon prepared from coir pith, an agricultural solid waste, Dyes Pigments, 54 (2002) 47-58.

[155] M. Shirmardi, A. Mesdaghinia, A.H. Mahvi, S. Nasseri, R. Nabizadeh, Kinetics and equilibrium studies on adsorption of acid red 18 (Azo-Dye) using multiwall carbon nanotubes (MWCNTs) from aqueous solution, Journal of Chemistry, 9 (2012) 2371-2383.

[156] E. Bazrafshan, F.K. Mostafapour, A.R. Hosseini, A. Raksh Khorshid, A.H. Mahvi, Decolorisation of reactive red 120 dye by using single-walled carbon nanotubes in aqueous solutions, Journal of chemistry, 2013 (2012).

[157] W.W. Ngah, S. Fatinathan, Chitosan flakes and chitosan–GLA beads for adsorption of p-nitrophenol in aqueous solution, Colloids Surf., A: Physico. Eng. Asp., 277 (2006) 214-222.

[158] S. Mishra, D. Mohapatra, D. Mishra, P. Chattopadhyay, G.R. Chaudhury, R. Das, Arsenic adsorption on natural minerals, Journal of Materials and Environmental Science, 5 (2014) 350-359.

[159] B. Royer, N.F. Cardoso, E.C. Lima, J.C. Vaghetti, N.M. Simon, T. Calvete, R.C. Veses, Applications of Brazilian pine-fruit shell in natural and carbonized forms as adsorbents to removal of methylene blue from aqueous

solutions—Kinetic and equilibrium study, J. Hazard. Mater., 164 (2009) 1213-1222.

[160] I. Langmuir, The constitution and fundamental properties of solids and liquids. Part I. Solids, Journal of the American chemical society, 38 (1916) 2221-2295.

[161] M. Erdem, E. Yüksel, T. Tay, Y. Çimen, H. Türk, Synthesis of novel methacrylate-based adsorbents and their sorptive properties towards p-nitrophenol from aqueous solutions, J. Colloid Interface Sci., 333 (2009) 40-48.

[162] K.R. Hall, L.C. Eagleton, A. Acrivos, T. Vermeulen, Pore-and solid-diffusion kinetics in fixed-bed adsorption under constant pattern conditions, Industrial & Engineering Chemistry Fundamentals, 5 (1966) 212-223.

[163] G. McKay, Adsorption of dyestuffs from aqueous solutions with activated carbon I: Equilibrium and batch contact-time studies, Journal of chemical technology and biotechnology, 32 (1982) 759-772.

[164] C. Giles, T. MacEwan, S. Nakhwa, D. Smith, A system of classification of solution adsorption isotherms, and its use in the diagnosis of adsorption mechanisms and measurement of specific surface areas of solids, J. Chem. Soc, 111 (1960) 3973-3993.

[165] M.-H. Baek, C.O. Ijagbemi, O. Se-Jin, D.-S. Kim, Removal of Malachite Green from aqueous solution using degreased coffee bean, J. Hazard. Mater., 176 (2010) 820-828.

[166] Y.-q. Xia, T.-y. Guo, M.-d. Song, B.-h. Zhang, B.-l. Zhang, Adsorption dynamics and thermodynamics of Hb on the Hb-imprinted polymer beads, Reactive and Functional Polymers, 68 (2008) 63-69.

[167] Q. Hu, Y. Liu, C. Feng, Z. Zhang, Z. Lei, K. Shimizu, Predicting equilibrium time by adsorption kinetic equations and modifying Langmuir isotherm by fractal-like approach, Journal of Molecular Liquids, 268 (2018) 728-733.

[168] M.T. Sultana, H.S. Al-Lamib, A.H. Al-Dujialic, Synthesis and characterization of alumina-grafted acrylic acid monomer and polymer and its

adsorption of phenol and p-chlorophenol, Desal. Water Treat., 150 (2019) 192-203.

[169] H.B. Senturk, D. Ozdes, A. Gundogdu, C. Duran, M. Soylak, Removal of phenol from aqueous solutions by adsorption onto organomodified Tirebolu bentonite: Equilibrium, kinetic and thermodynamic study, J. Hazard. Mater., 172 (2009) 353-362.

[170] M. TEMKIN, V. PYZHEV, Application of Temkin adsorption isotherm, Acta Physiochim, 12 (1940) 217-222.

[171] Y. Meshram, J. Gunjate, R. Khope, Studies on adsorption characteristics of manganese onto coal based chemically modified activated carbon, Materials Today: Proceedings, (2020).

[172] S. Khandaker, Y. Toyohara, G.C. Saha, M.R. Awual, T. Kuba, Development of synthetic zeolites from bio-slag for cesium adsorption: Kinetic, isotherm and thermodynamic studies, Journal of Water Process Engineering, 33 (2020) 101055.

[173] E. Inam, U. Etim, E. Akpabio, S. Umoren, Process optimization for the application of carbon from plantain peels in dye abstraction, Journal of Taibah University for Science, 11 (2017) 173-185.

[174] K.Y. Foo, B.H. Hameed, Insights into the modeling of adsorption isotherm systems, Chem. Eng. J., 156 (2010) 2-10.

[175] N. Ayawei, A.N. Ebelegi, D. Wankasi, Modelling and interpretation of adsorption isotherms, Journal of Chemistry, 2017 (2017).

[176] A. Benhammou, A. Yaacoubi, L. Nibou, B. Tanouti, Adsorption of metal ions onto Moroccan stevensite: kinetic and isotherm studies, J. Colloid Interface Sci., 282 (2005) 320-326.

[177] M. Dubinin, The potential theory of adsorption of gases and vapors for adsorbents with energetically nonuniform surfaces, Chemical Reviews, 60 (1960) 235-241.

[178] A. Debrassi, T. Baccarin, C.A. Demarchi, N. Nedelko, A. Ślawska-Waniewska, P. Dłużewski, M. Bilska, C.A. Rodrigues, Adsorption of Remazol Red 198 onto magnetic N-lauryl chitosan particles: equilibrium,

kinetics, reuse and factorial design, Environ. Sci. Pollut. Res., 19 (2012) 1594-1604.

[179] A.-H. Chen, S.-C. Liu, C.-Y. Chen, C.-Y. Chen, Comparative adsorption of Cu (II), Zn (II), and Pb (II) ions in aqueous solution on the crosslinked chitosan with epichlorohydrin, J. Hazard. Mater., 154 (2008) 184-191.

[180] A.-H. Chen, C.-Y. Yang, C.-Y. Chen, C.-Y. Chen, C.-W. Chen, The chemically crosslinked metal-complexed chitosans for comparative adsorptions of Cu (II), Zn (II), Ni (II) and Pb (II) ions in an aqueous medium, J. Hazard. Mater., 163 (2009) 1068-1075.

[181] A.-H. Chen, S.-M. Chen, Biosorption of azo dyes from aqueous solution by glutaraldehyde-crosslinked chitosans, J. Hazard. Mater., 172 (2009) 1111-1121.

[182] V.J. Inglezakis, A.A. Zorpas, Heat of adsorption, adsorption energy and activation energy in adsorption and ion exchange systems, Desal. Water Treat., 39 (2012) 149-157.

[183] H.T. Xing, J.H. Chen, X. Sun, Y.H. Huang, Z.B. Su, S.R. Hu, W. Weng, S.X. Li, H.X. Guo, W.B. Wu, NH2-rich polymer/graphene oxide used as a novel adsorbent for removal of Cu (II) from aqueous solution, Chem. Eng. J., 263 (2015) 280-289.

[184] T. Manimekalai, G. Tamilarasan, N. Sivakumar, S. Periyasamy, Kinetic, equilibrium and thermodynamic studies of synthetic dye removal using plastic waste activated carbon prepared by CO2 activation, Int. J. Chemtech. Res, 8 (2015) 225-240.

[185] A.M. Ghaedi, S. Karamipour, A. Vafaei, M.M. Baneshi, V. Kiarostami, Optimization and modeling of simultaneous ultrasound-assisted adsorption of ternary dyes using copper oxide nanoparticles immobilized on activated carbon using response surface methodology and artificial neural network, Ultrasonics sonochemistry, 51 (2019) 264-280.

[186] S. Patil, S. Renukdas, N. Patel, Removal of methylene blue, a basic dye from aqueous solutions by adsorption using teak tree (Tectona grandis) bark powder, International Journal of Environmental Sciences, 1 (2011) 711.

[187] A.K. Yadav, C. Kaushik, A.K. Haritash, A. Kansal, N. Rani, Defluoridation of groundwater using brick powder as an adsorbent, J. Hazard. Mater., 128 (2006) 289-293.

[188] T. Egbosiuba, A. Abdulkareem, A. Kovo, E. Afolabi, J. Tijani, M. Auta, W. Roos, Ultrasonic enhanced adsorption of methylene blue onto the optimized surface area of activated carbon: Adsorption isotherm, kinetics and thermodynamics, Chem. Eng. Res. Des., 153 (2020) 315-336.

[189] H. Erdem, B. Yildiz, M. Şahin, M. Erdem, Etodolac adsorption onto activated carbon prepared by chemical activation and pyrolysis of biomasses mixture, Biomass Conversion and Biorefinery, (2020) 1-13.

[190] M. Islam, P.C. Mishra, R. Patel, Fluoride adsorption from aqueous solution by a hybrid thorium phosphate composite, Chem. Eng. J., 166 (2011) 978-985.

[191] A. Itodo, H. Itodo, Activation chemistry and kinetics of Shea nutshell biosorbents for textile wastewater treatment, Acad. Arena, 2 (2010) 51-60.

[192] A.S. Özcan, B. Erdem, A. Özcan, Adsorption of Acid Blue 193 from aqueous solutions onto BTMA-bentonite, Colloids Surf., A: Physico. Eng. Asp., 266 (2005) 73-81.

[193] C.H. Ko, C. Fan, P.N. Chiang, M.K. Wang, K.C. Lin, p-Nitrophenol, phenol and aniline sorption by organo-clays, J. Hazard. Mater., 149 (2007) 275-282.

[194] A. Gholizadeh, M. Kermani, M. Gholami, M. Farzadkia, Kinetic and isotherm studies of adsorption and biosorption processes in the removal of phenolic compounds from aqueous solutions: comparative study, Journal of environmental health science and engineering, 11 (2013) 29.

[195] A.E. Regazzoni, Adsorption kinetics at solid/aqueous solution interfaces: On the boundaries of the pseudo-second-order rate equation, Colloids Surf., A: Physico. Eng. Asp., 585 (2020) 124093.

[196] M.J. Rupa, A. Pal, B.B. Saha, Activated carbon-graphene nanoplatelets based green cooling system: Adsorption kinetics, heat of adsorption, and thermodynamic performance, Energy, 193 (2020) 116774.

[197] S. Patil, J. Patil, S. Renukdas, N. Patel, Mechanism of Adsorption of Ferrous Ions from Waste Water on Natural Adsorbents, World Journal of Pharmacy and Pharmaceutical Sciences, 4 (2015) 767-788.

[198] Y. Özdemir, M. Doğan, M. Alkan, Adsorption of cationic dyes from aqueous solutions by sepiolite, Microporous and Mesoporous Materials, 96 (2006) 419-427.

[199] H.N. Tran, S.-J. You, H.-P. Chao, Thermodynamic parameters of cadmium adsorption onto orange peel calculated from various methods: a comparison study, J. of Environ. Chem. Eng., 4 (2016) 2671-2682.

[200] O.A. Akinbulumo, O.J. Odejobi, E.L. Odekanle, Thermodynamics and adsorption study of the corrosion inhibition of mild steel by Euphorbia heterophylla L. extract in 1.5 M HCl, Results in Materials, 5 (2020) 100074.

[201] M.A. Ahmad, N.A.A. Puad, O.S. Bello, Kinetic, equilibrium and thermodynamic studies of synthetic dye removal using pomegranate peel activated carbon prepared by microwave-induced KOH activation, Water Resources and industry, 6 (2014) 18-35.

[202] Y. Önal, C. Akmil-Başar, D. Eren, Ç. Sarıcı-Özdemir, T. Depci, Adsorption kinetics of malachite green onto activated carbon prepared from Tunçbilek lignite, J. Hazard. Mater., 128 (2006) 150-157.

[203] D. Lin, F. Wu, Y. Hu, T. Zhang, C. Liu, Q. Hu, Y. Hu, Z. Xue, H. Han, T.-H. Ko, Adsorption of dye by waste black tea powder: parameters, kinetic, equilibrium, and thermodynamic studies, Journal of Chemistry, 2020 (2020).

[204] H. Ouassif, E.M. Moujahid, R. Lahkale, R. Sadik, F.Z. Bouragba, M. Diouri, Zinc-Aluminum layered double hydroxide: High efficient removal by adsorption of tartrazine dye from aqueous solution, Surfaces and Interfaces, 18 (2020) 100401.

[205] G.D. Vuković, A.D. Marinković, S.D. Škapin, M.Đ. Ristić, R. Aleksić, A.A. Perić-Grujić, P.S. Uskoković, Removal of lead from water by amino modified multi-walled carbon nanotubes, Chem. Eng. J., 173 (2011) 855-865.

[206] C.-C. Liu, M. Kuang-Wang, Y.-S. Li, Removal of nickel from aqueous solution using wine processing waste sludge, Industrial & engineering chemistry research, 44 (2005) 1438-1445.

[207] G.Z. Kyzas, N.K. Lazaridis, M. Kostoglou, Adsorption/desorption of a dye by a chitosan derivative: experiments and phenomenological modeling, Chem. Eng. J., 248 (2014) 327-336.

[208] O. Zanella, I.C. Tessaro, L.A. Féris, Desorption-and Decomposition-Based Techniques for the Regeneration of Activated Carbon, Chemical Engineering & Technology, 37 (2014) 1447-1459.

[209] L. Soldatkina, M. Zavrichko, Equilibrium, kinetic, and thermodynamic studies of anionic dyes adsorption on corn stalks modified by cetylpyridinium bromide, Colloids and Interfaces, 3 (2019) 4.

[210] A.A. Kamaru, N.S. Sani, N.A.N.N. Malek, Raw and surfactant-modified pineapple leaf as adsorbent for removal of methylene blue and methyl orange from aqueous solution, Desal. Water Treat., 57 (2016) 18836-18850.

[211] M. Vakili, S. Deng, G. Cagnetta, W. Wang, P. Meng, D. Liu, G. Yu, Regeneration of chitosan-based adsorbents used in heavy metal adsorption: A review, Sep. Purif. Technol., (2019).